Control of cell division orientation during vascular development in *Arabidopsis thaliana*

W.M.S. Smet

Control of cell division orientation during vascular development in *Arabidopsis thaliana*

Wouter Marcel Sander Smet

Control of cell division orientation during vascular development in *Arabidopsis thaliana*

Wouter Marcel Sander Smet

Contents

Chapter 1

Scope of the thesis

Wouter Smet[1,2,3]

1. Wageningen University, Laboratory of Biochemistry, Stippeneng 4, 6708 WE Wageningen, the Netherlands
2. Ghent University, Department of Plant Biotechnology and Bioinformatics, Technologiepark 927, 9052 Ghent, Belgium
3. VIB Center for Plant Systems Biology, Technologiepark 927, 9052 Ghent, Belgium

Unlike animals, plants have rigid cell walls which are fixed immediately after division. Hence, cell division and subsequent cell elongation of the daughter cells are the main ways to control three-dimensional (3D) growth in plants. Therefore, in order to properly pattern and grow, it is crucial to carefully position and orient the division plane. Before going into details regarding the role of oriented cell divisions for e.g. vascular development and the molecular pathways uncovered so far (see **Chapter 2: Introduction**); we want to provide a clear framework describing cell division orientation in plants. In this extended scope, we will thus first focus on the different types of cell divisions a plant has at its disposal to generate a 3D structure and introduce a clear nomenclature to define these different division types. We will end by formulating our research question and explain how this fits within the described framework for cell division orientation in plants.

A first type of cell divisions in plants is related to changes in the position of the division plane resulting in a symmetric or asymmetric division (**Figure 1A**). During a symmetric division, the cell division plane is positioned through the center of the cell which will result in two daughter cells with equal volumes after cell division. This happens for example in the majority of the cells in the root apical meristem leading to the replenishment of cells in the root apical meristem and resulting in longitudinal growth of the root. In contrast, during an asymmetric division the cell division plane is positioned off-center, resulting in daughter cells of different volume. Moreover, asymmetric divisions often result in daughter cells which obtain different cell fates, and is therefore of particular interest to developmental biologists. A prime example of asymmetric cell division is the first division of the *Arabidopsis* zygote (Jürgens, 1994; Scheres, et al., 1994).

Besides changes in the position of the division plane, a cell can also control the orientation of its division plane, which results in the addition of a cell in the X, Y or Z dimension (**Figure 1B**). Two basic types of oriented cell division are commonly used in literature: anticlinal and periclinal divisions. Anticlinal divisions are perpendicular to the organ surface and add more cells to an existing cell file and thus result in longitudinal growth. Periclinal divisions are parallel to the organ surface and result in the addition of new cell files and are generally speaking responsible for radial growth.

Conventional nomenclature for anticlinal and periclinal cell divisions as described above is applied to both longitudinal and radial 2D sections. In a longitudinal cross-section, this means that a periclinal cell division results in the formation of a new cell file whereas an anticlinal division adds an extra cell to the existing cell file

(**Figure 1B**). However, in a radial cross-section both anticlinal and periclinal cell divisions result in the formation of new cells files (**Figure 1B**). When applying the nomenclature described above to a 3D image, it becomes even clearer that anticlinal divisions are used for two distinct types of cell divisions. We believe that this nomenclature can be confusing and does not allow for proper distinction between the different types of cell division. Therefore, we propose a new nomenclature using a radial system; cell division planes perpendicular to the organ center will be termed **periclinal** divisions, parallel to the center will be **radial** division and divisions in Z will be termed **anticlinal** divisions. This will provide more consistency in nomenclature and allows for easier distinction of the different types of cell division.

Although it remains unclear how the positioning and orientation of the new cell plate is controlled, it will ultimately be dependent on the position and orientation of the cortical cytoskeleton. The future division plane is preceded by the formation of a structure named the preprophase band (PPB) (Vanstraelen, et al., 2006; Chan, et al., 2005). This is a ring of cortical microtubules held together by actin filaments which is assembled at the G2/M transition. The PPB recruits different protein complexes in order to be properly positioned and accurately predicts the future division plane. The PPB is not a permanent structure and is broken down once the mitotic spindle starts to form (Pickett-Heaps and Northcote, 1966). Once broken down it leaves behind a zone depleted of F-actin, known as the Cortical Division Zone (CDZ) (Mineyuki and Palevitz, 1990), which guides the mitotic spindle and phragmoplast and finally the new cell plate to the correct position (Walker, et al., 2007). Mutations in genes involved in positioning the PPB, CDZ or phragmoplast often result in abnormal, **oblique** division planes (**Figure 1C**) (Pietra, et al., 2013; Azimzadeh, et al., 2008; Xu, et al., 2008; Ambrose, et al., 2007; Walker, et al., 2007; Muller, et al., 2006; Bouquin, et al., 2003; Camilleri, et al., 2002; Bichet, et al., 2001; Burk, et al., 2001; Whittington, et al., 2001). These structures are thus all crucial for correct cell division, but are themselves not the determining factors.

Then what determines division plane orientation? Already in the nineteenth century, Errera and De Wildeman formulated rules stating that cells divide along the plane of the smallest surface that encloses a fixed cellular volume and is thus more commonly known as the 'shortest wall' rule (De Wildeman, 1893; Errera, 1888). As this rule always leads to symmetric divisions, clearly it cannot explain e.g. the first division of the zygote in Arabidopsis thaliana. Nevertheless, more recent work using 3D meshes of maize cells has shown that these rules can be used to accurately predict the PPB positioning (Martinez, et al., 2018). However, 3D analysis of the *Arabidopsis*

plant embryo has shown the phytohormone auxin is able to allow deviation from the shortest cell wall rule and change division plane orientation (see **Chapter 2**) (Yoshida, et al., 2014). Thus, it is hypothesized that this rule acts as a default mechanism of cell division orientation when internal or external cues are absent.

Ultimately deviating from this proposed 'shortest wall' default mechanism would require a shift in the cortical cytoskeletal organization because the PPB and finally also the actual cell plate will form in the same orientation as the cortical cytoskeleton. Therefore, in order to deviate from the shortest wall rule, a cell must receive other cues in order to position its division plane differently. These cues can be, but are not limited to, developmental programs (e.g. lateral root formation or vascular development), genetic factors (e.g. transcription factors), responses to hormones (e.g. auxin or gibberellic acid) or environmental inputs (e.g. light or mechanical pressure) (**Figure 1D-E**) (Chen, et al., 2014; De Rybel, et al., 2013; Vineyard, et al., 2013; Hamant, et al., 2008; Hush, et al., 1990; Hardham and Mccully, 1982; Lintilhac and Vesecky, 1981). Overruling the default state can be the result of only one cue or a combinatorial effect of multiple cues at the same time. While it is known that certain cues are able to overrule the default state and shift the cell division into a certain position, it remains unknown exactly how these cues determine the future division plane position and orientation. Hence, a real gap in our current understanding is how this variety of cues eventually influences the cortical cytoskeleton, which will lead to specific oriented cell divisions.

In this thesis, we aim to answer these questions by studying one specific genetic cue (the heterodimer complex formed by the TARGET OF MONOPTEROS5 (TMO5) and LONESOME HIGHWAY (LHW) transcription factors) capable of shifting the division plane orientation in order to dissect the downstream mechanisms that control division plane orientation.
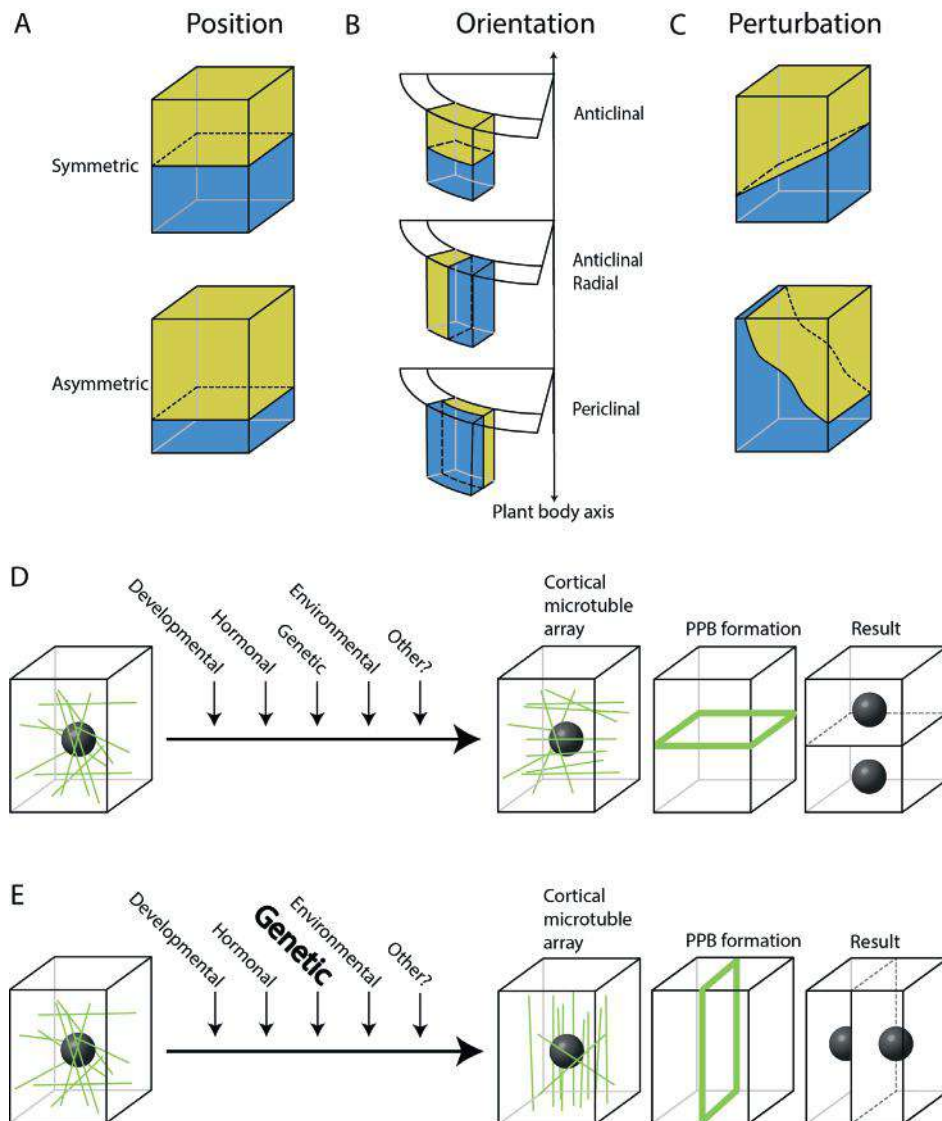
Figure 1: Overview of different ways a cell can position and orient its division plane and how different cues can affect cell division orientation. A. Cells can position their division plane symmetric or asymmetric which gives rise to daughter cells of the same or different size, respectively. **B.** Different ways how a cell can orient its division plane. Anticlinal divisions lead to more cells within a cell file. Radial cell divisions increase the amount of cell files within a cell type while periclinal divisions lead to additional cell files. **C.** Mutations in genes involved in positioning the PPB, CDZ or phragmoplast often result in perturbed division planes. **D.** A cell at interphase is subjected to different cues which affects how it will orient and position its array of cortical microtubules (green lines). This affects the formation of the PPB (green band) and ultimately how the daughter cells are positioned. **E**. An increase of a certain cue (in this case a genetic cue) can lead to reorientation of the cortical microtubule array changing the division plane orientation.

References

Ambrose, J.C., Shoji, T., Kotzer, A.M., Pighin, J.A., and Wasteneys, G.O. (2007). The Arabidopsis CLASP gene encodes a microtubule-associated protein involved in cell expansion and division. The Plant cell 19, 2763-75.

Azimzadeh, J., Nacry, P., Christodoulidou, A., Drevensek, S., Camilleri, C., Amiour, N., Parcy, F., Pastuglia, M., and Bouchez, D. (2008). Arabidopsis TONNEAU1 proteins are essential for preprophase band formation and interact with centrin. The Plant cell 20, 2146-59.

Bichet, A., Desnos, T., Turner, S., Grandjean, O., and Hofte, H. (2001). BOTERO1 is required for normal orientation of cortical microtubules and anisotropic cell expansion in Arabidopsis. The Plant journal : for cell and molecular biology 25, 137-48.

Bouquin, T., Mattsson, O., Naested, H., Foster, R., and Mundy, J. (2003). The Arabidopsis lue1 mutant defines a katanin p60 ortholog involved in hormonal control of microtubule orientation during cell growth. Journal of cell science 116, 791-801.

Burk, D.H., Liu, B., Zhong, R., Morrison, W.H., and Ye, Z.H. (2001). A katanin-like protein regulates normal cell wall biosynthesis and cell elongation. The Plant cell 13, 807-27.

Camilleri, C., Azimzadeh, J., Pastuglia, M., Bellini, C., Grandjean, O., and Bouchez, D. (2002). The Arabidopsis TONNEAU2 gene encodes a putative novel protein phosphatase 2A regulatory subunit essential for the control of the cortical cytoskeleton. The Plant cell 14, 833-45.

Chan, J., Calder, G., Fox, S., and Lloyd, C. (2005). Localization of the microtubule end binding protein EB1 reveals alternative pathways of spindle development in Arabidopsis suspension cells. The Plant cell 17, 1737-1748.

Chen, X., Grandont, L., Li, H., Hauschild, R., Paque, S., Abuzeineh, A., Rakusova, H., Benkova, E., Perrot-Rechenmann, C., and Friml, J. (2014). Inhibition of cell expansion by rapid ABP1-mediated auxin effect on microtubules. Nature 516, 90-3.

De Rybel, B., Möller, B., Yoshida, S., Grabowicz, I., Barbier de Reuille, P., Boeren, S., Smith, R.S., Borst, J.W., and Weijers, D. (2013). A bHLH complex controls embryonic vascular tissue establishment and indeterminate growth in Arabidopsis. Developmental cell 24, 426-37.

Errera, L. (1888). Über Zellformen und Seifenblasen. Botanisches Centralblatt, 395–399.

Hamant, O., Heisler, M.G., Jonsson, H., Krupinski, P., Uyttewaal, M., Bokov, P., Corson, F., Sahlin, P., Boudaoud, A., Meyerowitz, E.M., et al. (2008). Developmental Patterning by Mechanical Signals in Arabidopsis. Science 322, 1650-1655.

Hardham, A.R., and Mccully, M.E. (1982). Reprogramming of Cells Following Wounding in Pea (Pisum-Sativum-L) Roots .1. Cell-Division and Differentiation of New Vascular Elements. Protoplasma 112, 143-151.

Hush, J.M., Hawes, C.R., and Overall, R.L. (1990). Interphase Microtubule Reorientation Predicts a New Cell Polarity in Wounded Pea Roots. Journal of cell science 96, 47-61.

Jürgens, G.M., U. (1994). Arabidopsis. In Embryos: Colour Atlas of Development - Bard,Jbl. Nature 370, 190-190.

Lintilhac, P.M., and Vesecky, T.B. (1981). Mechanical-Stress and Cell-Wall Orientation in Plants .2. The Application of Controlled Directional Stress to Growing Plants - with a Discussion on the Nature of the Wound Reaction. Am J Bot 68, 1222-1230.

Martinez, P., Allsman, L.A., Brakke, K.A., Hoyt, C., Hayes, J., Liang, H., Neher, W., Rui, Y., Roberts, A.M., Moradifam, A., et al. (2018). Predicting division planes of three-dimensional cells by soap-film minimization. The Plant cell.

Mineyuki, Y., and Palevitz, B.A. (1990). Relationship between Preprophase Band Organization, F-Actin and the Division Site in Allium - Fluorescence and Morphometric Studies on Cytochalasin-Treated Cells. Journal of cell science 97, 283-295.

Muller, S., Han, S., and Smith, L.G. (2006). Two kinesins are involved in the spatial control of cytokinesis in Arabidopsis thaliana. Current biology : CB 16, 888-94.

Pickett-Heaps, J.D., and Northcote, D.H. (1966). Organization of microtubules and endoplasmic reticulum during mitosis and cytokinesis in wheat meristems. Journal of cell science 1, 109-20.

Pietra, S., Gustavsson, A., Kiefer, C., Kalmbach, L., Horstedt, P., Ikeda, Y., Stepanova, A.N., Alonso, J.M., and Grebe, M. (2013). Arabidopsis SABRE and CLASP interact to stabilize cell division plane orientation and planar polarity. Nature communications 4, 2779.

Scheres, B., Wolkenfelt, H., Willemsen, V., Terlouw, M., Lawson, E., Dean, C., and Weisbeek, P. (1994). Embryonic Origin of the Arabidopsis Primary Root and Root-Meristem Initials. Development 120, 2475-2487.

Vanstraelen, M., Van Damme, D., De Rycke, R., Mylle, E., Inze, D., and Geelen, D. (2006). Cell cycle-dependent targeting of a kinesin at the plasma membrane demarcates the division site in plant cells. Current Biology 16, 308-314.

Vineyard, L., Elliott, A., Dhingra, S., Lucas, J.R., and Shaw, S.L. (2013). Progressive transverse microtubule array organization in hormone-induced Arabidopsis hypocotyl cells. The Plant cell 25, 662-76.

Walker, K.L., Muller, S., Moss, D., Ehrhardt, D.W., and Smith, L.G. (2007). Arabidopsis TANGLED identifies the division plane throughout mitosis and cytokinesis. Current biology : CB 17, 1827-36.

Whittington, A.T., Vugrek, O., Wei, K.J., Hasenbein, N.G., Sugimoto, K., Rashbrooke, M.C., and Wasteneys, G.O. (2001). MOR1 is essential for organizing cortical microtubules in plants. Nature 411, 610-3.

De Wildeman, E.d. (1893). Études sur l'attache des cloisons cellulaires. Mémoires couronnés et mémoires des savants étrangers, 1-84.

Xu, X.F.M., Zhao, Q., Rodrigo-Peiris, T., Brkljacic, J., He, C.S., Muller, S., and Meier, I. (2008). RanGAP1 is a continuous marker of the Arabidopsis cell division plane. Proceedings of the National Academy of Sciences of the United States of America 105, 18637-18642.

Yoshida, S., Barbier de Reuille, P., Lane, B., Bassel, G.W., Prusinkiewicz, P., Smith, R.S., and Weijers, D. (2014). Genetic control of plant development by overriding a geometric division rule. Developmental cell

Chapter 2

Introduction

Wouter Smet[1,2,3,] Dolf Weijers[1] and Bert De Rybel[1,2,3]

1.   Wageningen University, Laboratory of Biochemistry, Stippeneng 4, 6708 WE Wageningen, the Netherlands
2.   Ghent University, Department of Plant Biotechnology and Bioinformatics, Technologiepark 927, 9052 Ghent, Belgium
3.   VIB Center for Plant Systems Biology, Technologiepark 927, 9052 Ghent, Belgium

The Arabidopsis root as a model system to study cell division orientation

Arabidopsis thaliana is heavily used as a plant model system because it is small and easy to grow, has a fully sequenced and small genome, has many genetic resources and collections, is easy to transform and has a short lifecycle of only 3 months. The *Arabidopsis* root provides an elegant system to study vascular development and cell division orientations due to its simple and very predictable cellular organization in files of cells (**Figure 1**). Furthermore, the roots can be easily grown *in vitro* on agar-based medium allowing easy access and observation. Moreover, the young roots are fully transparent, making them particularly suitable for microscopic analysis. Because of these main reasons, the *Arabidopsis root* is one of the most popular model systems for plant developmental biologists.

The root apical meristem consists of three different zones, which from root tip to shoot are; the meristematic, elongation and differentiation zone (**Figure 1**). Cell division is mostly limited to the meristematic zone close to the root tip and thus it is here where the new cells of the root meristem are formed during primary growth. Cells from the meristematic zone will reach the differentiation zone, which is marked by e.g. the occurrence of root-hair cells. The root meristem in *Arabidopsis* is organized in a simple radial manner (Dolan et al., 1993) consisting of concentric tissue layers with different functional properties. From outside to inside we can find the epidermis, the ground tissues (cortex and endodermis), and the centrally located vasculature. These different cell layers all originate from the stem cells in the root meristem, which generate all these cell-layers in a highly organized manner (**Figure 1**) (Dolan, et al., 1993). The stem cells surround an organizing center called the quiescent center (QC). The QC cells rarely divide and induce the surrounding stem cells to maintain their stem cell identity (van den Berg, et al., 1997). Cells close to the QC frequently proliferate and gradually progress away from the QC and start to differentiate and undergo regulated cell expansion (Kidner, et al., 2000). Because plant cells are fixed in their position directly after division they form cell files in the root meristem, facilitating lineage tracing of cells and cell divisions. Recent work suggests that instead of only having stem cells next to the QC, there likely is a gradient of stemness throughout the root meristem coupled to an opposing gradient of differentiation (**Figure 1**) (Wendrich, et al., 2017).
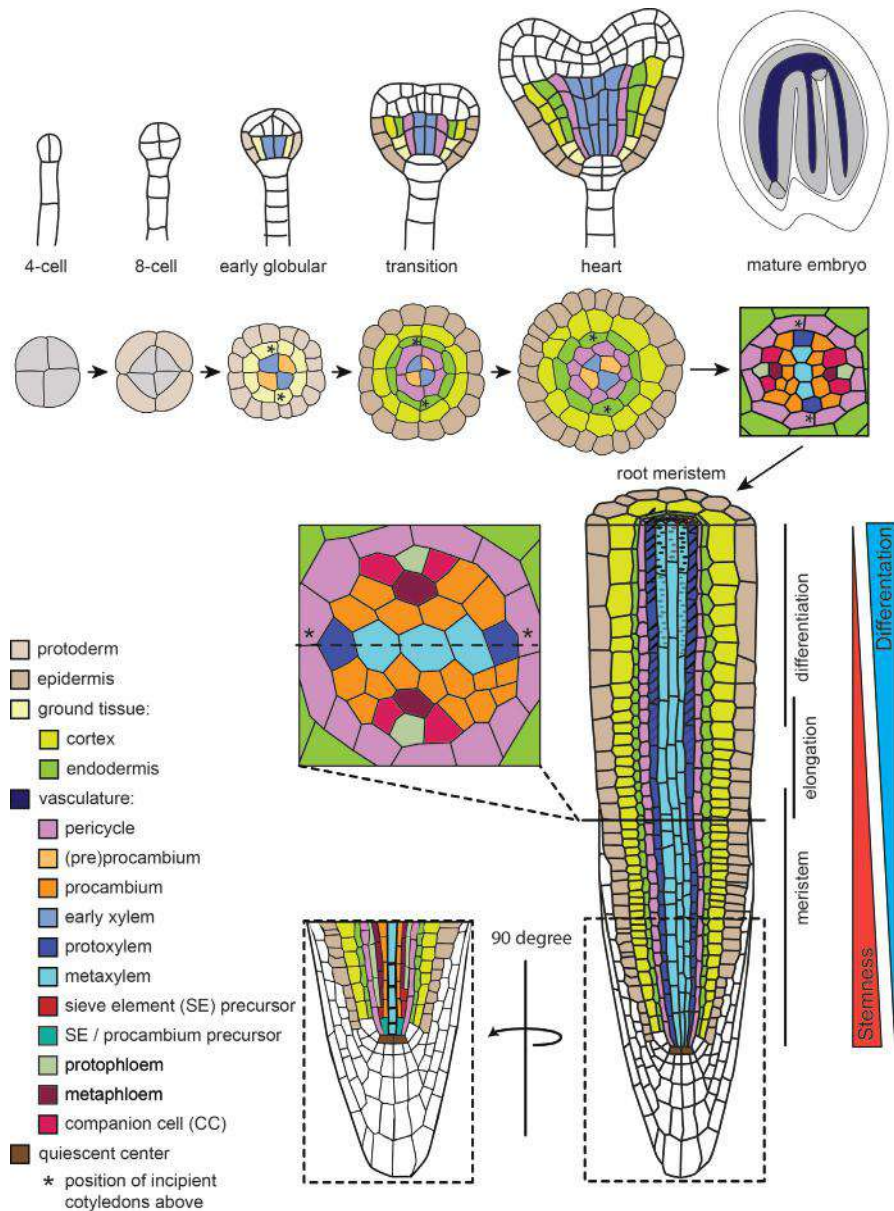
Figure 1: An overview of the cell-type organization in the developing embryo and root meristem.
Starting from a four cell stage embryo we can follow the cellular organization during embryogenesis (upper panel). At the end of embryogenesis all cell-types that are present can also be found in the root meristem (cross-section mature embryo vs. cross-section root meristem). The root meristem first of all consists of different zones (meristematic, elongation, differentiation). Recent work suggests that there is a gradient of stemness versus an opposing gradient of differentiation present in the root meristem. The root meristem on the right meristem shows the cellular organization of a longitudinal cross-section through the xylem. A 90 degree shifted cross-section also shows the cellular organization of the developing phloem lineage. Figure modified from Wendrich, et al., 2017; De Rybel, et al., 2016; De Rybel, et al., 2014b.

Vascular tissue function, ontogeny and development

Vascular tissues form an efficient fluid conducting system that stretches throughout the entire plant body. It is thought that the development of tissues was a crucial step that enabled plants to thrive on land and reach the heights we see today in giant trees (Xu, et al., 2014; Lucas, et al., 2013). The main functions of the vascular tissues are mechanical support of the plant and long-distance transport of water, sugars, nutrients, hormones and other signaling molecules. The vascular system also functions as an effective long-distance communication system transferring information about abiotic and biotic conditions between tissues below and above ground. This type of transfer can include hormones, peptides, proteins and RNA; and allows the vasculature to coordinate developmental and physiological processes at the whole-plant level.

As is the case for all tissue types in the mature root meristem, the vascular tissues originate during embryogenesis (Jürgens, 1994; Mansfield and Briarty, 1991). Embryogenesis starts at the fertilization of the zygote. After fertilization the zygote elongates and divides into a smaller apical cell and a larger basal cell. After two rounds of anticlinal and periclinal divisions the apical cell forms the eight-cell proembryo (octant stage) (**Figure 1**). The basal cells form the extraembryonic suspensor by a series of anticlinal divisions, which functions to anchor the embryo to the embryo sac and ovule tissue (Mansfield and Briarty, 1991). The upper part of the octant stage proembryo will give rise to the shoot while the lower part will develop the RAM. At the 16-cell stage additional periclinal divisions will generate 8 outer cells and 8 inner cells. The next stage (early globular) is the point where the vascular initials are generated. This is due to the inner four cells of the 16-cell stage embryo dividing periclinally and forming the vascular and ground tissue initial cells. At late globular stage also the upper cell of the suspensor divides asymmetrically and gives rise to a smaller lens-shaped apical cell and a larger basal cell. The lens-shaped cell will later develop into the QC while the larger basal cell develops into the columella root cap cells (Hamann, et al., 1999; Scheres, et al., 1994). At the transition stage the endodermis, cortex and pericycle lineages are formed. Further divisions increase the size of the embryo (e.g. hearth, torpedo stage) until a mature embryo is formed. At this point the embryo has established all the cell types that can also be found in the mature root. From this we can conclude that all vascular cell types originate from the first vascular initial cells in the early embryo (De Rybel, et al., 2014a; Yoshida, et al., 2014; Scheres, et al., 1995; Scheres, et al., 1994). Provascular initial cells thus need to develop into a vast array of cell identities.

Broadly speaking, the vascular system throughout the plant consists of three major tissue types: xylem, phloem and (pro)cambium cells (**Figure 1**). All these cell types are arranged in a highly organized manner and each cell type has a specialized function. While the different vascular cell types described above all originate from only a few pro-vascular initial cells in the early embryo, they do not differentiate during embryogenesis.

Xylem tissues differentiate into several cell types including tracheary elements, xylem fibers and xylem parenchyma cells (Esau, 1965). Xylem is responsible for the root to shoot transport of water and minerals and also provides the plant with mechanical support. The xylem tracheary elements are the water conducting cells, while both tracheary elements and xylem fibers provide mechanical support and possess thick secondary cell walls. Xylem parenchyma provides various functions including aiding the lignification of secondary cell walls in neighboring vessel elements and fibers (Pesquet, et al., 2013; Smith, et al., 2013). Xylem parenchyma cells lack well defined secondary cell walls. All these different cell types are formed from procambium cells. Xylem tracheary and xylem fiber cells undergo programmed cell death in order to develop distinct lignified secondary cell walls (Oda and Fukuda, 2012; Mauseth, 1988). Tracheary elements are formed during different stages of plant development, and can be distinguished as protoxylem and metaxylem. Differentiated protoxylem cells typically have annular or helical secondary cell wall thickenings, while metaxylem cells have distinctive pitted or reticulate secondary cell wall thickenings.

Phloem on the other hand, differentiates into sieve elements, companion cells, phloem fibers and phloem parenchyma cells. The main function of the phloem is transporting photo-assimilates produced in the photosynthetic tissues throughout the plant. The sieve elements are the main conductive tissue of the phloem. They develop from phloem precursor cells in the procambium (**Figure 1**) (Mahönen, et al., 2000). During maturation of the sieve elements the organelles are degraded and at connecting cells walls of the sieve elements, sieve pores are formed (Lucas, et al., 1993). These enlarged plasmodesmata pores allow for effective transport in the phloem. Companion cells originated from the same phloem precursor as the sieve elements cells (Mahönen, et al., 2000). They are connected to the sieve elements by numerous plasmodesmata and ensure their survival by supplying the sieve elements with energy, assimilates and other macromolecules.

The organization of vascular tissues differs tremendously within species, within different organs and even depending on the developmental stage. Despite these
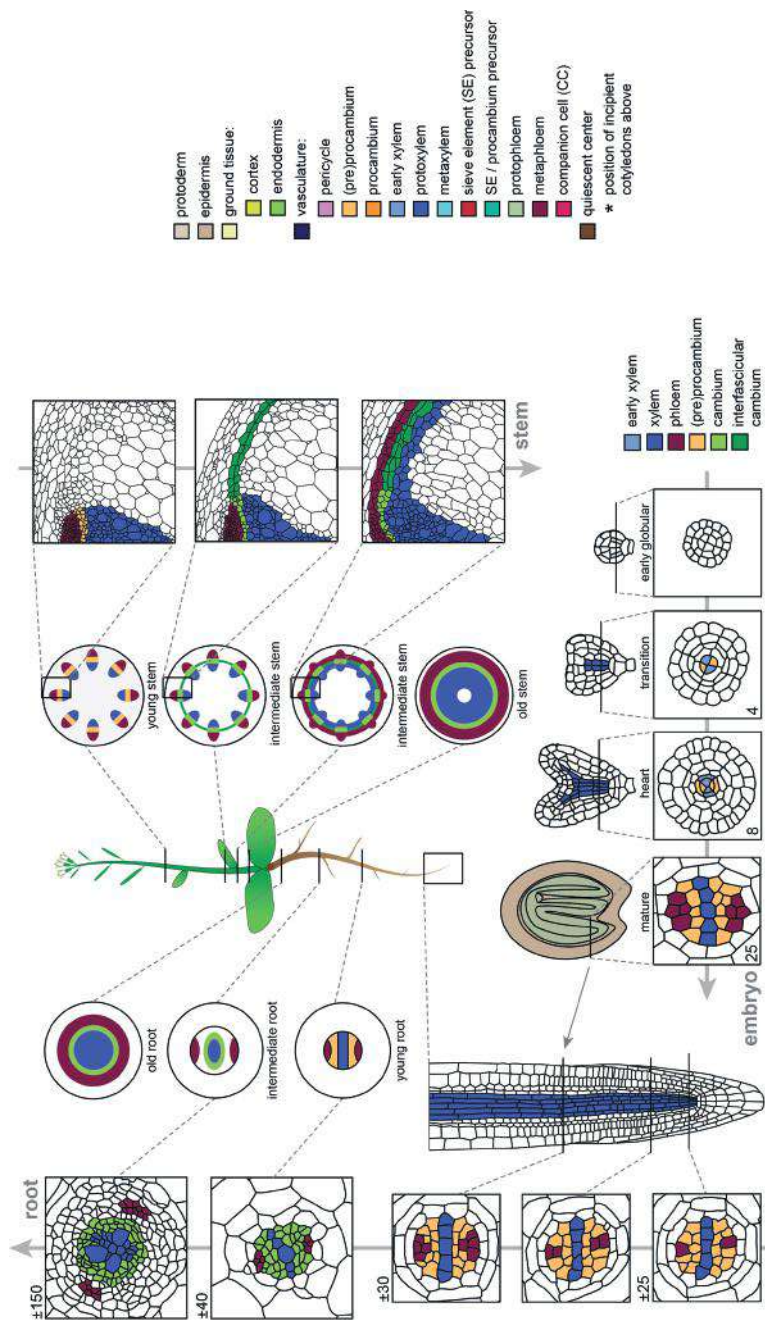
Figure 2: An overview of the organization of the vascular cell lineage throughout plant development. Starting from the early embryo (bottom panel) a diarch bisymmetrical pattern is established in the vasculature. This pattern is maintained in the root meristem. At the onset of secondary growth in the root, the inner cells divide and form concentric rings of phloem and procambium around a circle of xylem cells. In the young *Arabidopsis* shoot the vasculature is organized in separate bundles of xylem, procambium and phloem. At the onset of secondary growth, the interfascicular cambium starts to divide and connects the separate bundles. This eventually leads to the formation of concentric rings of phloem, cambium and xylem in the mature stem. For all sections, the location of cross sections is indicated on a young *Arabidopsis* seedling in the middle. The representative location of the section through the mature embryo in comparison to the post-embryonic root meristem is indicated with a thin arrow. The large gray arrows represent behind the cross sections represent the time axis during development. The numbers on or next to the cross sections represents the number of cells within the vasculature (excluding the pericycle cells).

differences, procambium is in general located between xylem and phloem cell types (**Figure 2**). In *Arabidopsis*, the vascular bundle in the root shows a bisymmetric or diarch organization. It consists of a central xylem axis, flanked on both sides by phloem poles with intervening cambium. However other dicotyledonous e.g. cotton plants show different organizations of the root vascular patterns (Scarpella and Meijer, 2004) and generally speaking, larger vascular bundles show higher order (triarch, tetrarch, etc.) organizations. Also within the plant itself, the vascular tissues show different organizations. The bisymmetric vascular anatomy of the meristematic root is established early during embryogenesis. Here, the future xylem axis is formed from the four inner cells at early globular stage. It is thought that the two cells that are connected in the middle by a "bridge" have higher auxin levels, and thus form the xylem axis (**Figure 2**) (De Rybel, et al., 2014a). The bisymmetric organization formed during embryogenesis is maintained in the post-embryonic root meristem. However, during secondary growth, this bisymmetric organization is changed into concentric rings of phloem and procambium around a circle of xylem cells (**Figure 2**). Very different from the root tissues, the young shoot vasculature is organized in separate bundles of xylem, procambium and phloem. Through cambial activity and the formation of interfascicular cambium, these bundles connect to form concentric rings of phloem, procambium with a central circle of xylem; similar to what is formed in the mature root (**Figure 2**).

Oriented cell divisions shape the vascular cell lineage

Because plant cells have rigid cell walls and are immobilized within a tissue context, cell expansion and oriented cell divisions are the main mechanisms to shape a three-dimensional organ and eventually the entire plant body. Three basic types of divisions occur in plants: Anticlinal, radial and periclinal (**described in Scope Figure 1**). Anticlinal cell divisions (AD) add more cells to an existing cell file and are thus the main driver of longitudinal growth along the main body axis of the plant. Radial divisions (RD) add more cell files to an existing to an existing cell type, increasing its width. Periclinal cell divisions (PD) however provide an increase in the number of cell files and thus control radial growth. These divisions often result in daughter cells of different size or identity and are therefore also referred to as 'formative divisions'(De Smet and Beeckman, 2011). The existence of these clearly distinct division types also suggests that control mechanisms must be present to specifically position the division plane and control its orientation. This process plays vital roles throughout plant development, starting with the very first division of the

zygote (van Dop, et al., 2015; Ueda and Laux, 2012). Later during embryogenesis, specific anticlinal and periclinal cell divisions generate all major tissue types of the plant (Scheres, et al., 1995; Scheres, et al., 1994). Post-embryonically, cell division orientations have also been shown to be of vital importance during e.g. root stem cell (Bennett and Scheres, 2010), stomatal development (Lau and Bergmann, 2012) and lateral root formation (Lavenus, et al., 2013; Peret, et al., 2009).

Although a tight control of cell division orientation is important throughout plant development, this is specifically true for vascular tissues. During the early globular stage of embryogenesis, only four provascular cells expressing early vascular marker genes (De Rybel, et al., 2014b) will undergo a series of periclinal cell divisions giving rise to a fully patterned vascular bundle containing about 25 cell files (excluding pericycle cells) in a mature embryonic root (**Figure 2**). Additional rounds of post-embryonic periclinal divisions in the meristematic vascular tissues will further increase the number of vascular cell files from 25 just above the quiescent center to about 30 in the elongation zone (**Figure 2**). Of particular interest in this case is the phloem cell lineage. Here, a single procambium cell undergoes a PD resulting in another procambium cell and a sieve element precursor cell. The latter undergoes another round of PD, generating a proto- and a meta-phloem cell file (**Figure 1**). Two more PD events generate the companion cell files on each side of the sieve element cell files from neighboring procambium cells (Rodriguez-Villalon, et al., 2014; Mahönen, et al., 2000).

Later in development during secondary growth, subsets of procambium cells will develop into vascular cambium; a meristem responsible for the secondary radial growth of stem and root tissues (**Figure 2**). During secondary growth, PRD are responsible for the dramatic increase in size of the vascular bundle. The organization of the root vascular tissues also changes during this process in which xylem proliferates in the center, phloem at the periphery and cambium in the middle (Nieminen, et al., 2015). This process starts at approximately five days after germination by periclinal cell divisions in the root procambium. The procambium and pericycle start to divide and subsequently a ring of continuous cambial cells is formed (Busse and Evert, 1999). At the transit stage, the cambium divides and forms secondary xylem inwards and secondary phloem outwards, leading to the concentric rings of phloem and procambium around a circle of xylem cells. In the young stem the vasculature is organized in separate vascular bundles. At secondary growth the vascular cambium is formed by divisions from the vascular bundles and between them. Fascicular cambium is formed by the dividing procambium cells in-

between the xylem and phloem cells. Interfascicular cambium forms in between these bundles and precedes the formation of the fascicular cambium. Formation of the interfascicular cambium meristem starts when the procambium cells in between the xylem and phloem start to divide inside the vascular bundles. The dividing interfascicular cambium forms a concentric ring that connects the vascular bundles and will then generate more phloem and xylem cells through cell division (Jouannet, et al., 2015); resulting in an organization similar to that of the root (**Figure 2**).

Genetic and hormonal control mechanisms

Over the past few years, our understanding of the hormonal and genetic control mechanisms of vascular development has increased tremendously. Genetic players ranging from early embryogenesis to late differentiation are now identified. However, despite the importance of oriented cell divisions for the vascular cell lineage, only a few pathways have been implicated in this process so far.

One major pathway controlling vascular periclinal and radial cell divisions (PRD) acts during early embryogenesis and also at least in the post-embryonic root. This pathway is dependent on the auxin-controlled transcription factor MONOPTEROS (MP) which is crucial for proper embryonic development of the procambium. Loss-of-function of *mp* leads to a reduction in the vascular cell file number. One of its downstream targets is a bHLH transcription factor TARGET OF MONOPTEROS5 (TMO5) and is first expressed in the four provascular initial cells during early globular stage (Schlereth, et al., 2010). TMO5 and its closest homologs form heterodimer complexes with another bHLH transcription factor called LONESOME HIGHWAY (LHW) and its respective homologs (De Rybel, et al., 2013; Ohashi-Ito and Bergmann, 2007) (**Figure 3**). Loss-of-function of *tmo5* or *lhw* clade members results in strongly reduced vascular cell file numbers, whereas ectopic expression of both TMO5 and LHW is able to ubiquitously induce PRD in the root (De Rybel, et al., 2013; Ohashi-Ito, et al., 2013a; Ohashi-Ito, et al., 2013b). Intriguingly, the expression of both bHLH transcription factors overlaps in young xylem cells while the PRD mostly take place in the neighboring procambium cells; suggesting that a mobile signal acts downstream (De Rybel, et al., 2013). More recently, the cytokinin (CK) biosynthetic gene *LONELY GUY4 (LOG4)* and its close homolog *LOG3* were identified as direct targets of the TMO5/LHW dimer complex (De Rybel, et al., 2014a; Ohashi-Ito, et al., 2014). CK is a good candidate to act as this mobile signal because CK-signaling is clearly required for PRD. This is reflected by the fact that mutants in

the biosynthetic pathway (e.g. *log1,2,3,5,6,7,8* (Tokunaga, et al., 2012; Kuroha, et al., 2009)), perception by the CK receptors (e.g. *wooden leg* (Mahönen, et al., 2000)) and mutants in downstream signaling events (e.g. *arr1,10,12* (Ishida, et al., 2008; Yokoyama, et al., 2007)) all show strongly reduced PRDs in the vascular bundle. In all these mutants, patterning within the vascular bundle is also disturbed; indicating that cell division orientation and patterning events are tightly linked. Although TMO5/LHW-dependent CK production along the xylem axis is able to trigger PRD in neighboring procambium cells, it seems unlikely that this pathway also controls the high number of PRD in the more distantly positioned phloem cell lineage.
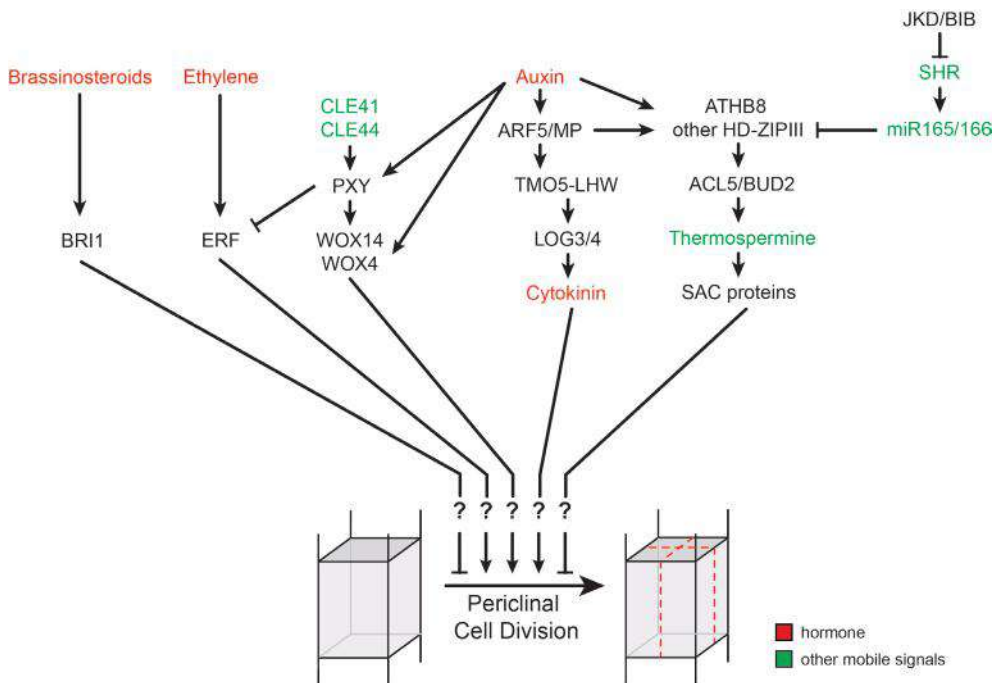
Figure 3: Schematic representation of the known hormonal and genetic pathways controlling vascular proliferation. Several pathways acting in different tissues during distinct developmental stages have been implicated in vascular proliferation resulting from an increase in periclinal cell division activity. It remains unclear if these pathways control the same downstream target genes or whether these are distinct. Moreover, the identity of these factors controlling the actual orientation of cell divisions remains unknown. The hormonal inputs to this network are highlighted in red.

Besides auxin and CK, brassinosteroid have also been implicated in controlling the amount of vascular cell files in the root meristem. Computational modeling has suggested that brassinosteroids can enhance the number of vascular bundles in the shoot by increasing the number of provascular cells and this has

been confirmed with observations in *Arabidopsis* mutants (Fabregas, et al., 2010; Ibanes, et al., 2009). A mutant of the *BRASSINOSTEROID INSENSITIVE 1 (BRI1)* gene and its two closest homologs results in a small meristem size which is due to reduced cell elongation and is accompanied by supernumerary formative cell divisions in the radial dimension (Kang, et al., 2017). Surprisingly, the majority of these mutant phenotypes can be rescued by protophloem specific expression of BRI1, suggesting an important role of BR-signaling in these tissue types.

A second major pathway controlling periclinal cell divisions within the hypocotyl, stem and leaf veins involves *ACAULIS5/THICKVEIN (ACL5/TKV)* (Clay and Nelson, 2005; Hanzawa, et al., 2000; Hanzawa, et al., 1997). Loss of ACL5 function causes vascular cell proliferation in combination with increased xylem cell differentiation (Imai, et al., 2008; Imai, et al., 2006). The polyamine thermospermine produced by ACL5 has been shown to repress the translational inhibitory effect of the up-stream open reading frames (uORFs) located in the 5' leader sequence of *SUPRESSOR OF ACAULIS51 (SAC51), SAC52* (Imai, et al., 2008; Imai, et al., 2006) and other *SAC* genes. *SAC51* encodes yet another bHLH transcription factor (Imai, et al., 2006), while *SAC52* was found to be *RIBOSOMAL PROTEIN L10 (RPL10A)* (Imai, et al., 2008). Recently it has been shown that ACL5 controlled SACLs are involved in a negative feedback loop controlling TMO5/LHW dimer activity. TMO5 and its close homolog T5L1 are both capable of binding LHW and increasing SACL protein levels by either directly increasing their transcription of through ACL5 thermospermine-mediated translation. The increased amount of SACL proteins can repress TMO5/LHW dimer activity by directly binding to LHW (Vera-Sirera, 2015). *ACL5* itself is also regulated by auxin through the homeodomain - leucine zipper (HD-ZIPIII) protein ARABIDOPSIS THALIANA HOMEOBOX 8 (ATHB8) (Baima, et al., 2014; Milhinhos, et al., 2013) (**Figure 3**). Loss-of-function of *HD-ZIPIII* and *KANADI* genes show increased vascular PRD in the hypocotyl, while increased levels show strongly reduced vascular cell numbers (Carlsbecker, et al., 2010; Ilegems, et al., 2010). Moreover, *HD-ZIPIII* levels in the primary root are controlled by the mobile SHORT-ROOT (SHR) transcription factor and micro-RNAs MIR165/166 (Miyashima, et al., 2011; Carlsbecker, et al., 2010). SHR which is expressed in the stele, moves outwards to the endodermis where it triggers MIR165/166 expression. SHR movement itself is restricted by the BIRD zinc finger transcription factor family and is necessary for border establishment between stele and ground tissue (Long, et al., 2015). Interestingly, a double mutant in two members of this family, *JACKDAW* and *BALD IBIS*, results in a strong increase in the number of vascular PRD (Long, et al., 2015).

Two other genes are involved in controlling boundary formation in the vasculature, these are *AT-HOOK MOTIF NUCLEAR LOCALIZED 3 (AHL3)* and the gene encoding its interacting homologue (*AHL4*). These genes are expressed in the procambium cells adjacent to the xylem axis and are cytokinin inducible. AHL3 and AHL4 proteins move towards the xylem where they regulate the tissue boundaries between xylem and procambium. Based on their expression and the fact that they are controlled by cytokinin it has been suggested that they function downstream of the TMO5/LHW pathway.

Later in development during secondary growth, PRD in the hypocotyl and stem are controlled by the CLE41/44 or TRACHEARY ELEMENT DIFFERENTIATION INHIBITORY FACTOR (TDIF) peptide and its PHLOEM INTERCALATED WITH XYLEM / TDIF RECEPTOR (PXY/TDR) receptor (Hirakawa, et al., 2010; Hirakawa, et al., 2008; Fisher and Turner, 2007) (**Figure 3**). This CLE-type peptide, produced in the secondary phloem, travels to the cambium where it binds the PXY/TDR receptor and induces the expression of the WUSCHEL-RELATED HOMEOBOX4 (WOX4) and WOX14 transcription factors (Etchells, et al., 2013; Etchells and Turner, 2010; Hirakawa, et al., 2010; Hirakawa, et al., 2008; Fisher and Turner, 2007). Mutants in these factors all show reduced numbers of vascular cell files, indicating a key role during lateral growth both in *Arabidopsis* and poplar (Etchells and Turner, 2010). Moreover, WOX4 and WOX14 act redundantly in controlling the number of vascular cell files within the cambium as the *wox4/wox14* double mutant shows a further reduction in cell files compared to the *wox4* single mutant (Etchells, et al., 2013; Suer, et al., 2011). This regulatory pathway is also profoundly controlled by hormonal input. For example, similar to primary vascular proliferation, CK is required for secondary growth, as procambium divisions are absent in a CK biosynthesis mutant and can be reinstalled by cytokinin treatments (Matsumoto-Kitano, et al., 2008). Also, *WOX4* was shown to be auxin-responsive in a PXY/TDIF independent manner, while ETHYLENE RESPONSE FACTORs (ERFs) are upregulated in the stem and hypocotyl of the *pxy/tdr* and *wox4* single mutants. Additionally, the *pxy erf109 erf018* triple mutant shows a reduction of vascular cell files within the hypocotyl (Etchells, et al., 2012).

Two other LRR-RLK named REDUCED IN LATERAL GROWTH 1 (RUL1) and MORE LATERAL GROWTH 1 (MOL1) have been shown to affect cambium activity during secondary growth. In contrast to the *pxy* mutant which has altered interfascicular cambium formation, mutants of *rul1* and *mol1* do not show impaired interfascicular cambium formation. *Rul1* and *mol1* show, respectively, a decrease and increase in interfascicular cambium-derived tissue, suggesting that they mediate the opposing

signals that regulate cambium activity. In recent work genes involved in ethylene and jasmonic acid signaling have been found downstream of *MOL1*, these signaling pathways are known to control lateral growth in the *Arabidopsis* stem (Gursanscky, et al., 2016).

Although the genetic and hormonal pathways discussed above all seem to control vascular proliferation; it remains entirely unclear how they exert their effect on the actual orientation of cell divisions in the vascular tissues. Indeed, there appears to be a gap in our understanding of how these regulatory networks are linked to cell division plane orientation.

Bridging the gap

A large number of proteins required to correctly execute oriented cell divisions have been identified. Many of these affect actin or microtubule (MT) dynamics and organization during different stages of cell division, while others determine a plasma membrane domain where the cell plate will fuse at the end of cytokinesis (Wu and Bezanilla, 2014; Pietra, et al., 2013; Azimzadeh, et al., 2008; Xu, et al., 2008; Ambrose, et al., 2007; Walker, et al., 2007; Muller, et al., 2006; Bouquin, et al., 2003; Camilleri, et al., 2002; Bichet, et al., 2001; Burk, et al., 2001; Whittington, et al., 2001; McClinton and Sung, 1997; Smith, et al., 1996; Traas, et al., 1995). In all cases, mutations do not cause a 90-degree rotation of the cell division plane, but result in randomly oriented cell divisions. Hence, these factors do not control the exact switching of the division plane between anticlinal or periclinal divisions, but are rather part of the canonical cell division machinery itself.

Nevertheless, as the preprophase band (PPB) normally forms in the same orientation as the cortical cytoskeletal organization (Mineyuki, 1999), the switch in cell division orientation required to generate a PRD should be preceded by a similar 90-degree rotation of the cortical MT array from transverse to longitudinal. This type of cytoskeletal rotation can be induced by light stimulus in hypocotyl epidermis cells through KATANIN-dependent MT severing and plus-end polymerization (Lindeboom, et al., 2013) and TONNEAU2/FASS-dependent branching nucleation (Kirik, et al., 2012). Similarly, short-term auxin treatments (Chen, et al., 2014) also provoke similar interphase MT reorientations, although an opposite reorientation from longitudinal to transverse by auxin and auxin in combination with gibberellic acid treatments has also been reported (Vineyard, et al., 2013). Besides hormones, sensing physical

pressure is also able to switch the orientation of cortical MT (Hamant, et al., 2008; Hush, et al., 1990; Hardham and Mccully, 1982; Lintilhac and Vesecky, 1981). It is however not straightforward to imagine how cells in the vascular system would feel differential pressure, or how light could induce the required MT reorientation in root vascular cells. Despite these considerations, KATANIN and TONNEAU2/FASS are good molecular targets to act downstream of the genetic pathways we have described previously. Other candidates present in root vascular cells are AURORA kinases. Especially during lateral root development in *aur1-2 aur2-2* double mutants, the highly elongated pericycle cells frequently undergo PD, instead of the normal AD (Van Damme, et al., 2011). It is thus conceivable that some or all of these molecular players will eventually be found as common downstream targets of the genetic pathways regulating vascular proliferation described above.

Future perspectives

In order to form functional vascular tissues, specifically oriented cell divisions have to occur in the correct cell at the right time; suggesting that this is a highly coordinated developmental process. Several genetic and hormonal pathways controlling vascular proliferation have been identified over the past years. However, these act during different stages of development and in different parts of the plant. Therefore, a major future challenge will be to determine if these pathways independently provide cues for vascular proliferation, or whether they interconnect to control common target genes.

Although it is currently entirely unknown what the identity of these downstream regulators might be, it is very likely that they will eventually control MT orientation and/or subsequent PPB positioning. Future work will have to show if such factors can be identified in vascular tissues or if for example cell polarity plays an important role; similar to stomatal development (Zhang, et al., 2015; Dong, et al., 2009). Finally, it remains possible that control of oriented cell divisions occurs through non-genetic determinants such as mechanical stress and light; or a combination of all these factors.

References

Ambrose, J.C., Shoji, T., Kotzer, A.M., Pighin, J.A., and Wasteneys, G.O. (2007). The Arabidopsis CLASP gene encodes a microtubule-associated protein involved in cell expansion and division. The Plant cell 19, 2763-75.

Azimzadeh, J., Nacry, P., Christodoulidou, A., Drevensek, S., Camilleri, C., Amiour, N., Parcy, F., Pastuglia, M., and Bouchez, D. (2008). Arabidopsis TONNEAU1 proteins are essential for preprophase band formation and interact with centrin. The Plant cell 20, 2146-59.

Baima, S., Forte, V., Possenti, M., Penalosa, A., Leoni, G., Salvi, S., Felici, B., Ruberti, I., and Morelli, G. (2014). Negative feedback regulation of auxin signaling by ATHB8/ACL5-BUD2 transcription module. Molecular plant 7, 1006-25.

Bennett, T., and Scheres, B. (2010). Root Development-Two Meristems for the Price of One? Curr Top Dev Biol 91, 67-102.

Bichet, A., Desnos, T., Turner, S., Grandjean, O., and Hofte, H. (2001). BOTERO1 is required for normal orientation of cortical microtubules and anisotropic cell expansion in Arabidopsis. The Plant journal : for cell and molecular biology 25, 137-48.

Bouquin, T., Mattsson, O., Naested, H., Foster, R., and Mundy, J. (2003). The Arabidopsis lue1 mutant defines a katanin p60 ortholog involved in hormonal control of microtubule orientation during cell growth. Journal of cell science 116, 791-801.

Burk, D.H., Liu, B., Zhong, R., Morrison, W.H., and Ye, Z.H. (2001). A katanin-like protein regulates normal cell wall biosynthesis and cell elongation. The Plant cell 13, 807-27.

Busse, J.S., and Evert, R.F. (1999). Vascular differentiation and transition in the seedling of Arabidopsis thaliana (Brassicaceae). Int J Plant Sci 160, 241-251.

Camilleri, C., Azimzadeh, J., Pastuglia, M., Bellini, C., Grandjean, O., and Bouchez, D. (2002). The Arabidopsis TONNEAU2 gene encodes a putative novel protein phosphatase 2A regulatory subunit essential for the control of the cortical cytoskeleton. The Plant cell 14, 833-45.

Carlsbecker, A., Lee, J.Y., Roberts, C.J., Dettmer, J., Lehesranta, S., Zhou, J., Lindgren, O., Moreno-Risueno, M.A., Vaten, A., Thitamadee, S., et al. (2010). Cell signalling by microRNA165/6 directs gene dose-dependent root cell fate. Nature 465, 316-21.

Chen, X., Grandont, L., Li, H., Hauschild, R., Paque, S., Abuzeineh, A., Rakusova, H., Benkova, E., Perrot-Rechenmann, C., and Friml, J. (2014). Inhibition of cell expansion by rapid ABP1-mediated auxin effect on microtubules. Nature 516, 90-3.

Clay, N.K., and Nelson, T. (2005). Arabidopsis thickvein mutation affects vein thickness and organ vascularization, and resides in a provascular cell-specific spermine synthase involved in vein definition and in polar auxin transport. Plant physiology 138, 767-77.

De Rybel, B., Adibi, M., Breda, A.S., Wendrich, J.R., Smit, M.E., Novák, O., Yamaguchi, N., Yoshida, S., Van Isterdael, G., Palovaara, J., et al. (2014a). Plant development. Integra-

tion of growth and patterning during vascular tissue formation in Arabidopsis. Science 345, 1255215.

De Rybel, B., Breda, A.S., and Weijers, D. (2014b). Prenatal plumbing--vascular tissue formation in the plant embryo. Physiologia plantarum 151, 126-33.

De Rybel, B., Mahönen, A.P., Helariutta, Y., and Weijers, D. (2016). Plant vascular development: from early specification to differentiation. Nature reviews. Molecular cell biology 17, 30-40.

De Rybel, B., Möller, B., Yoshida, S., Grabowicz, I., Barbier de Reuille, P., Boeren, S., Smith, R.S., Borst, J.W., and Weijers, D. (2013). A bHLH complex controls embryonic vascular tissue establishment and indeterminate growth in Arabidopsis. Developmental cell 24, 426-37.

De Smet, I., and Beeckman, T. (2011). Asymmetric cell division in land plants and algae: the driving force for differentiation. Nature reviews. Molecular cell biology 12, 177-88.

Dolan, L., Janmaat, K., Willemsen, V., Linstead, P., Poethig, S., Roberts, K., and Scheres, B. (1993). Cellular organisation of the Arabidopsis thaliana root. Development 119, 71-84.

Dong, J., MacAlister, C.A., and Bergmann, D.C. (2009). BASL controls asymmetric cell division in Arabidopsis. Cell 137, 1320-30.

Esau, K. (1965). Plant anatomy. Wiley.

Etchells, J.P., Provost, C.M., Mishra, L., and Turner, S.R. (2013). WOX4 and WOX14 act downstream of the PXY receptor kinase to regulate plant vascular proliferation independently of any role in vascular organisation. Development 140, 2224-34.

Etchells, J.P., Provost, C.M., and Turner, S.R. (2012). Plant vascular cell division is maintained by an interaction between PXY and ethylene signalling. PLoS genetics 8, e1002997.

Etchells, J.P., and Turner, S.R. (2010). The PXY-CLE41 receptor ligand pair defines a multifunctional pathway that controls the rate and orientation of vascular cell division. Development 137, 767-74.

Fabregas, N., Ibanes, M., and Cano-Delgado, A.I. (2010). A systems biology approach to dissect the contribution of brassinosteroid and auxin hormones to vascular patterning in the shoot of Arabidopsis thaliana. Plant signaling & behavior 5, 903-6.

Fisher, K., and Turner, S. (2007). PXY, a receptor-like kinase essential for maintaining polarity during plant vascular-tissue development. Current biology : CB 17, 1061-6.

Gursanscky, N.R., Jouannet, V., Grunwald, K., Sanchez, P., Laaber-Schwarz, M., and Greb, T. (2016). MOL1 is required for cambium homeostasis in Arabidopsis. Plant Journal 86, 210-220.

Hamann, T., Mayer, U., and Jürgens, G. (1999). The auxin-insensitive bodenlos mutation affects primary root formation and apical-basal patterning in the Arabidopsis embryo. Development 126, 1387-1395.

Hamant, O., Heisler, M.G., Jonsson, H., Krupinski, P., Uyttewaal, M., Bokov, P., Corson, F., Sahlin, P., Boudaoud, A., Meyerowitz, E.M., et al. (2008). Developmental Patterning by Mechanical Signals in Arabidopsis. Science 322, 1650-1655.

Hanzawa, Y., Takahashi, T., and Komeda, Y. (1997). ACL5: an Arabidopsis gene required for internodal elongation after flowering. The Plant journal : for cell and molecular biology 12, 863-74.

Hanzawa, Y., Takahashi, T., Michael, A.J., Burtin, D., Long, D., Pineiro, M., Coupland, G., and Komeda, Y. (2000). ACAULIS5, an Arabidopsis gene required for stem elongation, encodes a spermine synthase. The EMBO journal 19, 4248-56.

Hardham, A.R., and Mccully, M.E. (1982). Reprogramming of Cells Following Wounding in Pea (Pisum-Sativum-L) Roots .1. Cell-Division and Differentiation of New Vascular Elements. Protoplasma 112, 143-151.

Hirakawa, Y., Kondo, Y., and Fukuda, H. (2010). TDIF peptide signaling regulates vascular stem cell proliferation via the WOX4 homeobox gene in Arabidopsis. The Plant cell 22, 2618-29.

Hirakawa, Y., Shinohara, H., Kondo, Y., Inoue, A., Nakanomyo, I., Ogawa, M., Sawa, S., Ohashi-Ito, K., Matsubayashi, Y., and Fukuda, H. (2008). Non-cell-autonomous control of vascular stem cell fate by a CLE peptide/receptor system. Proceedings of the National Academy of Sciences of the United States of America 105, 15208-13.

Hush, J.M., Hawes, C.R., and Overall, R.L. (1990). Interphase Microtubule Reorientation Predicts a New Cell Polarity in Wounded Pea Roots. Journal of cell science 96, 47-61.

Ibanes, M., Fabregas, N., Chory, J., and Cano-Delgado, A.I. (2009). Brassinosteroid signaling and auxin transport are required to establish the periodic pattern of Arabidopsis shoot vascular bundles. Proceedings of the National Academy of Sciences of the United States of America 106, 13630-5.

Ilegems, M., Douet, V., Meylan-Bettex, M., Uyttewaal, M., Brand, L., Bowman, J.L., and Stieger, P.A. (2010). Interplay of auxin, KANADI and Class III HD-ZIP transcription factors in vascular tissue formation. Development 137, 975-84.

Imai, A., Hanzawa, Y., Komura, M., Yamamoto, K.T., Komeda, Y., and Takahashi, T. (2006). The dwarf phenotype of the Arabidopsis acl5 mutant is suppressed by a mutation in an upstream ORF of a bHLH gene. Development 133, 3575-85.

Imai, A., Komura, M., Kawano, E., Kuwashiro, Y., and Takahashi, T. (2008). A semi-dominant mutation in the ribosomal protein L10 gene suppresses the dwarf phenotype of the acl5 mutant in Arabidopsis thaliana. The Plant journal : for cell and molecular biology 56, 881-90.

Ishida, K., Yamashino, T., Yokoyama, A., and Mizuno, T. (2008). Three type-B response regulators, ARR1, ARR10 and ARR12, play essential but redundant roles in cytokinin signal transduction throughout the life cycle of Arabidopsis thaliana. Plant & cell physiology 49, 47-57.

Jouannet, V., Brackmann, K., and Greb, T. (2015). (Pro)cambium formation and proliferation: two sides of the same coin? Current opinion in plant biology 23, 54-60.

Jürgens, G.M., U. (1994). Arabidopsis. In Embryos: Colour Atlas of Development - Bard,Jbl. Nature 370, 190-190.

Kang, Y.H., Breda, A., and Hardtke, C.S. (2017). Brassinosteroid signaling directs formative cell divisions and protophloem differentiation in Arabidopsis root meristems. Development 144, 272-280.

Kidner, C., Sundaresan, V., Roberts, K., and Dolan, L. (2000). Clonal analysis of the Arabidopsis root confirms that position, not lineage, determines cell fate. Planta 211, 191-9.

Kirik, A., Ehrhardt, D.W., and Kirik, V. (2012). TONNEAU2/FASS Regulates the Geometry of Microtubule Nucleation and Cortical Array Organization in Interphase Arabidopsis Cells. The Plant cell 24, 1158-1170.

Kuroha, T., Tokunaga, H., Kojima, M., Ueda, N., Ishida, T., Nagawa, S., Fukuda, H., Sugimoto, K., and Sakakibara, H. (2009). Functional analyses of LONELY GUY cytokinin-activating enzymes reveal the importance of the direct activation pathway in Arabidopsis. The Plant cell 21, 3152-69.

Lau, O.S., and Bergmann, D.C. (2012). Stomatal development: a plant's perspective on cell polarity, cell fate transitions and intercellular communication. Development 139, 3683-92.

Lavenus, J., Goh, T., Roberts, I., Guyomarc'h, S., Lucas, M., De Smet, I., Fukaki, H., Beeckman, T., Bennett, M., and Laplaze, L. (2013). Lateral root development in Arabidopsis: fifty shades of auxin. Trends in plant science 18, 450-8.

Lindeboom, J.J., Nakamura, M., Hibbel, A., Shundyak, K., Gutierrez, R., Ketelaar, T., Emons, A.M., Mulder, B.M., Kirik, V., and Ehrhardt, D.W. (2013). A mechanism for reorientation of cortical microtubule arrays driven by microtubule severing. Science 342, 1245533.

Lintilhac, P.M., and Vesecky, T.B. (1981). Mechanical-Stress and Cell-Wall Orientation in Plants .2. The Application of Controlled Directional Stress to Growing Plants - with a Discussion on the Nature of the Wound Reaction. Am J Bot 68, 1222-1230.

Long, Y., Smet, W., Cruz-Ramírez, A., Castelijns, B., de Jonge, W., Mahönen, A.P., Bouchet, B.P., Perez, G.S., Akhmanova, A., Scheres, B., et al. (2015). Arabidopsis BIRD Zinc Finger Proteins Jointly Stabilize Tissue Boundaries by Confining the Cell Fate Regulator SHORT-ROOT and Contributing to Fate Specification. The Plant cell.

Lucas, W.J., Ding, B., and Vanderschoot, C. (1993). Tansley Review No. 58 Plasmodesmata and the Supracellular Nature of Plants. New Phytologist 125, 435-476.

Lucas, W.J., Groover, A., Lichtenberger, R., Furuta, K., Yadav, S.R., Helariutta, Y., He, X.Q., Fukuda, H., Kang, J., Brady, S.M., et al. (2013). The Plant Vascular System: Evolution, Development and Functions. J Integr Plant Biol 55, 294-388.

Mahönen, A.P., Bonke, M., Kauppinen, L., Riikonen, M., Benfey, P.N., and Helariutta, Y.

(2000). A novel two-component hybrid molecule regulates vascular morphogenesis of the Arabidopsis root. Genes & development 14, 2938-43.

Mansfield, S.G., and Briarty, L.G. (1991). Early Embryogenesis in Arabidopsis-Thaliana .2. The Developing Embryo. Can J Bot 69, 461-476.

Matsumoto-Kitano, M., Kusumoto, T., Tarkowski, P., Kinoshita-Tsujimura, K., Vaclavikova, K., Miyawaki, K., and Kakimoto, T. (2008). Cytokinins are central regulators of cambial activity. Proceedings of the National Academy of Sciences of the United States of America 105, 20027-20031.

Mauseth, J. (1988). Plant anatomy. Benjamin/Cummings Publ.CO.

McClinton, R.S., and Sung, Z.R. (1997). Organization of cortical microtubules at the plasma membrane in Arabidopsis. Planta 201, 252-60.

Milhinhos, A., Prestele, J., Bollhoner, B., Matos, A., Vera-Sirera, F., Rambla, J.L., Ljung, K., Carbonell, J., Blazquez, M.A., Tuominen, H., et al. (2013). Thermospermine levels are controlled by an auxin-dependent feedback loop mechanism in Populus xylem. Plant Journal 75, 685-698.

Mineyuki, Y. (1999). The preprophase band of microtubules: Its function as a cytokinetic apparatus in higher plants. Int Rev Cytol 187, 1-49.

Miyashima, S., Koi, S., Hashimoto, T., and Nakajima, K. (2011). Non-cell-autonomous micro-RNA165 acts in a dose-dependent manner to regulate multiple differentiation status in the Arabidopsis root. Development 138, 2303-13.

Muller, S., Han, S., and Smith, L.G. (2006). Two kinesins are involved in the spatial control of cytokinesis in Arabidopsis thaliana. Current biology : CB 16, 888-94.

Nieminen, K., Blomster, T., Helariutta, Y., and Mahonen, A.P. (2015). Vascular Cambium Development. The Arabidopsis book / American Society of Plant Biologists 13, e0177.

Oda, Y., and Fukuda, H. (2012). Secondary cell wall patterning during xylem differentiation. Current opinion in plant biology 15, 38-44.

Ohashi-Ito, K., and Bergmann, D.C. (2007). Regulation of the Arabidopsis root vascular initial population by LONESOME HIGHWAY. Development 134, 2959-68.

Ohashi-Ito, K., Matsukawa, M., and Fukuda, H. (2013a). An atypical bHLH transcription factor regulates early xylem development downstream of auxin. Plant & cell physiology 54, 398-405.

Ohashi-Ito, K., Oguchi, M., Kojima, M., Sakakibara, H., and Fukuda, H. (2013b). Auxin-associated initiation of vascular cell differentiation by LONESOME HIGHWAY. Development 140, 765-9.

Ohashi-Ito, K., Saegusa, M., Iwamoto, K., Oda, Y., Katayama, H., Kojima, M., Sakakibara, H., and Fukuda, H. (2014). A bHLH complex activates vascular cell division via cytokinin ac-

tion in root apical meristem. Current biology : CB 24, 2053-8.

Peret, B., Larrieu, A., and Bennett, M.J. (2009). Lateral root emergence: a difficult birth. Journal of experimental botany 60, 3637-43.

Pesquet, E., Zhang, B., Gorzsas, A., Puhakainen, T., Serk, H., Escamez, S., Barbier, O., Gerber, L., Courtois-Moreau, C., Alatalo, E., et al. (2013). Non-Cell-Autonomous Postmortem Lignification of Tracheary Elements in Zinnia elegans. The Plant cell 25, 1314-1328.

Pietra, S., Gustavsson, A., Kiefer, C., Kalmbach, L., Horstedt, P., Ikeda, Y., Stepanova, A.N., Alonso, J.M., and Grebe, M. (2013). Arabidopsis SABRE and CLASP interact to stabilize cell division plane orientation and planar polarity. Nature communications 4, 2779.

Rodriguez-Villalon, A., Gujas, B., Kang, Y.H., Breda, A.S., Cattaneo, P., Depuydt, S., and Hardtke, C.S. (2014). Molecular genetic framework for protophloem formation. Proceedings of the National Academy of Sciences of the United States of America 111, 11551-6.

Scarpella, E., and Meijer, A.H. (2004). Pattern formation in the vascular system of monocot and dicot plant species. New Phytologist 164, 209-242.

Scheres, B., Dilaurenzio, L., Willemsen, V., Hauser, M.T., Janmaat, K., Weisbeek, P., and Benfey, P.N. (1995). Mutations Affecting the Radial Organization of the Arabidopsis Root Display Specific Defects Throughout the Embryonic Axis. Development 121, 53-62.

Scheres, B., Wolkenfelt, H., Willemsen, V., Terlouw, M., Lawson, E., Dean, C., and Weisbeek, P. (1994). Embryonic Origin of the Arabidopsis Primary Root and Root-Meristem Initials. Development 120, 2475-2487.

Schlereth, A., Möller, B., Liu, W., Kientz, M., Flipse, J., Rademacher, E.H., Schmid, M., Jürgens, G., and Weijers, D. (2010). MONOPTEROS controls embryonic root initiation by regulating a mobile transcription factor. Nature 464, 913-6.

Smith, L.G., Hake, S., and Sylvester, A.W. (1996). The tangled-1 mutation alters cell division orientations throughout maize leaf development without altering leaf shape. Development 122, 481-489.

Smith, R.A., Schuetz, M., Roach, M., Mansfield, S.D., Ellis, B., and Samuels, L. (2013). Neighboring Parenchyma Cells Contribute to Arabidopsis Xylem Lignification, while Lignification of Interfascicular Fibers Is Cell Autonomous. The Plant cell 25, 3988-3999.

Suer, S., Agusti, J., Sanchez, P., Schwarz, M., and Greb, T. (2011). WOX4 imparts auxin responsiveness to cambium cells in Arabidopsis. The Plant cell 23, 3247-59.

Tokunaga, H., Kojima, M., Kuroha, T., Ishida, T., Sugimoto, K., Kiba, T., and Sakakibara, H. (2012). Arabidopsis lonely guy (LOG) multiple mutants reveal a central role of the LOG-dependent pathway in cytokinin activation. The Plant journal : for cell and molecular biology 69, 355-65.

Traas, J., Bellini, C., Nacry, P., Kronenberger, J., Bouchez, D., and Caboche, M. (1995). Normal Differentiation Patterns in Plants Lacking Microtubular Preprophase Bands. Nature

375, 676-677.

Ueda, M., and Laux, T. (2012). The origin of the plant body axis. Current opinion in plant biology 15, 578-84.

Van Damme, D., De Rybel, B., Gudesblat, G., Demidov, D., Grunewald, W., De Smet, I., Houben, A., Beeckman, T., and Russinova, E. (2011). Arabidopsis alpha Aurora kinases function in formative cell division plane orientation. The Plant cell 23, 4013-24.

van Dop, M., Liao, C.Y., and Weijers, D. (2015). Control of oriented cell division in the Arabidopsis embryo. Current opinion in plant biology 23, 25-30.

vandenBerg, C., Willemsen, V., Hendriks, G., Weisbeek, P., and Scheres, B. (1997). Short-range control of cell differentiation in the Arabidopsis root meristem. Nature 390, 287-289.

Vera-Sirera, F.D.R., B.; Úrbez, C.; Kouklas, E.; Pesquera, M.; Álvarez-Mahecha, J. C.; Minguet, E. G.; Tuominen, H.; Carbonell, J.; Borst, J. W.; Weijers, D.; Blázquez, M. A. (2015). A bHLH-based feedback loop restricts vascular cell proliferation in plants. Developmental cell (accepted).

Vineyard, L., Elliott, A., Dhingra, S., Lucas, J.R., and Shaw, S.L. (2013). Progressive transverse microtubule array organization in hormone-induced Arabidopsis hypocotyl cells. The Plant cell 25, 662-76.

Walker, K.L., Muller, S., Moss, D., Ehrhardt, D.W., and Smith, L.G. (2007). Arabidopsis TANGLED identifies the division plane throughout mitosis and cytokinesis. Current biology : CB 17, 1827-36.

Wendrich, J.R., Möller, B.K., Li, S., Saiga, S., Sozzani, R., Benfey, P.N., De Rybel, B., and Weijers, D. (2017). Framework for gradual progression of cell ontogeny in the Arabidopsis root meristem. Proceedings of the National Academy of Sciences of the United States of America 114, E8922-E8929.

Whittington, A.T., Vugrek, O., Wei, K.J., Hasenbein, N.G., Sugimoto, K., Rashbrooke, M.C., and Wasteneys, G.O. (2001). MOR1 is essential for organizing cortical microtubules in plants. Nature 411, 610-3.

Wu, S.Z., and Bezanilla, M. (2014). Myosin VIII associates with microtubule ends and together with actin plays a role in guiding plant cell division. eLife 3.

Xu, B., Ohtani, M., Yamaguchi, M., Toyooka, K., Wakazaki, M., Sato, M., Kubo, M., Nakano, Y., Sano, R., Hiwatashi, Y., et al. (2014). Contribution of NAC Transcription Factors to Plant Adaptation to Land. Science 343, 1505-1508.

Xu, X.F.M., Zhao, Q., Rodrigo-Peiris, T., Brkljacic, J., He, C.S., Muller, S., and Meier, I. (2008). RanGAP1 is a continuous marker of the Arabidopsis cell division plane. Proceedings of the National Academy of Sciences of the United States of America 105, 18637-18642.

Yokoyama, A., Yamashino, T., Amano, Y., Tajima, Y., Imamura, A., Sakakibara, H., and Mizuno, T. (2007). Type-B ARR transcription factors, ARR10 and ARR12, are implicated in

cytokinin-mediated regulation of protoxylem differentiation in roots of Arabidopsis thaliana. Plant & cell physiology 48, 84-96.

Yoshida, S., Barbier de Reuille, P., Lane, B., Bassel, G.W., Prusinkiewicz, P., Smith, R.S., and Weijers, D. (2014). Genetic control of plant development by overriding a geometric division rule. Developmental cell 29, 75-87.

Zhang, Y., Wang, P., Shao, W., Zhu, J.K., and Dong, J. (2015). The BASL polarity protein controls a MAPK signaling feedback loop in asymmetric cell division. Developmental cell 33, 136-49.

Chapter 3

Generation of a high-resolution transcriptomics dataset to identify TMO5/LHW target genes

Wouter Smet[1,2,3], Jo Gysens[2,3], Jenny Jansen[4], Mark Boekschoten[4], Dolf Weijers[1] and Bert De Rybel[1,2,3]

1. Wageningen University, Laboratory of Biochemistry, Stippeneng 4, 6708 WE Wageningen, the Netherlands
2. Ghent University, Department of Plant Biotechnology and Bioinformatics, Technologiepark 927, 9052 Ghent, Belgium
3. VIB Center for Plant Systems Biology, Technologiepark 927, 9052 Ghent, Belgium
4. Wageningen University, Laboratory of Human Nutrition, Stippeneng 4, 6708 WE Wageningen, the Netherlands

Abstract

Because plant cells are unable to move during development, plants rely on highly-coordinated oriented cell divisions to correctly develop a three-dimensional (3D) structure. Among these oriented divisions, anticlinal divisions (AD) generate more cells within a cell file and drive longitudinal growth; while, periclinal and radial divisions (abbreviated throughout the rest of the thesis to PRD) generate additional cell files and thus result in radial growth. The basic Helix Loop Helix (bHLH) transcription factor heterodimer formed by TARGET OF MONOPTEROS5 (TMO5) and LONESOME HIGHWAY (LHW) has been shown to be required and sufficient for PRD in a dose dependent manner. Thus far, these are the only factors known to be able to control PRD during primary growth in the vascular tissues. As it is unclear exactly how TMO5/LHW transcription factor activity is translated into the induction of PRD at a molecular level, we aim to identify novel downstream targets by generating a high-resolution temporal transcriptomics dataset. Here, we first created a double dexamethasone inducible line for both the TMO5 and LHW transcription factors and next show that this line is capable of rapid and synchronous induction of PRD; thus, providing the perfect starting material for our transcriptomics approach. Validation of the obtained dataset confirmed induction of known TMO5/LHW targets and furthermore revealed for the first time a consecutive activation of cytokinin biosynthesis and cytokinin response genes. In conclusion, our approach yielded a high-resolution temporal dataset containing both direct TMO5/LHW targets and more downstream genes putatively involved in executing TMO5/LHW activity towards PRD.

Introduction

Unlike their animal counterparts, plant cells are immobilized within a network of rigid cell walls. Therefore, plants need to rely on the processes of highly oriented cell division and directional cell elongation for their growth and development into a 3D structure. Oriented cell division can either occur perpendicular (anticlinal) or parallel (periclinal or radial) to the surface of the plant (Refer to the **Chapter 1** for a more detailed explanation about these division types). Here, we define anticlinal cell divisions (AD) to add more cells to an existing cell file in the root resulting in longitudinal growth; whereas both radial and periclinal cell divisions increase the number of cell files, thus contributing to radial growth. Asymmetric periclinal divisions are sometimes also referred to as 'formative' divisions (Gunning, et al., 1978). Although important throughout growth and development, PRD play a particularly important role in the development of vascular tissues. In the root, this tissue type originates from only 4 provascular cells in the early globular embryo and increases to approximately 30 cell files in the mature root tip (De Rybel, et al., 2014; Yoshida, et al., 2014; Scheres, et al., 1995; Scheres, et al., 1994). At the onset of secondary growth, about 10 days after germination, over 100 cell files are already present, and this number continues to rapidly increase during later stages of development (Nieminen, et al., 2015).

One of the major modules controlling vascular PRD in the early embryo and in the post-embryonic root is the TMO5/LHW pathway (De Rybel, et al., 2013; Ohashi-Ito, et al., 2013a; Ohashi-Ito, et al., 2013b). In this module (described in detail in Chapter 2), the auxin dependent *TARGET OF MONOPTEROS5 (TMO5)* gene encoding for a bHLH transcription factor is first expressed in the four provascular initial cells during early globular stage (Schlereth, et al., 2010). TMO5 and its three TMO5-LIKE homologs form heterodimer complexes with members from another bHLH transcription factor subfamily called LONESOME HIGHWAY (LHW) and its respective LHW-LIKE1, LHW-LIKE2 and LHW-LIKE3 homologs (Ohashi-Ito, et al., 2014; De Rybel, et al., 2013; Ohashi-Ito, et al., 2013a). Both factors overlap in expression from the early globular stage embryo onwards in the provascular cells and are restricted to the young xylem cells in the post embryonic root (De Rybel, et al., 2013; Ohashi-Ito, et al., 2013a; Ohashi-Ito, et al., 2013b). Loss-of-function of *tmo5* or *lhw* clade members results in a reduction in vascular cell file number. On the other hand, ectopic expression of both bHLH transcription factors results in additional periclinal and radial cell divisions in all tissue types of the root meristem (De Rybel, et al., 2014; Ohashi-Ito, et al., 2014; Ohashi-Ito, et al., 2013a). TMO5 and LHW form a heterodimer complex which

activates the expression of the *LONELY GUY4 (LOG4)* gene and its closest homolog *LOG3* (De Rybel, et al., 2014; Ohashi-Ito, et al., 2014). These genes are involved in the final and rate-limiting step of cytokinin biosynthesis (Kuroha, et al., 2009; Kurakawa, et al., 2007), linking this auxin induced pathway to cytokinin biosynthesis.

Cytokinin is required for PRD, as mutants in the biosynthetic pathway (e.g. *ipt* or *log* higher order mutants (Tokunaga, et al., 2012; Kuroha, et al., 2009)), mutants in the perception by the cytokinin receptors (e.g. the *wooden leg (wol)* mutant (Mahönen, et al., 2000)) and mutants in downstream signaling events (e.g. the *arr1,10,12* triple mutant (Ishida, et al., 2008; Yokoyama, et al., 2007)) all show strongly reduced PRD in the vascular bundle. However, treatment of *ipt, log* or *lhw* mutants with cytokinin results in rescuing the cell file number back to wild type levels (De Rybel, et al., 2014; Matsumoto-Kitano, et al., 2008); indicating the importance of cytokinin biosynthesis, perception and signaling for TMO5/LHW dependent PRD induction. Nevertheless, exogenous applications of cytokinin never lead to the massive proliferation seen in e.g. TMO5/LHW misexpression. This suggests that other, so far unknown, downstream targets are important for the TMO5/LHW dependent PRD effect. Furthermore, it is unclear what part of the cytokinin response pathway is required for the TMO5/LHW effect and what other factors might be induced further downstream. Therefore, in this chapter, we aim to identify novel downstream targets of the TMO5/LHW heterodimer complex by generating a high-resolution temporal transcriptomics dataset.

Results

Generating an inducible line to study cell division orientation

In order to provide a detailed understanding of the downstream transcriptional responses upon activation of the TMO5/LHW heterodimer complex, we need to be able to induce both subunits of the complex at the same time. The existing transgenic lines are not adequate as, for example, the double misexpression line (p*RPS5A*::*TMO5* x p*RPS5A*::*LHW*) described previously (De Rybel, et al., 2013) is constitutive and thus does not allow temporal control necessary for establishing early and late events using transcriptional analysis. Moreover, these seedlings show a very high variability in the number of vascular cell files (De Rybel, et al., 2014), which does not make this line the ideal starting material. Besides this, a TMO5 inducible line (p*RPS5A*::*TMO5*:GR) has been used to identify downstream targets (De Rybel, et al., 2013). However, because the TMO5 and LHW transcription factors act in a

heterodimer complex, this single TMO5 inducible line might not capture the full range of downstream effects of the two transcription factors combined. This is further supported by the rather limited effect on PRD by only inducing TMO5 (De Rybel, et al., 2013). Finally, an inducible cell-culture system of LHW and T5L1 has been used to identify direct targets of these transcription factors (Ohashi-Ito, et al., 2014). However, this system lacks the context in which these transcription factors are normally expressed and thus might give a limited or different downstream transcriptional response.

Because of these restrictions in the available transgenic lines, we chose to generate a double dexamethasone (DEX) inducible line of both TMO5 and LHW by first generating a p*RPS5A*::*LHW*:GR line and then crossing this to the available p*RPS5A*::*TMO5*:GR, resulting in a p*RPS5A*::*TMO5*:GR x p*RPS5A*::*LHW*:GR line (also called double GR or dGR line). In this line, both the TMO5 and LHW transcription factors are fused to the mammalian glucocorticoid receptor (GR) and are expressed in meristematic tissues by the strong ribosomal *RPS5A* promotor (Weijers, et al., 2005). Upon treatment with DEX, the TMO5:GR and LHW:GR fusion proteins undergo a conformational change in the GR tag that will shuttle them from the cytoplasm to the nucleus (Schena, et al., 1991); where they can activate downstream gene expression.

Simultaneous induction of TMO5 and LHW results in a fast and reproducible induction of PRD

First, we wanted to compare the strength and consistency of the induced PRD to the existing transgenic lines (De Rybel, et al., 2014; De Rybel, et al., 2013). We hypothesized that higher levels of the TMO5/LHW dimer should result in PRD that would lead to a decrease in root length and an increase in root width by boosting the number of cell files. To confirm this, constitutive p*RPS5A*::*TMO5* x p*RPS5A*::*LHW*, inducible p*RPS5A*::*TMO5*:GR, inducible p*RPS5A*::*LHW*:GR and the newly developed dGR seeds were grown on media supplemented with 10 µM DEX for 6 days and compared to the wild type control (Columbia-0 ecotype or Col-0). Representative plants of these lines are shown in **Figure 1A**. The constitutive p*RPS5A*::*TMO5* x p*RPS5A*::*LHW* line showed the variability as described in De Rybel, et al., 2013, ranging from moderately to extremely affected plants (**Figure 1A**).
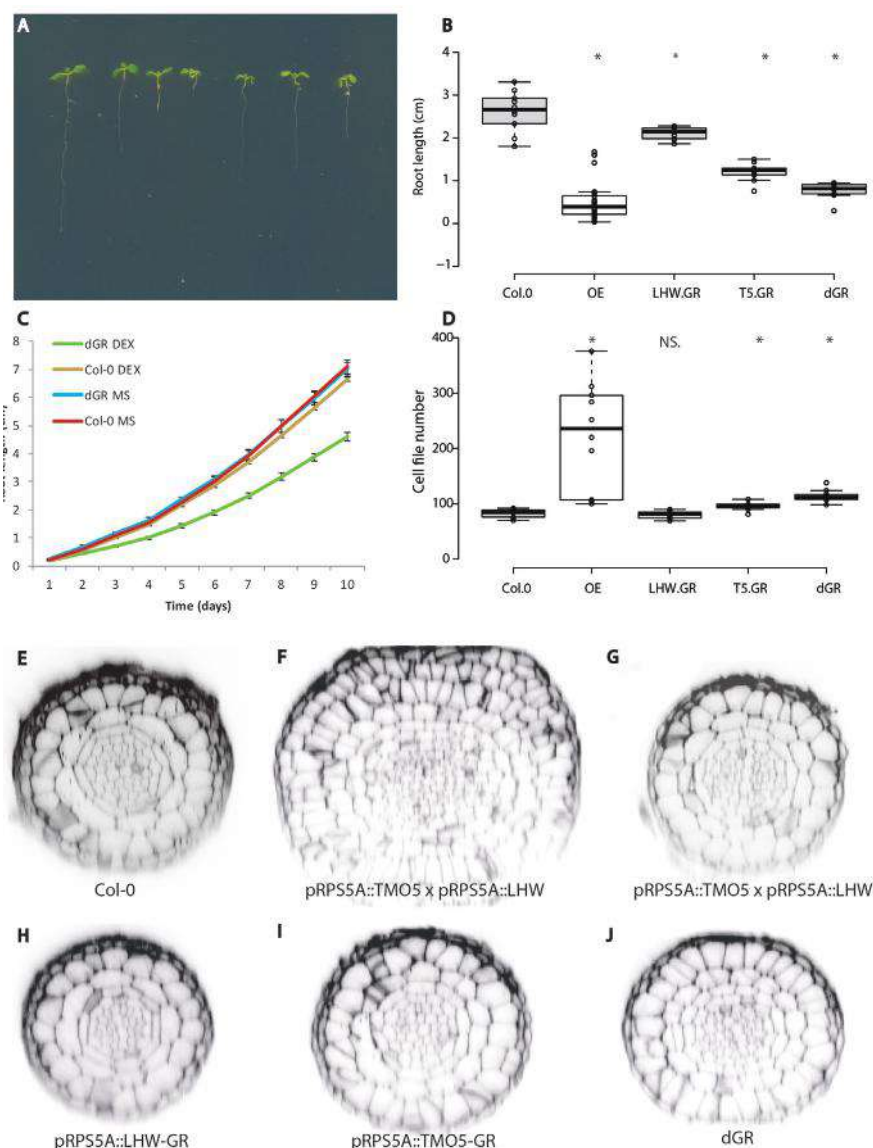
Figure 1: Phenotypical characterization of the newly developed dGR line in comparison to existing TMO-LHW overexpression lines. A. From left to right Col-0, p*RPS5A*::*TMO5* x p*RPS5A*::*LHW* (3 plants), p*RPS5A*::*LHW:*GR, p*RPS5A*::*TMO5*:GR, and dGR seeds grown on ½ MS plates supplemented with 10μM DEX for 6 DAG. **B.** Root length quantification of previous mentioned lines (n = respectively 10, 30, 10, 10 and 10). **C.** Root length quantification during 10 days of growth of dGR (Green/Blue) and Col-0 (Red/Yellow) on ½ MS and on ½ MS plates supplemented with 10μM DEX. **D.** Radial cell number quantification from confocal cross-sections of previous mentioned lines (n=10). Asterisks indicate a significant difference between sample and Col-0, as determined by a two-tailed t-test with *p*-value < 0.01. Quantified *p*-values for root length quantification can be found in **Supplemental Table 1**. **E-J** Radial confocal cross-sections of Col-0 (**E**), p*RPS5A*::*TMO5* x p*RPS5A*::*LHW* (variability in cell file number, strong (**F**) and weak (**G**)), p*RPS5A*::*LHW*:GR (**H**), p*RPS5A*::*TMO5*:GR (**I**), and dGR (**J**) seeds grown on ½ MS plates supplemented with 10μM DEX for 6 DAG.

47

Quantification of the root length and cell file number confirmed this initial observation with cell file numbers ranging from 100-300, while WT showed almost no variation and a value below 100 (**Figure 1B,D**). Representative pictures of radial sections used for cell file number quantification are shown in **Figures 1E-G**. All confocal sections were taken through the middle of the root meristem (see **Materials and Methods** section for details). The single inducible p*RPS5A*::*TMO5*:GR and p*RPS5A*::*LHW*:GR lines had a modest or no significant effect on root length and cell file number but showed high consistency (**Figure 1B,D**). In contrast, the dGR line showed a stronger and consistent increase in cell file number (**Figure 1B,D and H-J**). These results fit with the published effect of inducing TMO5 and LHW and with the hypothesis that inducing both TMO5 and LHW instead of constitutively overexpressing them results in a strong and consistent induction of PRD.

Next, we quantified the effect on root growth of the dGR line in comparison to Col-0 with and without 10µM DEX treatment during 10 days (**Figure 1C**). The dGR line showed no difference in root length compared to the Col-0 control when grown on control media, indicating that the GR constructs are not leaky. Upon DEX treatment, the dGR line showed a reduction in root growth, while the Col-0 control line grown on DEX showed no significant changes compared to growth on MS. These results indicate that DEX treatment itself has no effect on root growth.

To understand the temporal aspects of TMO5/LHW dependent induction of PRD, 5-day-old dGR roots were germinated and grown on DEX-free plates and then transferred to plates supplemented with 10µM DEX for 0h, 2h, 4h, 6h, 12h and 24h. As a control, a transfer from control media to control media was taken along in the analysis using the same time points (**Figures 2-4**).

We first used radial sections to quantify the increase in cell file number (**Figure 4A**). Representative pictures used for this quantification are shown in **Figure 2**. An increase in total cell number in dGR line was observed from 12h of DEX treatment onwards when comparing dGR on DEX with mock treatments (compare **Figure 3B-C to E-F; Figure 4A**). These additional divisions were never observed in the control treatment or in Col-0 plants. The increase in total cell number in the dGR was in line with the described phenotypes of both p*RPS5A*::*TMO5* and p*RPS5A*::*TMO5* x pRPS5A::*LHW* (De Rybel, et al., 2013). Quantification of individual cell-types showed that all cell-types had more PRD compared to the control except for xylem cells (**Supplemental Figure 1**), which are known not to divide or only divide very rarely (Mahönen, et al.,

2000). Our images did not allow distinguishing phloem cells from cambium cells and thus phloem and cambium cells were quantified together. These results indicate that the response in the dGR line is very homogeneous throughout the root meristem and that all cell types (except for the xylem) are susceptible to dGR induction.

When looking in more detail at single events of PRD in the radial cross-sections we could occasionally observe PRD already after 4h of DEX treatment. Therefore, we next looked at longitudinal cross-sections in order to study the first occurrence of TMO5/LHW induced PRD in more detail (**Figure 4B-E**). Longitudinal sections allowed for a faster screening of the whole meristem to look for PRD and confirmed that the first PRD occurrences could be observed as early as 4h after treatment. Moreover, we could see that PRD usually occur in clusters spread across the root meristem. This also explains why we only observe a significant increase in cell file number after 12h of treatment. The radial sections only capture a small amount of these clusters, which does not yield a significantly higher total cell number.

In conclusion, the dGR line outperforms all existing TMO5/LHW misexpression lines by providing strong and reliable induction of PRD. dGR provides a big advantage to the constitutive overexpression line as it enables us to study the PRDs and transcriptional changes upon induction by TMO5/ LHW in a temporal manner. Furthermore, we have established the minimum timeframe in which dGR induces the first PRD in the root meristem.

Whole genome transcriptomics and statistical analysis

Having established a time frame in which the dGR line is capable of reliably triggering ectopic PRD throughout the root meristem, we decided to perform the transcriptomics experiment. We sampled 5-day old seedlings of the dGR line that were transferred from ½ MS plates to 10µM DEX at the following time points: 0h, 0.5h, 1h, 2h, 3h, 4h, 5h and 6h. We collected 300 individual root tips per sample and three biological repeats per time point were sampled. Root tips were used instead of entire roots to enrich for meristematic *RPS5A* expressed tissue. After statistical analysis of the *Arabidopsis* Gene 1.0 ST micro-array data (see **Materials and Methods** section for details), we retained a list of 272 differentially up-regulated genes with a fold change of two or more (FC >2) at any of the time points (**Table 1**). Although we cannot exclude the involvement of down-regulated genes, we chose to focus on these up-regulated genes because in the experiments performed so far, TMO5 and LHW act as transcriptional activators.
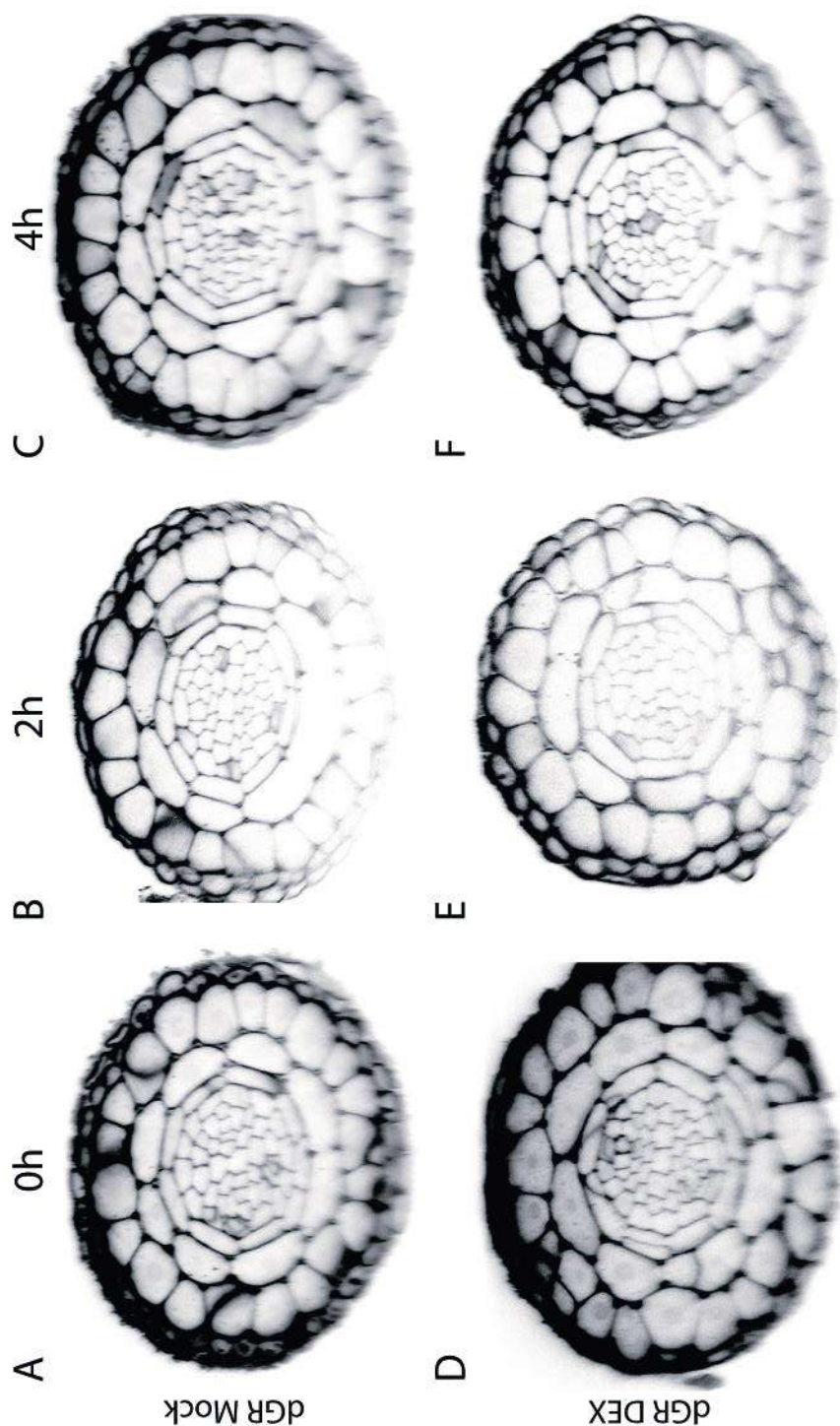
Figure 2: Temporal aspects of TMO5/LHW dependent induction of PRD on 5-day old dGR roots. A,B,C, showing radial cross-sections of roots transferred from ½ MS to ½ MS. **D,E,F** showing radial cross-sections of roots transferred from ½ MS to ½ MS containing 10μM DEX.
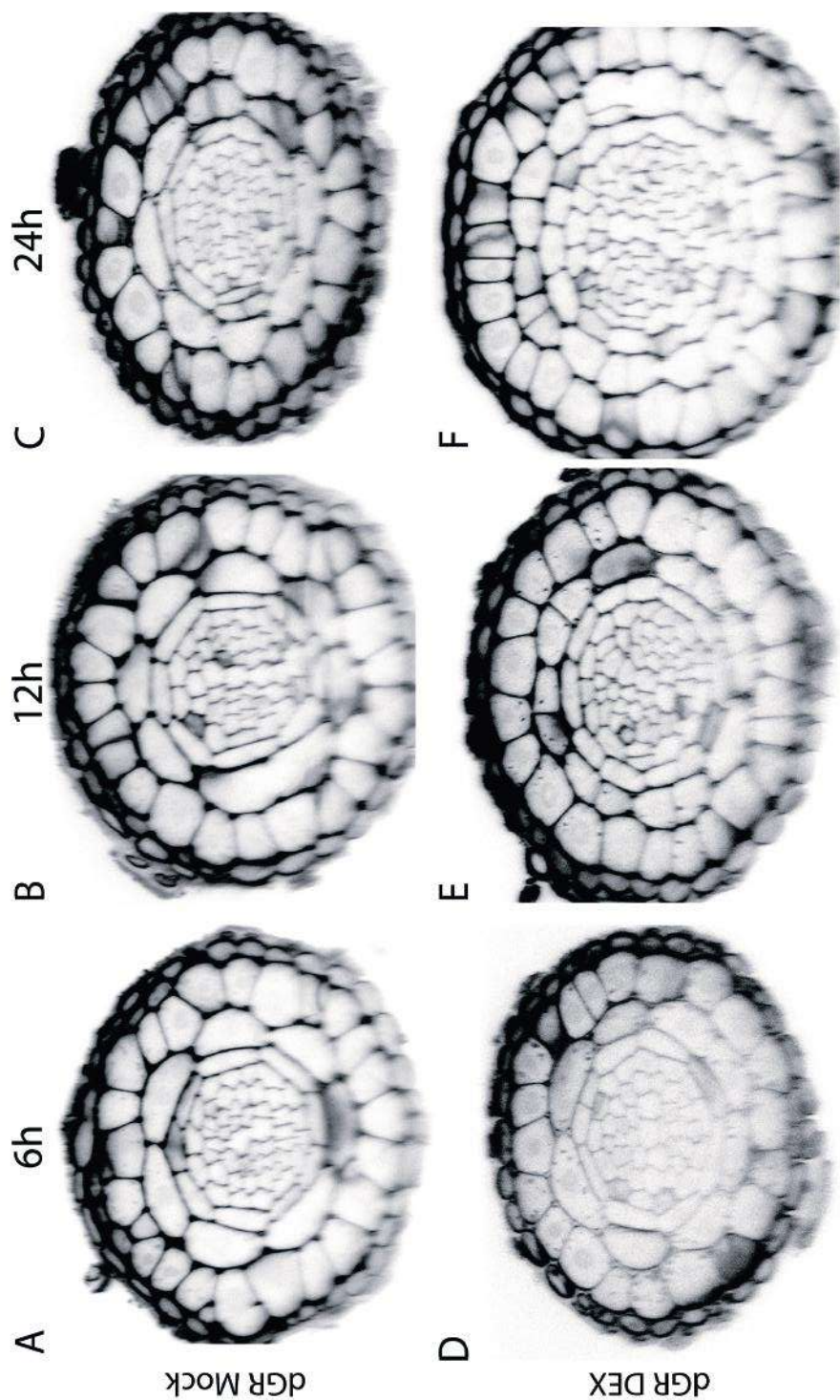
Figure 3: Temporal aspects of TMO5/LHW dependent induction of PRD on 5-day old dGR roots. A,B,C showing radial cross-sections of roots transferred from ½ MS to ½ MS. **D,E,F** showing radial cross-sections of roots transferred from ½ MS to ½ MS containing 10μM DEX.
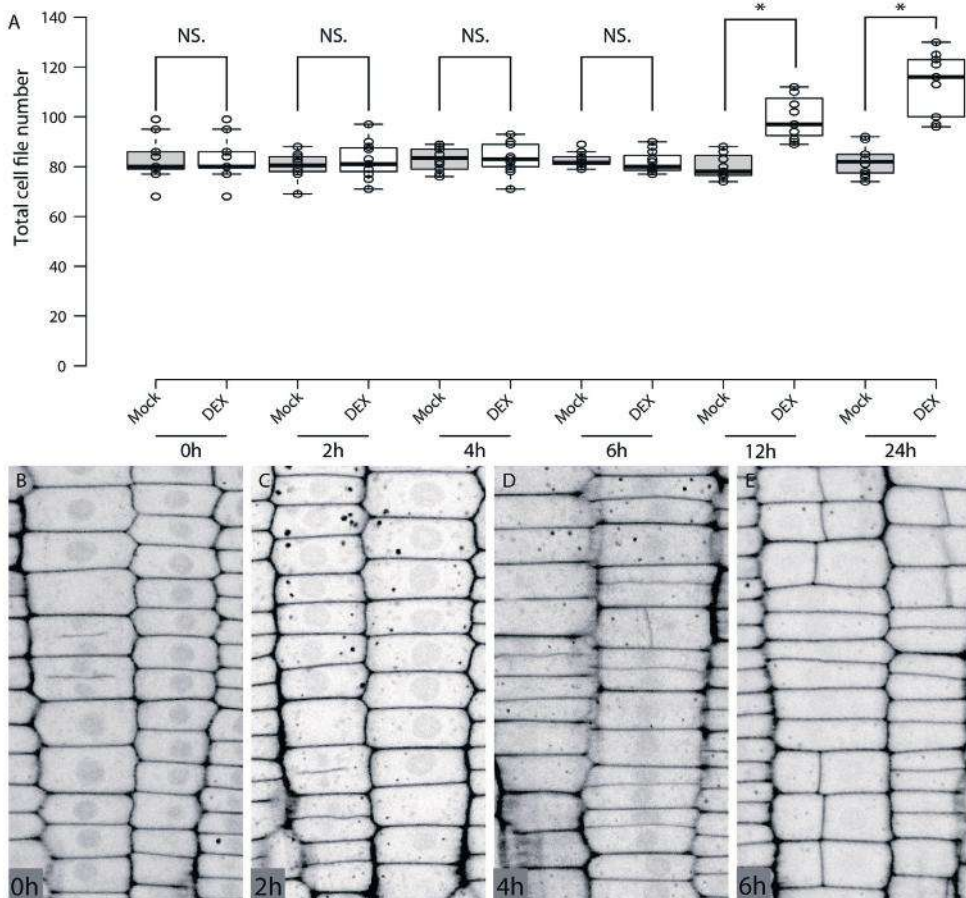
Figure 4: Temporal aspects of TMO5/LHW dependent induction of PRD. A. Quantification of cell number in radial sections of 5-day-old roots (n = 9, 8, 9, 10, 9, 12, 9, 10, 10, 10, 11 and 9 respectively). Asterisks indicates a significant difference in cell file number between DEX and mock treated roots of the same time point as indicated by a two-tailed t-test with p-value < 0.01 (NS: not significant). **B-E.** longitudinal sections of dGR roots transferred from ½ MS to ½ MS containing 10µM DEX.

BiNGO analysis reveals CK signaling as major downstream effect

To gain a first indication about the processes differentially regulated by inducing TMO5/LHW, the BiNGO (Biological Network Gene Ontology) plug-in tool for Cytoscape (Maere, et al., 2005) was used to assess the Biological Process categories that might be overrepresented in the list of differentially regulated genes. Biological Process categories were assessed to give a general overview of pathways downstream of TMO5/LHW. We used the BiNGO tool to compare

the obtained list of 272 genes with a fold change (FC) larger than 2 up-regulated genes and compared this to the entire genome of *Arabidopsis thaliana* using a Benjamini & Hochberg false discovery rate correction with *p*-value cutoff of 0.001. Because of the lack of annotation, 70 out of the 272 genes were discarded in this analysis. The overrepresented categories are shown in **Figure 5** and **Table 2**. This analysis revealed an enrichment of genes involved in, amongst others, cellular response to cytokinin stimulus and cytokinin-mediated signaling pathway in our dataset. Previous work has shown that constitutive overexpression of *TMO5* and *LHW* leads to ectopic *LOG4* expression, which in turn induces cytokinin production throughout the root meristem (De Rybel, et al., 2014; Ohashi-Ito, et al., 2014). Additionally, it has been shown that the synthetic cytokinin response marker TCSn (Zürcher, et al., 2013) is up-regulated during constitutive overexpression of *TMO5* and *LHW* and down-regulated in the *lhw* mutant (De Rybel, et al., 2014; Ohashi-Ito, et al., 2014). Overrepresentation of the biological processes in our BinGO analysis indeed suggests that that induction of TMO5/LHW triggered cytokinin biosynthesis and thus most likely also more downstream unannotated responses.

Table 1: Overview of the 272 differentially up-regulated genes. For the selection, a fold change >2 and *p*-value < 0.05 was applied. Listed are the At-code and the respective values at each of the time points that were sampled.

AGI	Description	FC 0.5h/0h	p-value	FC 1h/0h	p-value	FC 2h/0h	p-value	FC 3h/0h	p-value	FC 4h/0h	p-value	FC 5h/0h	p-value	FC 6h/0h	p-value
AT3G53450	LOG4	10,4	0,00	12,1	0,00	8,7	0,00	6,6	0,00	5,3	0,00	5,0	0,00	6,4	0,00
AT4G38650	GH10	4,6	0,00	7,8	0,00	5,6	0,00	3,0	0,00	2,2	0,00	1,9	0,00	2,1	0,00
AT4G23560	GH9B15	2,8	0,67	1,3	0,93	1,6	0,74	1,0	0,98	2,1	0,48	2,4	0,44	0,9	0,95
AT1G35820		2,8	0,72	1,5	0,86	1,2	0,93	1,3	0,91	0,9	0,92	1,3	0,81	2,0	0,53
AT1G29951	CPuORF35	2,8	0,00	3,0	0,00	2,5	0,00	2,0	0,00	2,0	0,00	1,7	0,00	1,8	0,00
AT1G29952	CPuORF34	2,8	0,00	3,0	0,00	2,5	0,00	2,0	0,00	2,0	0,00	1,7	0,00	1,8	0,00
AT1G29950	SACL3	2,7	0,00	3,0	0,00	2,6	0,00	1,9	0,00	1,9	0,00	1,6	0,00	1,8	0,00
AT1G20530		2,7	0,00	2,3	0,00	1,6	0,06	1,5	0,06	1,3	0,21	1,8	0,01	1,4	0,16
AT2G26440	PME12	2,6	0,00	3,2	0,00	3,3	0,00	3,1	0,00	2,5	0,00	3,1	0,00	2,7	0,00
AT3G58035		2,5	0,78	0,8	0,94	1,6	0,73	1,6	0,68	0,7	0,70	0,9	0,95	1,4	0,84
AT5G09600	SDH3-1	2,4	0,62	0,8	0,97	1,6	0,83	0,9	0,92	1,1	0,95	2,4	0,37	1,2	0,88
AT4G39010	GH9B18	2,3	0,03	1,5	0,36	1,2	0,77	1,0	0,97	0,8	0,48	0,9	0,78	0,9	0,69
AT2G40970	MYBC1	2,2	0,00	2,5	0,00	2,3	0,00	2,0	0,00	1,7	0,00	1,8	0,00	1,9	0,00
AT2G44460	BGLU28	2,2	0,31	1,8	0,34	1,9	0,20	1,2	0,68	1,0	0,94	1,4	0,44	1,1	0,86
AT3G20885		2,2	0,69	1,8	0,53	1,4	0,70	1,4	0,54	1,1	0,81	1,2	0,81	1,6	0,35
AT4G24110		2,2	0,00	1,3	0,34	1,0	0,94	1,0	0,94	1,0	0,85	0,9	0,85	1,0	0,94
AT5G07010	ST2A	2,1	0,00	1,6	0,10	1,4	0,27	1,4	0,18	1,4	0,19	1,3	0,19	1,2	0,39
AT2G43870		2,1	0,00	2,4	0,00	1,5	0,01	1,4	0,02	1,5	0,01	1,5	0,01	1,4	0,01
AT3G02000	ROXY1	2,0	0,12	2,4	0,01	2,0	0,05	1,7	0,08	1,6	0,15	1,8	0,05	1,8	0,04
AT5G39240		1,9	0,00	2,1	0,00	2,1	0,00	2,0	0,00	1,9	0,00	1,7	0,00	1,9	0,00
AT5G66440		1,9	0,00	2,0	0,00	2,0	0,00	1,9	0,00	1,9	0,00	1,6	0,00	1,6	0,00
AT1G03240		1,9	0,53	1,4	0,79	2,1	0,24	2,3	0,06	2,7	0,05	2,3	0,07	2,8	0,03
AT5G14120		1,8	0,01	1,9	0,00	2,1	0,00	1,6	0,00	1,6	0,01	1,5	0,01	1,6	0,01
AT1G47950		1,8	0,81	1,5	0,80	1,0	0,96	2,3	0,31	1,7	0,44	2,0	0,31	1,6	0,50
AT1G21651		1,7	0,71	3,1	0,18	2,4	0,20	2,4	0,12	1,6	0,49	2,0	0,20	2,0	0,21
AT1G20160	ATSBT5.2	1,7	0,01	2,4	0,00	2,7	0,00	3,6	0,00	3,0	0,00	3,0	0,00	2,7	0,00
AT1G60790	TBL2	1,7	0,06	2,1	0,00	1,4	0,20	1,2	0,38	1,2	0,49	1,1	0,85	1,2	0,42
AT5G17720		1,7	0,26	1,7	0,15	1,7	0,13	1,4	0,17	1,9	0,02	1,3	0,42	2,0	0,01
AT1G54680		1,7	0,48	1,2	0,85	2,2	0,07	1,4	0,35	1,7	0,13	1,5	0,30	1,7	0,13
AT5G57887		1,7	0,21	1,6	0,21	2,0	0,01	1,9	0,01	2,2	0,00	2,2	0,00	2,2	0,00
AT1G68470		1,6	0,06	2,3	0,00	2,2	0,00	2,0	0,00	2,4	0,00	1,7	0,01	1,8	0,00
AT4G00885	miRNA165	1,6	0,33	1,5	0,38	2,0	0,03	2,2	0,01	2,2	0,01	2,5	0,00	2,3	0,00
AT4G14690	ELIP2	1,6	0,07	2,4	0,00	2,1	0,00	1,6	0,02	1,6	0,02	1,7	0,01	1,8	0,01
AT3G45955		1,6	0,67	1,2	0,89	2,9	0,11	1,8	0,24	1,7	0,28	1,9	0,19	1,3	0,60

Gene														
AT1G14120	1,6	0,20	1,6	0,10	1,4	0,20	1,9	0,01	1,7	0,02	1,8	0,01	2,1	0,00
AT4G37390 AUR3	1,6	0,56	1,5	0,66	1,7	0,28	1,9	0,06	1,6	0,24	2,3	0,02	1,5	0,27
AT2G37390 KR2	1,6	0,00	2,5	0,00	2,7	0,00	2,6	0,00	2,8	0,00	2,8	0,00	2,6	0,00
AT5G56795 MT1B	1,6	0,76	2,4	0,41	1,9	0,47	3,2	0,03	2,9	0,07	2,9	0,06	3,0	0,04
AT1G67340	1,6	0,17	1,9	0,01	2,1	0,00	2,0	0,00	1,9	0,00	2,3	0,00	1,9	0,00
AT3G45390	1,6	0,68	1,2	0,85	1,9	0,23	1,6	0,34	2,3	0,07	2,1	0,09	1,9	0,16
AT5G39220	1,6	0,23	1,9	0,01	1,8	0,02	2,3	0,00	2,1	0,00	2,2	0,00	2,5	0,00
AT5G39080	1,6	0,25	3,1	0,00	3,1	0,00	2,1	0,00	2,7	0,00	2,4	0,00	2,8	0,00
AT5G38000	1,5	0,55	1,2	0,78	2,1	0,05	1,8	0,09	1,3	0,55	2,0	0,05	1,5	0,22
AT4G38780	1,5	0,62	1,5	0,59	1,4	0,51	1,4	0,37	1,1	0,90	1,4	0,39	2,4	0,02
AT2G25180 ARR12	1,5	0,00	2,0	0,00	2,0	0,00	1,8	0,00	1,7	0,00	1,6	0,00	1,7	0,00
AT3G10600 CAT7	1,5	0,77	1,2	0,93	1,8	0,36	2,1	0,17	1,3	0,81	1,3	0,59	1,7	0,33
AT3G59850	1,5	0,01	2,2	0,00	1,5	0,01	1,3	0,05	1,3	0,05	1,2	0,31	1,2	0,23
AT2G31540	1,5	0,76	0,7	0,75	0,9	0,90	2,3	0,08	2,0	0,18	2,7	0,04	2,6	0,03
AT3G03990	1,5	0,01	1,8	0,00	1,9	0,00	1,9	0,00	2,1	0,00	2,2	0,00	2,5	0,00
AT1G30760	1,5	0,51	1,3	0,64	1,7	0,15	2,0	0,01	2,0	0,02	1,6	0,12	1,4	0,24
AT4G04775	1,5	0,91	2,1	0,76	1,2	0,92	0,8	0,78	1,2	0,83	1,0	0,99	1,2	0,91
AT5G52450	1,5	0,34	1,5	0,22	2,0	0,00	1,9	0,00	1,9	0,01	1,7	0,02	1,6	0,03
AT1G63400	1,5	0,82	1,5	0,82	1,9	0,45	1,5	0,48	1,7	0,46	2,1	0,29	1,3	0,61
AT3G04440	1,5	0,80	1,2	0,96	1,7	0,45	2,1	0,18	1,7	0,45	1,5	0,40	1,5	0,41
AT3G16690 SWEET16	1,4	0,66	1,3	0,70	1,5	0,40	2,6	0,00	2,3	0,01	1,8	0,06	2,2	0,01
AT1G03850 GRXS13	1,4	0,62	1,4	0,55	1,5	0,42	1,9	0,05	2,0	0,05	2,1	0,03	2,0	0,04
AT3G24300 AMT1;3	1,4	0,66	1,6	0,27	1,7	0,12	2,5	0,00	1,8	0,04	1,7	0,06	1,9	0,01
AT5G16000 NIK1	1,4	0,10	1,9	0,00	2,0	0,00	1,9	0,00	2,0	0,00	1,9	0,00	1,8	0,00
AT5G40270	1,4	0,57	1,4	0,57	1,7	0,09	2,3	0,00	2,2	0,00	2,4	0,00	2,1	0,00
AT4G20362	1,4	0,14	1,8	0,00	2,1	0,00	1,9	0,00	1,5	0,01	1,2	0,18	1,3	0,09
AT1G23140	1,4	0,58	1,1	0,92	1,5	0,30	2,0	0,01	1,8	0,04	1,9	0,02	2,2	0,00
AT5G18930 BUD2	1,4	0,49	2,1	0,01	1,6	0,09	1,3	0,23	1,3	0,31	1,3	0,41	1,2	0,40
AT4G23500	1,4	0,13	1,6	0,01	1,7	0,00	2,0	0,00	1,8	0,00	1,8	0,00	1,8	0,00
AT4G18510 CLE2	1,4	0,68	1,3	0,67	1,5	0,35	1,9	0,05	2,0	0,03	2,1	0,02	2,5	0,00
AT4G17788	1,4	0,38	1,8	0,02	1,9	0,01	1,9	0,00	2,3	0,00	2,4	0,00	2,3	0,00
AT5G18661	1,4	0,51	1,4	0,35	1,4	0,27	2,0	0,01	1,8	0,02	1,4	0,17	1,6	0,06
AT1G13080 CYP71B2	1,4	0,66	1,4	0,58	1,7	0,18	1,6	0,15	2,0	0,03	2,8	0,00	2,8	0,00
AT5G67520 APK4	1,4	0,72	2,0	0,09	2,1	0,03	2,2	0,01	2,5	0,00	1,7	0,08	2,0	0,02
AT2G24580	1,4	0,10	1,7	0,00	1,7	0,00	1,9	0,00	2,2	0,00	2,2	0,00	2,5	0,00

AT5G43370 APT1	1,4	0,58	0,9	0,92	1,4	0,30	2,5	0,00	1,9	0,01	2,4	0,00	2,3	0,00
AT1G55740 SIP1	1,4	0,50	1,6	0,08	1,9	0,01	2,0	0,00	1,8	0,01	2,0	0,00	2,0	0,00
AT2G38760 ANT3	1,4	0,41	1,0	0,97	1,2	0,59	1,7	0,01	1,8	0,00	2,0	0,00	1,9	0,00
AT4G02005	1,4	0,75	2,0	0,12	1,5	0,42	1,8	0,07	1,7	0,20	1,2	0,59	1,8	0,07
AT4G32950 PP2C	1,4	0,82	1,5	0,57	2,8	0,02	2,9	0,01	1,6	0,20	1,1	0,79	0,8	0,74
AT4G16540	1,4	0,89	2,5	0,45	1,3	0,94	2,0	0,53	0,8	0,84	1,4	0,62	1,2	0,79
AT4G29905	1,4	0,65	1,3	0,65	1,3	0,51	2,2	0,01	2,5	0,00	2,4	0,00	2,8	0,00
AT5G58360 OFP3	1,3	0,84	1,2	0,91	1,5	0,49	2,0	0,07	1,9	0,10	1,8	0,12	1,9	0,07
AT3G50610	1,3	0,82	1,5	0,72	1,4	0,67	1,5	0,43	1,6	0,34	2,0	0,15	1,3	0,55
AT5G23980 FRO4	1,3	0,93	1,1	0,97	1,9	0,31	2,7	0,04	3,1	0,02	3,3	0,01	3,2	0,01
AT1G74458	1,3	0,42	1,2	0,54	1,5	0,07	1,8	0,00	2,0	0,00	1,7	0,01	2,1	0,00
AT3G17130	1,3	0,77	1,4	0,51	1,2	0,81	2,2	0,01	2,2	0,01	2,7	0,00	2,7	0,00
AT4G27730 OPT6	1,3	0,52	1,5	0,09	2,3	0,00	1,8	0,00	1,9	0,00	2,3	0,00	2,0	0,00
AT2G46690	1,3	0,48	1,6	0,04	2,0	0,00	2,6	0,00	2,2	0,00	2,5	0,00	2,3	0,00
AT1G57560 MYB50	1,3	0,76	1,3	0,78	1,5	0,30	2,1	0,02	1,8	0,06	2,1	0,02	2,0	0,02
AT2G38380	1,3	0,66	1,2	0,67	1,7	0,06	2,3	0,00	2,5	0,00	2,8	0,00	2,8	0,00
AT1G03950 VPS2.3	1,3	0,74	1,4	0,59	1,1	0,78	1,9	0,05	1,8	0,07	2,0	0,03	2,1	0,01
AT2G05440 GRP9	1,3	0,91	1,3	0,93	1,3	0,80	1,3	0,75	2,4	0,25	2,6	0,18	3,5	0,09
AT1G02380	1,3	0,75	1,3	0,64	1,4	0,40	2,1	0,01	1,8	0,04	1,8	0,04	1,7	0,08
AT1G22050 MUB6	1,3	0,71	1,6	0,18	2,1	0,01	1,9	0,01	1,7	0,05	1,7	0,03	1,9	0,01
AT1G68740 PHO1;H1	1,3	0,61	1,5	0,19	1,5	0,14	2,0	0,00	2,4	0,00	2,5	0,00	2,7	0,00
AT1G60050 UMAMIT35	1,3	0,83	1,3	0,75	1,6	0,45	3,4	0,00	3,1	0,00	2,9	0,01	2,4	0,02
AT5G13900	1,3	0,77	1,2	0,80	1,2	0,77	1,7	0,10	1,8	0,07	2,4	0,01	1,6	0,15
AT1G08430 ALMT1	1,3	0,79	1,4	0,47	1,6	0,21	1,8	0,04	1,6	0,10	2,2	0,01	1,8	0,03
AT1G31770 ABCG14	1,3	0,21	1,6	0,00	1,8	0,00	2,0	0,00	2,0	0,00	1,9	0,00	1,9	0,00
AT4G30450	1,3	0,72	1,4	0,44	1,6	0,09	1,8	0,02	2,2	0,00	2,4	0,00	2,2	0,00
AT3G46880	1,3	0,62	1,5	0,17	1,3	0,45	1,7	0,01	2,3	0,00	1,9	0,00	2,3	0,00
AT5G51790 bHLH120	1,3	0,65	1,7	0,05	2,1	0,00	2,0	0,00	2,2	0,00	2,4	0,00	3,0	0,00
AT3G10912 CPuORF63	1,3	0,63	1,2	0,61	1,3	0,41	1,8	0,01	1,6	0,03	1,9	0,00	2,1	0,00
AT3G10910	1,3	0,63	1,2	0,61	1,3	0,41	1,8	0,01	1,6	0,03	1,9	0,00	2,1	0,00
AT5G46845	1,3	0,77	1,0	0,97	1,2	0,75	1,5	0,10	1,6	0,11	1,9	0,02	2,4	0,00
AT2G35384	1,3	0,92	2,1	0,45	1,4	0,76	2,0	0,24	1,8	0,43	1,7	0,41	1,7	0,44
AT5G26300	1,3	0,92	1,2	0,95	1,6	0,67	2,5	0,08	2,0	0,29	2,3	0,15	3,2	0,03
AT2G34810	1,3	0,70	1,1	0,80	1,5	0,15	1,6	0,05	1,5	0,07	1,9	0,01	2,0	0,00
AT5G19530 ACL5	1,3	0,44	1,6	0,01	2,4	0,00	1,9	0,00	1,8	0,00	1,5	0,00	1,6	0,00

Gene														
AT5G58770 PT4	1,3	0,86	1,4	0,61	1,6	0,45	2,0	0,04	2,0	0,05	2,4	0,01	2,4	0,01
AT1G20380	1,2	0,62	1,3	0,38	1,4	0,12	1,8	0,00	2,1	0,00	2,0	0,00	2,0	0,00
AT1G34910	1,2	0,96	1,8	0,76	1,0	0,98	1,0	0,98	2,8	0,15	2,4	0,22	2,3	0,50
AT1G75440 UBC16	1,2	0,68	1,3	0,57	1,2	0,45	1,7	0,01	1,8	0,00	2,1	0,00	1,9	0,00
AT1G07690	1,2	0,89	1,5	0,64	2,7	0,02	2,1	0,04	1,6	0,25	1,1	0,81	1,0	0,95
AT1G01340 ACBK1	1,2	0,87	1,3	0,84	1,4	0,57	2,5	0,01	2,1	0,05	2,3	0,03	2,1	0,03
AT3G59340	1,2	0,78	1,2	0,71	1,4	0,32	1,5	0,08	1,6	0,05	2,0	0,00	2,2	0,00
AT1G21110 IGMT3	1,2	0,93	1,9	0,47	1,7	0,45	3,3	0,02	2,1	0,25	2,4	0,09	2,2	0,16
AT1G73910 ARP4A	1,2	0,89	2,2	0,14	1,5	0,46	0,9	0,77	1,5	0,47	1,3	0,65	1,4	0,56
AT3G51340	1,2	0,92	1,7	0,40	1,4	0,54	1,9	0,07	2,0	0,05	2,2	0,03	2,2	0,03
AT4G29080 IAA27	1,2	0,86	1,6	0,48	1,4	0,51	2,0	0,05	2,2	0,04	2,4	0,02	1,9	0,06
AT5G67620	1,2	0,65	1,3	0,17	2,0	0,00	2,8	0,00	2,5	0,00	2,5	0,00	2,4	0,00
AT3G46130 MYB48	1,2	0,82	1,3	0,57	1,2	0,76	1,3	0,33	1,4	0,20	1,6	0,10	2,0	0,01
AT5G14920	1,2	0,73	1,6	0,04	2,0	0,00	2,0	0,00	2,1	0,00	2,1	0,00	2,3	0,00
AT4G40010 SSNRK2.7	1,2	0,86	1,2	0,85	1,6	0,38	1,8	0,09	1,8	0,10	1,8	0,08	2,2	0,02
AT4G20450	1,2	0,86	1,4	0,75	2,2	0,10	3,3	0,00	2,2	0,05	2,9	0,01	2,6	0,02
AT5G16900	1,2	0,80	1,4	0,44	1,9	0,06	2,6	0,00	2,1	0,01	2,1	0,02	1,7	0,05
AT4G10670 GTC2	1,2	0,80	2,1	0,00	1,1	0,79	1,0	0,89	1,3	0,35	1,2	0,39	1,1	0,87
AT2G28990	1,2	0,77	1,1	0,92	1,4	0,26	1,9	0,00	1,8	0,01	1,9	0,00	2,0	0,00
AT5G07460 PMSR2	1,2	0,74	1,4	0,27	1,8	0,00	2,2	0,00	1,8	0,00	1,4	0,06	1,4	0,05
AT1G55320 AAE18	1,2	0,72	1,1	0,85	1,3	0,33	1,6	0,01	1,9	0,00	2,0	0,00	2,2	0,00
AT1G60140 TPS10	1,2	0,75	1,1	0,90	1,4	0,18	1,7	0,00	2,0	0,00	1,9	0,00	2,1	0,00
AT4G03420	1,2	0,92	1,5	0,63	1,4	0,67	2,4	0,02	1,6	0,26	1,5	0,34	1,8	0,16
AT2G37210 LOG3	1,2	0,85	2,0	0,03	1,2	0,77	1,0	0,97	0,8	0,38	1,0	0,95	0,9	0,63
AT1G13740 AFP2	1,2	0,83	1,6	0,17	2,1	0,01	2,1	0,00	2,2	0,00	2,3	0,00	2,1	0,00
AT2G23910	1,2	0,80	1,1	0,91	1,2	0,59	2,0	0,00	2,1	0,00	2,5	0,00	2,5	0,00
AT5G63600 FLS5	1,2	0,78	1,2	0,56	1,7	0,01	2,3	0,00	2,0	0,00	2,1	0,00	2,1	0,00
AT3G02020 AK3	1,1	0,89	0,9	0,95	1,2	0,81	1,8	0,10	1,8	0,13	2,6	0,06	2,2	0,02
AT2G16930	1,1	0,92	1,0	0,98	2,6	0,01	1,3	0,47	1,4	0,41	1,1	0,94	1,2	0,69
AT5G22410 RHS18	1,1	0,88	1,2	0,78	1,3	0,60	2,0	0,01	1,9	0,03	1,9	0,03	2,0	0,02
AT3G54600 DJ1F	1,1	0,90	1,3	0,63	1,4	0,34	1,8	0,02	1,9	0,01	2,4	0,00	2,2	0,00
AT4G27410 RD26	1,1	0,82	1,3	0,45	1,1	0,70	1,5	0,05	1,5	0,06	2,1	0,00	2,2	0,00
AT3G18280	1,1	0,84	1,5	0,14	1,6	0,06	2,0	0,00	1,9	0,00	2,0	0,00	2,2	0,00
AT1G31320 LBD4	1,1	0,87	1,3	0,61	1,4	0,26	2,1	0,00	2,3	0,00	1,7	0,02	1,8	0,01
AT1G78390 NCED9	1,1	0,93	1,2	0,79	1,7	0,13	2,6	0,00	2,2	0,01	3,1	0,00	2,3	0,00

Gene														
AT4G15480 UGT84A1	1,1	0,89	1,3	0,62	1,4	0,31	3,0	0,00	3,0	0,00	3,8	0,00	3,7	0,00
AT4G12470 AZI1	1,1	0,94	1,0	0,99	1,2	0,83	1,3	0,47	1,4	0,45	1,6	0,23	2,2	0,03
AT3G51540	1,1	0,87	1,2	0,72	1,4	0,28	2,2	0,00	2,0	0,01	2,2	0,00	2,4	0,00
AT5G48880 PKT2	1,1	0,81	1,0	0,95	1,1	0,89	1,5	0,01	1,7	0,00	2,1	0,00	2,2	0,00
AT3G21560 UGT84A2	1,1	0,82	1,1	0,87	1,4	0,06	2,1	0,00	1,9	0,00	2,2	0,00	2,2	0,00
AT1G22570	1,1	0,88	1,3	0,43	2,0	0,00	1,7	0,01	1,6	0,03	1,5	0,08	1,6	0,02
AT3G26125 CYP86C2	1,1	0,94	1,2	0,90	1,4	0,51	1,2	0,71	1,6	0,25	1,5	0,24	2,1	0,03
AT3G02242	1,1	0,93	1,0	0,97	1,4	0,47	2,1	0,03	1,7	0,11	1,4	0,31	1,5	0,21
AT2G35155	1,1	0,87	1,1	0,85	1,2	0,65	1,5	0,10	1,5	0,14	2,1	0,01	1,7	0,03
AT4G25640 DTX35	1,1	0,82	1,0	0,97	1,2	0,25	1,8	0,00	1,9	0,00	2,1	0,00	2,2	0,00
AT3G63540 hypothetical protein	1,1	0,92	1,2	0,73	1,3	0,58	1,5	0,15	1,5	0,16	1,6	0,08	2,0	0,01
AT3G27170 CLC-B	1,1	0,86	1,3	0,41	1,4	0,15	2,0	0,00	1,9	0,00	1,9	0,00	1,9	0,00
AT4G04840 MSRB6	1,1	0,87	1,0	0,99	1,1	0,68	1,4	0,07	1,6	0,02	2,6	0,00	2,8	0,00
AT1G33260	1,1	0,93	1,1	0,93	1,1	0,92	2,0	0,05	1,2	0,65	1,3	0,52	1,0	0,92
AT2G47460 MYB12	1,1	0,88	1,2	0,51	1,3	0,27	1,7	0,01	1,7	0,01	1,9	0,00	2,1	0,00
AT3G49860 ARLA1B	1,1	0,93	1,1	0,95	1,2	0,88	1,6	0,27	2,0	0,15	1,8	0,21	2,0	0,11
AT3G02240 RGF7	1,1	0,94	1,2	0,75	1,7	0,08	2,0	0,01	1,7	0,03	1,6	0,05	1,6	0,05
AT2G16910 AMS	1,1	0,89	1,0	0,96	1,2	0,44	1,1	0,66	1,4	0,08	2,0	0,00	1,2	0,36
AT2G28510 Dof2.1	1,1	0,91	1,6	0,04	2,1	0,00	2,2	0,00	2,1	0,00	1,9	0,00	2,1	0,00
AT2G29330 TRI	1,1	0,98	0,9	0,93	1,3	0,72	2,0	0,15	2,1	0,17	1,8	0,28	1,4	0,49
AT4G15765	1,1	1,00	1,1	0,91	1,1	0,87	1,0	0,98	1,3	0,55	2,0	0,10	1,5	0,27
AT4G15390	1,1	0,91	1,2	0,58	1,5	0,11	2,1	0,00	2,0	0,00	1,7	0,01	1,8	0,00
AT4G27030 FADA	1,1	0,92	1,2	0,83	1,5	0,47	1,7	0,21	1,6	0,20	1,5	0,25	2,1	0,05
AT1G31885 NIP3;1	1,1	0,92	1,2	0,66	1,8	0,03	2,7	0,00	2,5	0,00	2,3	0,00	2,7	0,00
AT4G33730	1,1	0,92	1,2	0,79	1,4	0,38	2,2	0,00	1,8	0,02	1,9	0,01	1,7	0,02
AT1G26360 MES13	1,1	0,92	1,0	0,97	1,1	0,84	1,8	0,06	1,7	0,08	2,2	0,01	2,0	0,03
AT2G28850 CYP710A3	1,1	0,97	0,9	0,92	1,7	0,43	2,7	0,01	1,6	0,27	1,3	0,63	1,1	0,81
AT4G36430	1,1	0,98	1,6	0,76	1,7	0,48	2,4	0,10	1,8	0,24	1,8	0,27	1,3	0,58
AT1G05390	1,1	1,00	1,2	0,99	2,0	0,79	2,2	0,52	0,9	0,99	1,5	0,72	1,2	0,98
AT1G51870	1,1	0,96	1,5	0,44	1,4	0,45	2,0	0,03	1,6	0,19	2,3	0,01	2,7	0,00
AT3G56080	1,1	0,95	1,5	0,24	1,2	0,73	1,7	0,03	1,9	0,01	2,4	0,00	2,5	0,00
AT2G32270 ZIP3	1,1	0,96	1,4	0,37	2,2	0,00	3,0	0,00	2,7	0,00	2,8	0,00	2,7	0,00
AT3G44990 XTH31	1,1	0,95	1,1	0,84	1,3	0,20	2,2	0,00	2,1	0,00	2,3	0,00	2,5	0,00
AT3G25190	1,1	0,93	1,1	0,71	1,4	0,06	1,9	0,00	1,8	0,00	2,1	0,00	1,9	0,00
AT4G08620 SULTR1;1	1,1	0,92	1,1	0,94	1,5	0,55	2,6	0,02	2,7	0,02	3,0	0,01	3,1	0,01

Gene														
AT3G21510 AHP1 E	1,1	0,95	1,0	0,98	1,1	0,90	1,5	0,04	1,8	0,00	2,0	0,00	2,1	0,00
AT1G54970 PRP1	1,0	0,99	0,9	0,97	0,7	0,42	1,6	0,25	1,6	0,26	1,8	0,16	2,2	0,04
AT1G04110 SDD1	1,0	0,98	1,6	0,28	2,1	0,02	1,7	0,07	1,3	0,45	1,5	0,17	1,2	0,52
AT5G07680 AC079	1,0	0,97	1,0	0,98	1,0	1,00	1,7	0,03	1,9	0,01	2,3	0,00	1,9	0,01
AT3G05936	1,0	0,97	0,9	0,95	1,3	0,41	2,1	0,00	1,7	0,03	1,8	0,02	2,0	0,01
AT1G59850	1,0	0,96	0,8	0,94	1,1	0,79	2,0	0,03	1,7	0,12	1,6	0,17	1,6	0,14
AT2G04070	1,0	0,99	1,2	0,94	0,8	0,85	2,1	0,52	0,7	0,62	0,8	0,85	0,9	0,86
AT4G18940	1,0	0,96	1,4	0,58	1,7	0,21	2,2	0,01	2,4	0,01	2,5	0,00	2,4	0,00
AT1G10470 ARR4	1,0	0,96	1,5	0,04	2,0	0,00	2,7	0,00	2,9	0,00	2,6	0,00	2,6	0,00
AT5G65800 ACS5	1,0	0,96	1,1	0,91	1,6	0,15	2,7	0,00	2,3	0,00	2,4	0,00	2,1	0,01
AT5G26080	1,0	0,99	1,0	1,00	1,0	0,94	1,6	0,14	1,8	0,09	1,8	0,09	2,0	0,03
AT1G62975 bHLH125	1,0	1,00	1,3	0,37	1,7	0,01	2,5	0,00	2,5	0,00	2,3	0,00	2,3	0,00
AT1G13420 ST4B	1,0	0,99	0,8	0,73	1,0	0,94	2,1	0,00	2,0	0,00	1,7	0,01	1,9	0,00
AT5G45380 DUR3	1,0	0,99	1,1	0,83	1,5	0,01	2,1	0,00	1,8	0,00	1,9	0,00	1,8	0,00
AT5G33355 Defensin-like family protein	1,0	0,96	0,9	0,95	1,1	0,97	1,3	0,78	1,3	0,69	1,4	0,68	2,6	0,11
AT5G37260 RVE2	1,0	1,00	1,4	0,17	1,6	0,03	1,9	0,00	2,0	0,00	1,8	0,00	2,1	0,00
AT1G30840 PUP4	1,0	0,99	1,4	0,30	1,4	0,20	2,0	0,01	2,1	0,00	2,1	0,00	2,3	0,00
AT1G78990	1,0	0,99	1,1	0,99	0,9	0,96	1,2	0,73	1,5	0,41	1,4	0,55	2,0	0,11
AT3G01260	1,0	0,99	1,1	0,96	1,3	0,54	2,0	0,01	2,1	0,01	2,2	0,00	2,4	0,00
AT1G15380 GLYI4	1,0	0,99	1,1	0,97	1,3	0,56	1,8	0,05	2,3	0,01	2,4	0,01	2,6	0,00
AT4G14440 HCD1	1,0	0,99	1,0	0,99	1,0	1,00	1,7	0,14	1,2	0,67	2,0	0,05	1,3	0,43
AT5G65980	1,0	0,99	0,9	0,93	1,2	0,76	2,4	0,01	3,1	0,00	3,0	0,00	2,0	0,03
AT2G48080	1,0	0,99	1,0	0,99	1,3	0,27	2,4	0,00	1,7	0,00	1,6	0,01	1,4	0,04
AT5G62920 ARR6	1,0	0,99	1,9	0,01	2,3	0,00	3,2	0,00	3,5	0,00	3,7	0,00	3,5	0,00
AT5G47980	1,0	0,99	0,9	0,87	1,1	0,91	1,4	0,16	1,6	0,07	2,0	0,01	1,8	0,02
AT5G36740	1,0	0,95	0,9	0,95	1,6	0,75	2,2	0,22	1,0	0,98	1,4	0,65	0,7	0,49
AT3G46710	1,0	0,99	1,2	0,88	1,2	0,89	1,6	0,22	1,6	0,33	2,0	0,09	2,0	0,07
AT4G08780	1,0	0,99	0,7	0,70	1,2	0,82	2,4	0,03	0,8	0,74	0,9	0,82	1,1	0,76
AT3G04110 GLR1	1,0	0,99	1,1	0,95	1,3	0,52	1,5	0,13	2,3	0,00	2,0	0,01	2,3	0,00
AT1G51830	1,0	0,98	1,2	0,78	1,4	0,44	2,0	0,01	2,0	0,01	1,9	0,01	2,0	0,01
AT5G51780 bHLH36	1,0	0,99	1,7	0,25	2,5	0,01	3,4	0,00	3,1	0,00	3,7	0,00	3,0	0,00
AT1G54950	1,0	0,98	1,3	0,71	2,5	0,00	4,4	0,00	1,6	0,17	1,0	1,00	1,0	0,93
AT3G01730	1,0	0,99	1,1	0,93	1,2	0,60	2,5	0,00	2,1	0,01	1,9	0,02	1,9	0,02
AT1G61080	1,0	1,00	0,9	0,99	1,0	1,00	1,5	0,17	1,2	0,56	2,1	0,02	1,6	0,12
AT3G51350	0,9	0,97	1,2	0,90	1,2	0,84	2,3	0,02	1,9	0,07	1,6	0,16	1,8	0,08

Gene														
AT2G46650 CYTB5-C	0,9	0,95	1,1	0,93	1,3	0,45	1,9	0,01	2,1	0,00	2,3	0,00	2,0	0,00
AT5G19970	0,9	0,93	1,0	0,98	1,2	0,83	1,9	0,03	2,0	0,02	1,7	0,06	2,2	0,01
AT4G25410 bHLH126	0,9	0,95	1,1	0,94	1,7	0,06	1,8	0,02	1,7	0,04	2,0	0,01	2,5	0,00
AT2G36120 DOT1	0,9	0,95	1,1	0,93	1,4	0,43	1,7	0,04	2,0	0,02	2,1	0,01	2,2	0,00
AT3G02620	0,9	0,97	1,4	0,61	1,7	0,13	2,1	0,01	2,3	0,01	2,0	0,01	2,7	0,00
AT4G15233 ABCG42	0,9	0,93	1,0	0,96	1,5	0,43	1,6	0,26	1,8	0,16	2,0	0,08	1,8	0,15
AT5G38450 CYP735A1	0,9	0,92	1,0	0,97	1,7	0,12	1,9	0,02	2,0	0,01	2,0	0,01	2,0	0,01
AT1G73270 SCPL6	0,9	0,95	1,0	0,97	1,0	0,98	2,0	0,10	1,3	0,69	2,1	0,09	2,0	0,08
AT5G59680	0,9	0,99	0,8	0,95	1,5	0,57	2,9	0,04	3,0	0,04	2,8	0,05	2,7	0,06
AT4G04450 WRKY42	0,9	0,91	1,2	0,58	1,3	0,18	2,0	0,00	2,0	0,00	2,0	0,00	2,0	0,00
AT1G68880 bZIP	0,9	0,92	1,3	0,78	1,6	0,23	2,2	0,01	1,7	0,09	1,9	0,03	1,6	0,12
AT4G13390 EXT12	0,9	0,98	1,2	0,81	1,0	0,96	1,6	0,13	2,0	0,03	2,0	0,03	2,1	0,02
AT5G49770	0,9	0,93	1,1	0,93	1,2	0,80	2,4	0,00	2,1	0,01	1,9	0,03	2,5	0,00
AT1G08090 NRT2;1	0,9	0,90	1,1	0,85	1,6	0,07	4,4	0,00	3,3	0,00	2,3	0,00	2,3	0,00
AT3G50300	0,9	0,92	1,8	0,03	1,9	0,01	2,5	0,00	2,5	0,00	2,9	0,00	2,8	0,00
AT3G18080 BGLU44	0,9	0,97	1,3	0,81	4,3	0,00	4,2	0,00	4,6	0,00	5,3	0,00	6,1	0,00
AT2G43100 IPMI2	0,9	0,92	1,2	0,82	1,1	0,90	1,7	0,11	2,0	0,04	2,0	0,03	2,0	0,03
AT4G39070 BZS1	0,9	0,89	1,2	0,57	1,7	0,01	2,1	0,00	2,1	0,00	2,1	0,00	2,1	0,00
AT1G74880 NDH-O	0,9	0,91	1,1	0,91	1,4	0,41	1,8	0,03	2,0	0,00	2,2	0,00	2,5	0,00
AT2G26820 PP2-A3	0,9	0,87	1,2	0,73	1,7	0,02	2,4	0,00	1,8	0,00	1,8	0,00	1,6	0,01
AT1G68500	0,9	0,96	1,4	0,65	1,2	0,73	1,8	0,08	1,6	0,21	1,9	0,06	2,0	0,04
AT1G74890 ARR15	0,9	0,90	1,1	0,97	2,0	0,07	2,1	0,02	2,0	0,03	2,9	0,00	3,2	0,00
AT5G06570	0,9	0,84	1,0	1,00	1,3	0,56	1,9	0,01	2,1	0,00	2,1	0,00	2,0	0,00
AT1G67110 CYP735A2	0,9	0,92	1,2	0,80	1,3	0,64	1,8	0,08	2,6	0,00	2,2	0,01	2,2	0,01
AT4G29310	0,9	0,78	1,2	0,65	1,7	0,01	1,8	0,00	2,2	0,00	2,0	0,00	2,1	0,00
AT5G03995	0,9	0,85	1,0	0,96	1,7	0,01	2,3	0,00	2,0	0,00	2,0	0,00	2,1	0,00
AT1G13300 HRS1	0,9	0,86	1,1	0,95	1,4	0,37	2,4	0,00	2,3	0,00	2,2	0,00	2,1	0,00
AT3G18450	0,9	0,85	1,1	0,97	1,9	0,03	3,3	0,00	3,0	0,00	2,9	0,00	2,7	0,00
AT2G20080 TIE2	0,9	0,80	1,4	0,15	2,3	0,00	3,6	0,00	3,1	0,00	3,2	0,00	3,3	0,00
AT1G07560	0,9	0,92	0,8	0,70	1,3	0,58	2,2	0,01	1,8	0,03	1,8	0,03	2,1	0,01
AT1G53940 GLIP2	0,9	0,86	1,2	0,82	1,4	0,48	2,9	0,00	2,9	0,00	3,0	0,00	2,7	0,00
AT1G64780 ATAMT1;2	0,9	0,86	1,0	0,93	1,3	0,54	2,4	0,00	2,0	0,01	2,0	0,01	1,6	0,08
AT4G36220 FAH1	0,9	0,86	1,5	0,51	1,1	0,85	1,3	0,36	1,3	0,47	1,8	0,05	2,0	0,01
AT3G06390	0,9	0,94	0,9	0,95	1,2	0,91	1,6	0,39	1,8	0,36	1,9	0,27	2,0	0,15
AT3G57040 ARR9	0,9	0,81	1,0	0,98	1,6	0,09	1,9	0,01	2,1	0,00	2,1	0,00	2,1	0,00

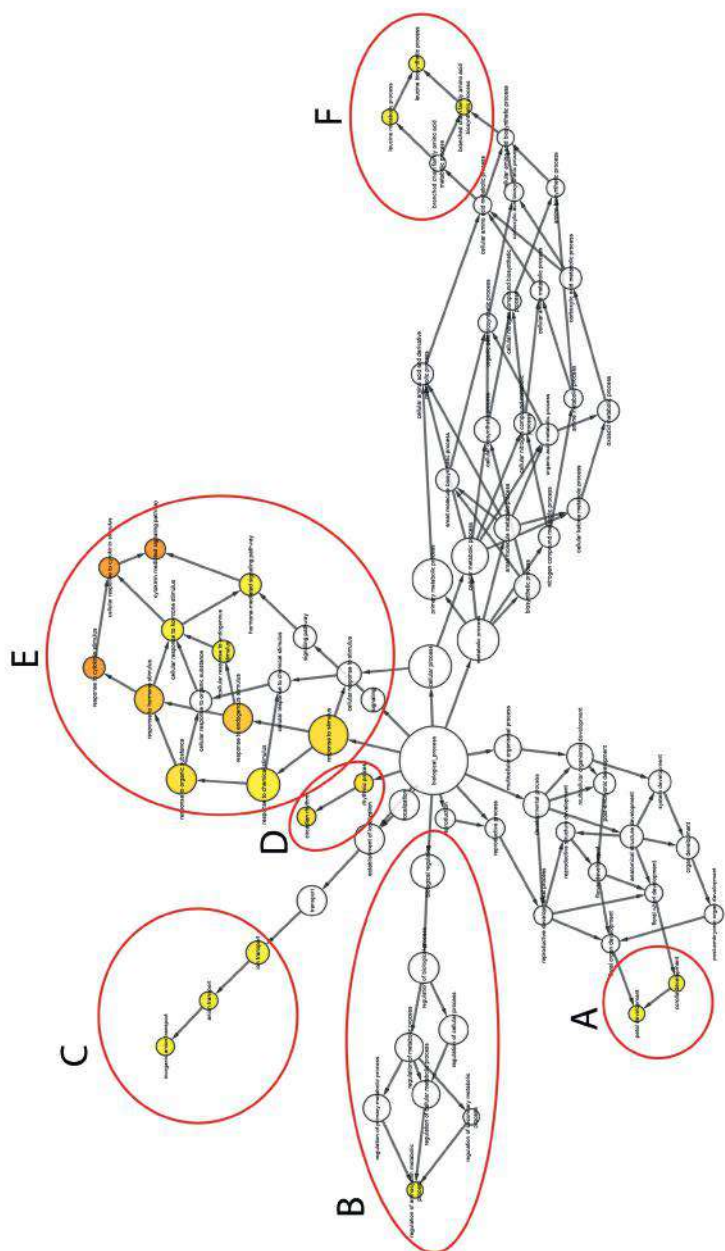| Gene														
AT3G48360 BT2	0,8	0,87	0,8	0,80	1,1	0,90	1,2	0,55	1,9	0,02	1,8	0,05	2,3	0,00
AT5G26320	0,8	0,89	1,0	0,98	1,5	0,43	2,3	0,02	1,9	0,07	2,2	0,02	2,2	0,03
AT2G22122	0,8	0,81	1,0	0,98	1,1	0,80	1,6	0,06	2,0	0,01	2,0	0,01	1,8	0,02
AT3G28510	0,8	0,94	0,9	0,95	0,7	0,78	2,1	0,55	1,3	0,89	0,8	0,81	0,8	0,70
AT5G10990 SAUR	0,8	0,73	2,3	0,00	2,1	0,00	3,6	0,00	3,3	0,00	4,9	0,00	3,6	0,00
AT2G41310 ARR8	0,8	0,75	1,3	0,41	1,7	0,01	1,9	0,00	2,1	0,00	2,0	0,00	2,0	0,00
AT4G11393 Defensin-like family protein	0,8	0,87	0,7	0,64	1,3	0,52	2,7	0,00	3,1	0,00	4,3	0,00	4,2	0,00
AT2G04050	0,8	0,92	0,8	0,92	0,8	0,81	2,8	0,20	0,8	0,77	0,9	0,88	0,8	0,79
AT1G28170 SOT7	0,8	0,93	0,9	0,97	1,9	0,13	1,9	0,06	1,5	0,28	2,2	0,03	2,1	0,03
AT5G38940	0,8	0,91	1,6	0,73	2,6	0,12	6,4	0,00	6,1	0,00	5,4	0,00	4,9	0,00
AT3G48100 ARR5	0,8	0,78	1,8	0,28	1,9	0,13	2,5	0,01	2,0	0,04	2,3	0,01	2,0	0,03
AT3G58990 IPMI1	0,8	0,77	1,0	1,00	1,2	0,84	1,6	0,09	1,9	0,03	2,1	0,01	2,1	0,01
AT5G48430	0,8	0,61	1,3	0,42	2,3	0,00	2,5	0,00	1,6	0,03	1,3	0,21	1,2	0,38
AT3G02850 SKOR	0,8	0,52	0,9	0,87	1,1	0,76	1,5	0,01	1,8	0,00	2,2	0,00	2,3	0,00
AT1G49860 GSTF14	0,8	0,88	1,0	1,00	1,3	0,72	2,3	0,06	3,4	0,03	1,7	0,32	2,4	0,05
AT3G46340	0,8	0,82	1,0	0,99	1,4	0,65	1,4	0,34	1,5	0,28	1,5	0,29	2,4	0,03
AT2G13960	0,8	0,96	0,4	0,54	0,8	0,95	2,0	0,36	0,7	0,72	1,0	0,96	0,6	0,65
AT1G34520	0,8	0,87	1,1	0,96	1,6	0,40	2,4	0,04	1,4	0,44	2,2	0,07	1,9	0,10
AT4G13420 HAK5	0,7	0,91	2,1	0,84	0,8	0,86	2,5	0,46	1,0	0,97	1,0	0,97	0,8	0,87
AT1G64400 LACS3	0,7	0,62	0,9	0,93	1,0	0,99	2,0	0,01	1,6	0,08	1,6	0,10	1,7	0,04
AT2G01520 ZCE1	0,7	0,87	1,0	1,00	0,9	0,93	1,1	0,87	2,2	0,46	1,9	0,37	2,6	0,12
AT1G27020	0,7	0,38	1,4	0,30	1,4	0,21	2,7	0,00	1,7	0,01	1,2	0,36	1,5	0,03
AT3G27950	0,7	0,15	0,9	0,84	1,3	0,17	2,0	0,00	1,5	0,03	1,3	0,10	1,3	0,08
AT4G11650 ATOSM34 /// OSM34	0,7	0,90	1,2	1,00	0,6	0,78	2,6	0,49	3,3	0,66	1,1	0,97	0,8	0,85
AT5G23020 MAM3	0,7	0,73	0,9	0,95	0,9	0,98	1,5	0,38	2,1	0,14	2,0	0,09	2,6	0,03
AT1G10550 XTH33	0,7	0,53	0,9	0,79	1,5	0,34	2,7	0,00	1,9	0,04	2,2	0,01	1,8	0,06
AT3G47710 BNQ3	0,6	0,23	1,9	0,02	3,0	0,00	3,5	0,00	2,9	0,00	3,2	0,00	3,0	0,00
AT1G05700	0,5	0,42	1,0	0,90	1,8	0,30	3,4	0,01	2,2	0,07	2,1	0,08	1,9	0,13

Figure 5: BiNGO analysis network constructed in Cytoscape. Network shows hubs of Biological processes found in the 272 differentially expressed genes from our selection with FC >2 and *p*-value < 0.05. Benjamini & Hochberg false discovery rate correction with *p*-value cutoff of 0.01. Color scale shows the corrected *p*-value of the biological process hubs. 65 genes of 272 total genes were discarded from the analysis because of lack of annotation. Circles mark the major biological process found as followed: **A.** Petal development, **B**. Regulation of anthocyanin metabolic process, **C.** Inorganic anion transport, **D.** Circadian rythm, **E.** Cytokinin response, **F.** Leucine biosynthetic process.

Table 2: GO enrichment analysis on the significant up-regulated genes at any time point. Table of Biological processes found in the 272 differentially expressed genes from our selection with FC >2 and *p*-value < 0.05. Benjamini & Hochberg false discovery rate correction with *p*-value cutoff of 0.01. 65 genes of 272 total genes were discarded from the analysis because of lack of annotation.

Biological process	Number of genes in biological process	p-value
cellular process	67	9,59E-1
metabolic process	62	9,55E-1
primary metabolic process	57	9,38E-1
response to stimulus	55	9,21E-1
cellular metabolic process	45	8,22E-1
biological regulation	36	7,86E-1
response to chemical stimulus	34	7,65E-1
regulation of biological process	28	7,46E-1
localization	26	6,81E-1
establishment of localization	26	6,46E-1
transport	26	6,20E-1
response to organic substance	26	6,11E-1
response to endogenous stimulus	25	4,25E-1
regulation of cellular process	24	4,20E-1
response to hormone stimulus	24	3,54E-1
regulation of metabolic process	22	3,06E-1
regulation of cellular metabolic process	21	2,89E-1
regulation of primary metabolic process	20	2,76E-1
multicellular organismal process	19	2,75E-1
developmental process	18	2,56E-1
multicellular organismal development	18	1,57E-1
biosynthetic process	17	1,48E-1
cellular biosynthetic process	17	1,43E-1
small molecule metabolic process	17	1,26E-1
cellular response to stimulus	14	1,24E-1
signaling	13	1,09E-1
anatomical structure development	12	9,34E-2
signaling pathway	12	8,50E-2
small molecule biosynthetic process	12	7,33E-2
ion transport	12	7,32E-2
system development	11	7,27E-2
organ development	11	7,00E-2
post-embryonic development	10	6,72E-2
cellular ketone metabolic process	10	6,72E-2
organic acid metabolic process	10	6,49E-2
oxoacid metabolic process	10	6,44E-2
carboxylic acid metabolic process	10	6,44E-2
cellular amino acid and derivative metabolic process	10	6,19E-2

cellular response to chemical stimulus	10	4,36E-2
cellular response to organic substance	10	1,65E-2
cellular response to endogenous stimulus	10	1,51E-2
cellular response to hormone stimulus	10	1,38E-2
hormone-mediated signaling pathway	10	1,37E-2
response to cytokinin stimulus	10	1,16E-2
nitrogen compound metabolic process	9	1,09E-2
cellular nitrogen compound metabolic process	9	8,35E-3
cellular response to cytokinin stimulus	8	5,66E-3
cytokinin mediated signaling pathway	8	2,84E-3
reproduction	7	2,66E-3
reproductive process	7	2,09E-3
reproductive developmental process	6	1,79E-3
reproductive structure development	6	1,60E-3
amine metabolic process	6	1,56E-3
cellular amine metabolic process	6	9,16E-4
organic acid biosynthetic process	6	4,04E-4
carboxylic acid biosynthetic process	6	4,04E-4
post-embryonic organ development	6	3,97E-4
rhythmic process	6	3,30E-4
circadian rhythm	6	2,10E-4
cellular nitrogen compound biosynthetic process	5	2,10E-4
cellular amino acid metabolic process	5	1,38E-4
flower development	5	9,79E-5
amine biosynthetic process	5	8,98E-5
floral organ development	5	6,35E-5
floral whorl development	5	5,45E-5
anion transport	5	4,88E-5
inorganic anion transport	5	1,94E-5
cellular amino acid biosynthetic process	4	5,96E-6
regulation of secondary metabolic process	3	5,96E-6
branched chain family amino acid metabolic process	3	4,15E-6
petal development	3	3,00E-6
corolla development	3	2,67E-7
regulation of anthocyanin metabolic process	3	2,13E-7
branched chain family amino acid biosynthetic process	3	2,31E-9
leucine metabolic process	3	2,31E-9
leucine biosynthetic process	3	1,24E-9

Known TMO5/LHW target genes are induced in the dGR dataset

To further validate our micro-array dataset, we studied the relative expression levels of known targets of the TMO5/LHW dimer in our dataset. Thus far only a handful of genes are shown to be direct target genes of TMO5/LHW: *LOG4* (Katayama, 2015; Vera-Sirera, 2015; De Rybel, et al., 2014); *AT4G38650/GH10* (Margo Smit and Bert De Rybel - unpublished work) and *SUPRESSOR OF AUCALIS5-LIKE3 (SACL3)*. SACL proteins control the activity of the TMO5/LHW dimer by binding to LHW, thereby titrating away LHW for the TMO5/LHW interaction (Katayama, 2015; Vera-Sirera, 2015; Imai, et al., 2006). The relative expression levels of these genes in our dataset are shown in **Figure 6**. *LOG4, GH10* and *SACL3* already show up-regulation after 0.5h and peak at 1h after of treatment. Validation of these expression levels was done by performing Q-RT-PCR on dGR roots harvested in a separate time course experiment using 0h, 2h, 4h and 6h time points. *LOG4, GH10* and *SACL3* were found to be increased by 7.7 fold, 9.8 fold and 2.7 fold, respectively after 2h of treatment (**Figure 6**) after which expression was reduced. Thus, the Q-RT-PCR data corresponded to the fold-changes and time points in the micro-array data, showing that our dataset reproduces the published responses upon TMO5/LHW induction.

TMO5/LHW induction leads to subsequent cytokinin biosynthesis and response

In order to have a more detailed look at cytokinin biosynthesis and subsequent response, marker lines for CK biosynthesis (p*LOG4*::n3xGFP) and CK signaling (pTCSn::tdTomato) were introduced into the dGR background. 5-day-old dGR roots of these lines were grown on DEX-free control plates and transferred to plates supplemented with 10µM DEX for 24h. DEX-free to DEX-free transfers were used as a control. The roots of these plants were fixed and cleared using ClearSee (Kurihara, et al., 2015) and stained with Calcofluor White (Ursache, et al., 2018). Next the roots were imaged using confocal microscopy (**Figure 7**). Induced p*LOG4* fused to a nuclear triple GFP fluorescent tag (n3GFP) roots showed ectopic expression mainly in the cortex cell layer and an overall increase in expression level. Similarly, induced pTCSn fused to a nuclear tandem-Tomato fluorescent protein (ntdT) roots showed ectopic expression throughout the root meristem and an increase in expression levels. It is worth noticing that pTCSn expression is absent in the ground tissues, while clear expression is observed upon inducing TMO5/LHW. Taken together, these results confirm that cytokinin biosynthesis and responses are increased in the
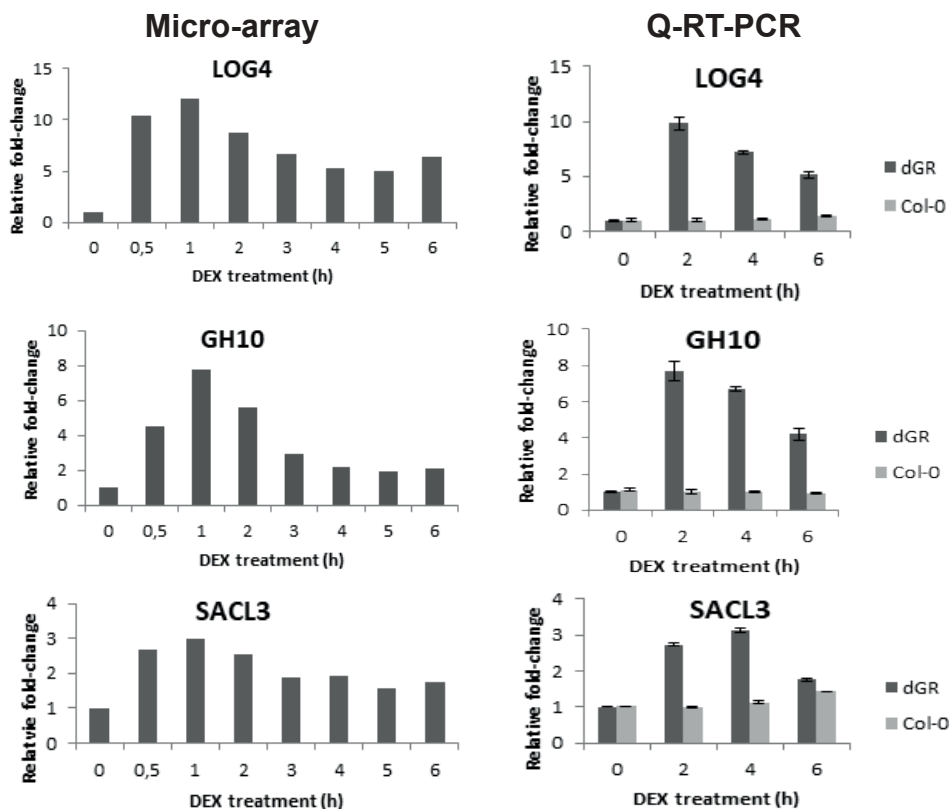
Figure 6: Q-RT-PCR validation of known TMO5/LHW induced genes. Left panels: transcriptome data showing relative fold-changes of *LOG4*, *GH10* and *SACL3* in dGR root tips from 0-6h after treatment on ½ MS supplemented with 10µM DEX. Right panel: Q-RT-PCR data using *EEF* and *CDKA* as reference genes showing relative fold-changes of *LOG4*, *GH10* and *SACL3* in roots of both *Col-0* and dGR from 0-6h after treatment on ½ MS supplemented with 10µM DEX.

root meristem, matching with published results in De Rybel, et al., 2014; Ohashi-Ito, et al., 2014. This further strengthens the validity of our transcriptomics dataset.

Although induction of the TCSn reporter is a good indication that cytokinin signaling is activated upon TMO5/LHW induction; up regulation of A-type A*RABIDOPSIS RESPONSE REGULATORS (ARRs)* provides better evidence. These A-type *ARR* genes act as negative regulators of the actual effectors of cytokinin signaling: B-type *ARRs* (To, et al., 2004). Some of these B-type *ARRs* have been shown to be involved in controlling vascular development as the *arr1,arr10,arr12* mutant has a reduced vascular bundle (Ishida, et al., 2008). Thus far, none of the existing datasets (De Rybel, et al., 2014; Ohashi-Ito, et al., 2014) have been able to show induction of the downstream A-type *ARR* genes. Due to the high temporal resolution of the dGR dataset, we found seven A-type *ARR* and one B-type *ARR* genes to be

transcriptionally up-regulated in the dataset (see **Table 4**) and we tested the relative expression levels of *ARR15* by Q-RT-PCR (**Figure 8**). We could see a clear increase in the *ARR15* transcript levels upon DEX treatment, suggesting that our dataset also captures the downstream cytokinin response.
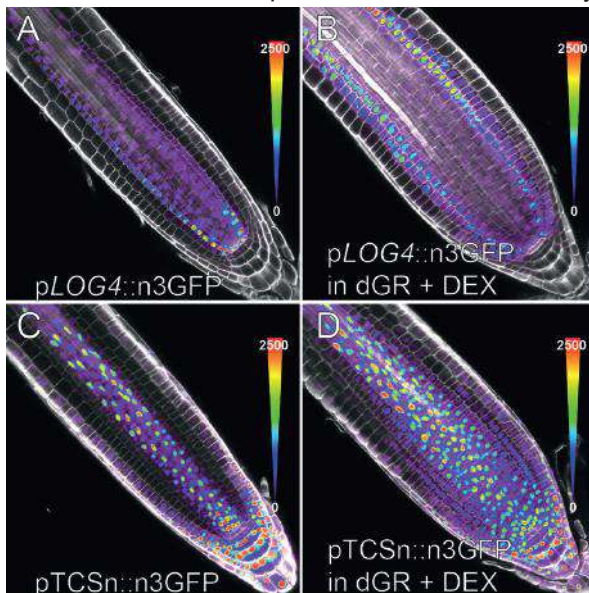
Figure 7: TMO5/LHW induction induces reporter lines for cytokinin biosynthesis and response. Confocal imaging of cytokinin biosynthesis and response using p*LOG4*::n3xGFP and pTCSn::ntdT crossed in the dGR background. **A** and **C** show the lines transferred from ½ MS to ½ MS. **B** and **D** show lines transferred from ½ MS to ½ MS containing 10µM DEX. Lines were imaged after 24h of treatment.
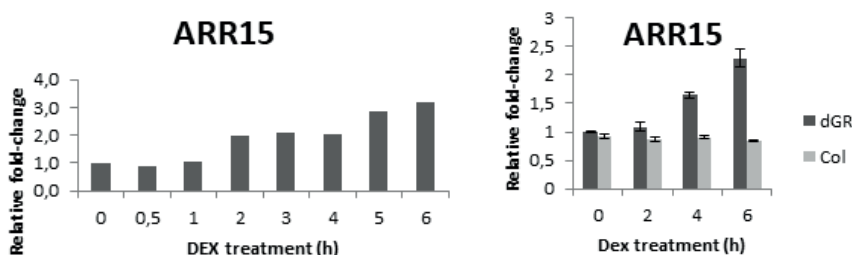
Figure 8: Q-RT-PCR validation of *ARR15* gene expression. Left panel: transcriptome data of *ARR15*. Right panel: Q-RT-PCR data using *EEF* and *CDKA* as reference genes.

A limited set of genes in the dGR dataset is cytokinin inducible

As our dataset allows detecting cytokinin response genes upon TMO5/LHW induction, we next wanted to evaluate how many of the TMO5/LHW induced genes are cytokinin inducible. In order to do so, we compared our list of 272 up-regulated

genes with the "Golden List" of 226 cytokinin regulated genes (Bhargava, et al., 2013), a list of ARR10 target genes (Zubo, et al., 2017) and a list of ARR1, ARR10, ARR12 target genes (Xie, et al., 2018). ARR1, ARR10 and ARR12 are the major B-type ARRs responsible for proper vascular development (Ishida, et al., 2008; Yokoyama, et al., 2007). A total of 70 genes were found in the overlaps between the different cytokinin datasets and the dGR dataset. Only 11 genes were found in the overlap amongst all these datasets (**Figure 9A** and **Supplemental Table 2**) and, as expected, several of these genes were A-type *ARR* genes (*ARR4, 5, 6, 9* and *15*) while the remaining genes belong to different gene families. This suggests that although dGR induction leads to cytokinin production via LOG4 throughout the root meristem, it results in the induction of a specific subset of cytokinin response genes. None of the other genes have thus far been reported to be involved in controlling PRD.
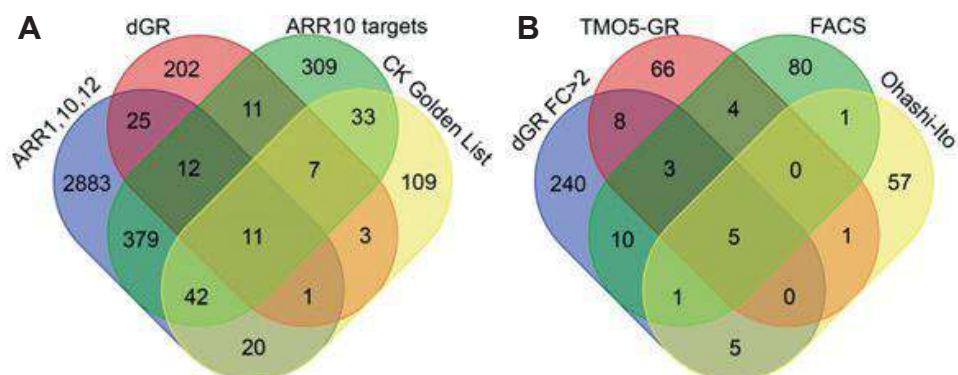
Figure 9: Overlap between the dGR dataset and published dataset related to TMO5/LHW. A. Overlap between dGR and CK golden list, and ARR10 target genes **B.** Overlap between dGR/DEX_ CHX/FACS and Ohashi-Ito dataset. dGR: List of 272 FC2> up-regulated genes after induction of both TMO5 and LHW. TMO5-GR: Genes differentially up-regulated FC2>2 in p*RPS5A*:TMO5:GR after induction of 1h on dexamethasone compared to mock treated. FACS: differentially regulated genes in J0571>>pUAS:TMO5:GR sorted ground tissue cells after 1h of induction. Ohashi-Ito: genes differentially regulated after 12h induction of TMO5 and LHW in *Arabidopsis* suspension cell.

The dGR dataset contains all known and putative novel regulators of PRD

Finally we compared our list of 272 up-regulated genes to previously published TMO5/ LHW related datasets; including a short term (1h) root based p*RPS5A*::*TMO5*:GR induction (Ohashi-Ito, et al., 2014; De Rybel, et al., 2013); a short term (1h) FACS sorted ground tissue cells (Ohashi-Ito, et al., 2014; De Rybel, et al., 2013) and a long term (12h) cell culture based p*MDC7*::*TMO5LIKE1* – p*MDC7*::*LHW*:GR induction system (Ohashi-Ito, et al., 2014; De Rybel, et al., 2013). Overlapping between all these sets were the expected candidates: *LOG4*, *GH10* and *uORF34* (an upstream open reading

frame at the 5' of *SACL3*) (**Figure 9B** and **Supplemental Table 3**). Furthermore, the overlap between the dGR and the Ohashi-Ito dataset contains *LOG3*, *ACL5* and 3 other genes. *LOG3* and *ACL5* were only lowly expressed in the other datasets therefor they do not overlap with all sets even though they are known downstream regulators. An overview of the other genes and overlaps are summarized in **Supplemental Table 3**.

Conclusion and discussion

In order to understand the downstream factors responsible for the TMO5/LHW dependent trigger of periclinal and radial cell division, we performed a whole genome transcriptomic analysis using a newly generated dGR line. Compared to the existing tools, this double inducible line generates both fast and homogeneous induction of PRD throughout the root meristem and thus provides the perfect tool for a high density temporal transcriptomic analysis.

Using a combination of Q-RT-PCR and reporter lines, we confirmed the early and strong induction of known target genes, including the cytokinin biosynthesis gene *LOG4* (Kuroha, et al., 2009). The subsequent induction of A-type *ARR* cytokinin response genes further strengthens the validity of our dataset. Intriguingly, we also observed the up-regulation of the B-type *ARR12* gene. As the *arr1/arr10/arr12* triple mutant is known to have a reduction in the amount of vascular cell files (Ishida, et al., 2008) and TMO5/LHW induction does not happen in the *wol* cytokinin perception mutant (Mahönen, et al., 2000), it would be good to investigate what part of the cytokinin signaling cascade is specifically required for the TMO5/LHW dependent induction of PRD.

Given the high temporal resolution, this dataset allows to sketch a detailed timeline of the subsequent transcriptional events that occur between TMO5/LHW heterodimer complex induction and the first actual PRD (**Figure 7**). As a first step, direct target genes *LOG4* and *GH10* were found to be induced within 30 minutes, with a peak at 1h after induction. Although not shown previously, the logical next step is activation of cytokinin signaling through B-type *ARR* genes. This is usually visualized at the transcriptional level through up regulation of A-type *ARR* genes, which are the negative regulators of the B-type *ARR* genes. We observed that at least eight A-type *ARR* genes start to be up-regulated after 2h of treatment and hit a plateau at 4h after treatment (**Figure 7**). As no other genes are currently known to be involved in PRD, it is difficult to speculate on the function of genes induced at later time point. Finally, confocal analysis has indicated that the first radial divisions already occur from 4h

after dexamethasone treatment onwards. Although cells will have to reorient their interphase microtubule arrays and undergo cytokinesis and cell division, this would still allow for additional waves of gene expression in-between cytokinin signaling (starting at 2h) and PRD (starting at 4h) (**Figure 7**). Following this hypothesis, by focusing on genes induced at the 3-4h time point, we might be able to find genes which are expressed downstream or at the same level of cytokinin response and thus might allow us to find cytokinin dependent and independent genes that are involved in PRD.

Although it is clear that cytokinin is required for the TMO5/LHW dependent induction of PRD (De Rybel, et al., 2014), exogenous cytokinin application does not result in similar over-proliferation phenotypes (Mahönen, et al., 2006). Thus, other cytokinin independent pathways will very likely be required for TMO5/LHW controlled PRD (**Figure 7**). For this class of genes, it is difficult to predict at what time points these might be induced, but a good time point to start investigating these non-cytokinin related genes would be the earlier 1-2h time points.
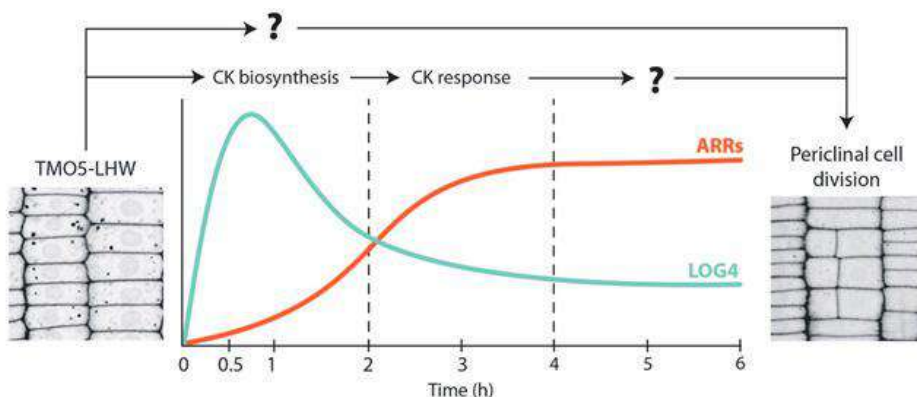
Figure 7: Model of genes down-stream of TMO5/LHW and time points of their induction in our obtained dataset. Cells in the root meristem receive the TMO5/LHW heterodimer complex induction. This quickly (0.5-1h) leads to up-regulated LOG4 levels which increased CK biosynthesis (cyan). Up-regulated CK biosynthesis is followed by increased *ARR* genes marking the cytokinin response (2-4h) (orange). However, what is down-stream of the cytokinin response genes that is shifting the division plane is thus far unknown (4-6h). Although these divisions CK plays an important role in this process it remains possible that a parallel pathway is necessary for shifting the division plane.

Besides the temporal aspects, the dGR line also allowed us to make some intriguing observations regarding the control on cell proliferation and cell division orientation. For example, although induction of TMO5/LHW in the dGR line results in fast and homogenous phenotypes at the plant and tissue level, it is interesting to note that not all cells undergo PRD at the same time upon TMO5/LHW induction. There are several reasons why this could be the case. First, it could be that cells need to be in the correct stage of the cell-cycle when perceiving

the TMO5/LHW signal in order to start dividing. Another explanation could be that the levels of TMO5/LHW protein are not sufficient upon induction to trigger PRD in a certain cell, or inhibitors further downstream are preventing PRD.

Furthermore, although prolonged induction of TMO5/LHW (e.g. 12-24h or even longer) resulted in an ever-increasing percentage of cells undergoing PRD, these roots continue some longitudinal growth. Indeed, mainly cells close to the QC still undergo AD, while most surrounding cells seem to be responding to the TMO5/LHW induction. It is known that the auxin controlled PLT genes are responsible for controlling the activity of the root meristem (Galinha, et al., 2007; Aida, et al., 2004). This observation is in line with the hypothesis that the auxin-dependent PLT pathway induces cells near the QC to undergo AD, while cells higher up in the root meristem have lower levels of auxin and PLTs and could thus undergo PRD through the TMO5/LHW pathway (De Rybel, et al., 2016).

Another interesting observation was that the first cells that divided after TMO5/LHW induction were in most cases cortex cells. It seems that these cells are more prone to the TMO5/LHW signal. One explanation for this is that auxin response (as reported by DR5V2) and cytokinin response (as reported by TCSn) are generally lower in the ground tissue, and especially in the cortex cells, compared to the other cell-types in the root meristem (Liao, et al., 2015; Zürcher, et al., 2013). As TCSn expression is strongly induced in cortex cells upon TMO5/LHW induction, and these cells usually have very low levels of cytokinin response, it is possible that this is the reason why cortex cells respond first.

Finally, one could imagine that if cells are suddenly forced to switch their division planes, this might in some cases result in oblique or partially formed division planes. As TMO5/LHW induction always leads to clean 90 degree switches in division plane orientation, we hypothesize that those cells responding to the PRD trigger are in a state in which they still have to position the preprophase band. It therefore also seems unlikely that TMO5/LHW would directly influence and/or disturbs the actual cell division machinery itself; but rather acts on the upstream (transcriptional) controlling mechanisms. It is remarkable that the overlap between the published data sets and our obtained dataset mainly consists of known targets, but that the remaining overlap is limited. One would expect that all the genes differentially expressed in e.g. the TMO5-GR set would be overlapping with the dGR dataset because the differentially expressed genes in the TMO5-GR set are early expressed genes upon TMO5 induction.

The fact that this does not seem to be the case, could be explained by the fact that TMO5/LHW acts as an obligate heterodimer and thus that the combined misexpression results in different transcriptional responses compared to the single misexpression. Alternatively, it could be due to the different set-up and materials that were sampled. The Ohashi-Ito data set is obtained by using cell cultures and thus TMO-LHW are induced in a different developmental context. Therefore one could expect a different transcriptional response, especially upon longer treatment. Furthermore, this also highlights the intriguing possibility that combined induction of TMO5 and LHW might result in a different transcriptional response compared to TMO5 or LHW single induction. A separate experiment would need to be set up in order to prove or disprove this hypothesis and is outside of the scope of this work.

In conclusion, in this chapter we have generated and validated a high temporal resolution dataset of the transcriptional events that occur upon TMO5/LHW induction. We will next use this repository to identify and unravel the downstream transcriptional networks that together control PRD.

Materials and Methods

Plant material and growth conditions

All seeds were surface sterilized, sown on solid on ½ MS plates without sucrose and vernalized for 24h at 4°C before growing in a growth room at 22°C in continuous light conditions. Ten-day old seedlings were transferred to soil and grown in green house conditions. Dexamethasone treatment was performed by either germinating seeds on 10μM dexamethasone supplemented medium or by transferring plants from ½ MS to 10μM dexamethasone supplemented medium and continuing growth for the indicated time. The dGR line was generated by crossing p*RPS5A*::*TMO5*:GR (De Rybel, et al., 2013) with p*RPS5A*::*LHW*:GR (see below). The A*rabidopsis thaliana* (L.) Heynh. Col-0 ecotype served as wild-type control. dGR marker lines of p*LOG4*::n3xGFP (De Rybel, et al., 2014), TCSn::tdT were generated by crosses.

Cloning and plant transformation

p*RPS5A*::*LHW*:GR construct was generated by extension PCR of *LHW* and GR using primers containing Ligation Independent Cloning (LIC) adapters. The obtained fragments were then cloned in the pPLV028 vector using LIC (Wendrich,

et al., 2015; De Rybel, et al., 2011). The pTCSn::ntdT-pDR5v2::n3xGFP (Liao, et al., 2015; Zürcher, et al., 2013) construct was generated by using PCR to generate both promoter fragments with LIC adapters. These were then cloned using LIC. All constructs were verified by sequencing and were transformed into Col-0 using simplified floral dipping (De Rybel, et al., 2011). All primer sequences used for cloning and sequencing can be found in **Supplemental Table 4**.

Plant imaging and image processing

Seedlings for DIC analysis were mounted in a solution of 20% glycerol 60% lactic acid. DIC microscopy was performed using an Olympus BX53 DIC microscope. For mPS-PI staining, roots were stained as described previously (Truernit, et al., 2008). Seedlings used in the marker line analysis were stained using the ClearSee protocol as described in Kurihara, et al., 2015). Cell walls in these seedlings were stained using a 0.1% Calcofluor White staining solution in ClearSee (Ursache, et al., 2018). Confocal microscopy was performed on Leica SP8 (63X) Zeiss LSM710 (63X) and Leica SP2 (63X) (all water corrected objective (NA 1.2) lenses) confocal microscopes. Calcofluor White, GFP, tandemTomato (tdT) and propidium iodide (PI) samples were imaged at an excitation of 405nm, 488nm, 561nm and 514nm respectively. Calcofluor White, GFP, tdT and PI were visualized at an emission of 425-475 nm, 500-535nm, 580-630nm and 600-700nm respectively. Quantifications for both root length analysis and cell file numbers were performed using the Image J software package.

Root length measurements

Root length analysis was performed by marking growth of roots (n=10 per sample) every 24h on ½ MS plates. Plates with markings were scanned after 10 days and lengths were measured using the Image J software package.

Quantification of cell numbers

Roots were fixed and stained using a modified Pseudo Schiff – Propidium Iodine (mPS-PI) staining (Truernit, et al., 2008). The stained roots were imaged by using confocal microscopy and radial cross-sections were taken in the middle of root meristem (defined as the middle between the first elongating cortex cells and the QC).

Box Plots

All box plots were generated using the BoxPlotR webtool using standard settings. Center lines represent the medians; box limits indicate the 25th and 75th percentiles as determined by R software; whiskers extend 1.5 times the interquartile range from the 25th and 75th percentiles, outliers are represented by dots.

Venn diagrams

Venn diagrams were generated using the PSB Venn Diagram webtool using symmetric and colored settings http://bioinformatics.psb.ugent.be/webtools/Venn/.

Q-RT-PCR

RNA was extracted using the RNeasy kit (Qiagen). Poly(dt) cDNA was generated from 1µg of total RNA using Superscript II reverse transcriptase (Invitrogen) and analyzed on a LightCycler 480 (Roche Molecular Systems, Inc) with SYBR Green I Master kit (Roche Diagnostics) according to manufacturer's instructions. Primer pairs were designed using Universal Probe Library Assay Design Center (Roche Molecular Systems, Inc). All primers used for Q-RT-PCR analysis can be found in **Supplemental Table 4**. All reactions were done in triplicate. Data was analyzed using qBase+ software package (Biogazelle). Expression levels were normalized to those of *EEF1α4* and *CDKA1;1*.

Micro-array and statistical analysis

p*RPS5A*::TMO5:GR x p*RPS5A*::LHW:GR (dGR) and Col-0 seeds were bleach sterilized and vernalized for 24h at 4°C. Seeds were sown on ½ MS plates and grown for 5 days in a growth room at 22°C. 5-day old plants of both Col-0 and dGR were transferred to ½ MS plates containing 10µM DEX and mock-plates and were sampled at the following time points: 0h, 0.5h, 1h, 2h, 3h, 4h, 5h and 6h. 300 individual root tips were sampled per sample and three biological repeats per time point were used. Root tips were harvested directly into liquid nitrogen, RNA was extracted using the RNeasy kit (Qiagen). Total RNA (100 ng) was labelled using an Ambion WT expression kit (Life Technologies) and hybridized to Arabidopsis Gene 1.0 ST arrays (Affymetrix), that probes the expression of 27,827 unique genes. Sample labelling; hybridization to chips and image scanning was performed according manufacturer's instructions. Microarray analysis was performed using MADMAX pipeline for statistical analysis

of microarray data (Lin, et al., 2011). Expression values were calculated using robust multichip average (RMA) method, which includes quantile normalisation (Bolstad, et al., 2003; Irizarry, et al., 2003). Probe sets on the array were redefined using current genome information (Dai, et al., 2005). In this study, probes were reorganized on the basis of the gene definitions as available in the TAIR10 database. Differentially expressed probe sets (genes) were identified by linear models and an intensity-based moderated t-statistic, taking into account the paired design (Sartor, et al., 2006). *P*-values were corrected for multiple testing by a false discovery rate method (Storey and Tibshirani, 2003), and probe sets that satisfied the criterion of $p < 0.05$ were considered to be significantly regulated. This yielded a list of 272 differentially up regulated genes with a fold change of two or more (FC >2) at any time point (**Table 1**).

Acknowledgements

References

Aida, M., Beis, D., Heidstra, R., Willemsen, V., Blilou, I., Galinha, C., Nussaume, L., Noh, Y.S., Amasino, R., and Scheres, B. (2004). The PLETHORA genes mediate patterning of the Arabidopsis root stem cell niche. Cell 119, 109-+.

Bhargava, A., Clabaugh, I., To, J.P., Maxwell, B.B., Chiang, Y.H., Schaller, G.E., Loraine, A., and Kieber, J.J. (2013). Identification of cytokinin-responsive genes using microarray meta-analysis and RNA-Seq in Arabidopsis. Plant physiology 162, 272-94.

Bolstad, B.M., Irizarry, R.A., Astrand, M., and Speed, T.P. (2003). A comparison of normalization methods for high density oligonucleotide array data based on variance and bias. Bioinformatics 19, 185-93.

Dai, M., Wang, P., Boyd, A.D., Kostov, G., Athey, B., Jones, E.G., Bunney, W.E., Myers, R.M., Speed, T.P., Akil, H., et al. (2005). Evolving gene/transcript definitions significantly alter the interpretation of GeneChip data. Nucleic Acids Research 33, e175.

De Rybel, B., Adibi, M., Breda, A.S., Wendrich, J.R., Smit, M.E., Novák, O., Yamaguchi, N., Yoshida, S., Van Isterdael, G., Palovaara, J., et al. (2014). Plant development. Integration of growth and patterning during vascular tissue formation in Arabidopsis. Science 345, 1255215.

De Rybel, B., Mahönen, A.P., Helariutta, Y., and Weijers, D. (2016). Plant vascular development: from early specification to differentiation. Nature reviews. Molecular cell biology 17, 30-40.

De Rybel, B., Möller, B., Yoshida, S., Grabowicz, I., Barbier de Reuille, P., Boeren, S., Smith, R.S., Borst, J.W., and Weijers, D. (2013). A bHLH complex controls embryonic vascular tissue establishment and indeterminate growth in Arabidopsis. Developmental cell 24, 426-37.

De Rybel, B., van den Berg, W., Lokerse, A., Liao, C.Y., van Mourik, H., Möller, B., Peris, C.L., and Weijers, D. (2011). A versatile set of ligation-independent cloning vectors for functional studies in plants. Plant physiology 156, 1292-9.

Galinha, C., Hofhuis, H., Luijten, M., Willemsen, V., Blilou, I., Heidstra, R., and Scheres, B. (2007). PLETHORA proteins as dose-dependent master regulators of Arabidopsis root development. Nature 449, 1053-1057.

Gunning, B.E., Hughes, J.E., and Hardham, A.R. (1978). Formative and proliferative cell divisions, cell differentiation, and developmental changes in the meristem of Azolla roots. Planta 143, 121-44.

Imai, A., Hanzawa, Y., Komura, M., Yamamoto, K.T., Komeda, Y., and Takahashi, T. (2006). The dwarf phenotype of the Arabidopsis acl5 mutant is suppressed by a mutation in an upstream ORF of a bHLH gene. Development 133, 3575-85.

Irizarry, R.A., Bolstad, B.M., Collin, F., Cope, L.M., Hobbs, B., and Speed, T.P. (2003). Summaries of Affymetrix GeneChip probe level data. Nucleic Acids Research 31, e15.

Ishida, K., Yamashino, T., Yokoyama, A., and Mizuno, T. (2008). Three type-B response

regulators, ARR1, ARR10 and ARR12, play essential but redundant roles in cytokinin signal transduction throughout the life cycle of Arabidopsis thaliana. Plant & cell physiology 49, 47-57.

Katayama, H.I., K.; Kariya, Y.; Asakawa, T.; Kan, T.; Fukuda, H.; Ohashi-Ito, K. (2015). A negative feedback loop controlling bHLH complexes is involved in vascular cell division and differentiation in the root apical meristem. Current biology : CB In press.

Kurakawa, T., Ueda, N., Maekawa, M., Kobayashi, K., Kojima, M., Nagato, Y., Sakakibara, H., and Kyozuka, J. (2007). Direct control of shoot meristem activity by a cytokinin-activating enzyme. Nature 445, 652-5.

Kurihara, D., Mizuta, Y., Sato, Y., and Higashiyama, T. (2015). ClearSee: a rapid optical clearing reagent for whole-plant fluorescence imaging. Development 142, 4168-79.

Kuroha, T., Tokunaga, H., Kojima, M., Ueda, N., Ishida, T., Nagawa, S., Fukuda, H., Sugimoto, K., and Sakakibara, H. (2009). Functional analyses of LONELY GUY cytokinin-activating enzymes reveal the importance of the direct activation pathway in Arabidopsis. The Plant cell 21, 3152-69.

Liao, C.Y., Smet, W., Brunoud, G., Yoshida, S., Vernoux, T., and Weijers, D. (2015). Reporters for sensitive and quantitative measurement of auxin response. Nature methods 12, 207-210.

Lin, K., Kools, H., de Groot, P.J., Gavai, A.K., Basnet, R.K., Cheng, F., Wu, J., Wang, X., Lommen, A., Hooiveld, G.J., et al. (2011). MADMAX - Management and analysis database for multiple ~omics experiments. J Integr Bioinform 8, 160.

Maere, S., Heymans, K., and Kuiper, M. (2005). BiNGO: a Cytoscape plugin to assess overrepresentation of gene ontology categories in biological networks. Bioinformatics 21, 3448-9.

Mahönen, A.P., Bishopp, A., Higuchi, M., Nieminen, K.M., Kinoshita, K., Tormakangas, K., Ikeda, Y., Oka, A., Kakimoto, T., and Helariutta, Y. (2006). Cytokinin signaling and its inhibitor AHP6 regulate cell fate during vascular development. Science 311, 94-8.

Mahönen, A.P., Bonke, M., Kauppinen, L., Riikonen, M., Benfey, P.N., and Helariutta, Y. (2000). A novel two-component hybrid molecule regulates vascular morphogenesis of the Arabidopsis root. Genes & development 14, 2938-43.

Matsumoto-Kitano, M., Kusumoto, T., Tarkowski, P., Kinoshita-Tsujimura, K., Vaclavikova, K., Miyawaki, K., and Kakimoto, T. (2008). Cytokinins are central regulators of cambial activity. Proceedings of the National Academy of Sciences of the United States of America 105, 20027-20031.

Nieminen, K., Blomster, T., Helariutta, Y., and Mahönen, A.P. (2015). Vascular Cambium Development. The Arabidopsis book / American Society of Plant Biologists 13, e0177.

Ohashi-Ito, K., Matsukawa, M., and Fukuda, H. (2013a). An atypical bHLH transcription factor regulates early xylem development downstream of auxin. Plant & cell physiology 54, 398-405.

Ohashi-Ito, K., Oguchi, M., Kojima, M., Sakakibara, H., and Fukuda, H. (2013b). Auxin-associated initiation of vascular cell differentiation by LONESOME HIGHWAY. Development 140, 765-9.

Ohashi-Ito, K., Saegusa, M., Iwamoto, K., Oda, Y., Katayama, H., Kojima, M., Sakakibara, H., and Fukuda, H. (2014). A bHLH complex activates vascular cell division via cytokinin action in root apical meristem. Current biology : CB 24, 2053-8.

Sartor, M.A., Tomlinson, C.R., Wesselkamper, S.C., Sivaganesan, S., Leikauf, G.D., and Medvedovic, M. (2006). Intensity-based hierarchical Bayes method improves testing for differentially expressed genes in microarray experiments. BMC Bioinformatics 7, 538.

Schena, M., Lloyd, A.M., and Davis, R.W. (1991). A steroid-inducible gene expression system for plant cells. Proceedings of the National Academy of Sciences of the United States of America 88, 10421-5.

Scheres, B., Dilaurenzio, L., Willemsen, V., Hauser, M.T., Janmaat, K., Weisbeek, P., and Benfey, P.N. (1995). Mutations Affecting the Radial Organization of the Arabidopsis Root Display Specific Defects Throughout the Embryonic Axis. Development 121, 53-62.

Scheres, B., Wolkenfelt, H., Willemsen, V., Terlouw, M., Lawson, E., Dean, C., and Weisbeek, P. (1994). Embryonic Origin of the Arabidopsis Primary Root and Root-Meristem Initials. Development 120, 2475-2487.

Schlereth, A., Möller, B., Liu, W., Kientz, M., Flipse, J., Rademacher, E.H., Schmid, M., Jürgens, G., and Weijers, D. (2010). MONOPTEROS controls embryonic root initiation by regulating a mobile transcription factor. Nature 464, 913-6.

Storey, J.D., and Tibshirani, R. (2003). Statistical significance for genomewide studies. Proceedings of the National Academy of Sciences of the United States of America 100, 9440-5.

To, J.P.C., Haberer, G., Ferreira, F.J., Deruere, J., Mason, M.G., Schaller, G.E., Alonso, J.M., Ecker, J.R., and Kieber, J.J. (2004). Type-A Arabidopsis response regulators are partially redundant negative regulators of cytokinin signaling. The Plant cell 16, 658-671.

Tokunaga, H., Kojima, M., Kuroha, T., Ishida, T., Sugimoto, K., Kiba, T., and Sakakibara, H. (2012). Arabidopsis lonely guy (LOG) multiple mutants reveal a central role of the LOG-dependent pathway in cytokinin activation. The Plant journal : for cell and molecular biology 69, 355-65.

Truernit, E., Bauby, H., Dubreucq, B., Grandjean, O., Runions, J., Barthélémy, J., and Palauqui, J.C. (2008). High-resolution whole-mount imaging of three-dimensional tissue organization and gene expression enables the study of Phloem development and structure in Arabidopsis. The Plant cell 20, 1494-503.

Ursache, R., Andersen, T.G., Marhavý, P., and Geldner, N. (2018). A protocol for combining fluorescent proteins with histological stains for diverse cell wall components. The Plant journal : for cell and molecular biology 93, 399-412.

Vera-Sirera, F.D.R., B.; Úrbez, C.; Kouklas, E.; Pesquera, M.; Álvarez-Mahecha, J. C.; Minguet, E. G.; Tuominen, H.; Carbonell, J.; Borst, J. W.; Weijers, D.; Blázquez, M. A. (2015). A bHLH-based feedback loop restricts vascular cell proliferation in plants. Developmental cell (accepted).

Weijers, D., Sauer, M., Meurette, O., Friml, J., Ljung, K., Sandberg, G., Hooykaas, P., and Offringa, R. (2005). Maintenance of embryonic auxin distribution for apical-basal patterning by PIN-FORMED-dependent auxin transport in Arabidopsis. The Plant cell 17, 2517-26.

Wendrich, J.R., Liao, C.Y., van den Berg, W.A., De Rybel, B., and Weijers, D. (2015). Ligation-independent cloning for plant research. Methods in molecular biology 1284, 421-31.

Xie, M.T., Chen, H.Y., Huang, L., O'Neil, R.C., Shokhirev, M.N., and Ecker, J.R. (2018). A B-ARR-mediated cytokinin transcriptional network directs hormone cross-regulation and shoot development (vol 9, 1604, 2018). Nature communications 9.

Yokoyama, A., Yamashino, T., Amano, Y., Tajima, Y., Imamura, A., Sakakibara, H., and Mizuno, T. (2007). Type-B ARR transcription factors, ARR10 and ARR12, are implicated in cytokinin-mediated regulation of protoxylem differentiation in roots of Arabidopsis thaliana. Plant & cell physiology 48, 84-96.

Yoshida, S., Barbier de Reuille, P., Lane, B., Bassel, G.W., Prusinkiewicz, P., Smith, R.S., and Weijers, D. (2014). Genetic control of plant development by overriding a geometric division rule. Developmental cell 29, 75-87.

Zubo, Y.O., Blakley, I.C., Yamburenko, M.V., Worthen, J.M., Street, I.H., Franco-Zorrilla, J.M., Zhang, W., Hill, K., Raines, T., Solano, R., et al. (2017). Cytokinin induces genome-wide binding of the type-B response regulator ARR10 to regulate growth and development in Arabidopsis. Proceedings of the National Academy of Sciences of the United States of America 114, E5995-E6004.

Zürcher, E., Tavor-Deslex, D., Lituiev, D., Enkerli, K., Tarr, P.T., and Muller, B. (2013). A robust and sensitive synthetic sensor to monitor the transcriptional output of the cytokinin signaling network in planta. Plant physiology 161, 1066-75.

Supplemental Information

Supplemental Table 1: *p*-values quantifications **Figure 1B** and **1D**.

	OE	LHW	T5	dGR
Fig 1B	0,0	0,004	0,000	0,000
Fig 1D	0,000	0,382	0,001	0,000

Supplemental Table 2: Overlapping genes ARR1,10,12 ChIP-seq targets, ARR10 targets, cytokinin Golden List and FC2> dGR dataset.

AGI	Description
AT3G48360	BT2
AT3G48100	ARR5
AT1G13740	AFP2
AT2G40970	myb family TF
AT1G03850	glutaredoxin family protein
AT5G47980	transferase family protein
AT3G57040	ARR9
AT1G74890	ARR15
AT1G10470	ARR4
AT5G62920	ARR6
AT3G27170	CLC-B

Supplemental Table 3: Overlapping genes of the following datasets FC2>, *pRPS5A*::*TMO5*:GR induction (1h), J0571 pUAS::*TMO5*-GR FACS sorted ground tissue cells (1h) and cell culture based p*MDC7*::*TMO5LIKE1* - p*MDC7*::*LHW:*GR dataset.

Datasets	Number of genes	AGI	Description
FACS Ohashi-Ito TMO5-GR dGR FC>2	5	AT1G29952	CPuORF34
FACS Ohashi-Ito TMO5-GR dGR FC>2		AT3G53450	unknown protein
FACS Ohashi-Ito TMO5-GR dGR FC>2		AT1G29950	transcription factor
FACS Ohashi-Ito TMO5-GR dGR FC>2		AT1G29951	CPuORF35
FACS Ohashi-Ito TMO5-GR dGR FC>2		AT4G38650	glycosyl hydrolase family 10 protein
FACS TMO5-GR dGR FC>2	3	AT2G40970	myb family transcription factor
FACS TMO5-GR dGR FC>2		AT4G20362	other RNA
FACS TMO5-GR dGR FC>2		AT2G37390	heavy-metal-associated domain-containing protein
FACS Ohashi-Ito dGR FC>2	1	AT2G26440	pectinesterase family protein
TMO5-GR dGR FC>2	8	AT2G43870	polygalacturonase, putative / pectinase, putative
TMO5-GR dGR FC>2		AT1G21651	protein binding / zinc ion binding
TMO5-GR dGR FC>2		AT4G17788	MIR160B
TMO5-GR dGR FC>2		AT4G00885	MIR165

TMO5-GR dGR FC>2		AT5G39080	transferase family protein
TMO5-GR dGR FC>2		AT5G09600	SDH3-1; succinate dehydrogenase
TMO5-GR dGR FC>2		AT5G07010	ST2A
TMO5-GR dGR FC>2		AT1G20530	unknown protein
FACS dGR FC>2	10	AT5G52450	MATE efflux protein-related
FACS dGR FC>2		AT1G08430	ALMT1
FACS dGR FC>2		AT4G14690	ELIP2
FACS dGR FC>2		AT2G44460	BGLU28
FACS dGR FC>2		AT3G45390	lectin protein kinase family protein
FACS dGR FC>2		AT1G35820	unknown protein
FACS dGR FC>2		AT3G17130	invertase/pectin methylesterase inhibitor family protein
FACS dGR FC>2		AT1G54680	unknown protein
FACS dGR FC>2		AT5G07460	PMSR2
FACS dGR FC>2		AT2G29330	TRI
Ohashi-Ito dGR FC>2	5	AT5G19530	ACL5
Ohashi-Ito dGR FC>2		AT5G66440	unknown protein
Ohashi-Ito dGR FC>2		AT1G04110	SDD1
Ohashi-Ito dGR FC>2		AT3G58035	pre-tRNA
Ohashi-Ito dGR FC>2		AT2G37210	
FACS TMO5-GR	4	AT3G23880	F-box family protein
FACS TMO5-GR		AT1G01110	IQD18
FACS TMO5-GR		AT4G28870	unknown protein
FACS TMO5-GR		AT4G01020	helicase domain-containing protein
Ohashi-Ito TMO5-GR	1	AT3G12220	scpl16
FACS Ohashi-Ito	1	AT3G04430	anac049

Supplemental Table 4: Primer list.

Cloning		
TCSn	fw	AGTTGGAATAGGATTTGACTAGTCAAAGATCTTTAAAAG
	rv	GTATGGAGTTGGATTTTGTTATATCTCCTTGGATCGATCC
LHW	fw	TAGTTGGAATAGGTTCATGGGAGTTT TACTAAGAGA AGC
	rv	AGTATGGAGTTGGGGTTCCATTGAACAGCCACCAGTAACCGG
GR	rv	AAAAAACTGCAGTCATTTTTGATGAAACAGAAGC

Q-RT-PCR		
CDKA	fw	ATTGCGTATTGCCACTCTCATAGG
	rv	TCCTGACAGGGATACCGAATGC
EEF	fw	CTGGAGGTTTTGAGGCTGGTAT
	rv	CCAAGGGTGAAAGCAAGAAGA
GH10	fw	AAGTTAAGGCGACGACAG
	rv	ATGATGCCAACTCTATACTCTC

LOG4	fw	GGTTTGATGGGTTTGGTTTCGC
	rv	CTACTGTTTCACCGGTCAACTCTC
SACL3	fw	CTTGAATGCTACCGATAT
	rv	AGGAAGTGAGTATAGAGG
ARR15	fw	GAGAACATACAACCTCGTATAGAACAA
	rv	GCTAATTTCACCGGTTTTAGCA

Supplemental Figure 1: Quantification of individual cell types dGR timecourse. Phloem cells could not be distinguished from cambium cells and thus are always counted as 8 cells.
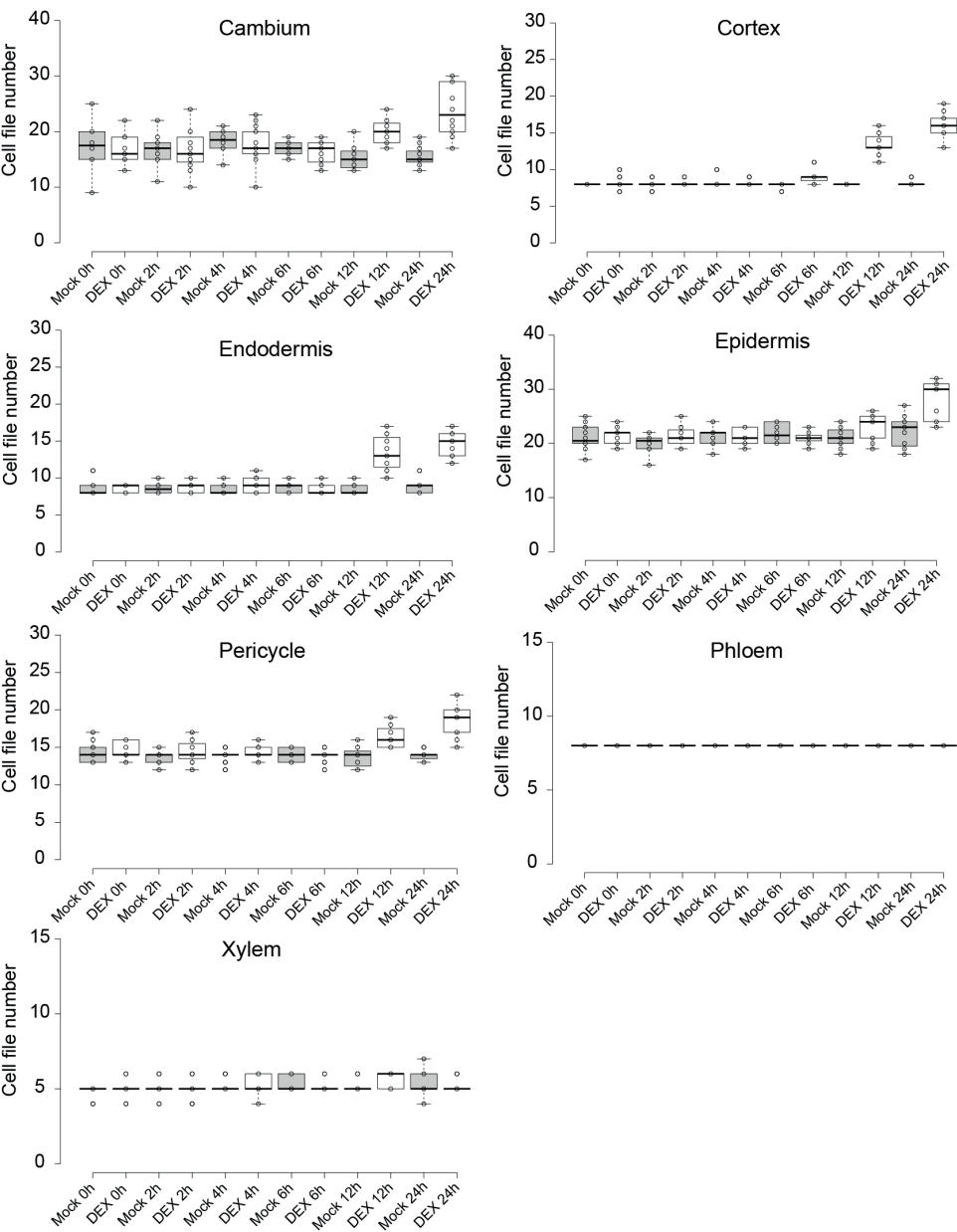
Chapter 4

The TMO5/LHW downstream target DOF2.1 promotes periclinal/radial cell proliferation

Wouter Smet[1,2,3], Iris Sevilem[4,5], Ykä Helariutta[4,5,6], Dolf Weijers[1] and Bert De Rybel[1,2,3]

1. Wageningen University, Laboratory of Biochemistry, Stippeneng 4, 6708 WE Wageningen, the Netherlands
2. Ghent University, Department of Plant Biotechnology and Bioinformatics, Technologiepark 927, 9052 Ghent, Belgium
3. VIB Center for Plant Systems Biology, Technologiepark 927, 9052 Ghent, Belgium
4. Institute of Biotechnology, University of Helsinki, Viikinkaari 5d, 00014 Helsinki, Finland
5. Department of Biological and Environmental Sciences, University of Helsinki, 00014 Helsinki, Finland
6. Sainsbury Laboratory, University of Cambridge, Bateman Street, Cambridge CB2 1LR, UK

Abstract

The TMO5 and LHW transcription factors dimerize to regulate a set of genes, culminating in the induction of periclinal and radial cell divisions (PRD) in *Arabidopsis* root tips. We have previously generated a transcriptomic dataset containing the downstream responses upon TMO5/LHW PRD. Here, we selected 55 target genes as potential candidates to be involved in controlling these divisions. Misexpression for one of these genes, the transcription factor DOF2.1, resulted in additional PRD throughout the root meristem and resulted in a shorter and thicker root, similar to TMO5/LHW misexpression. Loss-of-function of *DOF2.1* and its two closest homologs reduced PRDs in the primary root meristem. Furthermore, *DOF2.1* is cytokinin-inducible and expressed in cells around the protoxylem poles, suggesting it might respond to the TMO5/LHW-dependent CK biosynthesis. Interestingly, increasing CK levels results in an inhibition of protoxylem differentiation; which was not observed in misexpression of DOF2.1. In summary, these results suggest that DOF2.1 acts as a regulator of vascular cell proliferation downstream of TMO5/LHW and uncouples the induction of vascular cell proliferation from the inhibition of protoxylem differentiation. involved in controlling PRD. We identified DOF2.1 as a TMO5/LHW downstream factor capable of controlling PRD, without the pleiotropic effect on xylem differentiation.

Introduction

During evolution, the complexity and size of vascular tissues has increased tremendously. This has allowed vascular plants to grow to the sizes we can observe today. One plant-specific family of transcription factors (TFs) that is thought to have co-evolved with the increased complexity of the vascular tissues is the DNA-binding with one finger (Dof) gene family. In early-diverging land plants e.g. *Selaginella moellendorffii* and *Physcomitrella patens*, eight and nine Dof transcription factor genes have been found thus far, while in angiosperms an average of 30 Dof transcription factor genes can be found (Moreno-Risueno, et al., 2007). The model system used in this study, *Arabidopsis thaliana*, contains a total of 36 Dof TF genes.

Dof TFs are plant-specific and contain a zinc finger domain, consisting of a conserved region of 50 amino acids with a C2–C2 finger structure associated to a basic region that binds specifically to DNA. Furthermore they contain a bipartite nuclear localization domain that is highly conserved in the *Arabidopsis* Dof family (Krebs, et al., 2010). In *Arabidopsis thaliana*, the vast majority of these TFs have been found to be expressed in the vascular tissues (Le Hir and Bellini, 2013). Several of the Dof TFs have been described to be capable of moving from cell to cell (Chen, et al., 2013).

Dof TFs play a role in different stages of vascular development. *AtDof5.8* for example is already expressed during the embryogenesis and in young leaf primordia, flower buds and roots. It has been suggested that *AtDof5.8* plays a role in the early processes of vascular development (Konishi and Yanagisawa, 2007). Another TF that acts early during vascular development is *AtDof2.4,* which follows the expression of the early marker for procambium identity ATHB8 in the leaf (Scarpella, et al., 2004). Three other Dof factors: *AtDof2.1, AtDof4.6, and AtDof5.3/TMO6,* are also expressed in the root and in the pre-procambial cells during leaf vein development (Gardiner, et al., 2010). Nevertheless, the exact function of these Dof TFs described above remains unknown so far. Three other DOF TFs have been found to act during secondary development. AtDof5.6/HCA2 promotes interfascicular cambium formation, as the hca2 gain-of-function mutant shows premature formation of the interfascicular cambium (Guo, et al., 2009). Furthermore, this mutant shows increased cambial activity and high phloem proliferation, suggesting a function in (pro)cambium formation and/or divisions (Guo, et al., 2009). Two other Dof TFs AtDof3.4/OBP1 and AtDof2.3/CDF4 are suggested to control maintenance of cambium or cambium activity by affecting the cell cycle (Skirycz, et al., 2008). Recently it has been found that CDF4 promotes

differentiation and is repressed by WOX5, acting in opposite gradients (Pi, et al., 2015).

In the previous chapter, we generated a high-resolution transcriptomics dataset using a TMO5/LHW inducible line. Here we describe how we used this dataset to select and screen downstream genes of the TMO5/LHW dimer in order to identify factors involved in controlling PRD. We identified DOF2.1 as a TMO5/LHW downstream factor capable of controlling PRD, without the pleiotropic effect on xylem differentiation.

Results

Selecting genes downstream of TMO5/LHW involved in inducing PRD

In **Chapter 3**, we used a TMO5/LHW double inducible (dGR) line to generate a high-resolution dataset containing the detailed transcriptomic responses downstream of the TMO5/LHW dimer. We initially validated this dataset and identified sequential waves of gene expression. We established that the first wave of induced genes at the 0.5h-1h time point were direct target genes, including the cytokinin biosynthesis gene *LOG4*. This was followed by up-regulation of cytokinin response (marked by A-type *ARR* up regulation) around the 2h time point and reached a plateau at 4h of TMO5/LHW induction. Finally, the first actual PRD could be observed starting 4h-6h after induction. Given that it is currently unclear what downstream effectors execute the TMO5/LHW-dependent induction of PRD, we hypothesized that these could be amongst the genes induced around the 3h-4h time point. This is before the actual PRD occur, but after the initial wave of direct target genes and co-expressed with CK-responses. As such, we can predict to identify CK-induced genes, but also CK-unrelated targets induced at these time points. As described in the previous chapter, a list of genes with a fold change (FC) > 2 at any time point was generated. We focused on genes highly induced after 3h-4h of treatment to select genes for further screening. A list of 55 genes of interest was select and is shown in **Table 1,2**.

Because of the involvement of cytokinin in TMO5/LHW controlled PRD, we first focused on the cytokinin-regulated factors that were up-regulated upon TMO5/LHW induction. As described in the previous chapter, we compared a list of genes with a fold change (FC) > 2 at any time point with the "golden list" of cytokinin responsive factors (Bhargava, et al., 2013) and a list of ARR10 candidate target genes (Zubo, et al., 2017). From these we selected 14 genes based on their transcriptional profile and predicted expression patterns. These genes include a family of bHLH transcription factors, other types of TFs (MYB1C, HSR1, LBD4 and DOF2.1) and 5 other genes (**Table 3**).

Table 1: Target selection of 55 genes from dGR micro-array data and Q-RT-PCR validation. X marks plants screened in p*RPS5A* misexpression screen. ND marks samples where no data was obtained in the Q-RT-PCR validation.

Gene ID	Name	Description	Screened	MICRO-ARRAY FC 05h/0h	FC 01h/0h	FC 2h/0h	FC 3h/0h	FC 4h/0h	FC 5h/0h	FC 6h/0h	QPCR FC 2h/0h	FC 4h/0h	FC 6h/0h
AT1G67110	CYP735A2	CYP735A2 member of CYP709A	X	0,88	1,22	1,35	1,75	2,58	2,17	2,18	2,3	3,5	1,8
AT3G50300		HXXXD-type acyl-transferase family protein	X	0,91	1,83	1,90	2,54	2,52	2,90	2,78	0,9	1,8	1,7
AT1G31320	LBD4	LOB DOMAIN-CONTAINING PROTEIN 4	X	1,13	1,27	1,41	2,05	2,31	1,69	1,82	0,9	2,2	1,5
AT1G13740	AFP2	ABI FIVE BINDING PROTEIN 2 (AFP2)	X	1,16	1,58	2,15	2,08	2,20	2,25	2,12	1,5	1,7	1,3
AT1G13420	ATST4B	Encodes a sulfotransferase		1,02	0,84	1,05	2,07	1,98	1,73	1,86	1,5	4,7	3,2
AT5G51780	bHLH36	basix helix-loop-helix (bHLH) protein	X	0,96	1,68	2,52	3,38	3,06	3,67	3,02	1,32	2,91	1,79
AT5G51790	bHLH120	basix helix-loop-helix (bHLH) protein	X	1,26	1,68	2,13	2,02	2,17	2,38	2,95	1,41	2,58	1,53
AT1G62975	bHLH125	basix helix-loop-helix (bHLH) protein	X	1,02	1,31	1,70	2,53	2,51	2,31	2,33	0,97	2,49	1,33
AT4G25410	bHLH126	basix helix-loop-helix (bHLH) protein	X	0,94	1,08	1,74	1,78	1,72	2,04	2,49	1,38	2,47	1,34
AT2G40970	MYBC1	myb family transcription factor	X	2,23	2,50	2,26	1,96	1,70	1,77	1,95	2,01	1,79	1,38
AT1G13300	HRS1	myb family transcription factor	X	0,87	1,11	1,38	2,42	2,33	2,22	2,12	1,29	2,09	1,15
AT2G13960		myb family transcription factor		0,76	0,42	0,79	2,02	0,68	1,01	0,62	ND	ND	ND
AT3G46130	MYB48	myb family transcription factor	X	1,20	1,34	1,17	1,30	1,42	1,63	2,02	1,19	1,82	1,19
AT2G47460	MYB12	myb family transcription factor	X	1,10	1,24	1,30	1,67	1,68	1,91	2,08	0,56	1,61	1,99
AT5G59680		leucine-rich repeat protein kinase	X	0,93	0,82	1,48	2,88	2,98	2,82	2,67	ND	ND	ND
AT4G20450		leucine-rich repeat protein kinase	X	1,19	1,41	2,21	3,30	2,20	2,89	2,57	1,76	2,30	1,05
AT3G46340		leucine-rich repeat protein kinase		0,76	1,02	1,40	1,44	1,53	1,51	2,35	ND	ND	ND
AT1G07560		leucine-rich repeat protein kinase	X	0,86	0,76	1,29	2,17	1,84	1,82	2,08	0,99	1,28	0,64
AT2G28990		leucine-rich repeat protein kinase	X	1,18	1,06	1,35	1,87	1,78	1,90	2,04	1,10	1,83	1,08
AT1G05700		leucine-rich repeat protein kinase	X	0,51	0,98	1,79	3,36	2,20	2,10	1,87	1,53	1,96	1,02
AT5G16900		leucine-rich repeat protein kinase	X	1,19	1,43	1,92	2,64	2,14	2,08	1,74	1,33	2,27	1,34
AT5G49770		leucine-rich repeat protein kinase		0,91	1,09	1,19	2,44	2,13	1,89	2,46	ND	ND	ND
AT4G39070	BZS1	zinc finger (B-box type) protein	X	0,90	1,24	1,68	2,08	2,10	2,10	2,07	0,70	2,28	1,67
AT3G10910	DAFL1	zinc finger (C3HC4-type RING finger) protein	X	1,26	1,22	1,27	1,79	1,56	1,88	2,15	0,80	1,71	1,17
AT1G67340		zinc finger (MYND type) protein	X	1,58	1,95	2,13	1,97	1,92	2,33	1,93	1,34	1,53	1,24
AT2G20080	TIE2	unknown	X	0,87	1,45	2,27	3,56	3,12	3,22	3,30	0,85	2,78	1,66
AT4G29905		unknown	X	1,35	1,31	1,30	2,15	2,50	2,44	2,84	0,52	1,58	0,96
AT1G03240		unknown		1,88	1,40	2,05	2,32	2,66	2,31	2,78	ND	ND	ND
AT3G18450		unknown	X	0,87	1,05	1,87	3,29	2,99	2,88	2,67	1,23	2,42	1,21
AT3G51540		unknown	X	1,12	1,21	1,45	2,23	2,01	2,20	2,39	1,40	2,66	1,41
AT5G67620		unknown	X	1,20	1,34	1,99	2,77	2,46	2,54	2,39	1,16	2,43	1,48
AT3G46880		unknown	X	1,28	1,48	1,26	1,72	2,28	1,87	2,32	0,67	1,87	1,52
AT5G57887		unknown	X	1,66	1,57	1,99	1,90	2,21	2,16	2,24	1,54	1,86	1,24
AT3G59340		unknown	X	1,22	1,24	1,38	1,50	1,63	2,00	2,23	1,31	2,57	1,44
AT5G19970		unknown	X	0,94	1,04	1,20	1,92	1,96	1,73	2,21	0,74	1,47	0,83
AT1G74458		unknown	X	1,34	1,23	1,48	1,81	2,02	1,69	2,14	1,71	2,17	1,46
AT4G29310		unknown	X	0,88	1,18	1,69	1,84	2,20	1,99	2,12	1,13	1,95	1,75
AT5G03995		unknown	X	0,88	1,04	1,74	2,35	2,02	2,03	2,10	ND	ND	ND
AT1G68500		unknown	X	0,90	1,36	1,23	1,83	1,61	1,89	2,01	1,11	2,23	1,58
AT3G05936		unknown	X	1,05	0,93	1,34	2,14	1,73	1,79	1,98	1,06	3,22	2,83
AT3G01730		unknown	X	0,95	1,06	1,25	2,50	2,14	1,88	1,92	3,12	3,35	2,28
AT2G22122		unknown	X	0,83	1,02	1,13	1,61	1,99	2,00	1,75	0,75	0,93	0,60
AT4G03420		unknown	X	1,17	1,53	1,36	2,41	1,64	1,49	1,75	1,23	1,46	1,18
AT1G02380		unknown	X	1,29	1,30	1,42	2,06	1,81	1,80	1,66	2,37	2,28	1,53
AT5G18661		unknown	X	1,40	1,44	1,41	2,01	1,78	1,40	1,57	0,96	1,69	0,94

Annotation								ND	ND	ND
unknown	1,45	1,21	1,72	2,06	1,65	1,54	1,53	1,70	2,36	1,48
unknown (X)	0,72	1,35	1,36	2,69	1,71	1,20	1,48	1,95	1,02	1,23
unknown (X)	1,35	1,53	1,38	1,54	1,57	2,02	1,34	1,35	0,89	0,35
unknown (X)	1,23	1,46	2,72	2,15	1,56	1,12	1,04	3,61	1,21	0,28
unknown (X)	0,96	1,27	2,52	4,38	1,58	0,99	0,96			
manganese ion binding / nutrient reservoir (X)	0,80	1,64	2,58	6,39	6,12	5,37	4,85	3,25	2,71	2,00
B-S glucosidase 44 (X)	0,91	1,28	4,33	4,17	4,55	5,31	6,08	3,27	5,10	4,37

BGLU44

Table 2: *p*-values of Target selection of 55 genes from dGR micro-array data and Q-RT-PCR validation. X marks plants screened in p*RPS5A* misexpression screen. ND marks samples where no data was obtained in the Q-RT-PCR validation.

Gene ID	Name	Description	Screened	MICRO-ARRAY							QPCR		
				FC 05h/0h	FC 01h/0h	FC 2h/0h	FC 3h/0h	FC 4h/0h	FC 5h/0h	FC 6h/0h	FC 2h/0h	FC 4h/0h	FC 6h/0h
AT1G67110	CYP735A2	CYP735A2 member of CYP709A	X	0.92	0.80	0.64	0.08	0.00	0.01	0.01	0.06	0.10	0.04
AT3G50300		HXXXD-type acyl-transferase family protein	X	0.92	0.03	0.01	0.00	0.00	0.00	0.01	0.02	0.05	0.08
AT1G31320	LBD4	LOB DOMAIN-CONTAINING PROTEIN 4	X	0.87	0.61	0.26	0.00	0.00	0.02	0.01	0.05	0.07	0.04
AT1G13740	AFP2	ABI FIVE BINDING PROTEIN 2 (AFP2)	X	0.83	0.17	0.01	0.00	0.00	0.00	0.00	0.03	0.21	0.04
AT1G13420	ATST4B	Encodes a sulfotransferase	X	0.99	0.73	0.94	0.00	0.00	0.01	0.00	0.05	0.41	0.06
AT5G51780	bHLH36	basix helix-loop-helix (bHLH) protein	X	0.99	0.25	0.01	0.00	0.00	0.00	0.00	0.03	0.04	0.01
AT5G51790	bHLH120	basix helix-loop-helix (bHLH) protein	X	0.65	0.05	0.00	0.00	0.00	0.00	0.00	0.02	0.14	0.01
AT1G62975	bHLH125	basix helix-loop-helix (bHLH) protein	X	1.00	0.37	0.01	0.00	0.00	0.00	0.00	0.05	0.03	0.03
AT4G25410	bHLH126	basix helix-loop-helix (bHLH) protein	X	0.95	0.94	0.06	0.02	0.04	0.01	0.00	0.01	0.04	0.04
AT2G40970	MYBC1	myb family transcription factor	X	0.00	0.00	0.00	0.00	0.00	0.00	0.00	0.03	0.09	0.03
AT1G13300	HRS1	myb family transcription factor	X	0.86	0.95	0.37	0.00	0.00	0.00	0.00	0.04	0.06	0.01
AT2G13960		myb family transcription factor	X	0.96	0.54	0.95	0.36	0.72	0.96	0.65	ND	ND	ND
AT3G46130	MYB48	myb family transcription factor	X	0.82	0.57	0.76	0.33	0.20	0.10	0.01	0.02	0.04	0.04
AT2G47460	MYB12	myb family transcription factor	X	0.88	0.51	0.27	0.01	0.01	0.00	0.00	0.01	0.06	0.05
AT5G59680		leucine-rich repeat protein kinase		0.99	0.95	0.57	0.04	0.04	0.05	0.06	ND	ND	ND
AT4G20450		leucine-rich repeat protein kinase	X	0.86	0.75	0.10	0.00	0.05	0.01	0.02	0.10	0.28	0.09
AT3G46340		leucine-rich repeat protein kinase		0.82	0.99	0.65	0.34	0.28	0.29	0.03	ND	ND	ND
AT1G07560		leucine-rich repeat protein kinase	X	0.92	0.70	0.58	0.01	0.03	0.03	0.01	0.05	0.03	0.01
AT2G28990		leucine-rich repeat protein kinase	X	0.77	0.92	0.26	0.00	0.01	0.00	0.00	0.04	0.08	0.05
AT1G05700		leucine-rich repeat protein kinase	X	0.42	0.90	0.30	0.01	0.07	0.08	0.13	0.02	0.06	0.01
AT5G16900		leucine-rich repeat protein kinase	X	0.80	0.44	0.06	0.00	0.01	0.02	0.05	0.10	0.25	0.04
AT5G49770		leucine-rich repeat protein kinase		0.93	0.93	0.80	0.00	0.01	0.03	0.00	ND	ND	ND
AT4G39070	BZS1	zinc finger (B-box type) protein	X	0.89	0.57	0.01	0.00	0.00	0.00	0.00	0.02	0.06	0.04
AT3G10910	DAFL1	zinc finger (C3HC4-type RING finger) protein	X	0.63	0.61	0.41	0.01	0.03	0.00	0.00	0.01	0.05	0.02
AT1G67340		zinc finger (MYND type) protein	X	0.17	0.01	0.00	0.00	0.00	0.00	0.00	0.07	0.17	0.03
AT2G20080	TIE2	unknown	X	0.80	0.15	0.00	0.00	0.00	0.00	0.00	0.02	0.18	0.17
AT4G29905		unknown	X	0.65	0.65	0.51	0.01	0.00	0.00	0.00	0.04	0.04	0.05
AT1G03240		unknown		0.53	0.79	0.24	0.06	0.05	0.07	0.03	ND	ND	ND
AT3G18450		unknown	X	0.85	0.97	0.03	0.00	0.03	0.00	0.04	0.03	0.06	0.02
AT3G51540		unknown	X	0.87	0.72	0.28	0.00	0.01	0.00	0.00	0.02	0.06	0.04
AT5G67620		unknown	X	0.65	0.17	0.00	0.00	0.00	0.00	0.00	0.02	0.07	0.03
AT3G46880		unknown	X	0.62	0.17	0.45	0.01	0.00	0.00	0.00	0.05	0.05	0.13
AT5G57887		unknown	X	0.21	0.21	0.01	0.01	0.00	0.00	0.00	0.04	0.04	0.01
AT3G59340		unknown	X	0.78	0.71	0.32	0.08	0.05	0.00	0.00	0.05	0.12	0.02
AT5G19970		unknown	X	0.93	0.98	0.83	0.03	0.02	0.06	0.01	0.04	0.03	0.03
AT1G74458		unknown	X	0.42	0.54	0.07	0.00	0.00	0.01	0.00	0.05	0.04	0.02
AT4G29310		unknown	X	0.78	0.65	0.01	0.00	0.00	0.00	0.00	0.05	0.07	0.06
AT5G03995		unknown		0.85	0.96	0.01	0.00	0.00	0.00	0.00	ND	ND	ND
AT1G68500		unknown	X	0.96	0.65	0.73	0.08	0.21	0.06	0.04	0.06	0.04	0.08
AT3G05936		unknown	X	0.97	0.95	0.41	0.00	0.03	0.02	0.01	0.03	0.27	0.07
AT3G01730		unknown	X	0.99	0.93	0.60	0.00	0.01	0.02	0.02	0.07	0.11	0.05
AT2G22122		unknown	X	0.81	0.98	0.80	0.06	0.01	0.01	0.02	0.02	0.03	0.01
AT4G03420		unknown	X	0.92	0.63	0.67	0.02	0.26	0.34	0.16	0.10	0.11	0.02
AT1G02380		unknown	X	0.75	0.64	0.40	0.01	0.04	0.04	0.08	0.09	0.09	0.08
AT5G18661		unknown	X	0.51	0.35	0.27	0.01	0.02	0.17	0.06	0.02	0.15	0.02
AT3G04440		unknown		0.80	0.96	0.45	0.18	0.45	0.40	0.41	ND	ND	ND
AT1G27020		unknown	X	0.38	0.30	0.21	0.01	0.01	0.36	0.03	0.03	0.04	0.02
AT3G50610		unknown	X	0.82	0.72	0.67	0.43	0.34	0.15	0.55	0.07	0.03	0.03
AT1G07690		unknown	X	0.89	0.64	0.02	0.04	0.25	0.81	0.95	0.03	0.03	0.01

Gene ID	Name	Description												
AT1G54950		unknown	x	0.98	0.71	0.00	0.00	0.17	1.00	0.93	0.08	0.02	0.02
AT5G38940		manganese ion binding / nutrient reservoir	x	0.91	0.73	0.12	0.00	0.00	0.00	0.00	0.08	0.05	0.09
AT3G18080	BGLU44	B-S glucosidase 44	x	0.97	0.81	0.00	0.00	0.00	0.00	0.00	0.07	0.14	0.20
AT5G61650	CYCP4;2	P-type cyclin	x	0.86	0.95	0.97	0.17	0.17	0.13	0.03	0.07	0.06	0.070
AT5G07450	CYCP4;3	P-type cyclin	x	0.83	1.00	0.47	0.01	0.20	0.01	0.01	0.09	0.12	0.049
AT2G28510	DOF2.1	DOF-transcription factor	x	0.91	0.04	0.00	0.00	0.00	0.00	0.00	0.02	0.06	0.01

Furthermore, it is possible that factors parallel to the cytokinin response are required to control the divisions. To capture these as well, we selected 39 other genes based on being part of overrepresented gene families in our list of differential expressed genes with FC2 > 2 at any time point. This added 8 leucine-rich repeat genes, 3 Myb-domain TFs, 2 zinc finger proteins, 2 P-type cyclins (although not FC>2) and other 5 genes to our selection. Next, we included 23 unknown genes which are not present on the commonly used ATH1 arrays and therefore unexplored. Selection of these genes was done by taking the top up regulated genes at the 4h time point.

Selected target genes were validated by Q-RT-PCR on dGR root tips from a separate dexamethasone treated time course experiment using 0h, 2h, 4h and 6h time points (**Table 1,2**). All genes showed similar relative expression at 4h after treatment compared to the micro-array results, confirming that these selected genes are putative downstream regulators.

Table 3: Selected cytokinin regulated genes.

AGI	Name	Description
AT1G67110	CYP735A2	CYP735A2 member of CYP709A
AT3G50300		HXXXD-type acyl-transferase family protein
AT1G31320	LBD4	LOB DOMAIN-CONTAINING PROTEIN 4
AT1G13740	AFP2	ABI FIVE BINDING PROTEIN 2 (AFP2)
AT1G13420	ATST4B	Encodes a sulfotransferase
AT5G51780	bHLH36	basix helix-loop-helix (bHLH) protein
AT5G51790	bHLH120	basix helix-loop-helix (bHLH) protein
AT4G25410	bHLH126	basix helix-loop-helix (bHLH) protein
AT2G40970	MYBC1	myb family transcription factor
AT1G13300	HRS1	myb family transcription factor
AT4G39070	BZS1	zinc finger (B-box type) protein
AT3G10910	DAFL1	zinc finger (C3HC4-type RING finger) protein
AT2G20080	TIE2	unknown
AT3G59340		unknown
AT2G28510	DOF2.1	DOF-transcription factor

DOF2.1 misexpression induces PRD without pleiotropic effects on protoxylem differentiation

Given that we are searching for downstream effectors of the TMO5/LHW-dependent induction of PRD, it is plausible that these would be responsible for (part of the) observed phenotype. We thus took the approach to validate the involvement of
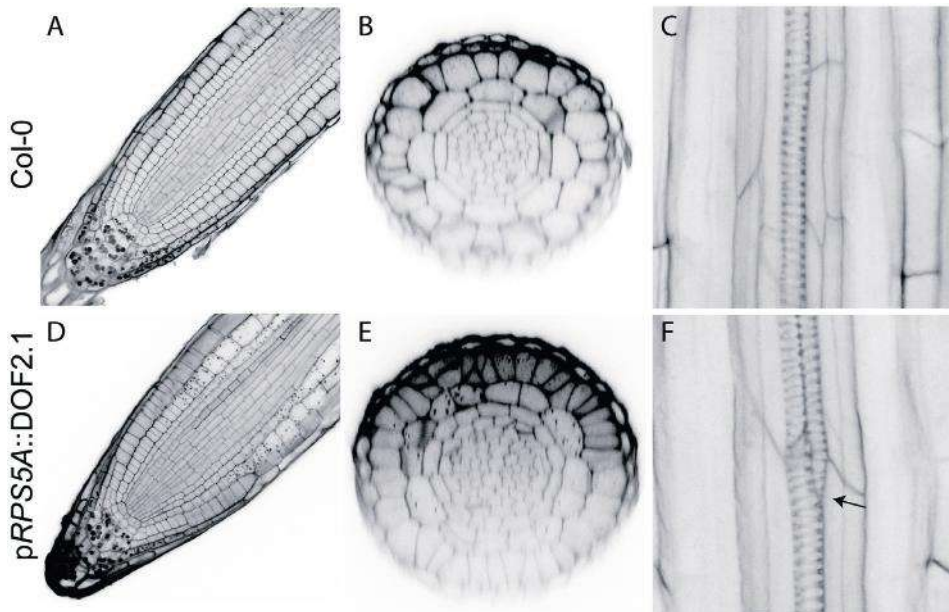
Figure 1: DOF2.1 misexpression causes additional PRD in the primary root meristem. A-C. Col-0 control, **D-E.** p*RPS5A*::*DOF2.1*. **A,D.** show longitudinal cross-sections of the root meristem using confocal microscopy. **B,E.** show radial cross-sections taken in the middle of the root meristem using confocal microscopy. **C,F.** show confocal images of the mature part of the root containing differentiated vasculature. Arrow in **F** indicates the point where the protoxylem gains an additional differentiated cell file.

our selected genes by driving these factors using the strong meristematic *RPS5A* promoter (Weijers, et al., 2001) and screening for altered division planes and disrupted organization of the primary root meristem by screening longitudinal sections using confocal microscopy. More general defects in root vascular development, architecture and anatomy were analyzed using differential interference contrast (DIC) light microscopy. Out of the 55 selected genes, 47 were successfully cloned and transformed into *Arabidopsis thaliana* (**Table 1**). Interestingly, only misexpression of DOF2.1 resulted in a strong phenotype, including a shorter and thicker root meristem compared to Col-0 (**Figure 1A,D**). Confocal cross-sections of p*RPS5A*::*DOF2.1* primary root meristems revealed that the increase in thickness was caused by additional PRD in almost all cell types throughout the root meristem (**Figure 1B,E**), similar to the TMO5/LHW misexpression phenotype. Thus, although it is possible we might have missed important genes using this approach, it has been successful to identify putative effectors downstream of TMO5/LHW.

The additional cell division in the p*RPS5A*::*DOF2.1* root also resulted in additional protoxylem cell files in the younger parts of the root (**Figure 1 C,F**). In the older part of the root, vascular organization was normal and protoxylem differentiated

as in WT roots (**Figure 1C,F**). This is intriguing, as TMO5/LHW misexpression prevents protoxylem differentiation, through LOG3/4-dependent CK biosynthesis (De Rybel, et al., 2014; Ohashi-Ito, et al., 2014). These results thus suggest that DOF2.1 uncouples the TMO5/LHW-dependent effects on PRD from the effects on protoxylem differentiation by acting downstream of CK signalling.

Levels of DOF2.1 affect the amount of PRD

To study the additional divisions caused by DOF2.1 misexpression in more detail we generated p*RPS5A*::*DOF2.1*:GR and p*WOL*-XVE::*DOF2.1* inducible lines. In the p*WOL*-XVE::*DOF2.1* inducible line, the promoter of *WOODENLEG* (*WOL*) is used to drive DOF2.1 expression only in the vasculature (**Figure 2A,C**). Treatment of p*WOL*-XVE::*DOF2.1* five-day-old seedlings with 10µM estradiol for 24h resulted in additional divisions within the vasculature and the surrounding endodermis layer when compared to untreated plants transferred to control medium (**Figure 2 B,D**). As the endodermis cells readily divide under stressed conditions, it is likely that the additional PRDs in this layer are caused by pressure of the expanding
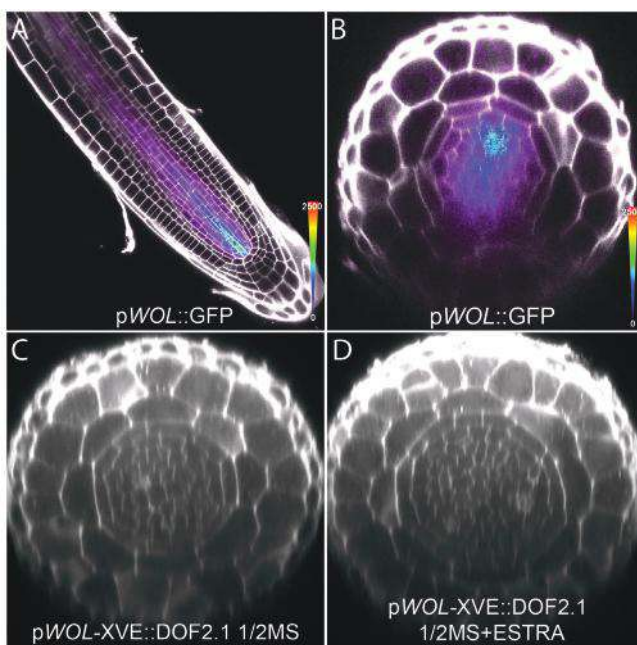
Figure 2: **Vascular specific overexpression of DOF2.1 causes vascular proliferation only. A.** expression of p*WOL*::GFP in the root meristem, **B.** expression of p*WOL*::GFP in a radial cross-section of the root meristem. **C.** radial cross-sections a root 5-DAG transferred from ½ MS to ½ MS for 24h. **D** radial cross-sections of a root transferred from ½ MS to ½ MS + 10µM estradiol for 24h.
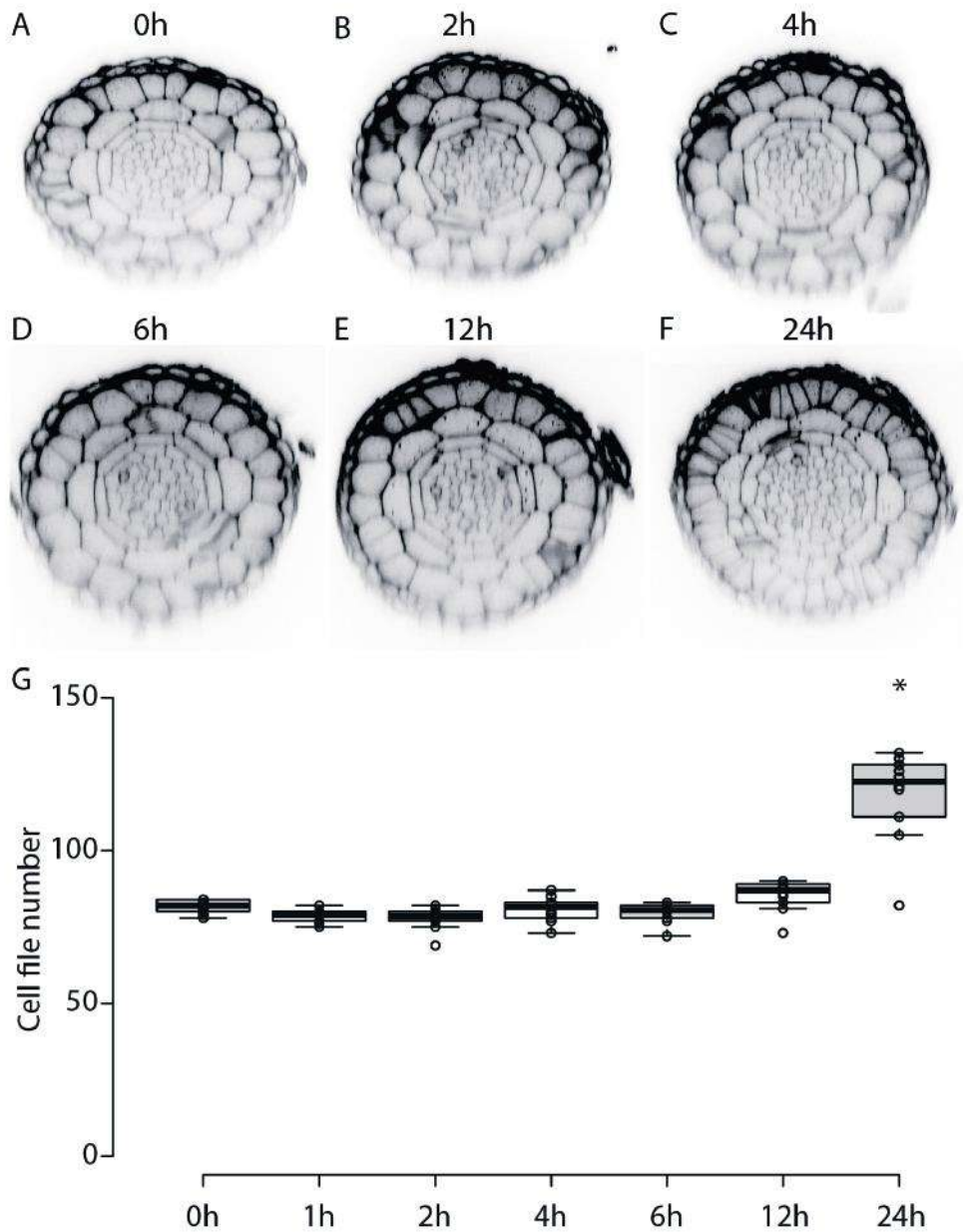
Figure 3: Temporal aspects of DOF2.1 dependent induction of PRD on 5-day old *pRPS5A::DOF2.1*:GR roots. A-F. showing radial cross-sections of roots transferred from ½ MS to ½ MS + 10μM DEX. **G.** Box plot showing total cell file number in root cross-sections of p*RPS5A*::*DOF2.1*:GR treated with dexamethasone. Asterisk marks significance compared to the 0h time point according to a two-sided Student T-test ($p < 0.05$) (n>10).
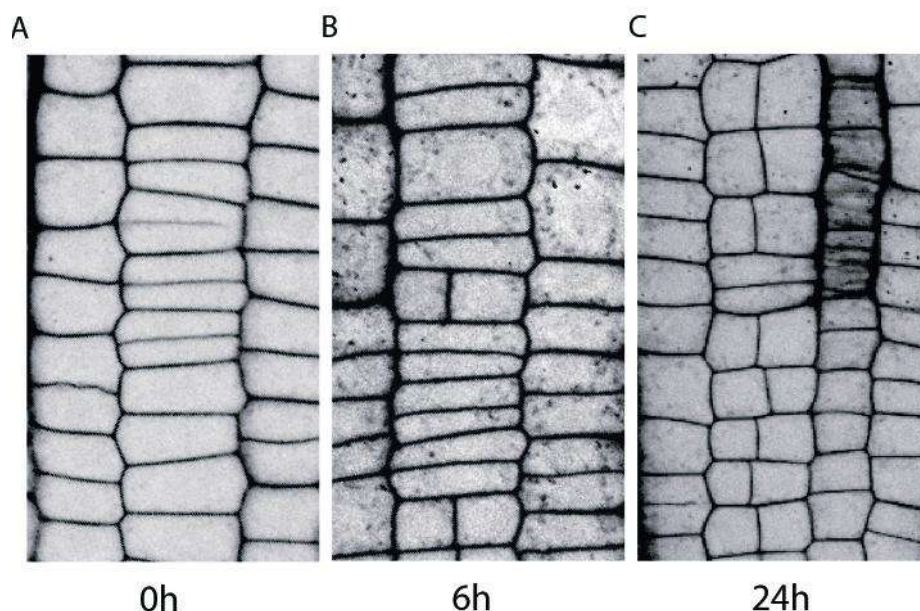
Figure 4: Temporal aspects of DOF2.1 dependent induction of radial divisions in longitudinal sections. A-C Longitudinal sections of epidermis of 5-day-old p*RPS5A*::*DOF2.1*-GR roots at different time points after dexamethasone treatment (n =10).

to the 0h time point (**Figure 3G**). When looking in more detail at single events of PRD in the longitudinal cross sections the earliest time point at which we could observe PRD was after 6h of treatment (**Figure 4A-C**). The first cells to divide were always epidermis cells, which is different when compared to dGR, where cortex are the first cells to divide. Together this shows that DOF2.1 misexpression has a similar effect compared to TMO5/LHW misexpression, but also shows distinct differences.

Next, we studied the effect of loss-of-function of DOF2.1 using the available *dof2.1* T-DNA insertion line (**Figure 5**). We quantified the reduction in DOF2.1 transcript using Q-RT-PCR. This showed that the T-DNA insertion line had a ~60% reduction of DOF2.1 transcript (**Figure 6**). We studied the root meristem of these plants but did not observe any statistically significant effect in the total amount of cell files or the number of vascular cell files (**Figure 7B,E,G**). Also vascular organization in these plants was unaffected. The *Arabidopsis* genome contains 36 Dof-type TF genes and thus it could be expected that other DOF family members might act in a redundant manner. DOF2.1 belongs to a small sub clade of the DOF family together with two closest homologs TMO6 and DOF6 (**Figure 6A**). Because DOF6 and TMO6 might act in a redundant manner, we quantified the relative expression levels of the *DOF6* and *TMO6* of in the *dof2.1* T-DNA insertion line using Q-RT-PCR (**Figure 6B**). Here
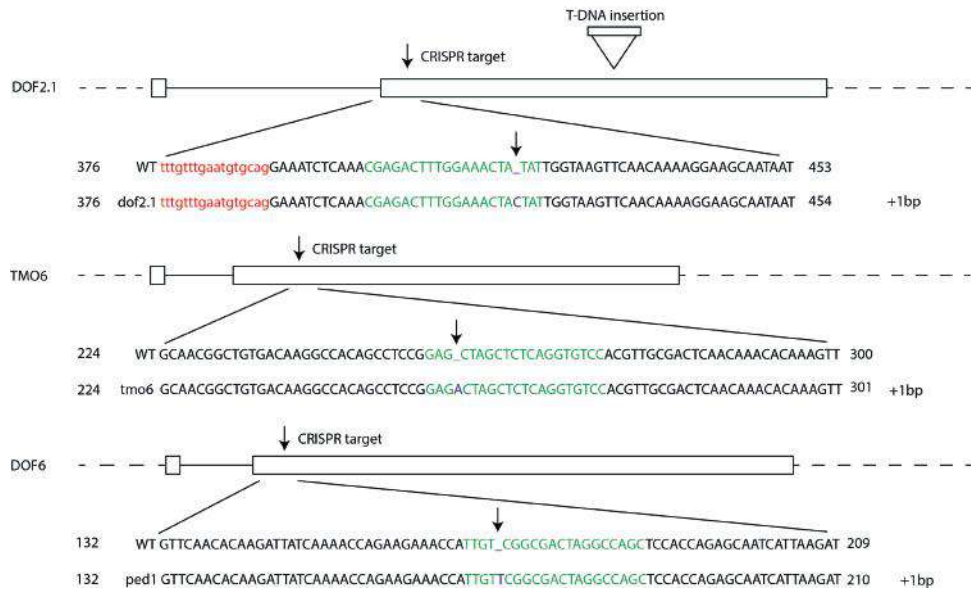
Figure 5: Overview of the CRISPR/Cas9 induced mutations in the dof triple mutant. Arrows indicate the base pairs mutated by CRISRP/CAS9. Striped lines represent 5' and 3' untranslated regions, boxes represent exons and lines represent introns. Red letters represent introns, black letters represent exons, and green letters represent the protospacer adjacent motifs selected for CRISPR mutations. Numbers show the distance from the start of the gene in base pairs.
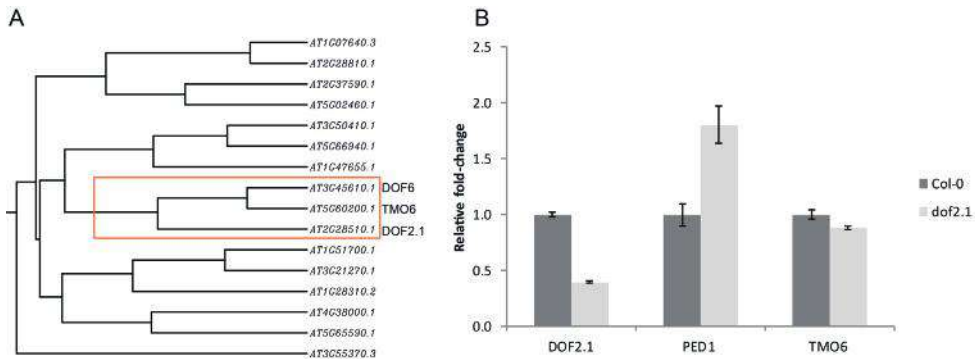
Figure 6: Q-RT-PCR of DOF2.1 clade members in the *dof2.1* T-DNA mutant background. A. Tree of Dof family members based on protein sequence alignment. Orange box marks DOF2.1 and its closest homologs. **B.** Relative fold-changes of *DOF2.1*, *DOF6* and *TMO6* in 5-day old *dof2.1* T-DNA seedlings compared to Col-0. *EEF* and *CDKA* were used as reference genes.

we observed an increase in the transcript levels of *DOF6*. Neither of these DOF genes showed any significant differential regulation in the dGR dataset and thusdo not seem to be co-regulated by TMO5/LHW. Because of the up regulation of *DOF6* transcript in the *dof2.1* T-DNA insertion line, we decided to generate a higher order mutant of both *DOF6* and *TMO6* to investigate the amount of redundancy within this clade of the DOF transcription factor family. We generated a homozygous
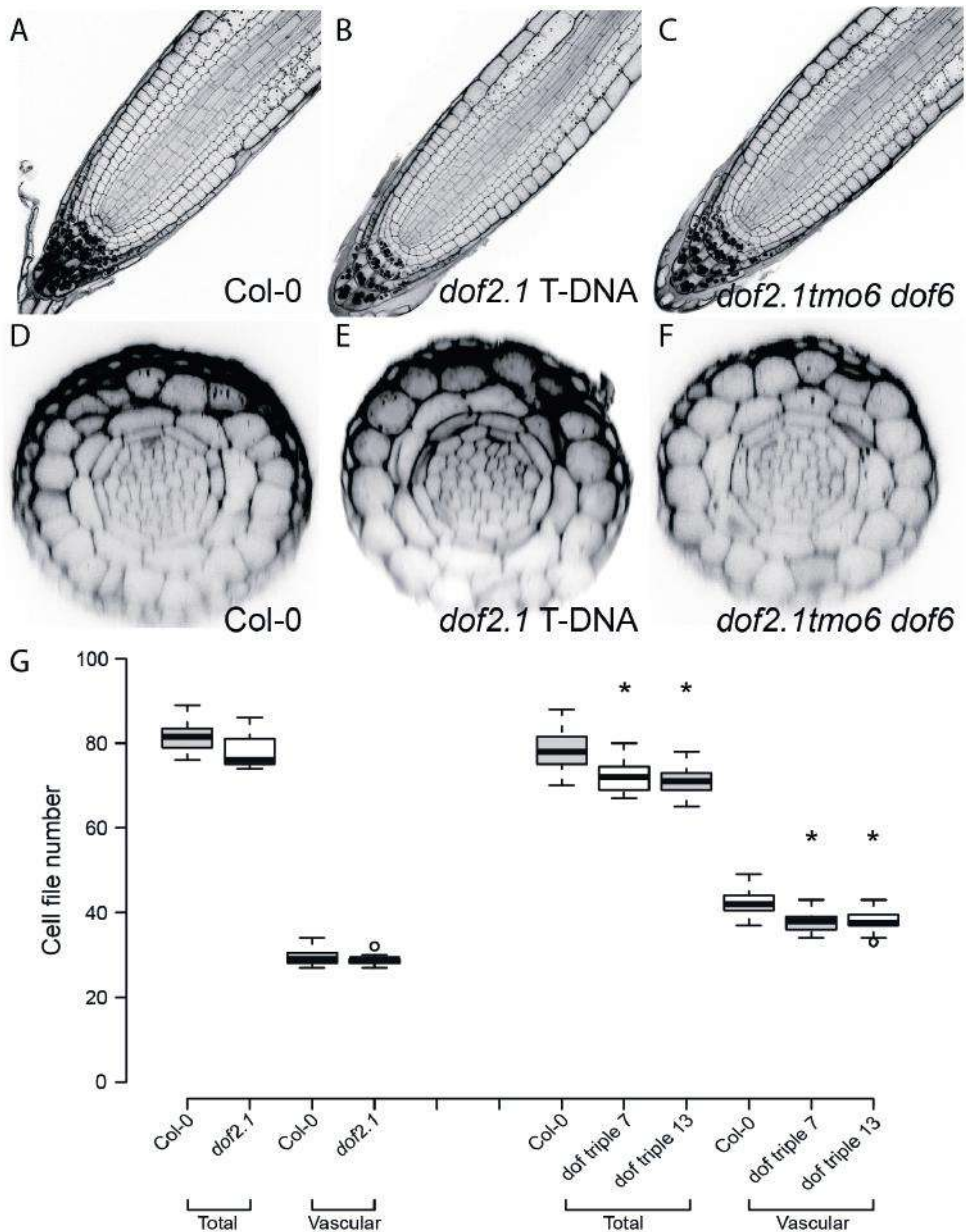
Figure 7: Loss-of-function effect of *DOF2.1* and family members on vascular cell proliferation. Roots meristems were stained using mPS-PI staining and imaged by confocal microscopy **A-C.** Longitudinal sections of root meristems of Col-0, *dof2.1* T-DNA and *dof triple* mutant. **D-F.** Radial sections of root meristems of Col-0, *dof2.1* T-DNA and *dof triple* mutant. **G.** Box plot of total cell file number of *dof2.1* vs Col-0 (Left, n=10 per sample) and two *dof triple* lines vs Col-0 (Right, n=30 per sample). n = 10 sample points. Asterisk marks significance compared to the 0h time point according to a two-sided Student T-test (*p*<0.05) (n>10).

vasculature on the inside of the root. If this is correct, this would mean that DOF2.1 only causes PRD in a cell autonomous manner, suggesting that the DOF2.1 protein might not be mobile. Additional tissue-specific experiments, driving DOF2.1 from e.g. the TMO5 promoter are currently being performed to confirm this hypothesis. To understand the temporal aspects of DOF2.1 controlled PRD, p*RPS5A*::*DOF2.1*:GR seeds were germinated and grown on DEX-free media for 5 days and then transferred to plates supplemented with 10µM DEX for 0h, 2h, 4h, 6h, 12h and 24h (**Figure 3**). A significant increase in total cell number in p*RPS5A*::*DOF2.1*:GR line was observed from 24h of DEX treatment onwards when comparing p*RPS5A*::*DOF2.1*:GR on DEX *dof2.1 tmo6 dof6* triple mutant (*dof triple*) using the CRISPR/CAS9 system. All three genes contained a +1 bp insertion in the second exon resulting in the appearanc e of premature stop codons (**Figure 5**). Imaging and quantification of radial cross-sections of the dof triple revealed a reduction in the amount of total and vascular cell files when compared to Col-0 (**Figure 7**). This suggests that DOF2.1, DOF6 and TMO6 act in a redundant manner to control the amount of cell files in the root meristem.

DOF2.1 is expressed in the vasculature and is cytokinin-inducible

If *DOF2.1* is indeed a downstream TMO5/LHW effector, it should either be expressed in or move towards the domain in which TMO5/LHW is active. Thus, we generated and analyzed transcriptional (p*DOF2.1*::GUS/GFP) and translational (p*DOF2.1*::*DOF2.1*:YFP) reporter lines (**Figure 8**). Although a short 2835 bp promoter fragment has been used previously (Gardiner, et al., 2010), we first generated a longer promoter region reporter using 3711bp upstream of the *DOF2.1* start codon. Both lines showed *DOF2.1* expression in vascular tissues of the root meristem and in the leaf veins in the shoot (**Figure 8A,B**). More detailed confocal analysis showed that p*DOF2.1* is expressed in the protoxylem pole associated-cambium, pericycle and endodermis cells starting from the QC and extending beyond the meristematic region (**Figure 8B,E**) into the mature root. An identical expression pattern was observed in the p*DOF2.1*::*DOF2.1*:YFP translational reporter (**Figure 8C,F**). This suggests that the DOF2.1 protein does not move outside the domain where the promoter is active; unlike what has been shown for other DOF-type TFs (Chen, et al., 2013). Interestingly, in the translational reporter line, additional PRDs could be observed in the endodermis and pericycle cell-layers showing that the addition of one *DOF2.1* copy is sufficient to induce additional PRD (**Figure 8C,F**).

The observed expression pattern of p*DOF2.1* does not perfectly match the TMO5/

LHW overlapping expression domain along the xylem axis, but strongly resembles the expression of the direct downstream targets *LOG3* and *LOG4* (De Rybel, et al., 2014; Ohashi-Ito, et al., 2014; Kuroha, et al., 2009). Therefore, we hypothesized that *DOF2.1* might not be a direct TMO5/LHW target but could instead be controlled through cytokinin. To test this, we analyzed the relative expression of *DOF2.1* by Q-RT-PCR upon exogenous CK treatment (**Figure 9**) by transferring five-day-old Col-0 seedlings from cytokinin-free plates to plates supplemented with 10 µM Benzyl Adenine (BA) for 0', 15', 30', 1h, 2h and 6h. As expected, *DOF2.1* relative expression levels were quickly induced upon BA treatment. Recent work showed by ChIP-seq that the B-type ARRs, ARR1, ARR10 and ARR12 bind to the *DOF2.1* promoter indeed suggesting that DOF2.1 is cytokinin controlled (Xie, et al., 2018). Next, to verify that TMO5/LHW indeed controls *DOF2.1* expression in the root, we introduced the p*DOF2.1*::nGUS/GFP transcriptional reporter into the dGR background. Five-day-old seedlings were grown on either DEX-free plates as a control or on plates supplemented with 10µM DEX. Upon induction, *DOF2.1* expression was extended from the protoxylem pole associated cells to an almost full ring of expression in the pericycle, endodermis and cortex cells (**Figure 10A,B,D,E**). Intriguingly, no expression was found at the metaxylem, the phloem pole positions or the epidermal cells. Both dGR and p*RPS5A*::*DOF2.1* result in PRD throughout the root meristem, suggesting a uniform expression of the p*RPS5A* promoter. To verify, we re-analyzed the *RPS5A* promoter in detail using a p*RPS5A*::nGFP/GUS reporter line. Indeed, expression could be found through-out the root meristem, however several cell per cell-file did not show expression (**Figure 10C,F**). Hence, it is possible that a downstream mobile system causes these divisions or that other factors inhibit DOF activity in these cells. In conclusion, these results confirm that TMO5/LHW controls *DOF2.1* expression and thus that DOF2.1 could be a downstream effector of TMO5/LHW-dependent PRD.

To test if DOF2.1-controlled PRDs are indeed fully dependent on TMO5/LHW activity, we crossed p*RPS5A*::*DOF2.1*-GR in the *tmo5/tmo5l1* double and *lhw* single loss-of-function mutants. Homozygous seeds of these lines were germinated and grown on ½MS plates containing 10µM DEX for 5 days. Plants grown on ½MS plates were used as a control. Quantification of radial cross-sections revealed a significant increase in the total amount of cell files upon dexamethasone treatment when compared to untreated samples (**Figure 11**). However, the amount of vascular cell files was not affected by DOF2.1 induction. Thus these results suggest that DOF2.1 requires TMO5/LHW or a downstream signal in order to control divisions in the vasculature, but is capable of controlling
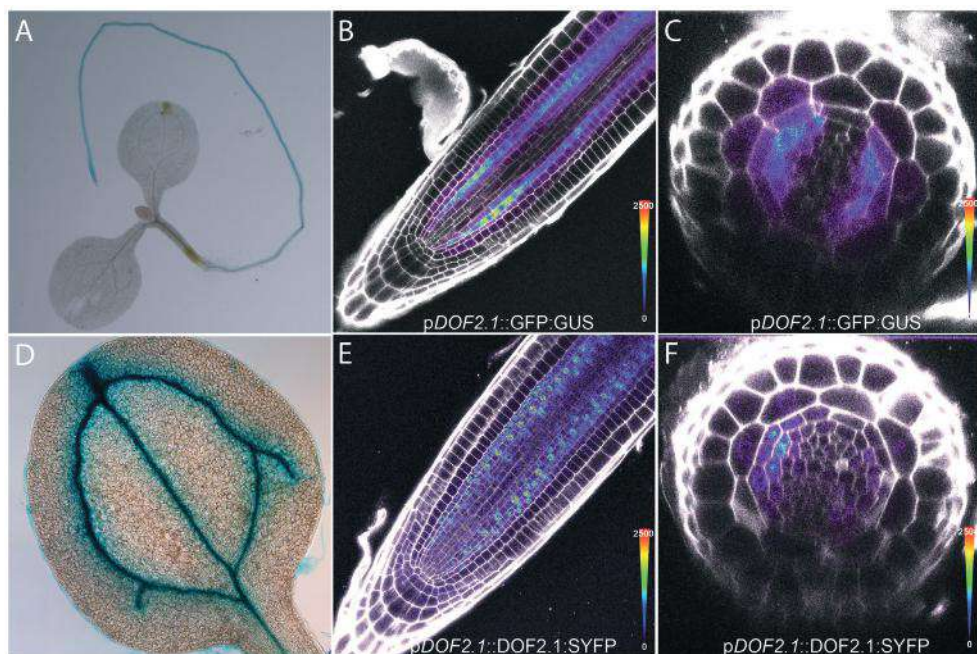
Figure 8: DOF2.1 is strongly expressed in xylem pole associated cells in the root. A-D. p*DOF2.1*::GFP/GUS transcriptional reporter line, **E-F.** p*DOF2.1::DOF2.1*-sYFP translational reporter line. **A.** 3-day old seedling stained with GUS staining for 15 minutes. **D** GUS stained cotyledon and shoot meristem of a 3-day old seedling stained for 24h. **B,E.** Longitudinal confocal cross-sections of the root meristem. **C,F.** Radial confocal cross-sections of the root meristem
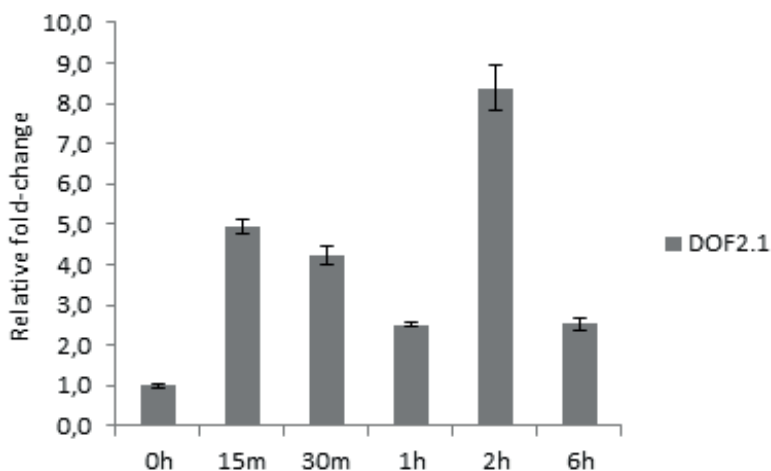

Figure 9: DOF2.1 is cytokinin inducible. Relative fold-changes of *DOF2.1* upon treatment with 10µM Benzyl Adenine (BA) for 0', 15', 30', 1h, 2h and 6h.

PRD in the outer cell-layers in a TMO5/LHW independent manner. Alternatively, the number of additional cell files in the vascular bundle might not be large enough to give significant differences, while this is the case for the entire root cross section.

103
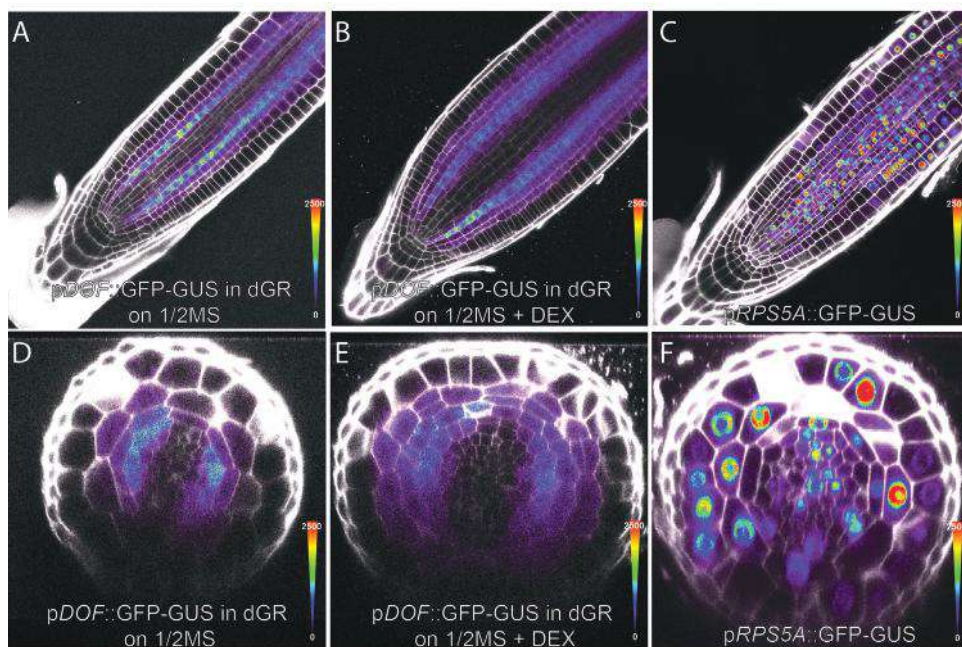
Figure 10: p*DOF2.1* reporter line is induced by TMO5/LHW. **A,B,D,E.** Confocal imaging of p*DOF2.1*:GFP:GUS in the dGR background. **A.** and **D.** show the lines transferred from ½ MS to ½ MS. **B.** and **E.** show lines transferred from ½ MS to ½ MS containing 10µM DEX. Lines were imaged after 24h of treatment. **C.** and **F.** show expression of p*RPS5A*::GFP-GUS.

Discussion and future perspectives

Based on the characterization of the TMO5/LHW misexpression line (dGR), we hypothesized that 3-4h after induction of TMO5/LHW we could find effectors that execute the TMO5/LHW dependent PRDs. Because this is before the actual PRDs occur, but after the initial wave of direct target genes and co-expressed with CK-responses. We selected CK dependent and independent genes that were highly up-regulated 3-4h after TMO5/LHW induction. Misexpression of these genes using the *RPS5A* promotor and analysis revealed that DOF2.1 had an effect on PRD as it showed additional PRD throughout the root meristem. However, we did not observe any phenotype when overexpressing any of the other genes. This could be due to the strength of the *RPS5A* promoter; due to the superficial nature of our screening in which we could have missed subtle phenotypes; or perhaps the capacity of a single gene to induce PRD is rarer than we hypothesized in advance. Nevertheless, DOF2.1 is capable of inducing PRD in the root meristem leading to an increase in cell-file number and subsequently to a reduction in root growth. Using an inducible line, we established that DOF2.1 can induce divisions as soon as 6h after induction, which
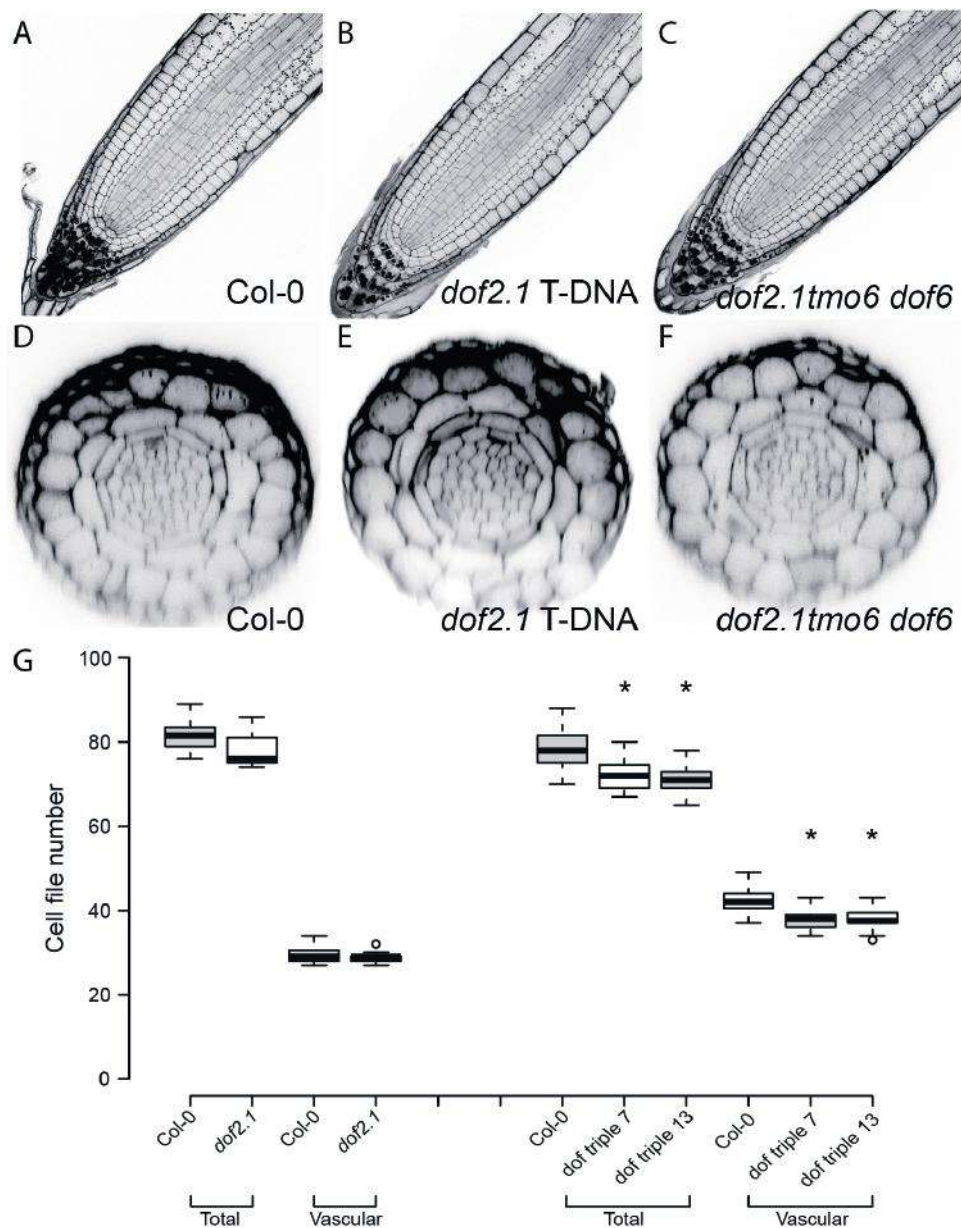
Figure 11: DOF2.1 is capable of inducing PRD *in lhw and tmo5/tmo5l1* mutant backgrounds. Total and vascular cell files were counted after constitutive induction of p*RPS5A*::*DOF2.1*-GR on ½ MS plates containing 10µM dexamethasone, ½ MS plates were used as a control. Asterisk marks significance compared to the 0h time point according to a two-sided Student T-test (*p*<0.05) (n>5).

is slightly slower compared to TMO5/LHW. This is surprising, as one would expect a faster response further downstream in the transcriptional cascade. It could be that DOF2.1 requires factors that are co-expressed upon induction of TMO5/LHW and therefore DOF2.1 misexpression is limited by the levels of the co-expressed genes, resulting in slower division when compared to TMO5/LHW. Another explanation is that *DOF2.1* is subjected to negative feedback which is down-regulated upon TMO5/LHW induction. It is also possible that this is purely an effect of the position of the transgene leading to a difference in expression levels and thus a difference in strength of the phenotype. In any case, we are currently unable to explain this observation.

Surprisingly, *DOF2.1* expression could never be observed at the phloem poles and metaxylem cells, even upon induction of TMO5/LHW, which is activated in these cells. Moreover, we know that CK signaling occurs in these cells as visualized using the TCSn or ARR5 reporters (De Rybel, et al., 2014; Zürcher, et al., 2013). This suggests that there could be active inhibition of DOF2.1 expression in the middle of the root. Intriguingly, HD-ZIPIII type TFs have been shown to be mainly expressed in exactly these cells in the center of the root (Carlsbecker et al 2010). Moreover, the quadruple loss-of-function mutant of the HD-ZIPIII genes, *athb8 cna phb phv* leads to an increased amount of cell files in the vascular bundle, while the gain-of-function mutant *phb-1d* leads to a reduction in vascular bundle size (Carlsbecker et al 2010). Finally, DOF-type TFs have been shown to bind the promoters of HD-ZIPIII genes and can activate their expression (Brady et al 2011). Taken together, these data suggest that HD-ZIPIII proteins could act as negative regulators of *DOF2.1* expression. In this hypothesis, there are high HD-ZIPIII protein levels in the inner cells of the vasculature and low levels in the outer cells, due to the activity of the micro-RNAs MIR165/166 (Carlsbecker et al 2010, Miyashima et al 2011). The resulting gradient of HD-ZIPIII proteins could as such generate the sharp border of *DOF2.1* expression observed upon TMO5/LHW induction.

Although we established that *DOF2.1* is a downstream target gene of the TMO5/LHW dimer, its expression pattern did not resemble the expression domain of TMO5 and LHW (De Rybel, et al., 2013). However the broader expression pattern suggested that it could be downstream of cytokinin as this is produced along the xylem axis and diffuses outwards. Indeed, exogenous cytokinin treatment quickly and strongly increased *DOF2.1* transcript abundance. A next step would be to show that DOF2.1 requires cytokinin for its function. Thus, it would be interesting to see if DOF2.1 still functions in for example the *wol* mutant background, in which cytokinin perception is

inhibited. Moreover, it was recently shown that ARR1, ARR10 and ARR12 bind to the *DOF2.1* promoter sequence (Xie et al 2018), suggesting that the cytokinin inducibility of DOF2.1 could go through these B-type ARRs. The loss-of-function phenotype of the *arr1, arr10, arr12* triple mutant is a severely reduced vascular bundle size (Ishida, et al., 2008) and thus *DOF2.1* could be involved in controlling these PRDs. However, the *arr1, arr10, arr12* triple mutant also shows only protoxylem cells in the vascular bundle and a stronger reduction in vascular bundle size than the dof triple mutant suggesting that ARR1, ARR10 and ARR12 regulate more factors involved in PRD.

Induction of p*RPS5A*::DOF2.1-GR in the *tmo5/tmo5l1* and *lhw* mutants resulted in an increase in the total amount of cell files when compared to the non-induced samples. This shows that DOF2.1 does not need TMO5/LHW for its activity; which is logical for a downstream target gene. However, it is puzzling that DOF2.1 induction did not increase in the amount of cell files in the vasculature itself. Perhaps the vasculature in both *tmo5/tmo5l1* and *lhw* mutants is so different from wild-type that potential additional factors required for DOF2.1 function might not be present at sufficient levels. One factor that could be crucial for DOF2.1 functioning is cytokinin, as it is shown to be required for TMO5/LHW-controlled PRDs, and is capable of restoring the *lhw* mutant phenotype. Therefore it would be worthwhile to observe the effect of p*RPS5A*::DOF2.1-GR induction in the *tmo5/tmo5l1* or *lhw* mutants in the presence of exogenously applied cytokinin.

Materials and Methods

Plant material and growth conditions

All seeds were surface sterilized, sown on solid on ½ MS plates without sucrose and vernalized for 24h at 4°C before growing in a growth room at 22°C in continuous light conditions. Ten day old seedlings were transferred to soil and grown in green house conditions. Dexamethasone treatment was performed by either germinating seeds on 10µM dexamethasone supplemented medium or by transferring plants from ½ MS to 10µM dexamethasone supplemented medium and continuing growth for the indicated time. Benzyl Adenine (BA) treatment was performed by transferring plants from ½ MS to 10µM BA supplemented medium and continuing growth for the indicated time. The *Arabidopsis thaliana* (L.) Heynh. Col-0 ecotype served as wild-type control. dGR marker line of p*DOF2.1*::GFP-GUS was generated by a cross. The *dof2.1* T-DNA line used was GK-668G12 from the Gabi-Kat collection (Kleinboelting, et al., 2012).

Cloning and plant transformation

All p*RPS5A* misexpression lines were created by cloning the respective coding sequence of the genes to be miss-expressed in either pK7m24GW,3/pH7m24GW,3/ pB7m24GW,3 destination vectors using Gateway cloning (Karimi, et al., 2007). p*RPS5A*::*DOF2.1*-GR was generated by cloning *DOF2.1* coding sequence without stop in the pDONR221 entry vector and subsequent recombination using Gateway cloning in pHm43GW destination vector. p*WOL*-XVE::*DOF2.1* was generated by cloning the p*WOL*-XVE inducible promoter and DOF2.1 coding sequence in the pHm43GW destination vector (Siligato, et al., 2016). *DOF2.1* promoter was cloned by using the region 3711 bp upstream of the start in pDONRP41R entry vector. p*DOF2.1*::GFP/GUS was generated by cloning the pDOF2.1 entry vector in pBGWFS7 destination vector using Gateway cloning. p*DOF2.1*::*DOF2.1*:sYFP was obtained by cloning the p*DOF2.1*, *DOF2.1* coding sequence minus stop, and sYFP entry clones in the pHm43GW destination vector using Gateway cloning. Primers used are listed in **Supplemental Table 1** Plant transformation was performed using floral dip (Clough and Bent, 1998).

CRISPR/CAS9 mutant generation

20-nt protospacer were selected using the CRISPR-P tool (Lei, et al., 2014). 2 Protospacers were designed per targeted gene. Protospacer oligos were ordered fused with the corresponding BbsI cut sites (-FW: 5'-ATTG + protospacer REV: 5'-AAAC + rev-com protospacer). Primers used can be found in Supplemental table 1. Oligos were annealed and cloned into corresponding pEN-Chimera plasmids (Steinert, et al., 2017) (containing different Golden Gate Assembly sites) using classic ligation (https://gateway.psb.ugent.be). pEN-Chimera plasmids were sequenced to verify insertion of appropriate protospacer. pEN-Chimera were cloned into the pFASTRK_AtCas9_AG expression vector (https://gateway.psb. ugent.be) using Golden Gate Assembly (Engler, et al., 2009). Expression vectors were sequenced to verify successful insertion of the protospacers. Positive expression vectors were transformed into *Agrobacterium tumefaciens*. Plants were transformed with *Agrobacterium* cultures using floral dip. Positive transformed seeds were selected based on red seed coat fluorescence and transferred to soil. Editing of target genes was confirmed in T1 generation by PCR on target genes and subsequent sequencing. Plants showing high CRISPR efficiency after TIDE analysis (https://www.deskgen.com/landing/tide.html) were harvested. Seeds lacking red seed coat fluorescence were transferred to soil and plants were again

screened for editing of target genes using PCR and sequencing. Plants containing homozygous desired editing events were selected and seeds were harvested. In T3 homozygous edited plants were selected and confirmed via sequencing.

Plant imaging and image processing

For DIC analysis, seedlings were mounted in a solution of 20% glycerol 60% lactic acid. DIC microscopy was performed using an Olympus BX53 DIC microscope. For mPS-PI staining, roots were stained as described previously (Truernit, et al., 2008). GUS staining was performed as described in (Vanneste, et al., 2005). Confocal microscopy was performed on Leica SP8 (40X) Zeiss LSM710 (63X) and Leica SP2 (63X) (all water corrected objective (NA 1.2) lenses) confocal microscopes. Calcofluor White, GFP, YFP, tandemTomato (tdT) and propidium iodide (PI) samples were imaged at an excitation of 405nm, 488nm, 514 nm, 561nm and 514nm respectively. GFP and PI were visualized at an emission of 425-475 nm, 500-535nm, 515-550 nm and 600-700nm respectively. Quantifications of cell file numbers were performed using the Image J software package.

Quantification of cell numbers

Roots were fixed and stained using a modified Pseudo Schiff – Propidium Iodine (mPS-PI) staining (Truernit, et al., 2008). The stained roots were imaged by using confocal microscopy and radial cross-sections were taken in the middle of root meristem (defined as the middle between the first elongating cortex cells and the QC).

Box Plots

All box plots were generated using the BoxPlotR webtool using standard settings. Center lines represent the medians; box limits indicate the 25th and 75th percentiles as determined by R software; whiskers extend 1.5 times the interquartile range from the 25th and 75th percentiles, outliers are represented by dots.

Q-RT-PCR

RNA was extracted using the RNeasy kit (Qiagen). Poly(dt) cDNA was generated from 1µg of total RNA using Superscript II reverse transcriptase (Invitrogen) and analyzed on a LightCycler 480 (Roche Molecular Systems, Inc) with SYBR Green I Master kit (Roche

Diagnostics) according to manufacturer's instructions. Primer pairs were designed using Universal Probe Library Assay Design Center (Roche Molecular Systems, Inc). All primers used for Q-RT-PCR analysis can be found in Supplemental Table 1. All reactions were done in triplicate. Data was analyzed using qBase+ software package (Biogazelle). Expression levels were normalized to those of *EEF1α4* and *CDKA1;1*.

Acknowledgements

References

Bhargava, A., Clabaugh, I., To, J.P., Maxwell, B.B., Chiang, Y.H., Schaller, G.E., Loraine, A., and Kieber, J.J. (2013). Identification of cytokinin-responsive genes using microarray meta-analysis and RNA-Seq in Arabidopsis. Plant physiology 162, 272-94.

Chen, H., Ahmad, M., Rim, Y., Lucas, W.J., and Kim, J.Y. (2013). Evolutionary and molecular analysis of Dof transcription factors identified a conserved motif for intercellular protein trafficking. New Phytologist 198, 1250-1260.

Clough, S.J., and Bent, A.F. (1998). Floral dip: a simplified method for Agrobacterium-mediated transformation of Arabidopsis thaliana. Plant Journal 16, 735-743.

De Rybel, B., Adibi, M., Breda, A.S., Wendrich, J.R., Smit, M.E., Novák, O., Yamaguchi, N., Yoshida, S., Van Isterdael, G., Palovaara, J., et al. (2014). Plant development. Integration of growth and patterning during vascular tissue formation in Arabidopsis. Science 345, 1255215.

De Rybel, B., Möller, B., Yoshida, S., Grabowicz, I., Barbier de Reuille, P., Boeren, S., Smith, R.S., Borst, J.W., and Weijers, D. (2013). A bHLH complex controls embryonic vascular tissue establishment and indeterminate growth in Arabidopsis. Developmental cell 24, 426-37.

Engler, C., Gruetzner, R., Kandzia, R., and Marillonnet, S. (2009). Golden gate shuffling: a one-pot DNA shuffling method based on type IIs restriction enzymes. PloS one 4, e5553.

Gardiner, J., Sherr, I., and Scarpella, E. (2010). Expression of DOF genes identifies early stages of vascular development in Arabidopsis leaves. Int J Dev Biol 54, 1389-1396.

Guo, Y., Qin, G., Gu, H., and Qu, L.J. (2009). Dof5.6/HCA2, a Dof transcription factor gene, regulates interfascicular cambium formation and vascular tissue development in Arabidopsis. The Plant cell 21, 3518-34.

Ishida, K., Yamashino, T., Yokoyama, A., and Mizuno, T. (2008). Three type-B response regu-

lators, ARR1, ARR10 and ARR12, play essential but redundant roles in cytokinin signal transduction throughout the life cycle of Arabidopsis thaliana. Plant & cell physiology 49, 47-57.

Karimi, M., Bleys, A., Vanderhaeghen, R., and Hilson, P. (2007). Building blocks for plant gene assembly. Plant physiology 145, 1183-1191.

Kleinboelting, N., Huep, G., Kloetgen, A., Viehoever, P., and Weisshaar, B. (2012). GABI-Kat SimpleSearch: new features of the Arabidopsis thaliana T-DNA mutant database. Nucleic Acids Res 40, D1211-D1215.

Konishi, M., and Yanagisawa, S. (2007). Sequential activation of two Dof transcription factor gene promoters during vascular development in Arabidopsis thaliana. Plant Physiol Bioch 45, 623-629.

Krebs, J., Mueller-Roeber, B., and Ruzicic, S. (2010). A novel bipartite nuclear localization signal with an atypically long linker in DOF transcription factors. J Plant Physiol 167, 583-586.

Kuroha, T., Tokunaga, H., Kojima, M., Ueda, N., Ishida, T., Nagawa, S., Fukuda, H., Sugimoto, K., and Sakakibara, H. (2009). Functional analyses of LONELY GUY cytokinin-activating enzymes reveal the importance of the direct activation pathway in Arabidopsis. The Plant cell 21, 3152-69.

Le Hir, R., and Bellini, C. (2013). The plant-specific Dof transcription factors family: new players involved in vascular system development and functioning in Arabidopsis. Front Plant Sci 4.

Lei, Y., Lu, L., Liu, H.Y., Li, S., Xing, F., and Chen, L.L. (2014). CRISPR-P: A Web Tool for Synthetic Single-Guide RNA Design of CRISPR-System in Plants. Molecular plant 7, 1494-1496.

Moreno-Risueno, M.A., Martinez, M., Vicente-Carbajosa, J., and Carbonero, P. (2007). The family of DOF transcription factors: from green unicellular algae to vascular plants. Mol Genet Genomics 277, 379-390.

Ohashi-Ito, K., Saegusa, M., Iwamoto, K., Oda, Y., Katayama, H., Kojima, M., Sakakibara, H., and Fukuda, H. (2014). A bHLH complex activates vascular cell division via cytokinin action in root apical meristem. Current biology : CB 24, 2053-8.

Pi, L., Aichinger, E., van der Graaff, E., Llavata-Peris, C.I., Weijers, D., Hennig, L., Groot, E., and Laux, T. (2015). Organizer-Derived WOX5 Signal Maintains Root Columella Stem Cells through Chromatin-Mediated Repression of CDF4 Expression. Developmental cell 33, 576-88.

Scarpella, E., Francis, P., and Berleth, T. (2004). Stage-specific markers define early steps of procambium development in Arabidopsis leaves and correlate termination of vein formation with mesophyll differentiation. Development 131, 3445-3455.

Siligato, R., Wang, X., Yadav, S.R., Lehesranta, S., Ma, G.J., Ursache, R., Sevilem, I., Zhang, J., Gorte, M., Prasad, K., et al. (2016). MultiSite Gateway-Compatible Cell Type-Specific Gene-Inducible System for Plants. Plant physiology 170, 627-641.

Skirycz, A., Radziejwoski, A., Busch, W., Hannah, M.A., Czeszejko, J., Kwasniewski, M.,

Zanor, M.I., Lohmann, J.U., De Veylder, L., Witt, I., et al. (2008). The DOF transcription factor OBP1 is involved in cell cycle regulation in Arabidopsis thaliana. Plant Journal 56, 779-792.

Steinert, J., Schmidt, C., and Puchta, H. (2017). Use of the Cas9 Orthologs from Streptococcus thermophilus and Staphylococcus aureus for Non-Homologous End-Joining Mediated Site-Specific Mutagenesis in Arabidopsis thaliana. Methods in molecular biology 1669, 365-376.

Truernit, E., Bauby, H., Dubreucq, B., Grandjean, O., Runions, J., Barthélémy, J., and Palauqui, J.C. (2008). High-resolution whole-mount imaging of three-dimensional tissue organization and gene expression enables the study of Phloem development and structure in Arabidopsis. The Plant cell 20, 1494-503.

Vanneste, S., De Rybel, B., Beemster, G.T.S., Ljung, K., De Smet, I., Van Isterdael, G., Naudts, M., Iida, R., Gruissem, W., Tasaka, M., et al. (2005). Cell cycle progression in the pericycle is not sufficient for SOLITARY ROOT/IAA14-mediated lateral root initiation in Arabidopsis thaliana. The Plant cell 17, 3035-3050.

Weijers, D., Franke-van Dijk, M., Vencken, R.J., Quint, A., Hooykaas, P., and Offringa, R. (2001). An Arabidopsis Minute-like phenotype caused by a semi-dominant mutation in a RIBOSOMAL PROTEIN S5 gene. Development 128, 4289-4299.

Xie, M.T., Chen, H.Y., Huang, L., O'Neil, R.C., Shokhirev, M.N., and Ecker, J.R. (2018). A B-ARR-mediated cytokinin transcriptional network directs hormone cross-regulation and shoot development (vol 9, 1604, 2018). Nature communications 9.

Zubo, Y.O., Blakley, I.C., Yamburenko, M.V., Worthen, J.M., Street, I.H., Franco-Zorrilla, J.M., Zhang, W., Hill, K., Raines, T., Solano, R., et al. (2017). Cytokinin induces genome-wide binding of the type-B response regulator ARR10 to regulate growth and development in Arabidopsis. Proceedings of the National Academy of Sciences of the United States of America 114, E5995-E6004.

Zürcher, E., Tavor-Deslex, D., Lituiev, D., Enkerli, K., Tarr, P.T., and Muller, B. (2013). A robust and sensitive synthetic sensor to monitor the transcriptional output of the cytokinin signaling network in planta. Plant physiology 161, 1066-75.

Supplemental Information

Supplemental Table 1: Primerlist

pDONR221 CDS
+ STOP

AT1G67110	CYP735A2	fw	GGGGACAAGTTTGTACAAAAAAGCAGGCTTA-ATGATGGTTACATTAGTACT
		rv	GGGGACCACTTTGTACAAGAAAGCTGGGTA-TCATAGATCAAGTGGCTTC
AT3G50300		fw	GGGGACAAGTTTGTACAAAAAAGCAGGCTTA-ATGGACGATGTGACCGTGAT
		rv	GGGGACCACTTTGTACAAGAAAGCTGGGTA-TCATGTAATTACATTCTCC
AT1G31320	LBD4	fw	GGGGACAAGTTTGTACAAAAAAGCAGGCTTA-ATGAAAGAAAGTAGCCGGAA
		rv	GGGGACCACTTTGTACAAGAAAGCTGGGTA-CTAGCAAGACCACATAGACT
AT1G13740	AFP2	fw	GGGGACAAGTTTGTACAAAAAAGCAGGCTTA-ATGGGTGAAGCAAGCAGACA
		rv	GGGGACCACTTTGTACAAGAAAGCTGGGTA-TTAAAAGGTCGAAGAAGAGG
AT1G13420	ATST4B	fw	GGGGACAAGTTTGTACAAAAAAGCAGGCTTA-ATGGGTGAGAAAGATATTCC
		rv	GGGGACCACTTTGTACAAGAAAGCTGGGTA-CTACAATTTCAAACCAGAGC
AT5G51780	bHLH36	fw	GGGGACAAGTTTGTACAAAAAAGCAGGCTTA-ATGGAGAAGATGATGCACAG
		rv	GGGGACCACTTTGTACAAGAAAGCTGGGTA-TTACTTCATTCTGATTAATC
AT5G51790	bHLH120	fw	GGGGACAAGTTTGTACAAAAAAGCAGGCTTA-ATGAATCCTTCTAACAATCC
		rv	GGGGACCACTTTGTACAAGAAAGCTGGGTA-TCAGTGCCTAGTCGTGG
AT1G62975	bHLH125	fw	GGGGACAAGTTTGTACAAAAAAGCAGGCTTA-ATGGATTGTGTTCCTTCATTG
		rv	GGGGACCACTTTGTACAAGAAAGCTGGGTA-CTACATAGTCATTATTTTATCC
AT4G25410	bHLH126	fw	GGGGACAAGTTTGTACAAAAAAGCAGGCTTA-ATGGATCCTTATAAGAATC
		rv	GGGGACCACTTTGTACAAGAAAGCTGGGTA-TCATAACGAAATTTCAAGAAG
AT2G40970	MYBC1	fw	GGGGACAAGTTTGTACAAAAAAGCAGGCTTA-ATGAGAGAAGATAATCCAAA
		rv	GGGGACCACTTTGTACAAGAAAGCTGGGTA-TTAATTTCCGGCAGGGAAGA
AT1G13300	HRS1	fw	GGGGACAAGTTTGTACAAAAAAGCAGGCTTA-ATGATTAAAAAGTTCAGCAA
		rv	GGGGACCACTTTGTACAAGAAAGCTGGGTA-TTAATTATTCTTGACGTAAT
AT2G13960		fw	GGGGACAAGTTTGTACAAAAAAGCAGGCTTA-ATGAGCTCAAGTTCGAATCC
		rv	GGGGACCACTTTGTACAAGAAAGCTGGGTA-TTACGTAAAATGAAAACCAA
AT3G46130	MYB48	fw	GGGGACAAGTTTGTACAAAAAAGCAGGCTTA-ATGATGCAAGAGGAGGGAAA
		rv	GGGGACCACTTTGTACAAGAAAGCTGGGTA-TTAACCTGACGACCATGGTG
AT2G47460	MYB12	fw	GGGGACAAGTTTGTACAAAAAAGCAGGCTTA-ATGGGAAGAGCGCCATGTTG
		rv	GGGGACCACTTTGTACAAGAAAGCTGGGTA-TCATGACAGAAGCCAAGCGA
AT5G59680		fw	GGGGACAAGTTTGTACAAAAAAGCAGGCTTA-ATGGAGAGGTCTCTTGAGC
		rv	GGGGACCACTTTGTACAAGAAAGCTGGGTA-CTATCTTGCTCTGGGAATC
AT4G20450		fw	GGGGACAAGTTTGTACAAAAAAGCAGGCTTA-ATGGAAGGTATTCACAAGC
		rv	GGGGACCACTTTGTACAAGAAAGCTGGGTA-CTAGCGTGCATCAGGGATA
AT3G46340		fw	GGGGACAAGTTTGTACAAAAAAGCAGGCTTA-ATGGAGTTTCCCCATTCGGT
		rv	GGGGACCACTTTGTACAAGAAAGCTGGGTA-CTACCTTGCACTAGGGACAGC
AT1G07560		fw	GGGGACAAGTTTGTACAAAAAAGCAGGCTTA-ATGAAAAACCTCCGTGGACT
		rv	GGGGACCACTTTGTACAAGAAAGCTGGGTA-CTAACGTGCCTTGGGGTTCA
AT2G28990		fw	GGGGACAAGTTTGTACAAAAAAGCAGGCTTA-ATGAAGATTCACCTTTTGTTGG
		rv	GGGGACCACTTTGTACAAGAAAGCTGGGTA-CTAGCGAGCTTGAGGTATTACC
AT1G05700		fw	GGGGACAAGTTTGTACAAAAAAGCAGGCTTA-ATGGAAGAGTTTCGTTTTCT
		rv	GGGGACCACTTTGTACAAGAAAGCTGGGTA-TCAATAGTTCTTGTTACTC
AT5G16900		fw	GGGGACAAGTTTGTACAAAAAAGCAGGCTTA-ATGGAGGATCGTCATCGTTA
		rv	GGGGACCACTTTGTACAAGAAAGCTGGGTA-CTAGGAACTTTTCGAGTCTA
AT5G49770		fw	GGGGACAAGTTTGTACAAAAAAGCAGGCTTA-ATGAAGATGAGTTCAAGAATTGG

		rv	GGGGACCACTTTGTACAAGAAAGCTGGGTA-TTAGGGTTTTGGAGTTGGGAAAA
AT4G39070	BZS1	fw	GGGGACAAGTTTGTACAAAAAAGCAGGCTTA-ATGAAGATTTGGTGTGCTGT
		rv	GGGGACCACTTTGTACAAGAAAGCTGGGTA-TCAAGAGAAGGGTTTGTGA
AT3G10910	DAFL1	fw	GGGGACAAGTTTGTACAAAAAAGCAGGCTTA-ATGGGTCGGTTGCTACTTG
		rv	GGGGACCACTTTGTACAAGAAAGCTGGGTA-CTATACGATGGAAACTACC
AT1G67340		fw	GGGGACAAGTTTGTACAAAAAAGCAGGCTTA-ATGTTACCCTCAAGAAAAAC
		rv	GGGGACCACTTTGTACAAGAAAGCTGGGTA-TTAACTCATTGGAAGCAAAA
AT2G20080	TIE2	fw	GGGGACAAGTTTGTACAAAAAAGCAGGCTTA-ATGGGAAGTACTTTCTTTGG
		rv	GGGGACCACTTTGTACAAGAAAGCTGGGTA-TCAAAGTGACAATCTCAACT
AT4G29905		fw	GGGGACAAGTTTGTACAAAAAAGCAGGCTTA-ATGTGTTTGGAAGTTGTGTA
		rv	GGGGACCACTTTGTACAAGAAAGCTGGGTA-TCAATAATACAAGACGAGAT
AT1G03240		fw	GGGGACAAGTTTGTACAAAAAAGCAGGCTTA-ATGACGATCAGAAGCAAAAAAGC
		rv	GGGGACCACTTTGTACAAGAAAGCTGGGTA-CTACGATATCACAGATGAAAAAAG
AT3G18450		fw	GGGGACAAGTTTGTACAAAAAAGCAGGCTTA-ATGGGTCGACCAGTTGGCCA
		rv	GGGGACCACTTTGTACAAGAAAGCTGGGTA-TCAACCCATCATTCGTTGAC
AT3G51540		fw	GGGGACAAGTTTGTACAAAAAAGCAGGCTTA-ATGAGTGATCGGAGTCTGAA
		rv	GGGGACCACTTTGTACAAGAAAGCTGGGTA-TCAGAGAGGAGAGAATAGAT
AT5G67620		fw	GGGGACAAGTTTGTACAAAAAAGCAGGCTTA-ATGGGGAATTGTCAAGCGGC
		rv	GGGGACCACTTTGTACAAGAAAGCTGGGTA-TCATGAGGATCCAAATTCCG
AT3G46880		fw	GGGGACAAGTTTGTACAAAAAAGCAGGCTTA-ATGGAGGGTAAAGGAAGAGT
		rv	GGGGACCACTTTGTACAAGAAAGCTGGGTA-TCAAACAATCAAATATTGTT
AT5G57887		fw	GGGGACAAGTTTGTACAAAAAAGCAGGCTTA-ATGCGTGACATCAAAGGCTT
		rv	GGGGACCACTTTGTACAAGAAAGCTGGGTA-CTAGAAAAGAAGAGAACTGC
AT3G59340		fw	GGGGACAAGTTTGTACAAAAAAGCAGGCTTA-ATGGCAATGGGTTTCGATTTC
		rv	GGGGACCACTTTGTACAAGAAAGCTGGGTA-CTATAACGATGTGTCTGGAAG
AT5G19970		fw	GGGGACAAGTTTGTACAAAAAAGCAGGCTTA-ATGAAACTACTCAATAAGTA
		rv	GGGGACCACTTTGTACAAGAAAGCTGGGTA-TTACAAAGAGAAGGTGAGGC
AT1G74458		fw	GGGGACAAGTTTGTACAAAAAAGCAGGCTTA-ATGGCGAGAAGACAACTCTT
		rv	GGGGACCACTTTGTACAAGAAAGCTGGGTA-TTAGCAATCAGAACAGTGAG
AT4G29310		fw	GGGGACAAGTTTGTACAAAAAAGCAGGCTTA-ATGGATCCATGTCCATTTGTACG
		rv	GGGGACCACTTTGTACAAGAAAGCTGGGTA-TCACGTGAGGGAGCTTTGGTCGT
AT5G03995		fw	GGGGACAAGTTTGTACAAAAAAGCAGGCTTA-ATGGTGGAGGACATCTTCAC
		rv	GGGGACCACTTTGTACAAGAAAGCTGGGTA-TTATAATCTAATATACAACT
AT1G68500		fw	GGGGACAAGTTTGTACAAAAAAGCAGGCTTA-ATGAAGAGACAGAGAAAAGATATGG
		rv	GGGGACCACTTTGTACAAGAAAGCTGGGTA-CTATGAGGAATGAGTTAAATTGTGG
AT3G05936		fw	GGGGACAAGTTTGTACAAAAAAGCAGGCTTA-ATGTTGCAGATTGTAGGCAAG
		rv	GGGGACCACTTTGTACAAGAAAGCTGGGTA-CTAACGGAATCCACCTCTTG
AT3G01730		fw	GGGGACAAGTTTGTACAAAAAAGCAGGCTTA-ATGAGAGCTTTCAGCTTAATG
		rv	GGGGACCACTTTGTACAAGAAAGCTGGGTA-TTAGAAGACGAAAGCCAAGGC
AT2G22122		fw	GGGGACAAGTTTGTACAAAAAAGCAGGCTTA-ATGTCTTCGATGGGAGCAAAC
		rv	GGGGACCACTTTGTACAAGAAAGCTGGGTA-TTAAGTCGACAACGGAGAAGA
AT4G03420		fw	GGGGACAAGTTTGTACAAAAAAGCAGGCTTA-ATGGTGTTTGGAAAAGGGTC
		rv	GGGGACCACTTTGTACAAGAAAGCTGGGTA-TCAGCCACGGTGAGCCATTC
AT1G02380		fw	GGGGACAAGTTTGTACAAAAAAGCAGGCTTA-ATGGATCAAATGTTATCAGG
		rv	GGGGACCACTTTGTACAAGAAAGCTGGGTA-TCATCTAGTAACGTCTCTCG
AT5G18661		fw	GGGGACAAGTTTGTACAAAAAAGCAGGCTTA-ATGGGTGGGATGTGTATGTC
		rv	GGGGACCACTTTGTACAAGAAAGCTGGGTA-TCAACGGCACCGGACGTAAC
AT3G04440		fw	GGGGACAAGTTTGTACAAAAAAGCAGGCTTA-ATGCCTACACCAACAAGCAACG
		rv	GGGGACCACTTTGTACAAGAAAGCTGGGTA-TCAACAATTGTTATAACTATC

AT1G27020		fw	GGGGACAAGTTTGTACAAAAAAGCAGGCTTA-ATGGGTTCTCTTGACTTGCC
		rv	GGGGACCACTTTGTACAAGAAAGCTGGGTA-TTACGCTGTGAAACGGGTGC
AT3G50610		fw	GGGGACAAGTTTGTACAAAAAAGCAGGCTTA-ATGGTATTTTACCAAACACC
		rv	GGGGACCACTTTGTACAAGAAAGCTGGGTA-TTAAGCTTTAGGTTCATCGT
AT1G07690		fw	GGGGACAAGTTTGTACAAAAAAGCAGGCTTA-ATGGCTTCTAATCTTCTCCT
		rv	GGGGACCACTTTGTACAAGAAAGCTGGGTA-TTAGACATGATCATCTGCTT
AT1G54950		fw	GGGGACAAGTTTGTACAAAAAAGCAGGCTTA-ATGGCTTCCACCAACTTTCC
		rv	GGGGACCACTTTGTACAAGAAAGCTGGGTA-TCAAGCAAGTTTTTGTAGTC
AT5G38940		fw	GGGGACAAGTTTGTACAAAAAAGCAGGCTTA-ATGTCTCATAAGTTTCTTATC
		rv	GGGGACCACTTTGTACAAGAAAGCTGGGTA-TTATTTCTTGAACTTGGTCTG
AT3G18080	BGLU44	fw	GGGGACAAGTTTGTACAAAAAAGCAGGCTTA-ATGAGACACCTTAGCTCACC
		rv	GGGGACCACTTTGTACAAGAAAGCTGGGTA-TCATTTGTTGTTTCGTTTC
AT5G61650	CYCP4;2	fw	GGGGACAAGTTTGTACAAAAAAGCAGGCTTA-ATGGCTGATCAGATTGAGATCC
		rv	GGGGACCACTTTGTACAAGAAAGCTGGGTA-TCAAGCAGCAGCGAGTTGC
AT5G07450	CYCP4;3	fw	GGGGACAAGTTTGTACAAAAAAGCAGGCTTA-ATGGCTTATCAGATTGATCAG
		rv	GGGGACCACTTTGTACAAGAAAGCTGGGTA-TCAAACAGCACTGGTGACTTG
AT2G28510	DOF2.1	fw	GGGGACAAGTTTGTACAAAAAAGCAGGCTTC-ATGGATCCTGAACAGGTAATTTCT
		rv	GGGGACCACTTTGTACAAGAAAGCTGGGTC-CTAGACCAAAGGAGTGTTGAGTAA

pDONR221 CDS
- STOP

| AT2G28510 | DOF2.1 | fw | GGGGACAAGTTTGTACAAAAAAGCAGGCTTC-ATGGATCCTGAACAGGTAATTTCT |
| | | rv | GGGGACCACTTTGTACAAGAAAGCTGGGTC-GACCAAAGGAGTGTTGAGTAAACCA |

pDONRP4P1R

| AT2G28510 | pDOF2.1 | fw | GGGGACAAGTTTGTACAAAAAAGCAGGCTTC-GGTATGGATCAGACGGTTTAAGTC |
| | | rv | GGGGACCACTTTGTACAAGAAAGCTGGGTC-CCATGTAACAAAGGATCGAAGCA |

CRISPR SG RNA

AT2G28510	DOF2.1 SG1	fw	ATTGCGAGACTTTGGAAACTATAT
		rv	AAACATATAGTTTCCAAAGTCTCG
	DOF2.1 SG2	fw	ATTGACTTCAGAACCCTTTAATTA
		rv	AAACTAATTAAAGGGTTCTGAAGT
AT5G60200	TMO6 SG1	fw	ATTGGGATCATTTGTTACAACACC
		rv	AAACGGTGTTGTAACAAATGATCC
	TMO6 SG2	fw	ATTGGGACACCTGAGAGCTAGCTC
		rv	AAACGAGCTAGCTCTCAGGTGTCC
At3g45610	PED1 SG1	fw	ATTGGCTGGCCTAGTCGCCGACAA
		rv	AAACTTGTCGGCGACTAGGCCAGC
	PED1 SG2	fw	ATTGTTTGCCGTCATGGGTCATCG
		rv	AAACCGATGACCCATGACGGCAAA

qPCR primers

AT1G67110	CYP735A2	fw	GAACAGCTCTCAAGTCTTACTTCGT
		rv	TCAAATGCCATTCTTGGTAAAA
AT3G50300		fw	AGAGAGTCGCTGCGGAGTAG
		rv	TCTTTATCAAGCGGAGGGTTT
AT1G31320	LBD4	fw	CGTCAACAAGATGCTTCAGG
		rv	CCTCGTAAACCATGCTGCTC

AT1G13740	AFP2	fw	CTGTGGTGTTGATTCCGATG
		rv	TTTCATCATTGCAGCTGTTTG
AT1G13420	ATST4B	fw	GTCCCTTATGGGAAAATGTGTT
		rv	GCACATGCTTAGGATCTTCCA
AT5G51780	bHLH36	fw	TTCTTCAAGTGCTTAGTGAATATGGT
		rv	TCAAAGCCATATCGTTGACCT
AT5G51790	bHLH120	fw	CGAGTCAACGAGAGGCTCAT
		rv	TCGTGGAAAGTACTAACTGCTCA
AT1G62975	bHLH125	fw	ACAGAGATTCATGCACACCATT
		rv	TTTATCCTTAAGCTCCAAAATATTGAT
AT4G25410	bHLH126	fw	CTCATGCACACTATTCAAGTAGAGG
		rv	CGTCGAAAGTATCAAATCCTCA
AT2G40970	MYBC1	fw	CCGCGATTTATCACCAGAAG
		rv	GTGGAGGAGTTGGAGTTGGA
AT1G13300	HRS1	fw	GACCACCCACTTCTTCCAAA
		rv	CTCATACTCTCATCTCTTGTCATCG
AT3G46130	MYB48	fw	GCTAAGTGGGGAAACAGGTG
		rv	GGACGCTTCTTTTCTTGAGC
AT2G47460	MYB12	fw	CAAGCGTGGAAACATAACTCC
		rv	GATGACCCGCGATTAGTGAC
AT4G20450		fw	AAAGAAGAAGCCATCCAAAGC
		rv	CCGCAACCTCTTCATAAGTATAGC
AT1G07560		fw	GCTCATCAAGCAGAAAAGGTC
		rv	CAAAACCCTTTCAAATTTCTTTGT
AT2G28990		fw	AGGCCAGCCCTTCAAATC
		rv	ACTATTGTGCCCGGGATTC
AT1G05700		fw	TGGGAGGGCCTTAATTGC
		rv	CCCGCTTGATGATAAGTTCAG
AT5G16900		fw	CGTCACCAAGAATCATTTCCTTA
		rv	CCAGTTTCTGTAGCTGGGTCA
AT4G39070	BZS1	fw	TGCTCCTCTTTGTGATATTTGC
		rv	CACATTCTCTGCATAGTATTGCTCT
AT3G10910	DAFL1	fw	CATGAAAGCTACGGAGTGTTTG
		rv	CCCTAACTTTTTCTCCATCTTCG
AT1G67340		fw	CGGAAGTCTCGAAGCTTGTT
		rv	CGCGGCTTTAGCCATTAAC
AT2G20080	TIE2	fw	TCTTTGTATCCTCAGATGGGAGT
		rv	TGGCTCTCTAAGATGCCGTAG
AT4G29905		fw	AACCAAAACAGAAAGAATGAAGAAA
		rv	TTGAGAGGAGAAGCAACCAAA
AT3G18450		fw	CATGGTTTTGACCCCATTCT
		rv	TCTCTTGCTGCTGTGCTTGT
AT3G51540		fw	AAATGGCTATCAATCACTTGGAC
		rv	CTACCACACGGTTTTCTTAGACC
AT5G67620		fw	ACCAAGATGGCGCTGATAAT
		rv	ACCACCACCTCTTCCTCCA
AT3G46880		fw	ACTCCATTTTCCCTCCTTCC
		rv	GGACCCATGTTTGGAGCTTA
AT5G57887		fw	GGGCAAGAAGATTCAGAGGA

		rv	ATGGAAGGAGCCTGACAAAA
AT3G59340		fw	GCTGGTGTTGTCATGGTACTCT
		rv	TCCAGCTAGAACAAGAAAATCTCC
AT5G19970		fw	GCTTATCAAATCGACCTCACG
		rv	GGTTTATTATCGAACCATCGTCA
AT1G74458		fw	TTGAATCGTCAGATTAGCCATC
		rv	GCACCGGATCCTGGATAA
AT4G29310		fw	AAGGGTTCGTGATGGGTTC
		rv	GTGGACCACAGGCTTGCT
AT1G68500		fw	CGGAAGAGGAGGAGCAATG
		rv	CCACACAGAGCTCCACGTTA
AT3G05936		fw	CATGGCGAGAGATTGACAAC
		rv	CCCCAAGTTCTGTCTTTTGG
AT3G01730		fw	GGGAACGACGAGACACTCAC
		rv	TACCAGTTGGTGACGGTGAA
AT2G22122		fw	AGAAGAGATGGCGGTGTTGA
		rv	CTCTATTACCGGCGGAAGAA
AT4G03420		fw	CACACTCTTTCATCTTCTTTCCAA
		rv	CCTTCCTTCCGGATCCTCT
AT1G02380		fw	ATGATTTTGCTCCCGTTGAG
		rv	CCCGAAATTCGCTTCCTC
AT5G18661		fw	GGTGGGATGTGTATGTCTGCT
		rv	TGTTAGTAAACTCGAACCTTCATCG
AT1G27020		fw	AAGTACTTTGGGGTCTTTAATTTGG
		rv	CGGCAAATTCGCTTTCTTT
AT3G50610		fw	AGCTGGATTTACAGATGATTTCG
		rv	TGTCCCACACCAGGACTGT
AT1G07690		fw	GGTCGTCGTCTTCTAACCAGA
		rv	GCTCTTAAGTTTCTTTTTCGCACT
AT1G54950		fw	CTTCCACCAACTTTCCTCTCA
		rv	CATTGGTAACCACAAGAAATGATTC
AT5G38940		fw	CCAACTTCAAGACTTTTGTGTCA
		rv	GGGTCCTTGCAGAACTTTCC
AT3G18080	BGLU44	fw	AAGATTGGAATGTGGAATTTGG
		rv	ACGAGTAAGCCCTTGGACCT
AT2G33460	RIC1	fw	GTCCAACCAACACCACACC
		rv	GGAAACGACTTGACCTTTCTCA
AT5G61650	CYCP4;2	fw	ATTTGGATCGGTTCGTGAAG
		rv	AGCCTATGGACATTAAAAGAATTGA
AT5G07450	CYCP4;3	fw	TTGATTCCTCTAATGTCCATAGACTC
		rv	CGCATAGAATGCATTATTGTAACAC
AT2G28510	DOF2.1	fw	CGGAGTTGTACCGGAGATTG
		rv	CCATTATTCCAAGATGAAACCAT
AT3G45610	PED1	fw	GATGGAGAACACGGGGTATG
		rv	CACTTGTCGCCATCTGCTC
AT5G60200	TMO6	fw	AGAAACCTTCTCCTGCAACG
		rv	AACGTGGACACCTGAGAGCTA

Chapter 5

Identification of novel bHLH transcriptional networks downstream of TMO5/LHW

Wouter Smet[1,2,3], Maria Angels de Luis Balaguer[4], Rosangela Sozzani[4], Dolf Weijers[1] and Bert De Rybel[1,2,3]

1. Wageningen University, Laboratory of Biochemistry, Stippeneng 4, 6708 WE Wageningen, the Netherlands
2. Ghent University, Department of Plant Biotechnology and Bioinformatics, Technologiepark 927, 9052 Ghent, Belgium
3. VIB Center for Plant Systems Biology, Technologiepark 927, 9052 Ghent, Belgium
4. Plant and Microbial Biology Department, North Carolina State University, NC 27695, Raleigh, United-States of America

Abstract

The TMO5/LHW heterodimer triggers periclinal and radial cell divisions through the regulation of a set of genes. In part, its action is mediated through promoting cytokinin biosynthesis, but it is unclear whether there are other, yet unknown target genes. Using a fine-resolution temporal transcriptomic dataset upon TMO5/LHW induction, we identified a novel target that is sufficient to trigger divisions. However, it is unlikely that action is relayed by a single target gene. Here, we re-analyzed our high temporal resolution transcriptomics dataset of TMO5/LHW using inferred network analysis to find more key regulatory hubs downstream of TMO5/LHW. The obtained gene regulatory network revealed a subfamily of bHLH transcription factors (TFs), acting as key nodes in the downstream responses. We show that most of the subclade members are expressed in the vasculature and are cytokinin-inducible. As single overexpression of these bHLH TFs using different promotors did not show any effect, we hypothesized that they require a heterodimerization partner. Indeed, using IP-MS/MS we identified that at least bHLH36 interacts with two bHLH TFs from yet another bHLH subfamily that are promising candidates for heterodimerization partners. In parallel, we generated *bhlh36, bhlh36 bhlh118* and *bhlh36 bhlh126* loss-of-function mutants using CRISPR/CAS9. As expected given the redundancy in the bHLH family, these single and double mutant combinations did not show a clear phenotype. Current efforts are focused on generating quadruple and hexuple mutant lines to understand the function of this novel bHLH subclade downstream of TMO5/LHW.

Introduction

The basic-loop-helix (bHLH) domain is a conserved amino acid motif that defines a family of transcription factors. While first discovered in animals it was later found in all the major eukaryotic lineages. Within these organisms, the bHLH family proteins have been described to function in numerous processes, from cell proliferation in animals to the formation of secondary metabolites in plants (Neuman, et al., 1995; Ludwig, et al., 1989). More than 170 bHLH family member genes are found in the *Arabidopsis thaliana* genome that fall within 26 subfamilies, and this is representative of other flowering plant model systems (Dolan, et al., 1993). About 20 of these subfamilies are also found in early land plants like lycophytes and mosses (Pires and Dolan, 2010). However, the genomes of chlorophytes and red algae only contain a small number of bHLH family genes (Pires and Dolan, 2010). Therefore it is hypothesized that the increased diversification of the bHLH family has co-evolved with the increase in anatomical complexity of multicellular organisms.

The bHLH domain defining this transcription factor family is characterized by 50–60 amino acids that form two separate regions. The N-terminal basic region that is a stretch of 10–15 amino acids with a high number of basic residues, is involved in DNA binding (Ferredamare, et al., 1994). The C-terminal helix-loop-helix region has a size of approximately 40 amino acids and forms two amphipathic α-helices separated by a loop of variable length. The helix-loop-helix domain promotes the formation of homo- or heterodimers between bHLH proteins, a prerequisite for these proteins for DNA binding to occur (Kadesch, 1993; Murre, et al., 1989).

In *Arabidopsis thaliana*, a number of bHLH family members have been described to function throughout plant development. For example, TARGET OF MONOPTEROS7 and its close relatives act early during embryonic development where they regulate hypophysis divisions and ensure proper embryo development. Another developmental process where bHLHs play a key role is the development of the stomata. Here, five bHLH genes from two different subfamilies promote stomatal lineage initiation and progression (Kanaoka, et al., 2008; MacAlister, et al., 2007; Ohashi-Ito and Bergmann, 2006). Three of these genes *SPEECHLESS (SPCH)*, *MUTE* and *FAMA* are members of the same subfamily and act sequentially to promote cellular transition during stomatal development. (MacAlister, et al., 2007; Pillitteri, et al., 2007; Ohashi-Ito and Bergmann, 2006).The activity of SPCH and MUTE is controlled by heterodimerization with two bHLH proteins from a different

subfamily: SCREAM (SCRM) and SCRM2. Finally, as described in **Chapter 1**, one of the major pathways controlling vascular development also requires regulation by interacting bHLH TFs. Here, TMO5 and LHW heterodimerize within the xylem axis cell to promote periclinal and radial divisions (PRDs) in the neighboring cambium cells through cytokinin production. TMO5/LHW dimer activity itself is limited by interaction of LHW with SACL proteins, another bHLH subfamily.

Given the low number of downstream genes identified with the misexpression strategy in **Chapter 3**, here we re-analyzed our TMO5/LHW transcriptomics dataset using inferred network analysis to find important players in the network downstream of TMO5/LHW. As such, we identified a novel subfamily of bHLH transcription factors which is under the control of TMO5/LHW and cytokinin, and their bHLH interaction partners.

Results

In **Chapter 4**, we described how genes were selected from our high temporal resolution TMO5/LHW transcriptomics data set by screening for PRD phenotypes upon misexpression. As it seems unlikely that only one additional gene would be involved in controlling PRD downstream of TMO5/LHW (see **Chapter 4**), we considered that our misexpression strategy might not have been ideal. Thus, we decided to re-analyze our dataset using a different approach to find more key players downstream of TMO5/LHW.

Network inference pinpoints a novel subfamily of bHLH transcription factors as major hubs downstream of TMO5/LHW

Gene expression datasets show expression levels of a large number of genes under specific conditions. In general, this data is then used to describe how genes behave under these conditions or how they are regulated. However, the expression levels of these genes can additionally be used to gain more knowledge about the relationship between genes, and ultimately gain a better understanding of the underlying gene regulatory networks (GRN) (Alina Sîrbu, 2011). Network inference uses wet-lab data in order to model GRNs, from which interactions can be verified experimentally. A modeled GRN represents a prediction of how molecular regulators (genes, proteins and/or metabolites) interact with each other and regulate gene expression. Studying the topology of the obtained network can reveal which genes are key regulators. The first step in using gene expression data for GRN inference

applies pattern analysis algorithms on both experimental and gene patterns seen in the data. Such algorithms include clustering, classification and feature selection techniques. The second step in GRN inference is using time series gene expression data for mathematical modelling. Modelling a GRN consists of a few main steps: choosing an appropriate model, inferring parameters from data, validating the model and conducting simulations of the GRN to predict its behavior under different conditions. The output GRN consists of nodes and edges connecting the different nodes. Nodes may represent genes, mRNA, protein or other molecules. Edges have a specific starting node and represent interaction or regulation of the starting node to the connected node. (Alina Sîrbu, 2011; Hecker, et al., 2009; Albert, 2007)

Having generated a high temporal resolution dataset, we were able to identify consecutive waves of gene expression upon TMO5/LHW induction (see **Chapter 2**). As such, this data-set should be ideal to identify transcriptional hubs downstream of TMO5/LHW using network inference analysis. It can then be assumed that these highly connected hubs would play an important role in executing the downstream effects upon TMO5/LHW induction and are worth studying in more detail.

In order to infer relationships and relative importance in the differentially expressed genes, we utilized the GENIST regulatory network inference algorithm (see **Materials and Methods** section for detailed description) (Balaguer, et al., 2017). The application of GENIST resulted in 6 individual networks, corresponding to pairwise comparisons between the 0 hour and all consecutive time-points of the TMO5/LHW induction time course in which 0.5h and 1h were combined into one set (0h-0.5+1h, 0h-2h, 0h-3h, 0h-4h, 0h-5h and 0h-6h). Both *TMO5* and *LHW* were artificially rooted in the network to be used as the start of the transcriptional cascade. To illustrate the cascade of regulations through time, the networks were color-coded for each time-point and jointly visualized (**Figure 1**). The thickness of each edge correlates with the probability with which the corresponding regulation was calculated, and the size of each node correlates with the number of genes that it directly regulates. Thus, predicted important regulators can be identified as the largest nodes in the network. As an intriguing first observation, the network places the initial time points at the center, and shows how the cascade of regulations expands outwards over time, suggesting that the network reproduces the consecutive waves of gene expression well (**Figure 1**).

When analyzing the obtained gene regulatory network in more detail, we first observed the position of the known TMO5/LHW targets in the network. We could

observe that TMO5 controls the expression of *LOG3/4*, *BUD2* and the upstream Open Reading Frames (*uORF34/35*) of *SACL3* at the 1h time point, confirming the proper interaction of the known direct target genes. At the 2h time point, the B-type *ARR12* gene and the A-Type *ARR3*, *ARR4* and *ARR6* genes were found as nodes indicating that also cytokinin response is incorporated into the network.

Within the network, we focused our attention on the 3-4h time points, for similar reasons as in **Chapter 3**: after the initial wave of direct target genes, but before PRD occur and co-expressed with CK-responses. With this selection criterion in mind, we should be able to identify both CK-induced and CK-unrelated targets genes which are induced at these time points. Intriguingly, the biggest hubs in the network were all linked to the 3-4h time points (**Figure 1**). One of these prominent nodes corresponded to *AT2G28510/DOF2.1* (**Figure 1B**), which is described in **Chapter 3** as an important player downstream of TMO5/LHW controlling PRD. This result confirms the power of the inferred network to identify novel downstream factors involved in PRD. The three other major nodes at these time points correspond to three bHLH family genes (*AT4G25410/bHLH126*, *AT5G51780/bHLH36*, *AT5G51790/bHLH120*) belonging to the same subfamily of bHLH TFs (**Figure 1B,C**). In total, this subfamily consists of 6 genes of which 4 are differentially regulated in our transcriptomics dataset and were included in the inferred network (**Table 1**, **Figure 2**).
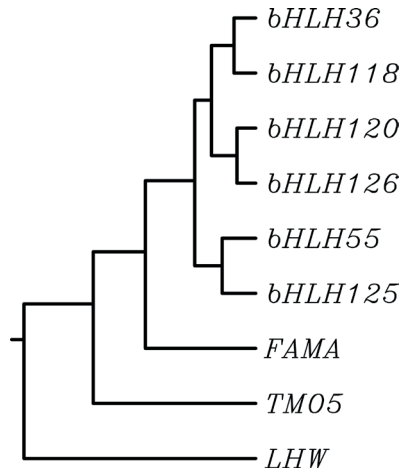
Figure 2: *Arabidopsis* bHLH transcription factor family tree based on protein sequence alignment. bHLH subfamily tree rooted to LHW, TMO5 and FAMA as unrelated bHLH factors. Alignment using ClustalW Omega on corresponding protein sequences.
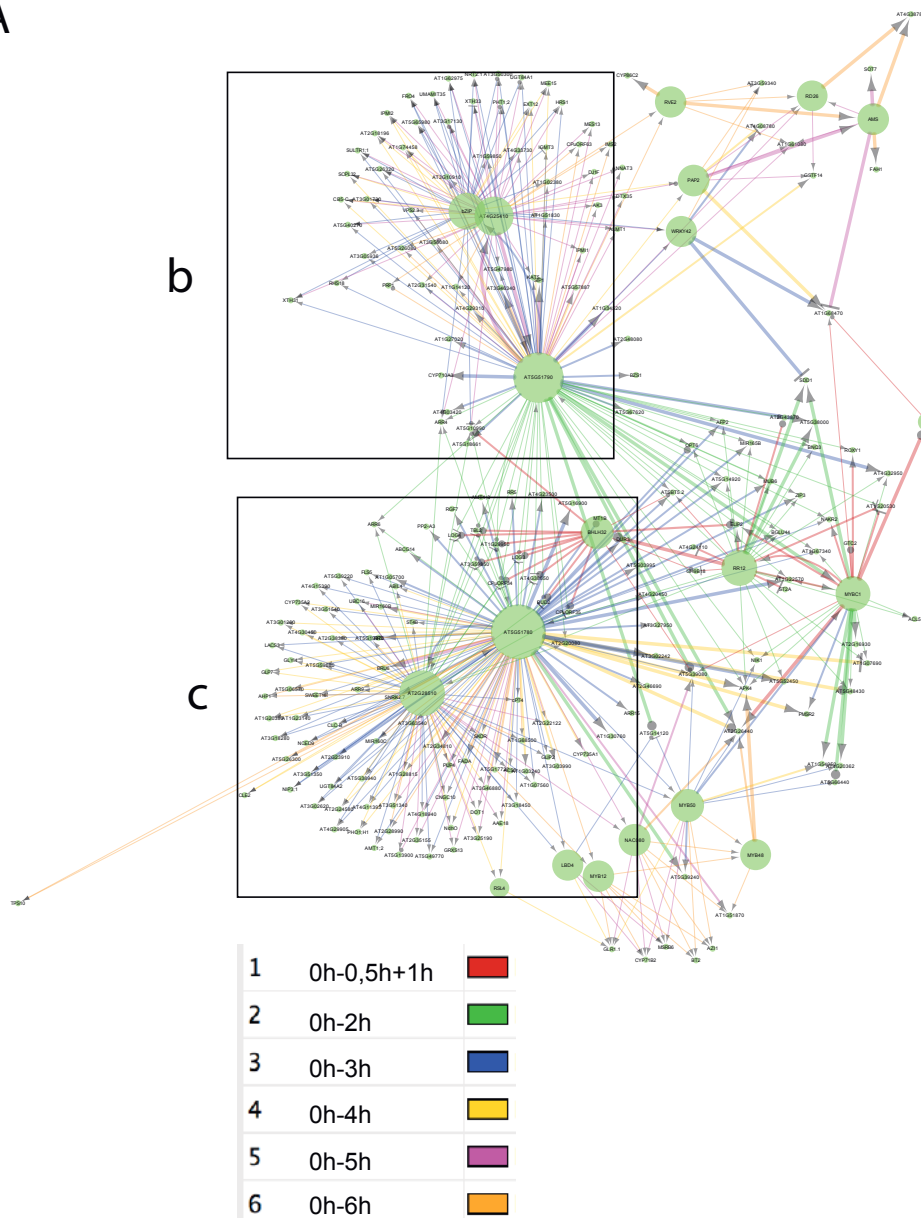
Figure 1: Inferred network of the dGR dataset. A. Overview of the network, b and c mark the more detailed view shown in **B.** and **C**. Nodes represent genes and, the size of the node correlates to the number of genes it directly regulates. The edges represent the interaction between nodes, the thickness of the edge correlates to the probability that the interaction was calculated. The color coding indicates the consecutive time-points of the TMO5/LHW induction time course 1-6 (0h-0.5+1h, 0h-2h, 0h-3h, 0h-4h, 0h-5h and 0h-6h).
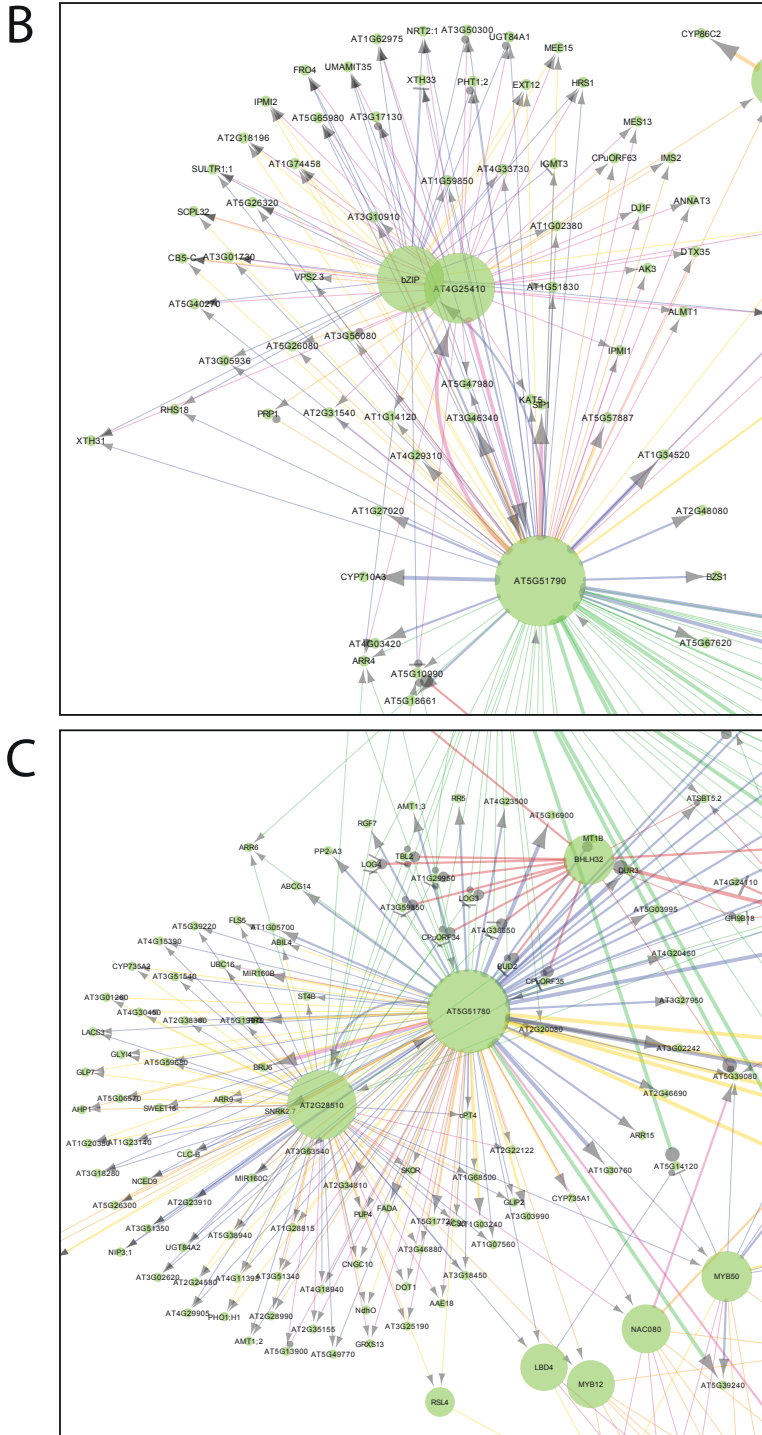
Table 1: Relative expression levels of bHLH subfamily members within the dGR micro-array dataset.
FC indicates fold-change depicted below. This is a ratio of the time point indicated compared to 0h time point.

	FC 0.5h/0h	FC 1h/0h	FC 2h/0h	FC 3h/0h	FC 4h/0h	FC 5h/0h	FC 6h/0h
bHLH36	1,0	1,7	2,5	3,4	3,1	3,7	3,0
bHLH55	1,0	1,1	1,0	0,9	1,1	0,9	1,0
bHLH118	0,9	1,1	1,2	1,4	1,2	1,2	1,2
bHLH120	1,3	1,7	2,1	2,0	2,2	2,4	3,0
bHLH125	1,0	1,3	1,7	2,5	2,5	2,3	2,3
bHLH126	0,9	1,1	1,7	1,8	1,7	2,0	2,5

The novel bHLH genes localize to distinct and overlapping regions in the root

To understand where these novel bHLH transcription factors might act, we first generated and analyzed transcriptional p*bHLH*::nGFP/GUS reporter lines (**Figure 3**) using confocal microscopy. All of these genes are expressed in the root; except for p*bHLH120*::nGFP/GUS for which none of the generated reporter line showed expression. We analyzed the root meristem of five-day-old p*bHLH*::nGFP/GUS seedlings in detail by imaging both longitudinal and radial cross-sections (**Figure 3**). p*bHLH36* shows expression in the root cap cells and cambium cells adjacent to the xylem axis (**Figure 3A,G**). p*bHLH55*::nGFP/GUS does not show any expression in the root meristem, however higher up in the root it is expressed in metaxylem, cambium and metaphloem cells (**Figure 3B,H,M,O**) p*bHLH126*::nGFP/GUS is expressed in the procambium cells, epidermis and root cap cells (**Figure 3F,L**). Neither p*bHLH118*::nGFP/GUS nor p*bHLH125*::nGFP/GUS are expressed in the vascular tissues in the root meristem (**Figure 3C,E,I,K**), but show a broad (**Figure 3N,P**) and cortex/epidermis expression (**Figure 3E,K**) respectively.

Most of the translational reporter lines did not show any expression except for p*bHLH36*::*bHLH36*:sYFP and p*bHLH120*::bHLH120:sYFP. This could indicate that the bHLH55, bHLH118, bHLH125 and bHLH126 have very low expression levels or that they are controlled post-transcriptionally. The expression of the pbHLH36::*bHLH36*:sYFP translational reporter line corresponded with the transcriptional reporter line and show mostly nuclear expression in the root cap both nuclear and mostly cytoplasmic expression in the procambium cells (**Figure 4A,C**). Unlike the transcriptional fusion, the translational p*bHLH120*::*bHLH120*:sYFP showed clear expression within the procambium cells higher up in the root meristem and is

localized in both the nucleus and cytoplasm (**Figure 4B,D**). The lack of transcriptional reporter of *bHLH120* is due to cloning difficulties and low transformation efficiency.
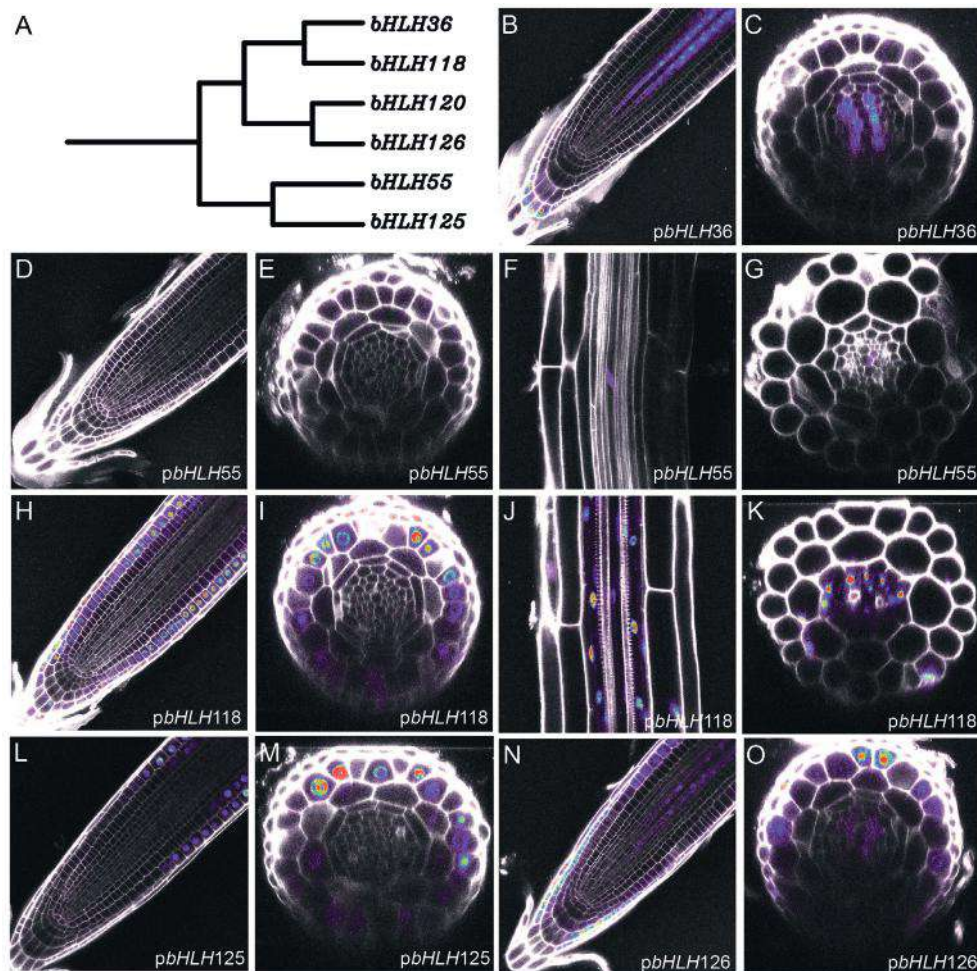

Figure 3: Confocal analysis transcriptional reporter lines p*bHLH*::nGFP-GUS transcriptional reporter lines. A. Arabidopsis bHLH transcription factor family tree based on protein sequence alignment. **B,D,H,L,N.** longitudinal cross-sections of the root meristem of the respective lines mentioned in the picure. **C,E,I,M,O.** Radial cross-sections in the center of the root meristem. **F,J.** Longitudinal section in the mature part of the root. **G,K.** Radial cross-section in the mature part of the root.

The novel bHLH genes are part of the TMO5/LHW cytokinin regulated targets

Interestingly, none of the observed expression patterns of the bHLH genes in this subfamily fully matches the TMO5/LHW overlapping expression domain along the xylem axis. Therefore, we hypothesized that these genes might be not be under direct control of TMO5/LHW but could instead be controlled through cytokinin. To

test this, we analyzed the relative expression of these bHLHs by Q-RT-PCR upon exogenous CK treatment (**Figure 5)** by transferring five-day-old Col-0 seedlings from cytokinin-free plates to plates supplemented with 10µM Benzyl Adenine (BA) for 0', 15', 30', 1h, 2h and 6h. As expected, relative expression level *bHLH36*, *bHLH120*, *bHLH125* and *bHLH126* were quickly induced upon BA treatment. The up regulation of the transcript of these bHLHs suggests that they are putative downstream effector of TMO5/LHW via CK-signaling. These data correspond to the observation that 5 out of 6 *bHLH* genes in this subfamily were recently found to be regulated by one or more of the main B-type ARRs (ARR1,ARR10 and ARR12) (Xie, et al., 2018; Zubo, et al., 2017), which are key cytokinin regulators necessary for proper vascular development (Ishida, et al., 2008; Yokoyama, et al., 2007).
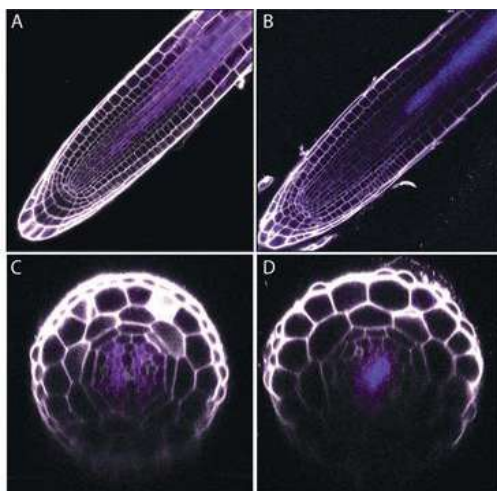
Figure 4: Confocal analysis translational reporter lines p*bHLH36*::*bHLH36*:sYFP and p*bHLH120*::*bHLH120*:sYFP A,B. show longitudinal sections of the root meristem of roots 4-DAG. **C,D.** show radial sections in the middle of the root meristem.

Next, to verify that TMO5/LHW indeed controls the expression of these expression in the root mersitem, we introduced the p*bHLH*::nGFP/GUS transcriptional reporter lines of p*bHLH36*, p*bHLH125* and p*bHLH126* into the dGR background. Five-day-old seedlings were grown on either DEX-free plates as a control or to plates supplemented with 10 µM DEX. Although *bHLH125* did not show any significant difference between treated and untreated roots in the root apical meristem, both the induced p*bHLH36*::nGFP/GUS and p*bHLH126*::nGFP/GUS lines showed increased expression in their normal domain and ectopic expression in the endodermis and cortex, suggesting that at least *bHLH36* and *bHLH126*, are under control of TMO5/LHW (**Figure 6**). The TCSn reporter also showed increased expression in these cells upon induction of

TMO5/LHW in the dGR background (**Chapter 3**). This suggests that the increased expression of the bHLHs in these goes through TMO5/LHW produced cytokinin.
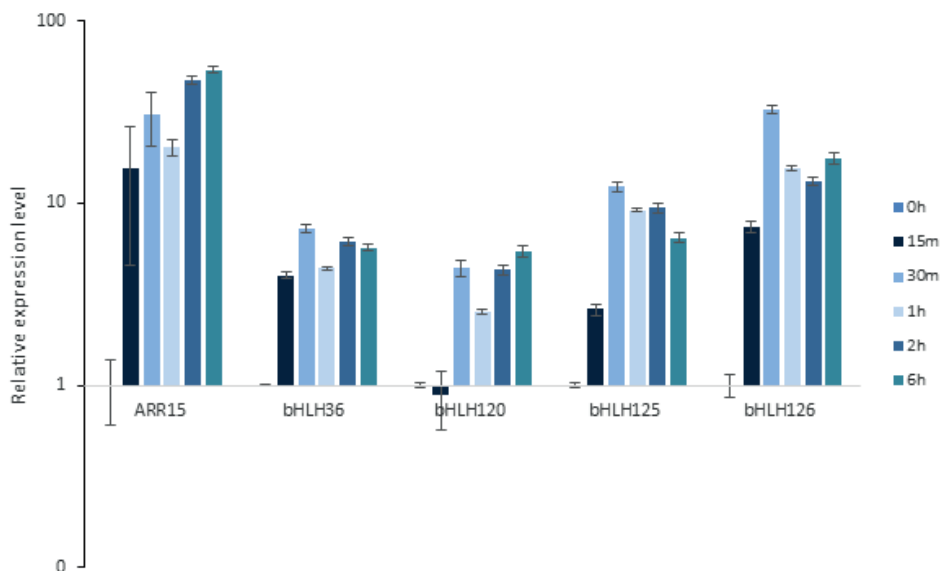

Figure 5: Relative expression levels of the bHLH subfamily upon BA treatment. Relative fold-changes of *bHLH36*, *bHLH120*, *bHLH125* and *bHLH126* in roots of five-day-old seedlings treated with 10μM BA. *EEF* and *CDKA* were used as reference genes. *ARR15* was used as a positive control.
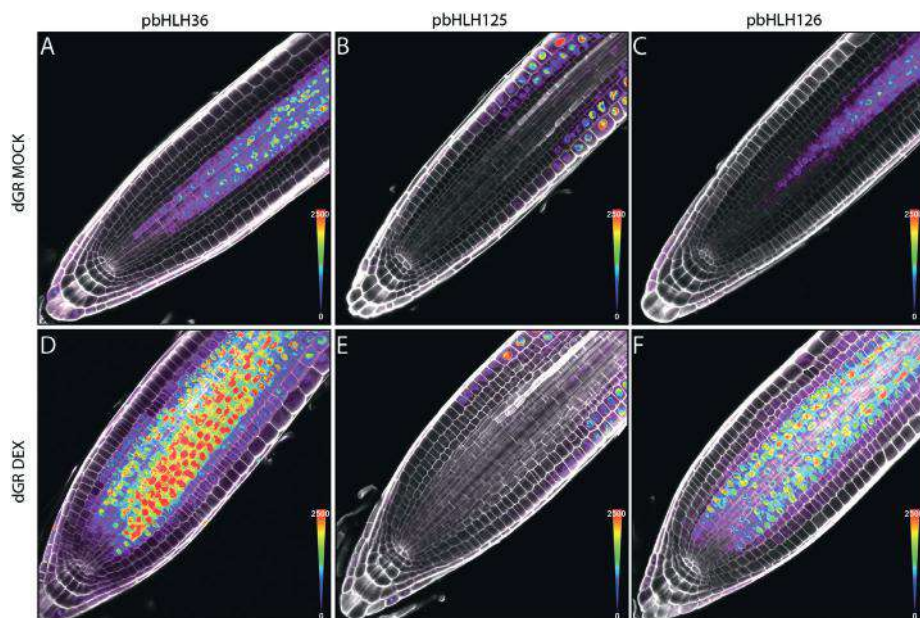

Figure 6: Confocal analysis of bHLH transcriptional reporters of p*bHLH36*, p*bHLH125* and *pbHLH126* in the dGR background A-C. mock treated samples **D-F.** samples treated with 10μM DEX.

The identified bHLH TFs might require interaction partners to execute their proper function

In **Chapter 3**, we selected 4 of these bHLH transcription factors (bHLH36, bHLH120, bHLH125 and bHLH126) as putative targets for our p*RPS5A* misexpression screen. However, no obvious phenotypes were found by confocal and DIC analysis. Misexpression of the other two bHLH TFs (bHLH55 and bHLH118) driven by the *RPS5A* promoter, also did not result in any obvious phenotype (data not shown). We hypothesized that this might be due to the strength of the promoter and we thus generated overexpression lines using the strong Cauliflower Mosaic Virus (CaMV) *35S* promoter. Plants of these overexpression lines also did not show any obvious phenotype, showing that increased and ectopic expression of single bHLH TFs from this subfamily does not result in obvious phenotypes. However, bHLH TFs are known to homo- or heterodimerize in order to bind DNA and active their downstream target (Kadesch, 1993; Murre, et al., 1989). We hypothesized that the lack of obvious phenotypes upon misexpression (using p*RPS5A*) or overexpression (using p*35S*) of these genes might be due to the fact that their putative interaction partner becomes limiting; similar to the TMO5/LHW heterodimer (Ohashi-Ito, et al., 2014; De Rybel, et al., 2013). To find potential interaction partners, we performed immunoprecipitation followed by tandem mass-spectrometry (IP-MS/MS) using the p*bHLH36*::*bHLH36*:sYFP translational reporter line and a p*35S*::*bHLH36*:GFP overexpression line. Using the obtained MS-data we compared protein groups found in the material of the previous described line and the Col-0 control. Ratios of protein abundance are found in **Table 2**, volcano plots of both samples can be found in **Supplemental Figures 2 and 3**. For both samples we could find our bait protein and fluorescent tag used to pull the protein indicating a technically successful experiment.

Intriguingly, the two first proteins on top of the list using the ratio of the translational fusion versus the control were two novel bHLH TFs (AT4G29930/bHLH27 and AT5G57150/bHLH35); both belonging to yet another novel subfamily of bHLH TFs (**Figures 8, 9, 10 and Table 2**). Peptide coverage of these proteins can be found in **Supplemental Figure 1**. To see if these bHLHs are controlled by TMO5 and LHW we looked in our obtained micro-array dataset, *bHLH35* shows a weak regulation of 1,6-fold at 6h upon TMO5/LHW induction, while *bHLH27* did not respond at all (**Table 3**), suggesting that these putative interacting bHLH TFs are not under the control of TMO5/LHW; adding another layer of control on the putative function of these TFs.
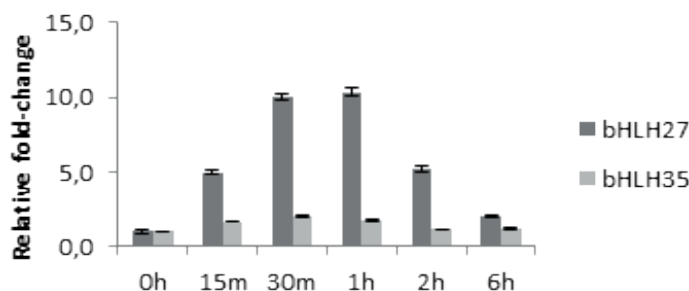
Figure 7: Relative expression levels of bHLH27 and bHLH35 upon cytokinin treatment. Relative fold-changes of *bHLH27* and *bHLH35* in roots of five-day-old seedlings treated with 10 µM BA. *EEF* and *CDKA* were used as reference genes.

Table 2: Overview of selected protein groups by IP-MS. Table shows ratio of highly abundant proteins found in material of seedling of p*bHLH36*::*bHLH36*:sYFP (genomic) and p*35S*::*bHLH36*:GFP (35S) compared to Col-0. Green color indicates the bait protein used to find potential interactors. Yellow color indicates GFP/YFP tag used to pull the bait protein. Unique peptides shows the amount of unique peptides found per protein ID.

Ratio Genomic/Col-0	p-value	Ratio 35S/Col-0	p-value	Unique peptides	Protein ID	Description
918,7	0,01	489,0	0,01	8	AT5G57150	bHLH35
154,1	0,02	75,9	0,04	7	AT4G29930	bHLH27
115,3	0,00	179,4	0,00	4	AT5G23060	CaS | calcium sensing receptor
111,4	0,01	1997,2	0,00	10	P42212;PSB_N_GFP	GFP
64,8	0,00	540,1	0,00	7	AT3G09440	Heat shock protein 70 family protein
59,1	0,00	1136,1	0,00	10	AT5G62390	BAG7
51,4	0,00	57,1	0,00	2	AT3G25860	LTA2, PLE2
44,1	0,00	47,4	0,00	1	AT1G14320	SAC52
38,5	0,00	68,2	0,00	2	AT5G21274	CAM6
38,5	0,00	3,0	0,37	3	AT4G27170	SESA4
34,5	0,00	72,1	0,00	9	AT5G51780	bHLH36
29,7	0,00	16,0	0,03	2	AT4G27140	SESA1
25,7	0,00	23,4	0,00	1	ATCG00790	RPL16
22,6	0,16	19,9	0,17	2	AT5G53800	unknown protein
16,7	0,05	24,8	0,02	1	AT3G26650	GAPA, GAPA-1
16,7	0,00	22,3	0,00	1	AT3G48930	EMB1080
12,1	0,12	56,8	0,00	3	AT3G17390	MTO3, SAMS3, MAT4
11,3	0,00	10,6	0,00	1	AT1G30380	PSAK
10,6	0,13	43,4	0,00	3	AT5G35630	GS2, GLN2, ATGSL1
10,6	0,11	4,1	0,46	2	AT3G16430	JAL31

To test if these bHLHs are also controlled by cytokinin, we analyzed the relative expression of these bHLHs by Q-RT-PCR upon exogenous CK treatment (**Figure 7**) by transferring five-day-old Col-0 seedlings from cytokinin-free plates to plates supplemented with 10µM Benzyl Adenine (BA) for 0', 15', 30', 1h, 2h and 6h. This showed that transcript levels of *bHLH27* are more than 10-fold induced upon CK treatment, while *bHLH35* was induced about 2-fold.

Although so far we have only analyzed putative interaction partners of bHLH36, it is likely that the other members of this subfamily might also interact with bHLH27/bHLH35 or other bHLH factors and require them for their function. Hence, it will be useful to further explore the interaction network of this novel bHLH subclade with other bHLH TFs.

Table 3: Relative expression levels of bHLH subfamily members within the dGR micro-array dataset. FC indicates fold-change depicted below. This is a ratio of the time point indicated compared to 0h time point.

	FC 0.5h/0h	FC 1h/0h	FC 2h/0h	FC 3h/0h	FC 4h/0h	FC 5h/0h	FC 6h/0h
bHLH27	1,1	0,9	1,1	1,1	1	1,1	1,1
bHLH35	0,9	0,9	1,1	1,3	1,3	1,3	1,6

bHLH candidate genes act in a redundant manner

Because the bHLH genes found in our inferred network analysis all belong to the same subfamily, we expected they might act in a redundant manner. Thus we aimed to generate higher order mutants of members of this bHLH subfamily by utilizing the CRISPR/CAS9 system. Using this system, so far, we obtained a *bhlh36* single, a *bhlh36 bhlh118* double and two *bhlh36 bhlh126* double mutant combinations in which the CRISPR/CAS9 construct has already been removed (**Figure 11A**). Although we are currently generating higher order quadruple and hexuple mutants to circumvent all genetic redundancy, we decided to already analyze these mutant combinations for an effect in vascular proliferation. We imaged the root meristems of five-day-old seedlings of these mutant lines and did not observe any difference when compared to the Col-0 control. When radial cross-sections of these roots were imaged and quantified for the amount of cell files; one of the two **b**hlh36 *bhlh126* loss-of-function mutant combinations showed a significantly higher cell file number when compared to the Col-0 control (**Figure 11B**). Because both *bhlh36 bhlh126* loss-of-function mutants result in frame shifts in the second exon and lead to premature stop codons, the difference in the effect is unexpected.

In the network analysis, *bHLH36, bHLH120* and *bHLH126* are found as the major regulators downstream of TMO5/LHW, also showing the biggest nodes. All three TFs are expressed in an overlapping manner within the vascular bundle and could thus act as part of the downstream TMO5/LHW response. Hence, a triple loss-of function of these genes might provide key insight how these bHLH TFs function downstream of TMO5/LHW. Additionally we might have to generate even higher order mutants and different combinations of loss-of-function mutants within this bHLH subfamily to fully understand the function of all the genes within this family.
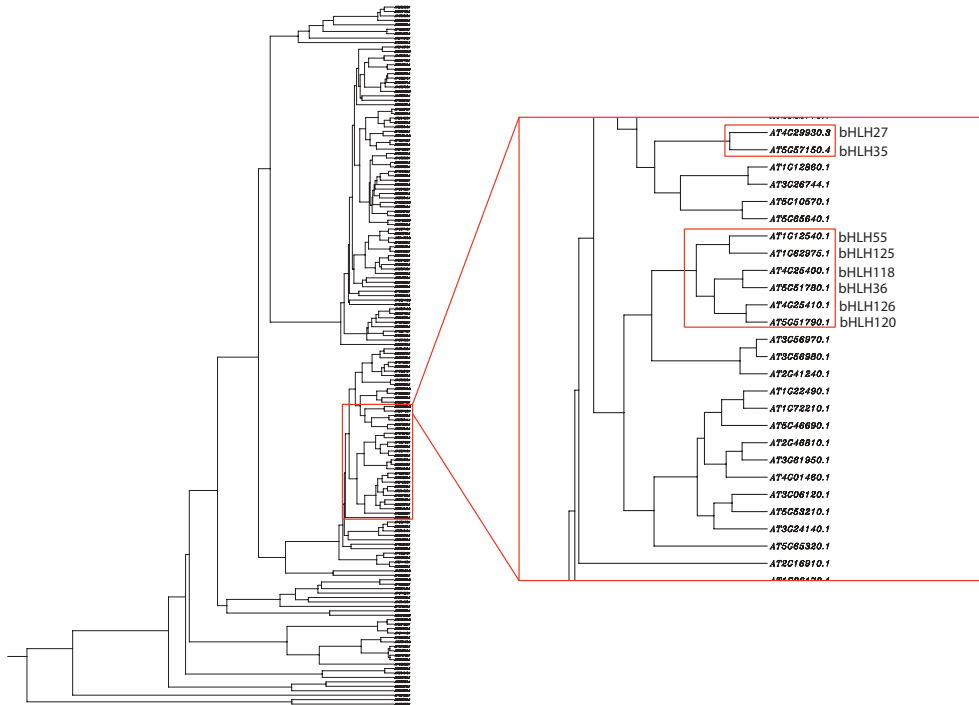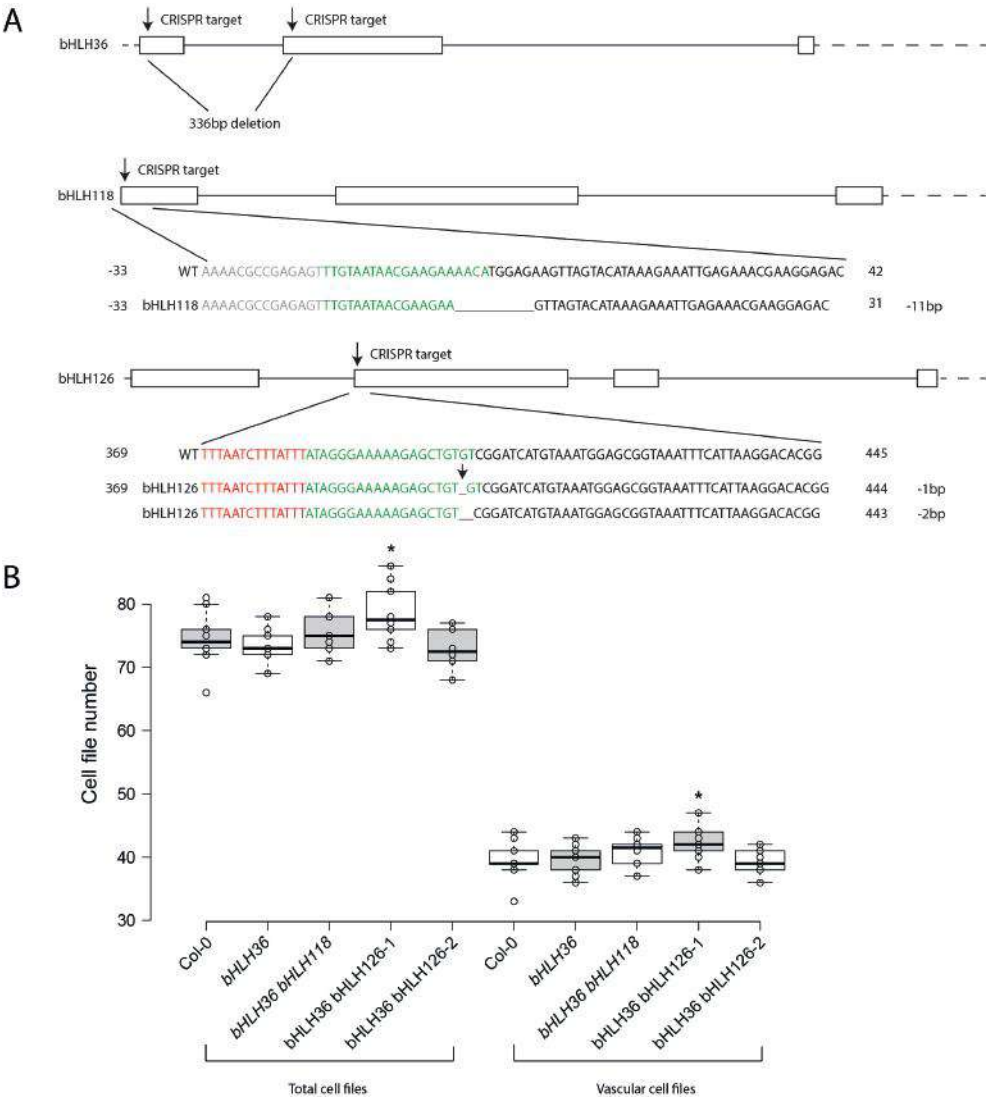
Figure 10: Arabidopsis bHLH transcription factor family tree based on protein sequence alignment. Orange boxes marks the bHLH subfamilies found in the IP-MS and network analysis.

lines represent 5' and 3' untranslated regions, boxes represent exons and lines represent introns. Grey letters represent intergenic regions. Red letters represent introns, black letters represent exons, and green letters represent the protospacer adjacent motifs selected for CRISPR mutations. Numbers show the distance from the start of the gene in base pairs. **B.** Box plot of cell file number in root meristems of Col-0, *bhlh36*, *bhlh36 bhlh18*, *bhlh36 bhlh126-1* and *bhlh36 bhlh126-2* loss-of-function mutants. Asterisk marks significance compared to the 0h time point according to a two-sided Student T-test ($p < 0.05$) (n>10).

Discussion and future perspectives

136

Because our misexpression strategy in **Chapter 4** yielded only one novel target gene showing an effect, we reanalyzed our high temporal resolution transcriptomics dataset of TMO5/LHW by using inferred network analysis. The obtained network reflected the consecutive waves of genes expression shown in **Chapter 3**, with early TMO5/LHW activation triggering cytokinin signaling and subsequent downstream responses; giving confidence in this strategy. This was further corroborated by identifying *DOF2.1* as one of the major nodes. Several of the other large nodes at the same time points belonged to a novel subfamily of bHLH TF. We thus decided to investigate this bHLH subfamily in more detail. While these bHLHs were also selected in **Chapter 4**, network inference proved to be a valuable tool to visualize the obtained data in a different way and pinpoint that these bHLH TFs might be important players, despite not having a single misexpression phenotype. Although network inference is a potent tool to find downstream factors, one should keep in mind that it is mainly oriented towards finding TFs and thus interesting other genes involved might be missed when using only this approach. Hence, although time consuming, a combination of several strategies will likely result in the best results regarding the selection of genes in a whole genome transcriptomics experiment.

Our expression analysis showed that these novel bHLH TFs have distinct and overlapping expression domains in the root. We further confirmed that several factors are likely downstream of the TMO5/LHW-dependent CK biosynthesis and signaling. This is further supported by the fact that all except one of the members of this family are putative transcriptional targets of one or more of the main B-type ARRs: ARR1, ARR10 and/or ARR12 (Xie, et al., 2018). These three ARRs are required for proper development of the vasculature as the *arr1,arr10,arr12* triple mutant has a major reduction in the amount of vascular cell files which are all differentiating into protoxylem cells (Ishida, et al., 2008). Confirming that CK signaling downstream of TMO5/LHW (leading to both vascular proliferation and inhibition of protoxylem differentiation) would go uniquely through these B-type ARRs would be a great step in understanding how TMO5/LHW produced cytokinin influences vascular development. However, it is very likely that other B-type ARRs might also play a role (Brecht Wybouw, personal communication of unpublished data).

Because at this point we lack both gain-of-function and loss-of-function phenotypes of the novel bHLH family members found in this chapter thus it is difficult to speculate about a specific function. It is crucial that we continue the generation of higher order loss-of-

function mutants within this family. Additionally we should investigate the combined overexpression of the bHLHs described here with their putative interaction partners.

Materials and Methods

TMO5/LHW Gene Network Inference

To infer a gene regulatory network (GRN) and predict the causal relationships of genes regulated by TMO5 and LHW, differentially expressed genes (DEGs) were identified using q < 0.05 & fold change > 2 as our selection criteria, when performing pairwise comparisons between hours 0-0.5, 0-1, 0-2, 0-3, 0-4, 0-5, and 0-6 of the TMO5/LHW induction time course. This resulted in the identification of 237 genes differentially expressed at 0.5, 1, 2, 3, 4, 5, and 6 hours after TMO5/LHW induction, which contained 22 transcription factors. To preserve the temporal cascade of regulations, the network was inferred as individual GRNs containing the DEGs at each time point, as opposed to predicting a GRN containing the 237 DEGs together. Specifically, because we assume that regulation between genes can occur, not only during concurrent time points, but also between consecutive time points, the DEGs from consecutive time points were grouped (0.5-1, 1-2, 2-3, 3-4, 4-5, 5-6 hours), and GRNs from each of the 6 resulting lists of genes were inferred. The GRN inference on each of the 6 sets of DEGs was performed by applying a dynamic Bayesian network (DBN)-based inference algorithm, GENIST (Balaguer, et al., 2017). Since GENIST offers the possibility of clustering genes based on their co-expression prior the inference step to improve the performance of the algorithm, GENIST was ran using a previously published TMO5-GR dataset (TMO5 induced for short time points and a cell sorted set) (De Rybel, et al., 2014) for the clustering step. Details about the application of GENIST to each of the 6 sets of genes are provided below.

1. Gene selection

The genes differentially expressed at each time point after induction of TMO5/ LHW, g_t, for $t \, \epsilon \{0.5, 1, 2, 3, 4, 5, 6 \}$ hours were selected. Then, the DEG from every two consecutive time points, g_t and $g_{(t+1)}$, were combined in sets S_τ, for $\tau \, \epsilon \{0.5\&1, 1\&2, 2\&3, 3\&4, 4\&5, 5\&6 \}$. Steps 2 and 3 were applied to the genes in each set S_τ individually.

2. Clustering

The expression values from the TMO5 induction from De Rybel et al., 2014 were used as the input data. Clustering of the genes in S_T was implemented by using the Silhouette index followed by linkage clustering. This resulted in a division of the S_T genes in c clusters.

3. GRN inference

3.1. Inferring intra-cluster connections for each cluster C_n, for n ε [1,c]:
The expression values in the TMO5/LHW induction time course for all genes in cluster C_n were used as the input data.

3.1.1 Selecting potential regulators: A gene g_r was selected as a potential regulator of a target gene g_s (denoted $g_r \rightarrow g_s$) if it exhibited a ±p×g_r change of expression immediately prior a change of expression of g_s of ±p×g_s:
$g_r \rightarrow g_s \leftrightarrow (g_r (t) > (1+p) \times g_r (t-1) | g_r (t) < (1-p) \times g_r (t-1)) \& (g_s (t + 1) > (1+p) \times g_s (t) | g_s (t + 1) < (1-p) \times g_s (t))$,   (1)
where we set a low threshold (p=0.1) to ensure that no regulators were missed.

3.1.2. DBN modeling: The GRN inference step was implemented as a Dynamic Bayesian Network (DBN) learning problem, where the dependences among the variables (genes) can be derived over adjacent time steps. Assuming stationarity and the genes to be modeled obeyed the first order Markov assumption, the joint probability distribution could be expressed as:
$P (X_1,...,X_m) = \prod_i P (X_i | X_1,...,X_{(i-1)}) = \prod_i P (X_i | Pa(X_i))$ (2)
where X_i is the expression of gene i, m = n(T − 1) is the number of genes (nodes), and Pa(X_i) is the set of regulators of gene i (parents of node i).

Given some observations of the variables over time, the DBN estimation was implemented by finding the structure of (2) that maximized the Bayesian Dirichlet equivalence uniform (BDeu) score [3]. Since the BDeu score of a DBN can be decomposed as the sum of the scores of the log conditional probabilities of each node, the log of the BDeu, BDeul, was used:

$$BDeu_l(D, G) = \log(P(G)) + \sum_{i=1}^{n} \sum_{j=1}^{q_i} \left(\log \left(\frac{\Gamma\left(\frac{\alpha}{q_i}\right)}{\Gamma\left(\sum_{k=1}^{r_i} N_{ijk} + \frac{\alpha}{q_i}\right)} \right) \right) + \sum_{k=1}^{r_i} \log(\frac{\Gamma(N_{ijk} + \frac{\alpha}{q_i})}{\Gamma(\frac{\alpha}{r_i q_i})})) \qquad (3)$$

139

the observations of the system, N_{ijk} indicates the number of data vectors in which gene i, X_i, has the value k while its parents are in the jth configuration, and α refers to the hyperparameters of the Dirichlet distribution.

From (2) and (3), the problem of deriving the DBN can be decomposed into finding the parents for each node. For this, the expression values of each gene were discretized in 2 levels (high and low). Then, for each gene, a list of all possible subsets of potential regulators was generated. To lower the complexity of the algorithm, which increases exponentially with the number of genes, the maximum size allowed for any subset (maximum number of regulators of a gene) was set to 3. The $BDeu_l$ was used to evaluate the likelihood that each gene was due to each subset of potential regulators. The regulators of gene i were selected as the ones contained in the subset that led to the highest value of the $BDeu_l$.

3.2. Inferring inter-cluster connections
Steps 3.1.1-3.1.2 were repeated for all hubs (cluster node with the largest degree of edges leaving the node (out-degree)) in all clusters Cn, for n ϵ [1,c]. This resulted in inter-cluster interactions among the cluster hubs.

3.3. Determining the sign of the interactions
A score was implemented to estimate whether the inferred interactions (edges) were activations or repressions. The score was calculated for each edge as the conditional probability that a gene is expressed (or not expressed) given that a parent was expressed (not expressed) in the prior time point, relative to the probability that a gene is expressed (or not expressed) given that a parent was not expressed (or viceversa expressed) in the prior time point. If the first conditional probability is larger (or smaller) than the second one, then the parent was found to be an activator (or repressor). In the case of a tight, the edge was found to have an undetermined sign.

The application of GENIST with this data resulted in 6 networks, corresponding to the 6 sets of DEGs, S_T. To illustrate the cascade of regulations through time, the networks for each set were jointly visualized in Cytoscape (Shannon, et al., 2003). The final network has 237 nodes, corresponding to the 237 DEGs, and 532 edges (regulations). The thickness each edge correlates with the probability with which the corresponding regulation was calculated (as in (3)), and the size of each node correlates with the number of genes that it directly regulates. The predicted most important regulators can be identified as the largest nodes in the network.

The network depicts the time cascade by color-coding the regulations inferred in the different time points: red (0.5-1), green (1-2), blue (2-3), yellow (3-4), pink (4-5), orange (5-6) hours. Overall, the network places the initial time points at the center, and shows how the cascade of regulations expands outwards over time.

Plant material and growth conditions

All seeds were surface sterilized, sown on solid on ½ MS plates without sucrose and vernalized for 24h at 4°C before growing in a growth room at 22°C in continuous light conditions. Ten day old seedlings were transferred to soil and grown in green house conditions. Dexamethasone treatment was performed by either germinating seeds on 10µM dexamethasone supplemented medium or by transferring plants from ½ MS to 10µM dexamethasone supplemented medium and continuing growth for the indicated time. Benzyl Adenine (BA) treatment was performed by transferring plants from ½ MS to 10µM BA supplemented medium and continuing growth for the indicated time. The *Arabidopsis thaliana* (L.) Heynh. Col-0 ecotype served as wild-type control. dGR marker lines of p*bHLH*::nGFP/ GUS were generated by crossing the respective marker lines with the dGR line

Cloning and plant transformation

All p*RPS5A* miss-expression lines were created by cloning the respective coding sequence of the genes to be miss-expressed in either pK7m24GW,3, pB7m24GW,3 destination vectors using Gateway cloning (Karimi, et al., 2007). p*35S*::*bHLH* overexpression lines were generated by cloning the respective coding sequence combined with a pDONRP41R-p35S in pK7m24GW,3. The p*35S*::*bHLH36*:GFP construct was generated by cloning the *bHLH36* coding sequence without stop in the pK7FWG2 Gateway destination vector. bHLH promoters were cloned by using the region upstream of the start and cloning this fragment in the pMK7S*NFm14GW destination vector using Gateway cloning. Size of promoter regions used can be found in **Supplemental Table 1**. Translational reporter lines were generated by cloning these promoter regions in pK7m34GW destination vector combined with the corresponding coding sequence without stop and fusing these to a sYFP using Gateway cloning. Primers used are listed in **Supplemental table 1**. Plant transformation was performed using floral dip. Immunoprecipitation followed by tandem mass-spectrometry (IP-MS) IP-MS/MS was performed as described in (Wendrich, et al., 2017). Up to 3 gram of five-

day-old seedlings of p*35S*::*bHLH36*:GFP and p*bHLH36*::*bHLH36*:sYFP was used. Col-0 was used as a control. Samples were performed in triplicate for follow-up statistics.

CRISPR/CAS9

Loss-of-function mutant generation by CRISPR/CAS9 was performed as described in Chapter 4. Primers of 20nt protospacers used can be found in **Supplemental Table 1**.

Plant imaging and image processing

Seedlings for DIC analysis were mounted in a solution of 20% glycerol 60% lactic acid. DIC microscopy was performed using an Olympus BX53 DIC microscope. For mPS-PI staining, roots were stained as described previously (Truernit, et al., 2008). GUS staining was performed as described in (Vanneste, et al., 2005). Confocal microscopy was performed on Leica SP8 (63X) Zeiss LSM710 (63X) and Leica SP2 (63X) (all water corrected objective (NA 1.2) lenses) confocal microscopes. Calcofluor White, GFP, sYFP and propidium iodide (PI) samples were imaged at an excitation of 405nm, 488nm, 514nm and 514nm respectively. Calcofluor White, GFP, sYFP and PI were visualized at an emission of 425-475 nm, 500-535nm, 515-550nm and 600-700nm respectively. Quantifications analysis and cell file numbers were performed using the Image J software package.

Quantification of cell numbers

Roots were fixed and stained using a slightly modified version of the Pseudo Schiff – Propidium Iodine (mPS-PI) staining protocol (Truernit, et al., 2008). The stained roots were imaged by using confocal microscopy and radial cross-sections were taken in the middle of root meristem (defined as the middle between the first elongating cortex cells and the QC).

Box Plots

All box plots were generated using the BoxPlotR webtool using standard settings. Center lines represent the medians; box limits indicate the 25th and 75th percentiles as determined by R software; whiskers extend 1.5 times the interquartile range from the 25th and 75th percentiles, outliers are represented by dots.

Q-RT-PCR

RNA was extracted using the RNeasy kit (Qiagen). Poly(dt) cDNA was generated from 1 µg of total RNA using Superscript II reverse transcriptase (Invitrogen) and analyzed on a LightCycler 480 (Roche Molecular Systems, Inc) with SYBR Green I Master kit (Roche Diagnostics) according to manufacturer's instructions. Primer pairs were designed using Universal Probe Library Assay Design Center (Roche Molecular Systems, Inc). All primers used for Q-RT-PCR analysis can be found in **Supplemental Table 1**. All reactions were done in triplicate. Data was analyzed using qBase+ software package (Biogazelle). Expression levels were normalized to those of *EEF1α4* and *CDKA1;1*.

Acknowledgements

References

Albert, R. (2007). Network inference, analysis, and modeling in systems biology. The Plant cell 19, 3327-3338.

Alina Sîrbu, H.J.R.a.M.C. (2011). Evolutionary Algorithms

Balaguer, M.A.D., Fisher, A.P., Clark, N.M., Fernandez-Espinosa, M.G., Möller, B.K., Weijers, D., Lohmann, J.U., Williams, C., Lorenzo, O., and Sozzani, R. (2017). Predicting gene regulatory networks by combining spatial and temporal gene expression data in Arabidopsis root stem cells. Proceedings of the National Academy of Sciences of the United States of America 114, E7632-E7640.

De Rybel, B., Adibi, M., Breda, A.S., Wendrich, J.R., Smit, M.E., Novák, O., Yamaguchi, N., Yoshida, S., Van Isterdael, G., Palovaara, J., et al. (2014). Plant development. Integration of growth and patterning during vascular tissue formation in Arabidopsis. Science 345, 1255215.

De Rybel, B., Möller, B., Yoshida, S., Grabowicz, I., Barbier de Reuille, P., Boeren, S., Smith, R.S., Borst, J.W., and Weijers, D. (2013). A bHLH complex controls embryonic vascular tissue establishment and indeterminate growth in Arabidopsis. Developmental cell 24, 426-37.

Dolan, L., Janmaat, K., Willemsen, V., Linstead, P., Poethig, S., Roberts, K., and Scheres, B. (1993). Cellular organisation of the Arabidopsis thaliana root. Development 119, 71-84.

Ferredamare, A.R., Pognonec, P., Roeder, R.G., and Burley, S.K. (1994). Structure and Function of the B/Hlh/Z Domain of Usf. Embo Journal 13, 180-189.

Hecker, M., Lambeck, S., Toepfer, S., van Someren, E., and Guthke, R. (2009). Gene regulatory network inference: Data integration in dynamic models-A review. Biosystems 96, 86-103.

Ishida, K., Yamashino, T., Yokoyama, A., and Mizuno, T. (2008). Three type-B response regulators, ARR1, ARR10 and ARR12, play essential but redundant roles in cytokinin signal transduction throughout the life cycle of Arabidopsis thaliana. Plant & cell physiology 49, 47-57.

Kadesch, T. (1993). Consequences of Heteromeric Interactions among Helix-Loop-Helix Proteins. Cell Growth Differ 4, 49-55.

Kanaoka, M.M., Pillitteri, L.J., Fujii, H., Yoshida, Y., Bogenschutz, N.L., Takabayashi, J., Zhu, J.K., and Torii, K.U. (2008). SCREAM/ICE1 and SCREAM2 specify three cell-state transitional steps leading to Arabidopsis stomatal differentiation. The Plant cell 20, 1775-1785.

Karimi, M., Bleys, A., Vanderhaeghen, R., and Hilson, P. (2007). Building blocks for plant gene assembly. Plant physiology 145, 1183-1191.

Ludwig, S.R., Habera, L.F., Dellaporta, S.L., and Wessler, S.R. (1989). Lc, a Member of the Maize R-Gene Family Responsible for Tissue-Specific Anthocyanin Production, Encodes a Protein Similar to Transcriptional Activators and Contains the Myc-Homology Region. Proceedings of the National Academy of Sciences of the United States of America 86, 7092-7096.

MacAlister, C.A., Ohashi-Ito, K., and Bergmann, D.C. (2007). Transcription factor control of asymmetric cell divisions that establish the stomatal lineage. Nature 445, 537-540.

Murre, C., Mccaw, P.S., Vaessin, H., Caudy, M., Jan, L.Y., Jan, Y.N., Cabrera, C.V., Buskin, J.N., Hauschka, S.D., Lassar, A.B., et al. (1989). Interactions between Heterologous Helix-Loop-Helix Proteins Generate Complexes That Bind Specifically to a Common DNA-Sequence. Cell 58, 537-544.

Neuman, K., Nornes, H.O., and Neuman, T. (1995). Helix-Loop-Helix Transcription Factors Regulate Id2 Gene Promoter Activity. Febs Lett 374, 279-283.

Ohashi-Ito, K., and Bergmann, D.C. (2006). Arabidopsis FAMA controls the final proliferation/differentiation switch during stomatal development. The Plant cell 18, 2493-2505.

Ohashi-Ito, K., Saegusa, M., Iwamoto, K., Oda, Y., Katayama, H., Kojima, M., Sakakibara, H., and Fukuda, H. (2014). A bHLH complex activates vascular cell division via cytokinin action in root apical meristem. Current biology : CB 24, 2053-8.

Pillitteri, L.J., Sloan, D.B., Bogenschutz, N.L., and Torii, K.U. (2007). Termination of asymmetric cell division and differentiation of stomata. Nature 445, 501-505.

Pires, N., and Dolan, L. (2010). Origin and Diversification of Basic-Helix-Loop-Helix Proteins in Plants. Mol Biol Evol 27, 862-874.

Shannon, P., Markiel, A., Ozier, O., Baliga, N.S., Wang, J.T., Ramage, D., Amin, N.,

Schwikowski, B., and Ideker, T. (2003). Cytoscape: A software environment for integrated models of biomolecular interaction networks. Genome Res 13, 2498-2504.

Truernit, E., Bauby, H., Dubreucq, B., Grandjean, O., Runions, J., Barthélémy, J., and Palauqui, J.C. (2008). High-resolution whole-mount imaging of three-dimensional tissue organization and gene expression enables the study of Phloem development and structure in Arabidopsis. The Plant cell 20, 1494-503.

Vanneste, S., De Rybel, B., Beemster, G.T.S., Ljung, K., De Smet, I., Van Isterdael, G., Naudts, M., Iida, R., Gruissem, W., Tasaka, M., et al. (2005). Cell cycle progression in the pericycle is not sufficient for SOLITARY ROOT/IAA14-mediated lateral root initiation in Arabidopsis thaliana. The Plant cell 17, 3035-3050.

Wendrich, J.R., Boeren, S., Möller, B.K., Weijers, D., and De Rybel, B. (2017). In Vivo Identification of Plant Protein Complexes Using IP-MS/MS. Methods in molecular biology 1497, 147-158.

Xie, M.T., Chen, H.Y., Huang, L., O'Neil, R.C., Shokhirev, M.N., and Ecker, J.R. (2018). A B-ARR-mediated cytokinin transcriptional network directs hormone cross-regulation and shoot development (vol 9, 1604, 2018). Nature communications 9.

Yokoyama, A., Yamashino, T., Amano, Y., Tajima, Y., Imamura, A., Sakakibara, H., and Mizuno, T. (2007). Type-B ARR transcription factors, ARR10 and ARR12, are implicated in cytokinin-mediated regulation of protoxylem differentiation in roots of Arabidopsis thaliana. Plant & cell physiology 48, 84-96.

Zubo, Y.O., Blakley, I.C., Yamburenko, M.V., Worthen, J.M., Street, I.H., Franco-Zorrilla, J.M., Zhang, W., Hill, K., Raines, T., Solano, R., et al. (2017). Cytokinin induces genome-wide binding of the type-B response regulator ARR10 to regulate growth and development in Arabidopsis. Proceedings of the National Academy of Sciences of the United States of America 114, E5995-E6004.

Supplemental Information

Supplemental Figure 1: bHLH27 and bHLH35 peptide coverage IP-MS. Different colors represent different peptides found in the obtained IP-MS data.

bHLH27

MEDLDHEYKNYWETTMFFQNQELEFDSWPMEEAFSGSGESSSPDGAATSPASSKNVVSERNRRQKLNQRLFALR
SVVPNISKLDKASVIKDSIDYMQELIDQEKTLEAEIRELESRSTLLENPVRDYDCNFAETHLQDFSDNNDMRSKKFKQ
MDYSTRVQHYPIEVLEMKVTWMGEKTVVVCITCSKKRETMVQLCKVLESLNLNILTTNFSSFTSRLSTTLFLQVTLSL
SPSLISLFGNVITSTNYKILNASREYCTCLVLV

bHLH35

MEDIVDQELSNYWEPSSFLQNEDFEYDRSWPLEEAISGSYDSSSPDGAASSPASKNIVSERNRRQKLNQRLFALRSV
VPNITKMDKASIIKDAISYIEGLQYEEKKLEAEIRELESTPKSSLSFSKDFDRDLLVPVTSKKMKQLDSGSSTSLIEVLELK
VTFMGERTMVVSVTCNKRTDTMVKLCEVFESLNLKILTSNLTSFSGMIFHTVFIELRPNIYWVVWFLVFMSIFGPTII
VIWSIWFIKKKIILSLWRMKKNKRCCG

Supplemental Figure 2: Volcano plot of IP-MS on p*bHLH36*::*bHLH36*:sYFP vs Col-0 control. All identified proteins after filtering and statistical analysis with their corresponding protein abundance ratios over the T-test *p*-value. Depicted in black circles are the significantly different samples from the control, with bait and GFP among these. Number indicates amount of significantly different samples from the control.
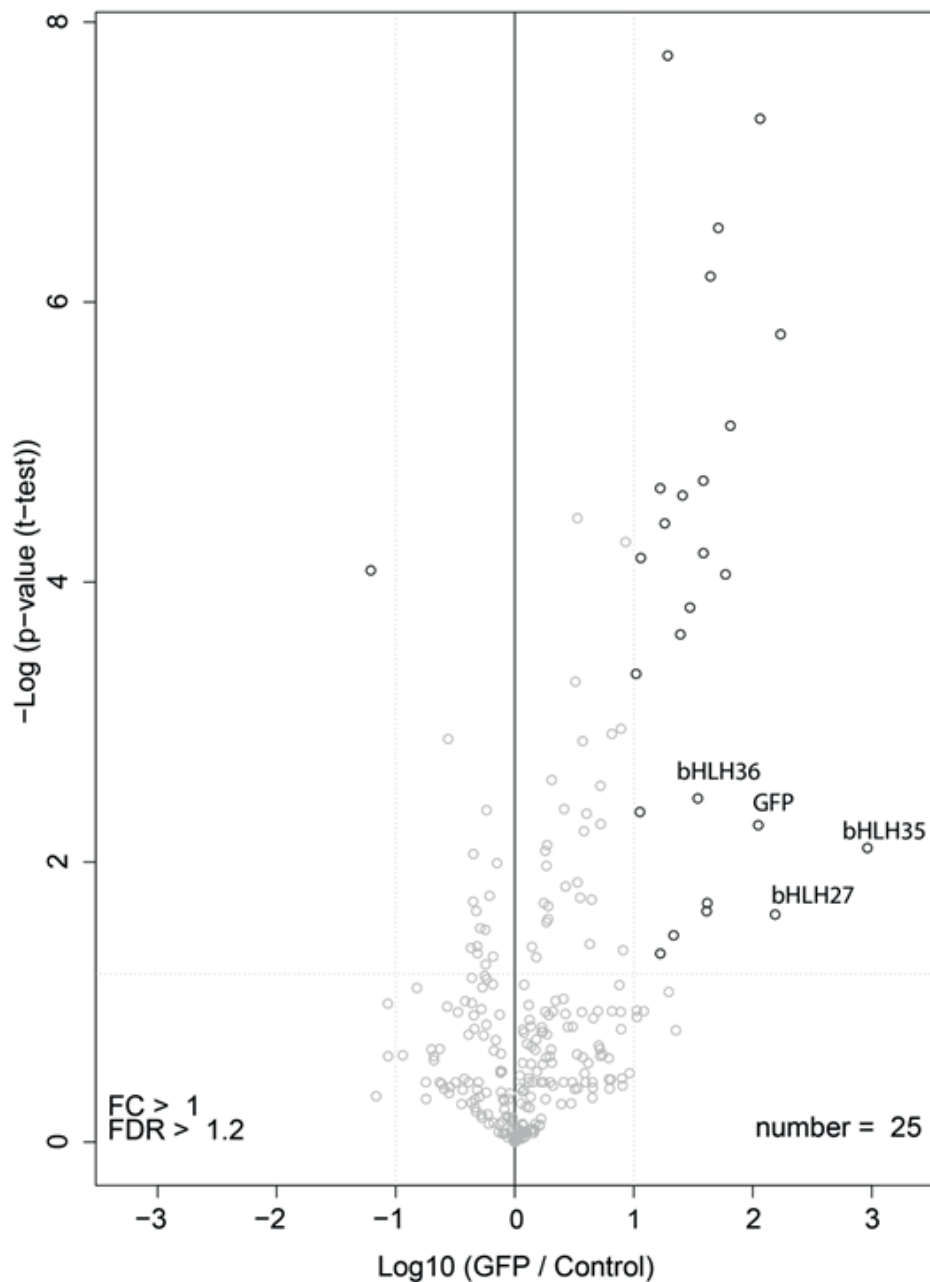
Supplemental Figure 3: Volcano plot of IP-MS on p*35S*::b*HLH36*:GFP vs Col-0 control. All identified proteins after filtering and statistical analysis with their corresponding protein abundance ratios over the T-test *p*-value. Depicted in black circles are the significantly different samples from the control, with bait and GFP among these. Number indicates amount of significantly different samples from the control.
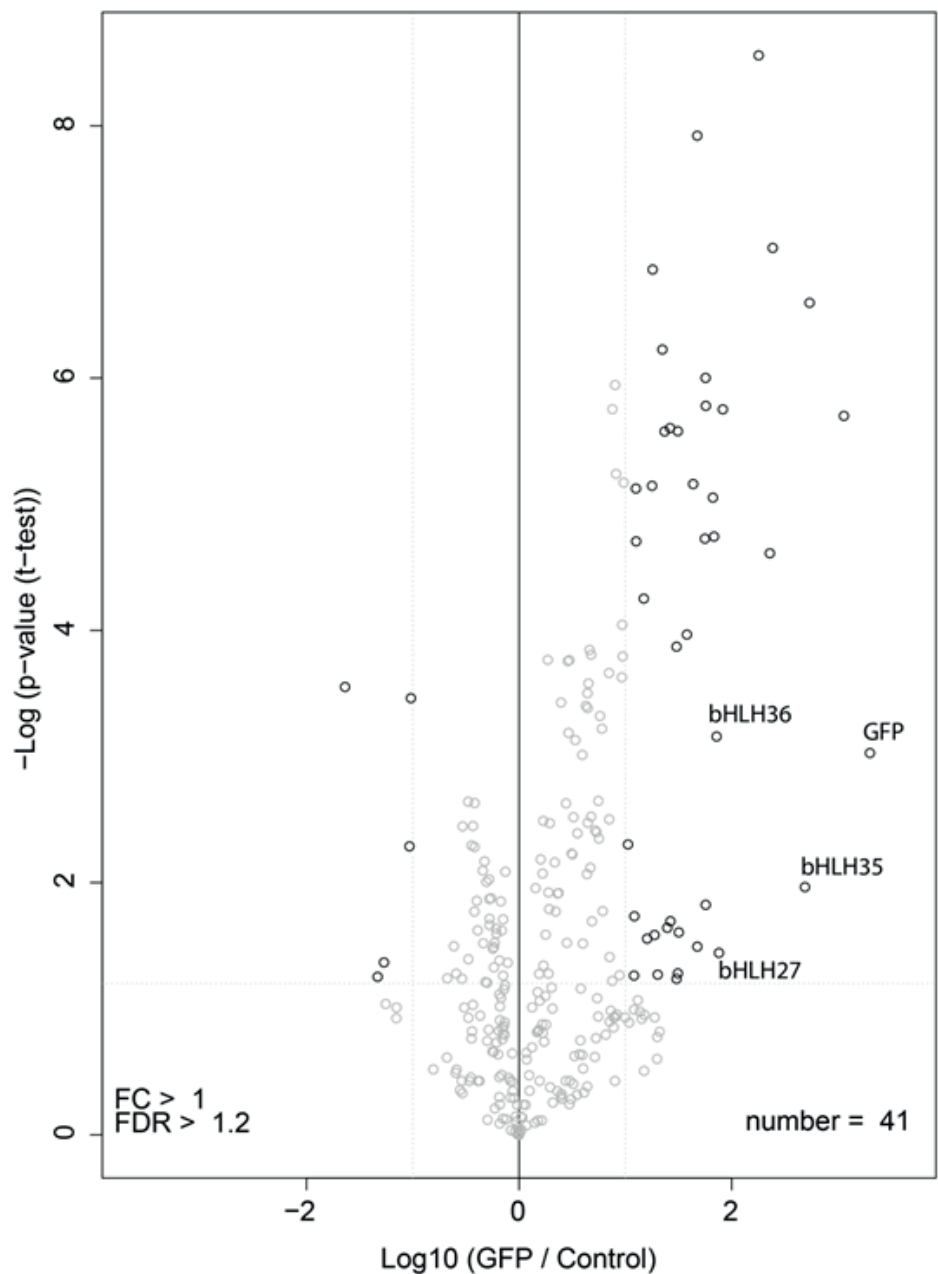
Supplemental Table 1: Primers

pDONR221 CDS +STOP

bHLH55	fw	GGGGACAAGTTTGTACAAAAAAGCAGGCTTA-ATGAATTTTCCAGATTCTTC
	rv	GGGGACCACTTTGTACAAGAAAGCTGGGTA-CTAGCGAGTAGTGACTCTTG
bHLH118	fw	GGGGACAAGTTTGTACAAAAAAGCAGGCTTA-ATGGAGAAGTTAGTACATAAAG
	rv	GGGGACCACTTTGTACAAGAAAGCTGGGTA-TTACTTCATCAGGGTAAGT
	fw	

pDONR221 CDS - STOP

bHLH36	fw	GGGGACAAGTTTGTACAAAAAAGCAGGCTTA-ATGGAGAAGATGATGCACAG
	rv	GGGGACCACTTTGTACAAGAAAGCTGGGTA-CTTCATTCTGATTAATCTCT
bHLH55	fw	GGGGACAAGTTTGTACAAAAAAGCAGGCTTA-ATGAATTTTCCAGATTCTTC
	rv	GGGGACCACTTTGTACAAGAAAGCTGGGTA-GCGAGTAGTGACTCTTGAGG
bHLH118	fw	GGGGACAAGTTTGTACAAAAAAGCAGGCTTA-ATGGAGAAGTTAGTACATAAAG
	rv	GGGGACCACTTTGTACAAGAAAGCTGGGTA-CTTCATCAGGGTAAGTGTA
bHLH120	fw	GGGGACAAGTTTGTACAAAAAAGCAGGCTTA-ATGAATCCTTCTAACAATCC
	rv	GGGGACCACTTTGTACAAGAAAGCTGGGTA-GTGCCTAGTCGTGGAAAGTA
bHLH125	fw	GGGGACAAGTTTGTACAAAAAAGCAGGCTTA-ATGGATTGTGTTCCTTCATTG
	rv	GGGGACCACTTTGTACAAGAAAGCTGGGTA-CATAGTCATTATTTTATCCT
bHLH126	fw	GGGGACAAGTTTGTACAAAAAAGCAGGCTTA-ATGGATCCTTATAAGAATC
	rv	GGGGACCACTTTGTACAAGAAAGCTGGGTA-AATTGTCGGAATATCGAAAA

pDONRP4P1R

1884 bp	pbHLH36	fw	GGGGACAACTTTGTATAGAAAAGTTG-AGCGGTTTCTTTGGTG
		rv	GGGGACTGCTTTTTTGTACAAACTTG-GTCGTTATTATCAGTACCAC
2188 bp	pbHLH55	fw	GGGGACAACTTTGTATAGAAAAGTTG-CTCTCACTCTTCCTTCCTTCC
		rv	GGGGACTGCTTTTTTGTACAAACTTG-GCCCTTTTTATTTTCTTGTTGG
1848 bp	pbHLH118	fw	GGGGACAACTTTGTATAGAAAAGTTG-CTAATTTAGGAATCATTTTG
		rv	GGGGACTGCTTTTTTGTACAAACTTG-GTTTTCTTCGTTATTACAAAC
3315 bp	pbHLH120	fw	GGGGACAACTTTGTATAGAAAAGTTG-GATCGGAAAATTATGTTTCCC
		rv	GGGGACTGCTTTTTTGTACAAACTTG-GGGTTGAGGTTTAGAAATGG
2847 bp	pbHLH125	fw	GGGGACAACTTTGTATAGAAAAGTTG-CACTGAAACAACAAAAGG
		rv	GGGGACTGCTTTTTTGTACAAACTTG-TGGAATTTGATATCTATGAG
3436 bp	pbHLH126	fw	GGGGACAACTTTGTATAGAAAAGTTG-TTCAAATAATCAAACGTTTT
		rv	GGGGACTGCTTTTTTGTACAAACTTG-AGTTTGACACTTTGAGCTTT

CRISPR SG RNA

bHLH36 sg1	fw	ATTGACAGAGAAACTGAGAGGCAA
	rv	AAACTTGCCTCTCAGTTTCTCTGT
bHLH36 s2	fw	ATTGGACGTCAGATCAAGTCAACG
	rv	AAACCGTTGACTTGATCTGACGTC
bHLH118 sg1	fw	ATTGTTGTAATAACGAAGAAAACA
	rv	AAACTGTTTTCTTCGTTATTACAA
bHLH118 sg2	fw	ATTGAAAACGTTCAACGTCAGATC

	rv	AAACGATCTGACGTTGAACGTTTT
bHLH126 sg1	fw	ATTGCTCTGTCTCTGGTAACCTTT
	rv	AAACAAAGGTTACCAGAGACAGAG
bHLH126 sg2	fw	ATTGatagGGAAAAAGAGCTGTGT
	rv	AAACACACAGCTCTTTTTCCctat

qPCR primers

bHLH27	fw	ATGGAAGATCTCGACCATGAG
	rv	CGAAAACGCTTCCTCCATC
bHLH35	fw	CGTCGACCAAGAATTAAGCAA
	rv	CTTCCAAAGGCCAGCTTCT
bHLH36	fw	TTCTTCAAGTGCTTAGTGAATATGGT
	rv	TCAAAGCCATATCGTTGACCT
bHLH120	fw	CGAGTCAACGAGAGGCTCAT
	rv	TCGTGGAAAGTACTAACTGCTCA
bHLH125	fw	ACAGAGATTCATGCACACCATT
	rv	TTTATCCTTAAGCTCCAAAATATTGAT
bHLH126	fw	CTCATGCACACTATTCAAGTAGAGG
	rv	CGTCGAAAGTATCAAATCCTCA

Chapter 6

General discussion

Wouter Smet[1,2,3],

1. Wageningen University, Laboratory of Biochemistry, Stippeneng 4, 6708 WE Wageningen, the Netherlands
2. Ghent University, Department of Plant Biotechnology and Bioinformatics, Technologiepark 927, 9052 Ghent, Belgium
3. VIB Center for Plant Systems Biology, Technologiepark 927, 9052 Ghent, Belgium

Digging deeper into the TMO5/LHW transcriptional responses

Plants, unlike animals, have rigid cell walls which are fixed immediately after division. As such, cell division and subsequent elongation of the divided cells results in growth of the plant. Therefore, in order to properly pattern and grow, it is crucial that plants carefully position and orient their division plane. However, how a cell determines where it will position its division plane and thus what kind of division it will undergo remains largely unknown. While the cell cycle machinery is necessary for a cell to divide in a correct manner, it is not determining the position of the division plane. The cell cycle machinery only acts on cues that make the cell divide in a certain manner. Concepts such as the shortest-cell-wall rule predict where a cell will position its division plane based on the shape of the cell and is seen as the default division state. However, cells often deviate from this rule during development in order to allow proper patterning of the plant. While it is known that certain cues are able to overrule the default state and shift the cell division into a certain position, it remains unclear how they determine the future division plane and act on the cell-cycle machinery. In this thesis we aimed to narrow this gap in our understanding by studying a genetic cue capable of shifting the division plane orientation.

We focused on two bHLH transcription factors TMO5 and LHW which are capable of triggering a shift in the division plane orientation (De Rybel et al 2014, De Rybel et al 2013, Ohashi-Ito et al 2013, Ohashi-Ito et al 2014). In **Chapter 3** we showed how we generated and used an inducible line of TMO5 and LHW (dGR) in order to study the reorientation of the division plane in more detail. Because TMO5 and LHW are transcriptions factors, we studied transcriptional changes upon their induction to find downstream genes involved in controlling PRD. While it is known that cytokinin is required to control the PRDs downstream of TMO5 and LHW (De Rybel et al 2014, Ohashi-Ito et al 2014), here we could show for the first time that cytokinin response is indeed triggered upon TMO5/LHW induction. Next, in both **Chapter 4** and **Chapter 5** we characterized new factors downstream of the TMO5/LHW controlled cytokinin response and tried to show their involvement in controlling cell division orientation. Although the exact function of the novel bHLH subfamily described in **Chapter 5** is unknown, but we could show that DOF2.1, described in **Chapter 4**, plays a role in controlling cell division orientation.

Position matters when responding to cell division orientation cues

In this thesis, we mainly focused on two genetic cues that can shift the division plane upon induction. Both TMO5/LHW and their downstream target DOF2.1 are capable of inducing PRD in any cell-type within the root. However, we could observe that not all cell-types and cells respond equally to induction of these cues. For example, cortical cells were the most responsive to the TMO5/LHW induction while upon induction of DOF2.1 the epidermis was most responsive. The difference in responsiveness could be due to several reasons. First of all, the auxin and CK levels in cortex cells are generally lower compared to the surrounding cell layers (Liao et al 2015, Zurcher et al 2013) and could thus be more responsive to the induced cues. As *DOF2.1* is part of the CK response, it is possible that both epidermis and cortex are cell layers where cytokinin signaling generally is lower and hence these would be more susceptible to the triggered CK response. However, we cannot exclude that the vasculature responds slower because it is more difficult to observe single events of PRD due to the high number of cells and their size. Another possibility is that the highest concentration of dexamethasone will be in the outer cells, leading to the strongest induction of these cues in the outer tissues.

Intriguingly, cells never showed PRDs before 4h after receiving the TMO5/LHW cue. One might expect that a downstream factor would trigger PRDs faster but we could not observe divisions earlier then 6h after triggering DOF2.1 expression. We attribute this to the requirement and accumulation of other genetic and/or cell-cycle machinery factors necessary to carry out the reorientation and division. It is possible that DOF2.1 requires or is limited by other factors that are normally regulated by TMO5/LHW leading to a slower response. On the other hand it is possible that DOF2.1 induction of PRD is more susceptible to a yet unknown negative feedback when compared to TMO5/LHW induction, or *DOF2.1* expression could be actively repressed. These cases would result in lower levels of the downstream factors that are required to facilitate the reorientation and division. We also observed that the response upon receiving both the TMO5/LHW and DOF2.1 cue did not lead to a homogenous response within a cell layer indicating the cells take a different time to respond to the cue. We also showed that the *RPS5A* promoter lacked expression in some cells however this does not fully explain the amount of difference in response we observed. Most cells within the root meristem are in different stage of the cell-cycle and thus it might take some cells longer to be able to orient their division plane and divide, when

compared to others. So depending on the stage of the cell-cycle up on receiving the cue it takes the cell at least 4-6h to reorient the division plane. This suggests that cell needs to be in a certain stage of the cell-cycle to perceived and act on the trigger.

Another interesting observation is that the induced divisions were always symmetrical and never asymmetrical (see **Figure 3 Chapter 3,4**). This suggests that there is an increase in the amount of cell files within a specific cell type, showing that TMO5/ LHW and DOF2.1 induce PRDs without affecting cell identity. Moreover, although both TMO5/LHW and DOF2.1 are capable of triggering periclinal and radial divisions, the majority of the induced reoriented cell divisions were radial divisions (see **Figure 3 Chapter 3,4**). It is possible that the cell shape in the root meristem might play a role. Generally, the majority of the cell types in the meristem have cells that are wider than they are long (personal communication Jos Wendrich). The observation that cells upon receiving the cues prefer to undergo radial divisions begs the question if the TMO5/LHW and DOF2.1 determine the future division site or rather inhibits the cell to divide in an anticlinal and periclinal manner. It is has previously been shown that auxin is required to allow cells to deviate from the shortest-cell-wall rule (Yoshida et al 2014). Thus, we can hypothesize that normally high levels of auxin in the root meristem (around the QC) promotes cell to divide in an anticlinal manner, driving longitudinal growth. However upon induction of TMO5/LHW cytokinin is produced and its downstream gene *DOF2.1* is triggered which both inhibit anticlinal divisions and allows cells to divide according to the shortest-cell-wall rule. This is supported by the observation that the upon induction of TMO5/LHW and DOF2.1 roots keep growing along the longitudinal axis because cells around the QC contain higher levels of auxin when compared to the more distal parts of the meristem. It is in this more distal zone of the root meristem where most PRDs are observed, suggesting that the area around the QC keeps driving longitudinal growth through auxin signaling. This is supported by the model in which the auxin controlled PLTs induce cells near the QC to undergo anticlinal divisions (Aida et al 2004, Galinha et al 2007). While this model of interplay between auxin and cytokinin is plausible in the context of the root meristem and is able to explain our observations, it is difficult to envision how it could be extrapolated to other developmental contexts such as lateral root development and secondary growth, where cells are generally longer than they are wide. Perhaps TMO5/LHW and DOF2.1 are simply specifying the future division plane to be radial instead of inhibiting anticlinal and periclinal divisions. This would however not explain the increased amount of periclinal divisions which can be seen upon prolonged induction of these cues. Hence,

although it is tempting to speculate how such a mechanism could function, more research will be required before any meaningful conclusions can be derived.

Bridging the gap

Identifying DOF2.1 as a transcriptional regulator involved in controlling division plane orientation downstream of the TMO5/LHW controlled cytokinin response is a first step in closing the gap between the upstream transcriptional responses and the downstream changes in cell division orientation (**Figure 1**). Moreover, it allows to further dissect the downstream responses, as the TMO5/LHW dependent inhibition of protoxylem formation does not occur during DOF2.1 misexpression. Hence, the division and differentiation effects downstream of the TMO5/LHW induced cytokinin response can be uncoupled (see **Figure 1, Chapter 4**). Recent work shows that the B-type cytokinin response factors ARR1, ARR10 and ARR12 can bind the promoter of *DOF2.1* (Xie et al 2018). Indeed, ARR12 was up-regulated in our obtained dataset, suggesting that TMO5/LHW activates DOF2.1 through these B-type ARRs. Together this would provide a model where TMO5/LHW activates cytokinin biosynthesis through LOG3, LOG4 within the xylem axis. In turn cytokinin diffuses outwards where it activates B-type ARR responses, possibly through ARR1, ARR10 and ARR12. These can activate *DOF2.1* expression and trigger PRD divisions in the vascular cells along the xylem axis.

Because *DOF2.1* is expressed throughout the root, it will be interesting to see if it is controlling PRD during secondary growth in a similar manner. Especially because during secondary growth there is a major increase in the amount of cell files generated. One DOF-type TF has already been shown to control PRD during secondary growth (Guo et al 2009) thus it is likely more factors will play a role at later stages of development. Given that the DOF-type transcription factor family acts in a redundant manner, investigating the function and regulation of the other family members might lead to a better understanding of how they control PRDs during plant development. In respect to this, recent developments in CRISPR/CAS9 technology have provided systems for easier and cleaner generation of high order mutants and will allow us to better study the function and redundancy of genes within large gene families.

The generation of the *dof2.1 tmo6 dof6* loss-of-function mutant revealed that these DOFs act in a redundant manner to control PRD in the vasculature. Recent work shows that TMO6, DOF6 and several other DOF-type TFs are also

controlled by cytokinin and are capable of inducing PRD in the root meristem (Unpublished work, Ykä Helariutta). However these genes are not up-regulated in our TMO5/LHW dataset suggesting they have other up-stream regulators.

Besides DOF2.1 we also found a subfamily of bHLH TFs to be downstream of TMO5/LHW and the subsequent cytokinin response (Figure 1). Overexpression of these genes did not show any obvious phenotype which we attributed to the lack of heterodimerization partners. Loss-of-function of *bHLH36* and *bHLH126* resulted in a small increase in cell number. Vascular organization and differentiation was not affected suggesting that the members of this family are repressors of vascular PRDs. However, analysis of higher order loss-of-function mutants and overexpression of these bHLH with their corresponding interaction partners will shed more light on the function of these genes.

Even though DOF2.1 brings us one step closer to understanding the transcriptional responses downstream of TMO5/LHW, we again identified a transcriptional regulator controlling these divisions and not an effector responsible for positioning the division plane itself. As such, it would be logical to repeat the approach used in **Chapter 2** and **Chapter 3** to look at the transcriptional changes upon DOF2.1 triggered divisions and to compare those to the obtained TMO5/LHW dataset. In this way, we can find common downstream genes which could be key regulators or effectors in orienting the division plane. *DOF2.1* was induced in our data set simultaneous with the cytokinin responses, thus it would be interesting to investigate the genes at the later time points of our dataset to try to find players downstream of DOF2.1 in order to unravel the entire transcriptional cascade leading to the changes in cell division orientation. Eventually, we hope to reach the end of this transcriptional signaling cascade and identify different classes of downstream factors such as for example polarity factors that more directly determine the orientation and positioning the division plane. However, the further downstream we go in this response, the less likely it becomes that we might find single factors capable or required to shift the division plane. In contrary, we might rather expect to find complex combinations of factors required for the control of this this important and fascinating developmental process.
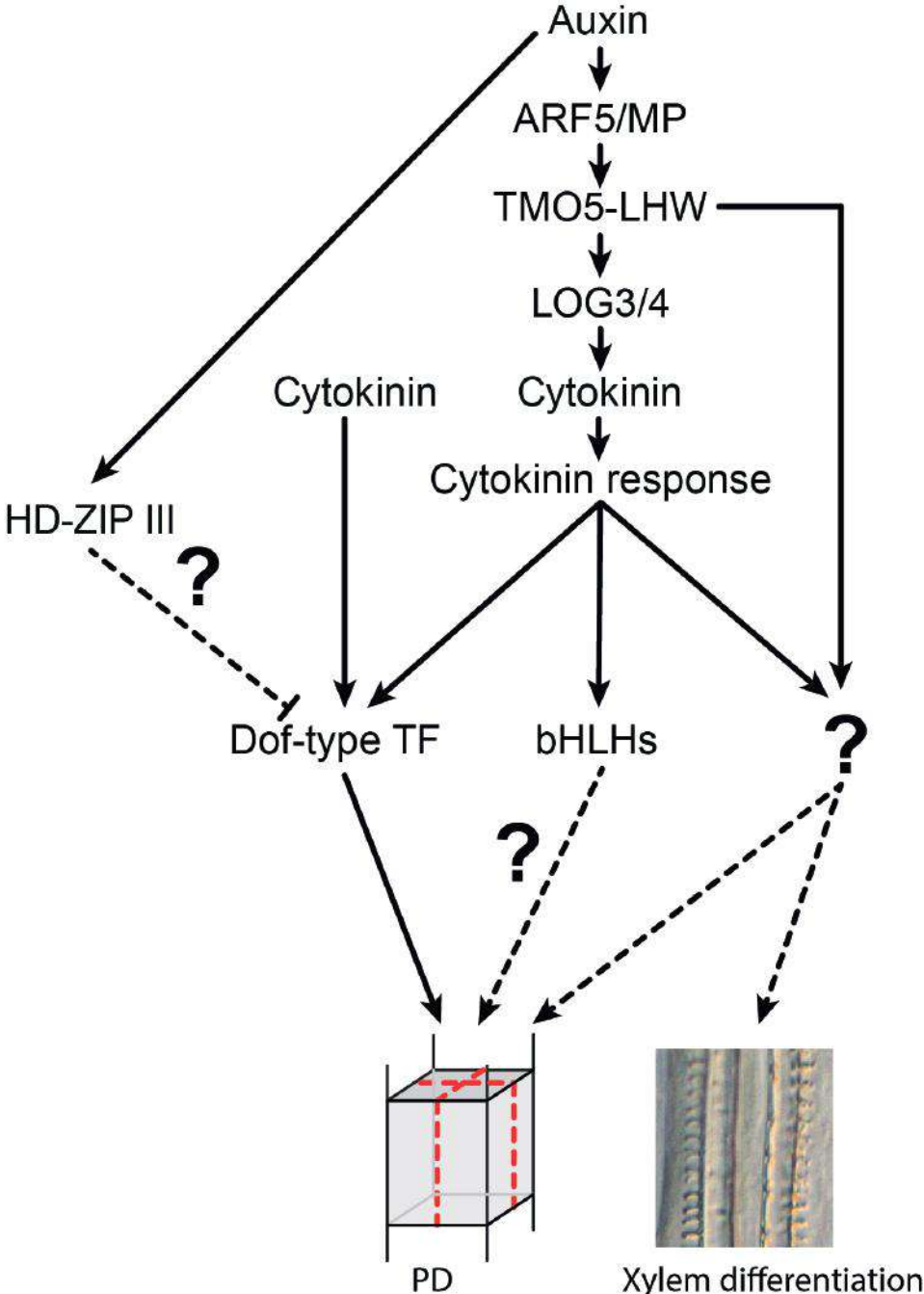
Figure 1: Model of TMO5/LHW pathway controlling PRDs. Full lines indicate known regulations. Dashed lines indicate possible regulations.

References

Aida M, Beis D, Heidstra R, Willemsen V, Blilou I, et al. 2004. The PLETHORA genes mediate patterning of the Arabidopsis root stem cell niche. Cell 119: 109-+

De Rybel B, Adibi M, Breda AS, Wendrich JR, Smit ME, et al. 2014. Plant development. Integration of growth and patterning during vascular tissue formation in Arabidopsis. Science 345: 1255215

De Rybel B, Moller B, Yoshida S, Grabowicz I, Barbier de Reuille P, et al. 2013. A bHLH complex controls embryonic vascular tissue establishment and indeterminate growth in Arabidopsis. Developmental cell 24: 426-37

Galinha C, Hofhuis H, Luijten M, Willemsen V, Blilou I, et al. 2007. PLETHORA proteins as dose-dependent master regulators of Arabidopsis root development. Nature 449: 1053-57

Guo Y, Qin G, Gu H, Qu LJ. 2009. Dof5.6/HCA2, a Dof transcription factor gene, regulates interfascicular cambium formation and vascular tissue development in Arabidopsis. The Plant cell 21: 3518-34

Liao CY, Smet W, Brunoud G, Yoshida S, Vernoux T, Weijers D. 2015. Reporters for sensitive and quantitative measurement of auxin response. Nature methods 12: 207-10, 2 p following 10

Ohashi-Ito K, Matsukawa M, Fukuda H. 2013. An atypical bHLH transcription factor regulates early xylem development downstream of auxin. Plant & cell physiology 54: 398-405

Ohashi-Ito K, Saegusa M, Iwamoto K, Oda Y, Katayama H, et al. 2014. A bHLH complex activates vascular cell division via cytokinin action in root apical meristem. Current biology : CB 24: 2053-8

Xie MT, Chen HY, Huang L, O'Neil RC, Shokhirev MN, Ecker JR. 2018. A B-ARR-mediated cytokinin transcriptional network directs hormone cross-regulation and shoot development (vol 9, 1604, 2018). Nature communications 9

Yoshida S, Barbier de Reuille P, Lane B, Bassel GW, Prusinkiewicz P, et al. 2014. Genetic control of plant development by overriding a geometric division rule. Developmental cell 29: 75-87

Zurcher E, Tavor-Deslex D, Lituiev D, Enkerli K, Tarr PT, Muller B. 2013. A robust and sensitive synthetic sensor to monitor the transcriptional output of the cytokinin signaling network in planta. Plant physiology 161: 1066-75

Summary

Growth of plants depends on cell division and elongation of the divided cells. After cell division, plant cells are fixed immediately within their tissue context. Thus, a carefully positioning and orientation of the division plane is crucial for plants to properly pattern and grow. Anticlinal cell divisions result in more cells within a cell file and lead to longitudinal growth; while periclinal and radial divisions (PRD) result in the addition of cell files during radial growth. So far, how a cell controls the position and orientation of its division plane remains poorly understood. In this thesis we focused on a complex of two proteins called TMO5 and LHW that are capable of shifting the division plane orientation towards PRD. Our main aim was to identify which genes are activated by the TMO5/LHW complex and characterize these to understand how plant cells control the positioning and orientation of their cell divisions to allow normal growth.

After introducing the main concepts and background information in **Chapter 2**, we continue to show in **Chapter 3** how we generated and characterized an inducible line of TMO5 and LHW (dGR). We compared this line to the existing TMO5-LHW misexpression and overexpression lines and concluded we created an excellent tool to study cell division orientation. Because TMO5 and LHW are transcription factors, we next studied the transcriptional changes upon induction. While it is commonly assumed that the plant hormone cytokinin is required to control these divisions, we could prove that indeed cytokinin response is triggered upon induction of TMO5/LHW.

In **Chapter 4** we used the transcriptional data to select putative targets, which were verified using a misexpression screen. We identified DOF2.1 as a factor capable of inducing PRD and continued to show how DOF2.1 functions downstream of TMO5-LHW and controls division plane orientation during vascular development. Analysis of loss-of-function mutants of DOF2.1 and the two closest family members revealed these Dof-type TF family members act in a redundant manner to control PRD.

Because our misexpression screen only yielded one factor controlling PRD, we reanalyzed our transcriptional data in **Chapter 5** using an inferred network analysis algorithm. We generated a gene regulatory network which indicated that a novel family of bHLHs acts as key transcriptional hubs downstream of TMO5-LHW. We could confirm that some of these factors are indeed TMO5-LHW regulated and are part of the downstream cytokinin response. Overexpression of these bHLH did not result in any obvious phenotype; however we showed that

they interact with members of a different family of bHLH TFs. This suggests that they might require this interaction in order to carry out their function. Loss-of-function of single genes did not reveal a clear phenotype, indicating that there is a high amount of redundancy within the novel bHLH subfamily. Analysis of higher order mutants will be required to identify the function of these bHLH genes.

In conclusion, the identification of DOF2.1 and its involvement in controlling PRD brings us one step closer to identify the key players that reorient and shift the division plane. However, the actual role of the novel bHLH subfamily acting downstream of TMO5-LHW is yet to be unraveled.

Samenvatting

De groei van planten is afhankelijk van celdeling en elongatie van de gedeelde cell. Na celdeling zijn planten cellen gefixeerd in hun weefselcontext. Daarom, is het nauwkeurig plaatsen en orienteren van het delingsvlak cruciaal voor de groei en patroonvorming van planten. Anticline cel delingen resulteren in meer cellen in een cellaag en zorgen voor longitudinale groei; terwijl pericline en radiale delingen (PRD) voor een toename in cellagen zorgt tijdens radiale groei. Dusverre, is het nog niet duidelijk hoe cellen de positie en orientatie van het delings vlak bepalen. In deze thesis focussen we op een complex van twee eiwitten genaamd TMO5 and LHW die in staat zijn om een cel te forceren het delings vlak te orienteren in de PRD richting. Het hoofddoel was om genen te identificeren die worden geactiveerd door het TMO5/LHW complex en deze te karakterisen om te begrijpen hoe planten cellen de positie en orientatie van hun celdeling controleren voor normale groei.

Na het introduceren van de hoofd concepten en achtergrond informatie in **Hoofdstuk 2**, tonen we in **Hoofdstuk 3** hoe we een induceerbare lijn van TMO5 en LHW genereerd en gekarakteriseerd hebben. We hebben deze lijn vergeleken met de bestaand TMO5-LHW misexpressie en overexpressie en concludeerde dat deze lijn uitstekend is om celdeling te bestuderen. Omdat TMO5 en LHW transcriptiefactoren zijn hebben we de transcriptionele veranderingen na inductie bestudeerd. Ondanks dat men aanneemt dat het planten hormoon cytokinine nodig is voor de controle van deze celdelingen, hebben wij aangetoond dat cytokinine respons wordt geactiveerd na inductie van TMO5/LHW.

In **Hoofdstuk 4** gebruikten we de transcriptionele data om mogelijk betrokken genen te selecteren, de betrokkenheid werd geverifeerd door middel van een misexpressie screen. We hebben DOF2.1 geidentificeerd als een factor die instaat is om PRD te induceren en vervolgens toonden we aan hoe DOF2.1 gereguleerd is door TMO5/LHW en het delingsvlak controleerd gedurdende vasculaire ontwikkeling. Anlyze van knock-out mutanten van DOF2.1 en twee dichtste familieleden toonde aan dat deze Dof-type transcriptie factoren redundant werken voor de controle van PRD.

Omdat onze misexprssie screen maar één factor die PRD controleerde opleverde hebben we onze transcriptionele data in **Hoofdstuk 5** opnieuw geanalyseerd doormiddel van een algoritme voor afgeleide netwerk analyze. We genereerde we een genregulatienetwerk wat aantoonde dat een nieuwe familie van bHLH

transcripiefactoren een belangrijke rol speelt bij transcriptionele respons bij de regulatie van TMO5/LHW. We konden bevestigen dat sommige van deze factoren inderdaad zijn gereguleerd door TMO5/LHW en dat ze een onderdeel zijn van de onderliggende cytokinine respons. Overexpressie van deze bHLH transcriptie factoren leide niet tot een duidelijk fenotype; maar we konden aantonen dat ze een interactie aangaan met leden van een andere familie van bHLH transcriptie factoren. Dit suggereerd dat deze interactie nodig is voor het uitvoeren van hun functie. Knock-out mutanten van enkele genen in deze familie resulteerde niet in duidelijke fenotypes, dit geeft aan dat er grote hoeveelheid redundantie is binnen deze nieuwe bHLH subfamilie. Analyze van hoger orde mutanten zal nodig zijn voor het identificeren om de functie van deze bHLH genen te achterhalen.

In conclusie, de identificatie van DOF2.1 en de betrokkenheid bij het controleren van PRD brengt ons een stap dichter bij het identificeren van de hoofdfactoren die betrokken zijn bij het reorienteren en verplaatsen van het delingsvlak. Echter, de precieze rol van de nieuwe bHLH subfamilie die gereguleerd wordt door TMO5-LHW zal nog moeten worden ontdekt.

Acknowledgements

I would like to thank everybody that helped and supported me throughout my PhD. Obtaining a PhD it is a difficult task which without all your support would not have been possible.

First of all, I would like to thank my promoters Dolf Weijers and Bert de Rybel. Thank you Dolf for letting me to join your lab during my master thesis, which brought me in contact with all the members from the WUR Plant Development group and allowed me to start a PhD with Bert. Even though I spent the majority of my PhD in Gent, when we met, your guidance and critical comments really put me and the project on track.

Bert, thank you for all your support and guidance throughout my PhD. I recall the job interview we had in Wageningen and from that moment I knew that joining you would be an amazing experience. It has been a privilege to be the first lab member of the group, working together in the lab allowed me to learn so many things and pushed the project along like crazy. During the years you have taught me many things, professionally and in life. It has been really great to see how the lab has grown in these few years and how you managed to establish that. It was also great that I was always able to walk in your office and ask or discuss what was on my mind. I am also really glad that you managed to push and guide me during the writing process, which was not the easiest job. Thanks for these amazing four years!

Next, I would like to thank the people from the Vascular Development group. The atmosphere in- and outside the lab was always great, which I think made us a great team. Jos, thank you for the helpful discussions, the coffee breaks and for bringing some Dutch power to the lab. Jonah, thanks for your help, support and making a great atmosphere in the lab. I especially would like to thank my fellow PhD students, Brecht and Eliana. Our corner was a great place to be in the lab, with many weird discussions and a lot of fun. We had so many memorable adventures, drinks, parties and dinners. I have been so lucky to have you as my colleagues. I will miss you guys. I want to thank the people in the Root Development lab and from the CSF, for the lunches, drinks and of course the nice period I spent there in my first years. Special thanks to Andrzej for the interesting discussions and regular lab visits. I also want to thank my amigo Wilson, who put a smile on my face every day and for providing some Chilean vibes to the lab. Sorry amigo for the huge amount of sequences and primers. Next, I want to thank the guys from the Nadine Crappéstraat, Nick, Lukas, Brecht. It was so cool that you guys moved into the same street. You adopted me in your friend group and made moving to Gent super easy. We had so

many good times together, I have been really lucky to have you as neighbors.

I also want to thank the people from Wageningen Plant Development Lab. I started my PhD there with this group of wonderful people and thus the decision to leave to Gent was not the easiest. Coming back to Wageningen once in a while and catching up with you guys was always a great experience. Also the Barcelona trip was very fun week with a lot of adventure, good science and a lot of laughs. Very happy that I could be a part of that, thank you Sacco!

I really want to thank Thijs, my fellow Zeeuw. We started the bachelor together in Breda and managed to follow each other's footsteps and eventually we both started the Plant Biotechnology master and ended up in the Weijers Lab. I am really glad we managed to stick together and get where we are now. We had so much fun during these years, the many memorable and crazy evenings will be difficult to match. Of course, I also want to thank Merel for the many times I could visit and stay over at your place.

Next, I want to thank Ikram Blilou. I started my bachelor internship with you in Utrecht together with Long. During this period you sparked my interest in plant development and it put me on the path towards the PhD. Your guidance and advice have helped me to get where I am today.

Of course I also want to thank my family for their continuous support through-out my studies. Especially my parents who allowed me to pursue my dreams and supported me in every way they could. Jeroen thanks helping your clumsy brother out once in a while, for the many games of hockey we played together, and for being an awesome brother. It is great to see how you and Anne are building on your future. Thank you all so much for everything, without you this would have never been possible.

Lastly, I would like to thank my fiancée Paula. Finding you was the greatest discovery I ever did. Who would have thought that this guy from Graauw would find this amazing girl from Arauco. It was amazing to spend all this time together in Gent and in Chile. You have always supported me in every way and brought out the better person in me. It was not always easy to live so far apart but we always managed to make it work and support each other. Now we are reunited and will start on the biggest experiment in our life, starting our little family. It is all I could ever dream of. Te amo mucho mi amor, besos.

Curriculum Vitae

Wouter Smet is born in Graauw, The Netherlands. He completed his secondary education degree (HAVO) in 2008. After this he started his Bachelor of Applied Science, studying Biology and Medical Lab Research with a specialization in Biotechnology at the Avans Hogeschool Breda. Here he completed two internships, the first at the Ben Scheres group at Utrecht University focused on protein interactions using FRET-FLIM in the *Arabidopsis thaliana* root meristem. The second internship was in the Tom Beeckman group at VIB in Ghent. Here he studied cell-cell communication during lateral root development in *Arabidopsis thaliana*. After receiving his degree in 2012, he started the master program Plant Biotechnology at Wageningen University. During this program he completed a minor and master thesis both focusing on plant molecular development. The minor thesis was completed in the group of Dolf Weijers at Wageningen University where he worked on analyzing auxin reporter lines and tracking polarity in *Arabidopsis thaliana* embryos. His thesis was completed at the Ben Scheres group which moved to Wageningen University; here he studied protein-protein interactions after site-directed mutagenesis in *Arabidopsis thaliana*. In 2014 Wouter started a Joint-PhD program with Dolf Weijers and Bert De Rybel at Wageningen University and VIB/Ghent University working on the control of periclinal cell division during vascular development in *Arabidopsis thaliana*, resulting in this thesis.

Publications

Smet W, Sevilem I, De Louis Balaguer MA, Wybouw B, Mor E, Sozzani R, Helariutta Y, De Rybel B: DOF2.1 controls vascular cell proliferation downstream of TMO5/LHW (Submitted)

Miyashima S, Roszak P, Sevilem I, Toyokura K, Blob B, Heo J,Mellor N, Help-Rinta-Rahko H, Otero S, **Smet W**, Boekschoten M, Hooiveld G, Hashimoto K, Wallner ES, Kondo Y, Melnyk C, Greb T, Nakajima K, Sozzani R, Bishopp A, De Rybel, Helariutta Y: Mobile PEAR transcription factors integrate hormone and miRNA cues to prime cambial growth (Submitted)

Long YC, Stahl Y, Weidtkamp-Peters S, **Smet W,** Du YJ, Gadella TWJ, Goedhart J, Scheres B, Blilou I: Optimizing FRET-FLIM Labeling Conditions to Detect Nuclear Protein Interactions at Native Expression Levels in Living Arabidopsis Roots. Frontiers in Plant Science 2018, 9.

Andersen TG, Naseer S, Ursache R, Wybouw B, **Smet W**, De Rybel B, Vermeer JEM, Geldner N: Diffusible repression of cytokinin signalling produces endodermal symmetry and passage cells. Nature 2018, 555:529-+.

Smet W, De Rybel B: Genetic and hormonal control of vascular tissue proliferation. Curr Opin Plant Biol 2016, 29:50-56.

Liao CY, **Smet W**, Brunoud G, Yoshida S, Vernoux T, Weijers D: Reporters for sensitive and quantitative measurement of auxin response. Nat Methods 2015, 12:207-210, 202 p following 210.

Long Y, **Smet W,** Cruz-Ramirez A, Castelijns B, de Jonge W, Mahonen AP, Bouchet BP, Perez GS, Akhmanova A, Scheres B, et al.: Arabidopsis BIRD Zinc Finger Proteins Jointly Stabilize Tissue Boundaries by Confining the Cell Fate Regulator SHORT-ROOT and Contributing to Fate Specification. Plant Cell 2015, 27:1185-1199.

Roberts I, Smith S, De Rybel B, Van Den Broeke J, **Smet W**, De Cokere S, Mispelaere M, De Smet I, Beeckman T: The CEP family in land plants: evolutionary analyses, expression studies, and role in Arabidopsis shoot development. J Exp Bot 2013, 64:5371-5381.

Education Statement of the Graduate School

The Graduate School **EXPERIMENTAL PLANT SCIENCES**

Experimental Plant Sciences

Issued to:	**Wouter Smet**
Date:	**09 November 2018**
Group:	**Laboratory of Biochemistry**
University:	**Wageningen University & Research**

1) Start-Up Phase

	date
► **First presentation of your project**	
Control of periclinal cell division during vascular development	12 Oct 2014
► **Writing or rewriting a project proposal**	
► **Writing a review or book chapter**	
Genetic and hormonal control of vascular tissue proliferation. Current Opinion in Plant Biology (2016), 29:50-56, DOI:10.1016/j.pbi.2015.09.008	Fall 2015
► **MSc courses**	
► **Laboratory use of isotopes**	
Subtotal Start-Up Phase	*7.5 **

2) Scientific Exposure

	date
► **EPS PhD student days**	
EPS PhD student days 'Get2Gether', Soest, the Netherlands	9-10 Feb 2017
EPS PhD student days 'Get2Gether', Soest, the Netherlands	15-16 Feb 2018
► **EPS theme symposia**	
EPS theme 1 'Developmental Biology of Plants', Leiden, the Netherlands	08 Jan 2015
EPS theme 1 'Developmental Biology of Plants', Wageningen, the Netherlands	21 Jan 2016
► **National meetings (e.g. Lunteren days) and other National Platforms**	
Annual meeting 'Experimental Plant Sciences', Lunteren, the Netherlands	13-14 Apr 2015
Annual meeting 'Experimental Plant Sciences', Lunteren, the Netherlands	11-12 Apr 2016
Annual meeting 'Experimental Plant Sciences', Lunteren, the Netherlands	10-11 Apr 2017
► **Seminars (series), workshops and symposia**	
Invited speakers and in house PI presentations WUR & VIB	2014-2018
► **Seminar plus**	
► **International symposia and congresses**	
Plant Organ Growth Symposium, Ghent, Belgium	10-12 Mar 2015
4th International Conference on Plant Vascular Biology (PVB2016), Shenzhen, China	19-23 Jul 2016
Vascular Get-Together 2015, Corsendonk, Belgium	23-25 Nov 2015
Vascular Development meeting 2016, Corsendonk, Belgium	14-16 Nov 2016
Vascular Development meeting 2017, Corsendonk, Belgium	13-15 Nov 2017
► **Presentations**	
Talk: Vascular Get-Together, Corsendonk, Belgium	24 Nov 2015
Talk: Vascular Development meeting 2016, Corsendonk, Belgium	15 Nov 2016
Talk: Vascular Development meeting 2017, Corsendonk, Belgium	14 Nov 2017
Talk: PhD trip to Center for Research in Agricultural Genomics (CRAG), Barcelona, Spain	17 May 2017
Poster: 4th International Conference on Plant Vascular Biology (PVB2016), Shenzhen, China	21 Jul 2016
► **IAB interview**	
► **Excursions**	
WUR PhD Trip to Agrasys, ICFO, CRAG & Synchotron, Barcelona, Spain	16-19 May 2017
Subtotal Scientific Exposure	*16.7 **

3) In-Depth Studies

	date
► **EPS courses or other PhD courses**	
VIB training 'Summer School on Advanced Light Microscopy', Ghent, Belgium	15-19 Jun 2015
EPS course 'Transcription Factors and Transcriptional Regulation', Wageningen, the Netherlands	12-14 Dec 2016
► **Journal club**	
Participation in weekly journal club (Dolf Weijers group/Tom Beeckman/Bert de Rybel)	2014-2018
► **Individual research training**	
Subtotal In-Depth Studies	*5.5 **

4) Personal Development

	date
► **Skill training courses**	
EPS Introduction Course, Wageningen, the Netherlands	22 Sep 2015
VIB training 'How to write a winning grant proposal', Zwijnaarde, Belgium	20 Jun 2017
Spanish language course A2, Ghent, Belgium	2018
Scientific Artwork - Vector graphics and images, Wageningen, the Netherlands	02-03 Oct 2017
Adobe InDesign Essential Training, Wageningen, the Netherlands	09-10 Oct 2017
► **Organisation of PhD students day, course or conference**	
► **Membership of Board, Committee or PhD council**	
Subtotal Personal Development	*10.1 **

TOTAL NUMBER OF CREDIT POINTS *39.8 **

Herewith the Graduate School declares that the PhD candidate has complied with the educational requirements set by the Educational Committee of EPS which comprises of a minimum total of 30 ECTS credits.

* A credit represents a normative study load of 28 hours of study.

Propositions

1. Key steps in plant development depend on the sequential action of different bHLH transcription factors
(this thesis)

2. Network inference as a method for analyzing transcriptional datasets promotes conservative gene selection
(this thesis)

3. Redundancy is no longer an excuse to disregard gene function in redundant gene families

4. Interdisciplinary collaborations should become a mandatory part of the PhD program

5. Ready-to-use products lead to a lack of understanding about the source, value and function of the components of the products.

6. Social media being a major news source for a large portion of the population makes critical-thinking ever more important

Propositions belonging to the thesis, entitled
Control of oriented cell division during vascular development in
Arabidopsis thaliana

Wouter Smet
Wageningen, 9th of November 2018